MOLECULAR INVESTIGATION OF PATHOGENIC BACTERIA IN THE PRESENCE OF PHENOLIC ACIDS

A Thesis Submitted to
the Graduate School of Engineering and Sciences of
İzmir Institute of Technology
in Partial Fulfillment of the Requirements for the Degree of

DOCTOR OF PHILOSOPHY

in Molecular Biology and Genetics

by
Özgün Öykü ÖZDEMİR

May 2019
İZMİR

We approve the thesis of **Özgün Öykü ÖZDEMİR**

Examining Committee Members:

Assoc. Prof. Dr. Ferda SOYER
Department of Molecular Biology and Genetics,
İzmir Institute of Technology

Assoc. Prof. Dr. Gülistan MEŞE ÖZÇİVİCİ
Department of Molecular Biology and Genetics,
İzmir Institute of Technology

Assist. Prof. Dr. Nur Başak SÜRMELİ
Department of Bioengineering,
İzmir Institute of Technology

Assist. Prof. Dr. Yavuz OKTAY
Department of Basic Medical Sciences, Dokuz Eylül University

Assist. Prof. Dr. Ayşe Banu DEMİR
Department of Basic Medical Sciences, İzmir University of Economics

20 May 2019

Assoc. Prof. Dr. Ferda SOYER
Supervisor, Department of Molecular Biology
and Genetics, İzmir Institute of Technology

Prof. Dr. Volkan SEYRANTEPE
Head of the Department of
Molecular Biology and Genetics

Prof. Dr. Aysun SOFUOĞLU
Dean of the Graduate School
of Engineering and Sciences

ACKNOWLEDGMENT

I sincerely thank to my advisor Assoc. Prof. Dr. Ferda SOYER for giving me the oppurtunity to work in her laboratory as well as her support and patience during the years of my Masters and PhD studies. I feel honored to be improved in science and life by her dependable guide and invaluable experiences which will lead me throughout my life. I wish to thank Assoc. Prof. Dr. Gülistan MEŞE ÖZÇİVİCİ and Assist. Prof. Dr. Nur Başak SÜRMELİ for being in my thesis supervising committee and their invaluable advices on the development of my PhD studies. I want to thank Assist. Prof. Dr. Ayşe Banu DEMİR and Assist. Prof. Dr. Yavuz OKTAY for being my PhD defense committee members. I am thankful to Prof. Dr. Talat YALÇIN for his kindness to allow me to use his laboratory facilities and his valuable help during my proteomics studies. I am also greatful to Assoc. Prof. Dr. Özden YALÇIN ÖZUYSAL for her kind help and invaluable guide in my RT-qPCR studies as well as allowing me to use her laboratory facility in c-DNA preparation step. In addition, I thank to Dr. Melike DİNÇ and Burcu FIRATLIGİL YILDIRIR for their valuable assistance in my proteomics and c-DNA preparation studies, respectively. I would also like to thank Özlem ECE for her kind help and assistance in my scanning electron microscopy studies.

I genuinely thank to my dear friend Dr. Deniz KEMAN for being not only a good labmate but also being one of my best friends. During the years we worked together I found out her intelligent, hard-working, supportive, humorous and sincere character, and I feel so lucky to have such a wonderful person in my life. I also wish to thank Ertuğrul ACAR for being such a good labmate and for his sincere and valuable friendship.

I wish to express my sincere gratitude to my dear family: my father Namık Kemal ÖZDEMİR, my mother Embiye ÖZDEMİR and my brother Seçkin Ozan ÖZDEMİR. They are always a loving family who supports me under every circumstance. I am very greatful for their limitless love and patience towards me as well as enormous mental and material supports throughout my life, especially in my PhD study period. I feel as I am the luckiest person for having such a wonderful family.

ABSTRACT

MOLECULAR INVESTIGATION OF PATHOGENIC BACTERIA IN THE PRESENCE OF PHENOLIC ACIDS

Pathogenic bacteria, including *P. aeruginosa*, are serious threats for human health with their antibiotic resistance and virulence factors. Since phenolic acids, secondary metabolites of plants, can be good candidates as antimicrobial agents, their mode of action should be investigated. Proteomics is one of the main approaches for elucidating the mode of action of such compounds. In addition, in order to enhance the antimicrobial effects and stabilities of phenolics, they can be encapsulated into nanoparticles. The nanoparticles can be produced from chitosan and alginate which are biocompatible polymers. In this study, the antimicrobial effects of 3-HPAA and 4-HBA were presented with MIC values of 2.1 and 1.9 mg/ml, respectively. The bacteriocidal effects of them were also shown as 2.3 mg/ml for 3-HPAA and 2.1 mg/ml for 4-HBA. The morphological changes of bacteria were determined after phenolic acid exposure via SEM. The LC-ESI-MS/MS technique was used to show changes in the protein profile of bacteria arose from antimicrobial effects. Both phenolic exposures resulted in various protein changes especially in membrane-related proteins as well as ribosome and protein synthesis related-proteins. In addition, they caused serious oxidative stress depending on the protein profile changes related to redox proteins. Alginate-chitosan nanoparticles resulted increased antimicrobial effects of the phenolics which were produced, characterized and tested on various pathogenic bacteria via agar diffussion and spectrophotometric measurements. Hence, free or encapsulated forms of phenolic acids were demonstrated as effective antimicrobial agents and based on proteomic results, the effect of phenolic acids may be multi targetted.

ÖZET

FENOLİK ASİTLERİN VARLIĞINDA PATOJEN BAKTERİLERİN MOLEKÜLER İNCELEMESİ

P. aeruginosa'nın da içinde bulunduğu patojen bakteriler antibiyotik dirençlilikleri ve virülans faktörleri nedeniyle insan sağlığı için önemli bir tehdit oluşturmaktadır. Bitkilerin sekonder metabolitleri olan fenolik asitler antimikrobiyal madde olmak için iyi adaylar olduklarından, etki mekanizmalarının çalışılması gereklidir. Proteomik çalışmalar, böyle maddelerin etki mekanizmalarının araştırılmasındaki önemli yaklaşımlardan biridir. Bunun yanısıra, kararlılıklarının ve antimikrobiyal etkilerinin arttırılması için, fenolik asitler nanopartiküller içerisine hapsedilebilirler. Nanopartiküller, biyo-uyumlu polimerler olan kitosan ve aljinattan sentezlenebilirler. Bu çalışmada, 3-HPAA ve 4-HBA'nın antimikrobiyal etkileri, sırasıyla 2.1 and 1.9 mg/ml olan minimum inhibe edici konsantrasyon değerleri ile sunulmuştur. Aynı zamanda bakterisidal etkiye sahip oldukları ise 3-HPAA için 2.3 mg/ml ve 4-HBA için 2.1 mg/ml minimum bakterisidal konsantrasyon değerleri ile gösterilmiştir. Buna ek olarak, bakterilerin morfolojilerinde fenolik asit uygulamasından sonra oluşan değişiklikler de taramalı elektron mikroskobu ile tespit edilmiştir. LC-ESI-MS/MS tekniği, antimikrobiyal etkiler nedeniyle protein profilinde oluşan değişiklikleri göstermek için kullanılmıştır. İki fenolik muamelesi de bakterinin protein profilinde, zarla ilgili proteinlerdeki, ribozom ve protein senteziyle ilgili proteinlerdeki değişimler başta olmak üzere, birçok değişime neden olmuştur. Bunun yanında, redox proteinlerindeki değişimler göz önüne alındığında, fenoliklerin bakterilerde ciddi oksidatif strese yol açtığı görülmüştür. Fenolik asitlerin enkapsüle edilmesini sağlayan, sentezlenen, tanımlanan ve antimikrobiyal etkileri birçok patojen bakteride agar difüzyon ve spektrofotometrik ölçümlerle test edilen aljinat-kitosan nanopartiküller ise, fenoliklerin antimikrobiyal etkilerinin artmasını sağlamıştır. Bu çalışmayla fenolik asitlerin hem serbest, hem de enkapsüle edilmiş hallerinin etkili antimikrobiyal maddeler oldukları sunulmuş ve proteomik çalışmanın sonuçlarına göre fenolik asitlerin çoklu-hedefli etkiler gösteriyor olabildikleri sonucuna varılmıştır.

This thesis is lovingly dedicated to my dear family.

TABLE OF CONTENTS

LIST OF FIGURES

Figure **Page**

Figure **Page**

Figure **Page**

Figure **Page**

LIST OF TABLES

Table **Page**

Table **Page**

LIST OF ABBREVIATIONS

ACN	Acetonitrile
Alg-Chi	Unloaded alginate-chitosan nanoparticles (null nanoparticles)
BER	Base excision repair
BSA	Bovine serum albumin
$CaCl_2$	Calcium chloride
cfu	Colony forming unit
ddH_2O	Double-distilled water
DLS	Dynamic Light Scattering
ESI	Electrospray ionization
FA	Formic acid
FT-IR	Fouirer Transfrom Infrared Spectrometry
g	Gram
h	Hours
HCl	Hydrochloric acid
HPLC	High pressure liquid chromatograpy
ICU	Intensive care units
LC	Liquid chromatography
LC-ESI-MS/MS	Liquid chromatography-electrospray ionization-tandem mass spectrometry
MBC	Minimum bacteriocidal concentration
MDR	Multidrug-resistant
MHB	Mueller Hinton broth
MHA	Mueller Hinton agar
MIC	Minimum inhibitory concentration
MRSA	Methicillin resistant *Staphylococcus aureus*
MSSA	Methicillin sensitive *Staphylococcus aureus*
MMR	Mismatch repair
M	Molar
mM	Milimolar
µl	Microliter

ml	Mililiter
mg	Miligram
NaOH	Sodium hydroxide
NER	Nucleotide excision repair
nm	Nanometer
O.D.	Optical density
OOWW	Olive oil waste water
PDI	Polydispersity index
RP	Reversed-phase
RT-qPCR	Real Time-Quantitative Polymerase Chain Reaction
ROS	Reactive oxygen species
SEM	Scanning Electron Microscopy
SCX	Strong cation exchange
SSC	Staphylococcal cassette chromosome
STRING	Search Tool for the Retrieval of Interacting Genes/Proteins
TSA	Tyrptic soy agar
T6SS	Type VI secretion system
v/v	Volume/Volume
WHO	World Health Organization
XDR	Extensively drug-resistant
x g	Gravity
3-HPAA	3-hydroxyphenylacetic acid
3-HPAA-Alg-Chi	Alginate chitosan nanoparticles loaded with 3-HPAA
4-HBA	4-hydroxybenzoic acid
4-HBA-Alg-Chi	Alginate chitosan nanoparticles loaded with 4-HBA

CHAPTER 1

LITERATURE REVIEW

1.1. Scope of the Study

Throughout the history, the human well-being is threatened by various diseases in which the bacterial infections cover a huge part. The bacterial infections arise from the pathogenic, opportunistic bacteria, which result in high mortality and morbidity as well as reduced life quality and high economic costs. Even today the bacteria still continue to cause various infections that are attempted to be controlled. The most effective way to combat these infections is using antimicrobial agents, specifically antibiotics, since the starting of usage of them lead a decline in these infections, worldwide. From the introduction of antibiotics for clinical use such as sulphonamides in 1935, penicillin in 1941, streptomycin in 1943 and many others since, the rapid decrease in these infections are reported (Aminov, 2017) which covers the duration of the discovery, development and use of the antibiotics between 1940-1970 (the golden age of antimicrobial therapy) (De Mol et al., 2018). However, the increased usage of the antibiotics in humans and animals are also result in the resistance development of the pathogenic bacteria since 20th century, which is still a serious problem (Caffrey et al., 2019). This is also presented by the important international agencies like World Health Organization (WHO) and the European Centre for Disease Prevention and Control (https://www.who.int/en/news-room/fact-sheets/detail/antibiotic-resistance, Access date: 06.04.2019; https://www.ecdc.europa.eu/en/publications-data/surveillance-antimicrobial-resistance-europe-2017, Access date: 06.04.2019). Various pathogenic bacteria are turn out to be multidrug-resistant (MDR) and even, extensively drug-resistant (XDR) bacteria (Durand et al., 2019). Thus, this period can be accepted as the post-antibiotic era (Murima et al., 2014). This situation shows that the continuation in antibiotics usage may result in elevated and formidable bacterial infections. It is assumed that by the year of 2050, the infections will globally cause ten million deaths per year (Maldonado-Carmona et al., 2019). In addition to the antibiotics resistance, the bacteria possess various other virulence factors to develop and maintain infections such

as biofilm formation and secretion of toxic substances (Bleves et al., 2010). Even in the hospitals, during the treatment of diseases such as in the cancer treatment (Galloway-Pena et al., 2017) or surgeries such as in the implant replacements (Zhou et al., 2015), these bacteria are the main reasons of the nosocomial infections. Infections that arise from food-borne pathogens also cause serious diseases and outbreaks, worldwide. Hence, in addition to development of new designs of existing antibiotics (Lewis, 2017), brand new antimicrobial agents and new routes for treatment of the bacterial infections are globally investigated.

Bioactive compounds such as phenolics, which are found naturally in almost all plants, are accepted as one of the promising agents for antimicrobial therapy. These compounds demonstrate a bacteriostatic effect through inhibition of bacterial growth or a bacteriocidal effect by killing the bacteria in a dose-dependent manner. However, the molecular basis of their antimicrobial effect must be investigated by –omics studies, such as changes at the proteomic level, in order to use them as new antimicrobial agents (Maldonado-Carmano et al., 2019). Additionally, since the encapsulation of these agents into nanoparticles can enhance and/or elongate the stability of their antimicrobial properties, it is considered as an important method for maintenance of antimicrobial activity.

a

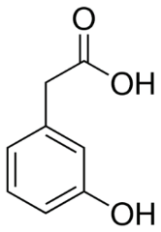

b

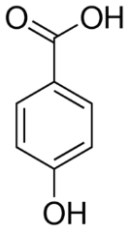

Figure 1.1. The chemical structures of phenolic acids focused in this study. a) 3-HPAA b) 4-HBA (Sources: Sigma-Aldrich)

The scope of our study covers the demonstration of water-soluble, simple phenolic acids with their high antimicrobial effects on *Pseudomonas aeruginosa* which is one of the most important pathogenic bacteria, as well as the proteomic changes in the protein profile of this bacteria to enlighten the action path of these agents. In addition, our scope

also covers the presentation of the antimicrobial effects and possible application route of the phenolic acids on various pathogenic bacteria *in vitro* after the encapsulation into alginate-chitosan nanoparticles.

1.2. Pathogenic Bacteria

The pathogenic bacteria, which are the causes of serious infections worldwide, were examined in this study for testing new antimicrobial agents. Among these, the well-known nosocomial pathogen, *Pseudomonas aeruginosa* was in the focus of this study to enlighten the proteomic changes for determination of the possible targets of the phenolic acids as promising antimicrobial agents.

1.2.1. *Pseudomonas aeruginosa*

Pseudomonas aeruginosa is a Gram negative bacterium which can be colonized in various environments (i.e. soil and water), plant and animal tissues (Ha and O'Toole, 2015; Valentini et al., 2018) as well as instruments and surfaces of the hospitals (Huber et al., 2016). As widely distributed opportunistic pathogens (Brown et al., 2012), they are accepted as one of the most important pathogenic bacteria in nosocomial (hospital-acquired) infections, worldwide (Klockgether and Tümmler, 2017) as well as in the community-acquired infections (Driscoll et al., 2007). Such that, *P. aeruginosa* are counted in the ESKAPE pathogens which stands for they are among six highly antibiotic resistant bacteria that mainly cause nosocomial infections: *Enterococcus faecium*, *Staphylococcus aureus*, *Klebsiella pneumoniae*, *Acinetobacter baumannii*, *Pseudomonas aeruginosa* and *Enterobacter* species (Murray et al., 2015). They take roles in serious infections such as pneumonia, meningitis, abscess, soft tissue infections, urinary tract infections and catheter associated infections (Chatterjee et al., 2016) as well as causing the infections that can result in deaths in immunocompromised individuals such as cancer, burn, HIV, cystic fibrosis and organ transplantation patients (Morita et al., 2014; Huber et al., 2016). *P. aeruginosa* may be the causative agent of both acute and chronic infections (Valentini et al., 2018). The important properties of *P. aeruginosa*, which show an extremely diverse genotype and phenotype (Silby et al., 2011; Huber et al., 2016), are the ability to adapt various environments via broad

changes in metabolism, possessing virulence factors such as proteases, lipopolysaccharides and exotoxins (Gellatly and Hancock, 2013) and to switching the life-style according to the conditions (Morita et al., 2014). The bacteria can be either in planktonic life-style by which causing acute infections or they can be in biofilm forming life-style which aids the attachment and continuation in chronic infections (Valentini et al., 2018). They also have the both intrinsic and adaptive resistance abilities against various antibiotics (Morita et al., 2014; Pang et al., 2019). This high resistance property may arise from the low permeability of outer membrane of *P. aeruginosa* against many antibiotics (Breidenstein et al., 2011). For instance, they have resistance to antibiotics in use such as penicillins, cephalosporins, carbapenems, monobactams and fluoroquinolones (Poole, 2011; Lister et al., 2009) which leads to the very limited therapeutic options for these bacteria. Since they are life-threatening pathogens with which to combat is highly challenging, it is required to discover, design and develop new antimicrobial agents and treatment routes against *P. aeruginosa*, urgently.

1.2.2. Other Pathogenic Bacteria

The other pathogenic bacteria in this study are important nosocomial pathogens; *Staphylococcus epidermidis*, *Acinetobacter haemolyticus*, Methicillin resistant *Staphylococcus aureus* (MRSA) and Methicillin sensitive *Staphylococcus aureus* (MSSA) in addition to serious food-borne pathogens; *Salmonella* Enteritidis, *Escherichia coli* O157:H7 and *Listeria monocytogenes*.

S. epidermidis are Gram positive bacteria (Neely and Maley, 2000) and they are normal occupants of skin and mucous membrane flora of humans and other mammals (Parlet et al., 2019; Argudin et al., 2015). As oppurtunistic pathogens, they are accepted as the cause of various infections since 1970s with the important virulence factors of biofilm formation and antibiotics resistance (Piette and Verschraegen, 2009). Among these, the antibiotic resistance is a major problem to fight against Staphylococci with a 91% resistance in clinical samples (Argudin et al., 2015). It can be stated that all infections caused by *S. epidermidis* are persistent against treatments (Schoenfelder et al., 2010). *S. epidermidis* with antibiotics resistance are colonized in patients and in/on hospital devices/areas by which the infections of these organisms take place (Piette and

Verschraegen, 2009). These infections resulted in significant outcomes for morbidity, mortality and economic costs.

S. aureus are Gram positive bacteria which are the causative agents of various hospital-acquired and community-acquired infections (Bitrus et al., 2018). Methicillin resistant *S. aureus* (MRSA) and Methicillin sensitive *S. aureus* (MSSA) are known as the "hospital pathogens" and "superbugs" with their resistance against many antibiotics (Nordmann et al., 2007). They are one of the ESKAPE pathogens since being in the aforementioned six highly antibiotic resistant nosocomial bacteria (Murray et al., 2015). They may cause acute infections by secreting virulence factors such as exotoxins and hydrolytic enzymes or chronic infections such as osteomyelitis, rhino sinusitis and otitis (François et al., 2010). The bacteria can survive by adapting to the environmental conditions immediately, for instance, the methicillin resistance was detected after six months of the initial clinical usage of methicillin in 1961 (François et al., 2010). The possession of the mobile genetic element staphylococcal cassette chromosome (SSC) which contains the *mec* gene in their chromosome (SSCmec genomic island), which has a broad genetic diversity, *S. aureus* strains (especially MRSA) gain the high antibiotic resistance (Bitrus et al., 2018). That result in the limited choices for the treatment of the infections of *S. aureus* and new antimicrobial agents are in search worldwide.

A. haemolyticus are Gram-negative opportunistic bacteria which are found in soil and waste waters in addition to being a normal occupant of healthy human skin, throat and intestine (Mujumdar et al., 2014). *Acinetobacter* species are considered as nosocomial pathogens which can cause various infections such as urinary tract infections, wound and burn infections and pneumonia and they are important agents of nosocomial outbreaks (Bergogne-Berezin, 1995). *Acinetobacter* develop resistance against common antibiotics in use and the infections caused by these bacteria are related especially with intensive care units (ICU) patients (Tripathi et al., 2014).

S. Enteritidis, *E. coli* O157:H7 and *L. monocytogenes* are food-borne pathogenic bacteria (Alegbeleye et al., 2018) that can lead food-borne infections via food poisoning. Food-borne diseases arise from contaminated food or water consumption by the food-borne pathogens or their toxins (Heredia and Garcia, 2018; Cisse, 2019). They are serious threats for human health, cause serious illnesses including diarrhea which may lead outbreaks in or between countries with high mortality and morbidity worldwide, as well as causing high economic costs (Alegbeleye et al., 2018; Franz et

al., 2019; Heredia and Garcia, 2018). According to WHO report in 2015, one of the 10 people experience diseases of food poisoning every year and about 420,000 deaths were presented, worldwide (Alegbeleye et al., 2018). The report indicates that the food-borne diseases resulted in nearly 23 million illness cases among which 5000 deaths occurred every year in Europe (Flynn et al., 2019). Although the food safety maintenance bears a high importance to reduce food-borne illnesses, it is a challenging process because of the errors at food processing and consumer levels as well as at the microorganism level (Franz et al., 2019). The resistance development of the microorganisms against antimicrobial agents is one of the primary reasons of problems in food safety (Franz et al., 2019) and new antimicrobial agents must be developed for both protection and treatments of food-borne diseases.

1.3. Phenolic Acids

The phenolic compounds, which are widely produced as secondary metabolites by almost all plants and fungi, are the phytochemicals which have various roles in plant metabolism such as pollination, pigmentation and growth as well as the defense against environmental stresses, predators and microorganisms (Hurtado-Fernandez et al., 2010; Duthie et al., 2003; Heleno et al., 2015). The phenolics also display many beneficial properties for human well-being by showing antimicrobial, anti-oxidant, anti-carcinogenic, cardio-protective and anti-inflammatory properties (Karaosmanoglu et al., 2010; Andjelkovic et al., 2006; Daglia, 2012; Gutiérrez-Larraínzar et al., 2012; Diaz-Gomez et al., 2013; Cueva et al.,2010). In addition, it was presented that phenolics enhance the composition and function of gut microbiota by supporting the beneficial bacteria (Cardona et al. 2013). Since they are found in nearly all plants, the foods in human diet which were derived from plants such as fruits, vegetables, olive oil, wine, tea, etc., widely contain phenolic compounds (Lima et al., 2019). For instance, the average phenolic acid consumption by humans is presented as about 200 mg/day depending on the preferences in their diet (Heleno et al., 2015). For the absorption of the consumed phenolics, they are conjugated via methylation, sulfation and glucuronidation first in the small intestine and then in the liver. These are the main processes for their detoxification and elevation of their hydrophilicity for elimination by urination in the human body (Heleno et al., 2015). Hence, the humans benefit from the

advantageous properties every time they consume plant-derived foods when avoiding the possible toxic effects.

The plants use phenylalanine or tyrosine as precursors to naturally synthesize the phenolic compounds via shikimate pathway (Heleno et al., 2015). The characteristic structures of phenolic compounds possess one or more benzene ring and hydroxyl groups as well as other radical groups (Hurtado-Fernandez et al., 2010). The phenolic compounds can be divided into two main groups based on their skeleton nature: Polyphenols and phenolic acids. The polyphenols which contain flavonoids and tannins have more than one benzene rings in their structures. On the other hand, the phenolic acids, which are the main topic of this study, are included in simple phenolics since they have one phenol ring in their structures. (Hurtado-Fernandez et al., 2010). The phenolic acids fall into two groups due to the attachment type of carboxylic group to the benzene ring: Hydroxybenzoic acids contain the carboxylic group as directly attached while hydroxycinnamic acids possess an ethylene group for the attachment of the carboxylic group (Andjelkovic et al., 2006). The chemical structures of hydroxybenzoic acids are presented as C_6-C_1 whereas those of hydroxycinnamic acids as C_6-C_3 (Tripoli et al., 2005). The two phenolic acids which were investigated in this study belong to these two distinct groups. The 3-hydroxyphenylacetic acid (3-HPAA) is included in hydroxycinnamic acids group while the 4-hydroxybenzoic acid (4-HBA) is in hydroxybenzoic acids group. The molecular weight of 3-HPAA and 4-HBA are 152.15 g/mole and 138.12 g/mole, respectively (Sigma-Aldrich). They are both water-soluble simple phenolic acids with one hydroxyl group on the benzene ring. The 3-HPAA is mostly detected in olive oil wastewater (OOWW) involving high degree of polyphenols which is the by-product of olive oil extraction process (Roig et al., 2006; Zafra et al., 2006). In the study performed in IYTE, 4-HBA is detected in extra virgin olive oils in west part of Turkey (Ocakoglu et al., 2009). Although both phenolic acids only have one hydroxyl group, its position differs (Figure 1.1) (Tang et al., 2016; Fletcher et al., 2019). As a matter of fact, the number and the position of the hydroxyl groups on the benzene rings are accepted to affect the antimicrobial and anti-oxidant properties of the phenolic compounds (Lima et al., 2019; Heleno et al., 2015). The selection of the phenolic acids in this study were done not only due to having similar structures in two distinct groups but also due to having one hydroxyl group at different positions. Hence, the comparison between these phenolic acids can be more relevant in terms of their

effects on bacterial growth and the protein profile. The chemical structures of 3-HPAA and 4-HBA are presented in Figure 1.1.a and Figure 1.1.b, respectively.

The antimicrobial properties of the phenolic compounds and phenolic-containing plant extracts against pathogenic bacteria were presented in various studies. These studies indicated that phenolic compounds may be potential effective antimicrobial agents. In the study of Cueva et al., the antimicrobial effects of 13 different phenolic compounds involving 3-hydroxybenzoic acid (3-HBA), 4-HBA, 3-HPAA and 4-hydroxyphenylacetic acid (4-HPAA) were individually tested in the concentration range of 62.5-10000 µg/ ml on the different strains of pathogenic bacteria; *E. coli*, *S. aureus*, *P. aeruginosa* (Cueva et al., 2010). It was found that *E. coli* and *S. aureus* were affected by phenolic compounds with respect to their structures and in a strain-specific, dose-dependent manner. The benzoic and phenylacetic acids were presented as in the most effective phenolic compounds among the tested chemicals. However, even 1000 µg/ ml concentrations of the compounds could not inhibit the *P. aeruginosa* which indicated that higher concentrations of phenolic acids are required for these bacteria. It was concluded that the usage of the phenolic acids at physiological concentrations results in the bacterial growth inhibition depending on the bacterial strain, phenolic acid dose and structure (Cueva et al., 2010). The antimicrobial tests of phenolic compounds, gallic acid and catechin, were performed on *Helicobacter pylori* which are the Gram negative bacteria causing peptic ulcer (Diaz-Gomez et al., 2013). Regardless of being applied individually or in combination, these phenolic compounds resulted in reduced bacterial growth in a dose-dependent manner. In addition, gallic acid resulted in higher antimicrobial effect than cathecin. Thus, the antimicrobial effect was found as phenolic compound type-dependent.

In another study, Sanhueza et al. tested the antimicrobial effects of phenolic acids and flavonoids including gallic acid, vanillic acid, syringic acid and catechin as well as various antibiotics on clinical strains of *S. aureus* and *E. coli* (Sanhueza et al., 2017). In addition, they compared those with the effect of grape pomace extract which contains all of the tested phenolics according to their HPLC study as well as testing the synergistic effects of the extract with antibiotics. The results showed that the tested bacteria were resistant to the antibiotics while phenolic compounds displayed high antimicrobial effects except (+)-catechin. The MIC values for phenolic acids were in the range of 0.062-3 mg/ml and the MIC values of flavonoids were found in 0.1-1.5 mg/ml

range for *S. aureus*. Whereas the phenolic acids showed MIC values in the range of 0.2-2.5 mg/ml and flavonoids showed 0.2-5 mg/ml for *E. coli*. They concluded that MIC values of the phenolic acids and flavonoids were similar to the MIC values of grape pomace extracts against antibiotic resistant bacteria (Sanhueza et al., 2017). Hence, the antimicrobial effect of the grape pomace extract may be due to its phenolic compound ingredients. Additionally, when the antibiotics were applied as a mixture with grape pomace extract, a synergistic effect was detected which may show that phenolic acids aid the bacterial growth inhibition of antibiotics (Sanhueza et al., 2017). Likewise, the study of Shen et al. indicated that the blueberry extract and the phenolic compounds chlorogenic acid, ellagic acid, quercetin and quercetin-3-galactoside, which were found in high levels in the blueberry extract, exhibited a dose-dependent bacterial growth inhibition of food-borne pathogens *L. monocytogenes* and *Salmonella* Enteritidis (Shen et al., 2014). Among the phenolic compounds tested, the least effective phenolic compound was found as the chlorogenic acid (500 µg/ml) while the most effective one was the ellagic acid (44 µg/ml) against *L. monocytogenes* and *Salmonella* Enteritidis (Shen et al., 2014). It was concluded that the phenolic contents of blueberry extracts may be the reason of the antimicrobial effect (Shen et al., 2014).

The distinct antimicrobial effects of the phenolic compounds are demonstrated on nosocomial or food-borne pathogenic bacteria in many studies. These studies mostly point out the higher antimicrobial effect of phenolic acids is associated with their smaller structures among all the phenolic compounds. It can be speculated that the small sizes of phenolic acids may lead the strong interactions with membranes or other targets in bacteria (Lima et al., 2019). For instance, outer membrane of Gram negative bacteria may be easily crossed by phenolic acids due to their small structures while the membrane does not usually allow big and hydrophobic molecules to be transported (Cueva et al., 2010). Relatedly, the antimicrobial effects of the phenolic compounds must be occurred due to the targeting some structures or metabolic pathways of the bacteria. Unfortunately, it is known that the antimicrobial agents can target human proteins as well as bacterial proteins which reduce the success of antimicrobial therapy (Chavali et al., 2012). Hence, the determination of the pathogen protein targets may be a starting point for the elucidation of action mechanisms of these compounds not only for further studies of future antimicrobial therapies but also elimination of the compounds targeting human proteins, leading specific antimicrobial agents for pathogens. A general

idea for possible pathogen protein targets of the antimicrobial agents can be achieved by using the proteomic approaches since the obstruct of checkpoints of important metabolic pathways is accepted as a useful way for antimicrobial therapy (Garg et al., 2018).

1.4. Proteomic Investigation of Antimicrobial Effects

The -omics sciences, including genomics, proteomics, transcriptomics, metabolomics, glycomics or the combinations of those, are accepted as dependable approaches with their related bioinformatics analyses due to their allowance to obtain wide informations that give clues about the action mechanisms of the bioactive compounds (Maldonado-Carmona et al., 2019). Among those, the proteomics may display useful results since the protein profiles possess the final state of the cell after the modifications. Hence, using the proteomics is a dependable approach for the determination of the bacterial protein profile changes for adaptations to different conditions such as growing in the presence of a chemical compound and it can aid reliable results in potential target determinations in the antimicrobial discovery area (François et al., 2010; Navare et al., 2015). For instance, the changes in the proteins functioned in bacterial cell processes which are required for the growth and survival can indicate the favorable targets (Lee et al., 2015). For this purpose, besides gel-based proteomic techniques, the mass spectrometry coupled with the liquid chromatography (LC) as well as electrospray ionization (ESI) is also a popular technique namely "Liquid Chromatography Electrospray Ionization Tandem Mass Spectrometry" (LC-ESI-MS/MS) (shot gun proteomics) with higher sensitivity and speed (François et al., 2010, Walther and Mann, 2010). In this technique, the protein samples are digested as the first step either with in-gel or in-solution digestion depending on the preference of a gel-based first separation of proteins or not, respectively (Choksawangkarn et al., 2012). The fractination which is performed after digestion step provides the enhancement of analytical dynamic range and proteome coverage (Yang et al., 2012). After that, the identification of high numbers of peptides can be obtained since this technique possesses two consecutive separation steps for peptides: LC and ESI-MS/MS (Stapels et al., 2004; Walther and Mann,2010). The first separation of the peptides is carried out by High Pressure Liquid Chromatograpy (HPLC) by either strong cation exchange (SCX)

chromatography depending on the charges or pH reversed-phase (RP) chromatography depending on the hydrophobic interactions (Batth et al., 2014). Either low or high pH HPLC columns can be used in RP chromatography (Wang et al., 2011). Since it results in enhanced protein identification, more clean samples excluding desalting, reducing sample loss as well as process time, high pH RP is more useful than low pH RP or SCX (Yang et al., 2012). Prior to second separation by HPLC using low pH columns, the samples are charged and transfered to gas form by ESI which allow the detection of the molecules in an electric field (Walther and Mann,2010). After the data is obtained and processed for the protein identification by search engines such as MASCOT (Walther and Mann, 2010), the functions of the proteins are determined in online databases (i.e.Uniprot, KEGG, Swissprot). The interaction network of the proteins can be detected for a deeper insight of the changes in the bacterial cell systems by databases such as STRING (Search Tool for the Retrieval of Interacting Genes/Proteins) which is a widely-used, open source database (http://string-db.org/) (Cafarelli et al., 2017). The interaction network of genes/proteins stands for the representation of the intractions between the genes/proteins of interest as a graphic by displaying each gene/protein as a node and their interaction as the connecting edge. The interaction informations are obtained from various sources such as primary databases as well as the predicted interactions via statistical methods and the interactions can be phyisical (direct) or functional (indirect) which are indicated by colors (Miryala et al., 2018; Cafarelli et al., 2017).

After the proteome elucidation, the protein data can be validated at the transcriptomic level by the technique named real time quantitative PCR (RT-qPCR). In this technique, the relative fold change of the gene expression of the protein of interest is determined based on the normalization to the expression of the reference gene and control group. A reference gene must be simultaneously analyzed with the investigated genes and specific primers for each gene must be designed by online tools such as Primer BLAST. The reference gene of the bacteria can be determined among the housekeeping genes such as gyrB, rpoA, rpoB, oriC, dnaJ, and rplI as well as 16S rRNA genes depending on the properties of the bacteria and the experimental conditions (Takahashi et al., 2017). For instance, in the study of Llanes et al. it was shown by RT-qPCR and immunoblotting that the overexpression of the genes of MexAB-OprM and MexXY efflux pumps were simultaneous (Llanes et al., 2004). In that study, 12

multidrug resistant *P. aeruginosa* strains were investigated and rpsL gene was used as the housekeeping gene for RT-qPCR. Based on the results, they concluded that the simultaneous overexpression of the efflux pump genes might aid the enhancement of the resistance of clinical strains (Llanes et al., 2004). Similarly, Dumas et al. used this technique for the investigation of expression of antibiotic resistance genes in wild-type and mutant, clinical and laboratory strains of *P. aeruginosa* (Dumas et al., 2006). Since the Mex drug efflux pumps, AmpC β-lactamase and OprD which is the porin of carbapenem are related to the antibiotic resistance of *P. aeruginosa*, they elucidated the expression of the genes of these proteins by RT-qPCR. As the reference gene, they also used ribosomal rpsL gene to normalize the results. Their results presented a high fold-increase in the expression of aforementioned genes and they concluded that RT-qPCR is a reliable technique for the investigation of expression of antibiotic resistance genes (Dumas et al., 2006). It is clear that rpsL gene, which is a 16S ribosomal protein gene, was used as the housekeeping gene in the RT-qPCR studies in the literature. Thus, this gene was chosen as the reference gene in our protein data validation study which was performed via RT-qPCR. Although the data of proteome and transcriptome may not always be overlapped due to the modifications of the proteins during or after their maturation, this type of validation is still accepted as a reliable technique to confirm the expression change of gene of protein of interest. For instance, Ma et al. investigated the mechanism of action of daptomycin antibiotic on *S. aureus* at the proteomic level by determining the whole proteome via LC-MS/MS and then validated the results via RT-qPCR for the genes of diphosphate kinase (NDK) and 5'-nucleotidase (NT5) enzymes by normalizing the results based on housekeeping gene, triosephosphate isomerase (TPI) gene (Ma et al., 2017). The proteomic data showed that the profile of membrane proteins and DNA metabolism were affected in the presence of daptomycin. The results displayed the relevant gene expression changes with the protein data by the increased expression of NDK gene and decreased expression of NT5 gene. These are both important enzymes which function in the purine metabolism. Thus, the changes of these proteins were not only confirmed at the proteomic level but also confirmed at the transcriptomic level. They concluded that doptamycin displayed a dual action mechanism by damaging the cell membrane and DNA metabolism of *S. aureus* which may explain its mode of action as a bacteriocidal antibiotic (Ma et al., 2017). In addition, various studies exist in the literature for the determination of the changes in

the protein profiles of bacteria, enlightening the bacterial metabolisms as well as the answers to different conditions which can aid the development of antimicrobial agents. In the study of Carrera et al., the proteome of 20 food-borne strains of *Staphylococcus aureus* were investigated by in-solution proteolytic digestion and LC-ESI-MS/MS analysis (Carrera et al., 2017). They used UniProt database to analyze the data sets and they determined the networks of the proteins by gene ontology (GO) analysis. They discussed that most common identified proteins of these strains were surface-associated proteins that were related to pathways and networks of energy, lipid metabolism and virulence (Carrera et al., 2017) which may be a clue for the target of new antimicrobials against these bacteria. Kılıç et al. elucidated the *P. aeruginosa* protein profile against chromium (VI) toxicity via proteomic approach. Since these bacteria are resistant against chromium (VI), the identifying the overexpressed proteins of these bacteria in high levels of the chromium (VI) may show the resistance scope of the bacteria (Kılıç et al., 2010). Since they used a gel based method, a small quatity of the proteins were detected. They used in-gel digestion of the protein spots prior to LC-ESI-MS/MS and determined 21 proteins which were expressed differently than the control group. The upregulated cytosolic proteins were detected which are related to stress response, protein biosynthesis, energy production metabolism and response to oxidative stress. The membrane bound proteins were upregulated functioned in the stress response, some ribosomal structural proteins, outer membrane proteins and energy metabolism proteins. Thus, the proteomic approach was successfully used to aid enlightening the resistance mechanism of *P. aeruginosa* against chromium (VI). The study of Sharma et al. demonstrated the proteome of clinical strain of *Klebsielle pneumoniae* in the presence of meropenem (a type of carbapenem) (Sharma et al., 2019). Since these bacteria possess a carbapenem resistance, Sharma et al. aimed to bring out the resistance mechanism of the bacteria to be able to detect the molecular targets to combat the resistant strains. They used LC- MS/MS and related bioinformatics tools, Gene Ontology, KEGG and STRING and demonstrated that 52 proteins were over expressed which might be used for bacterial resistance and survival. The overexpressed proteins were related mainly to protein translational machinery complex, DNA/RNA modification, carbapenems cleavage, energy metabolism and intermediary metabolism (Sharma et al., 2019). Thus, whole proteome of *Klebsielle pneumoniae* was enlightened in terms of carbapenem resistance-related proteins for further studies of antimicrobial

developments. Li et al. used the combination of proteomics and metabolomics data for the determination of the *E.coli* answer to ciprofloxacin (Li et al., 2018). They performed LC-MS/MS for protein identification of the bacteria growth in the environments with or without ciprofloxacin and compared those. They presented the changed protein profile with 143 decreased and 147 increased expressions. When they integrated proteomic data with the metabolomic data, they suggested a possible mode of action of this drug as blocking the DNA replication while increasing the DNA gyrase and DNA topoisomerase I. In addition, the ciprofloxacin exposure resulted in the changes of tRNA biosynthesis with the enhancement of aminoacyl-tRNAs ligases, but diminished the biosynthesis of related amino acids (Li et al., 2018).

As a consequence, proteomic approach is used for comparison between chemical of interest-treated or non-treated groups of the same organism to determine the molecular effects of the chemical on the organism. To the best of our knowledge, although the antimicrobial effects of the phenolic compounds are presented in a plenty of studies in the literature, the studies focusing on the molecular mechanism of their antimicrobial effects are very limited. Since our study aims to determine the changes in the whole protein profile of *P. aeruginosa* in the presence of phenolic acids, it may aid to fulfill the lack of information about the antimicrobial effects of these compounds at the molecular level. These informations can be a starting point to guide more detailed studies about the phenolic acid mode of action, in the future.

1.5. Encapsulation of Phenolic Acids

Nowadays, the encapsulation of the bioactive compounds, such as phenolic compounds, is a popular concept in the studies related to biomedical field. Although the phenolic acids are promising candidates for alternative treatments against pathogenic bacteria showing distinct antimicrobial effects, they have broad ranges of aqueus solubilities and rapid degradation profiles which may decrease their antimicrobial potential. The encapsulation of the phenolic acids into nanoparticles can solve these problems (Krausz et al, 2015). Nanoparticles are the particles which have a size range between 1-100 nm (Capaldi Arruda et al., 2015). But the ones that have sizes below 1000 nm are also accepted as nanoparticles in pharmaceutical science (Li et al., 2015). They are useful for encapsulation of drugs to be able to increase their stability and to

control their release properties. For encapsulation of the phytochemicals such as phenolic compounds into nanoparticles, hydrogen bonds and hydrophobic interactions are effective. These interactions encapsulate the phenolics in the nanoparticles not only to facilitate the aqueous solubility of phenolics but also to decrease the oxidation and/or degradation of the phenolics (Li et al., 2015). In the treatment of infections, the usage of the nanoparticles can be an alternative therapy route (Andonova and Urumova, 2013). Encapsulation would provide phenolic acids an increased stability, controlled release and protection against environmental changes. Relatedly, the antimicrobial effects of the phenolics can be achieved in higher levels when they are encapsulated compared to their effects of free form. In addition, because the resistance is not occurring in bacteria against phenolic acids so far, they can be alternative agents in infection treatments. In the encapsulation processes, polymers like chitosan and alginate are widely used. Chitosan is a biodegradable, biocompatible, non-toxic material with antimicrobial activity which can be used for variable applications. It is produced from chitin via deacetylation of chitin under alkaline conditions or by chitin deacetylase enzyme (Jayakumar et al., 2010). It has ability to comprise with vitamins, minerals, oils, proteins and biologically active natural products to form functional substances (Tang et al., 2013; Azevedo et al., 2014; Budnyak et al., 2016; Deka et al., 2016; Wu et al., 2018; Moschona and Liakopoulou-Kyriakides, 2018). Because of its extensive usage, easy preparation, known antimicrobial property and biodegradable nature, chitosan can be a good choice for encapsulation of phenolic acids for using as a possible treatment of infections in the future. Alginate is another important material which is used in encapsulation processes. It is an anionic polymer that is obtained from algae which consists of glucorinic acid and mannuronic acid residues. It is a commonly used material for encapsulation of chemicals because of its easy-to-use, non-toxic, biodegradable and biocompatible nature (Paques et al., 2014) and ability to synthesize hydrogels in the presence of divalent cations (Yang et al., 2011).

The alginate-chitosan nanoparticles, which possess alginate as a pre-gel and chitosan as a covering material, can be obtained depending on the electrostatic interactions of carboxyl groups of alginate and amino groups of chitosan (Zimet et al., 2018). In the production of alginate-chitosan nanoparticles, ion-gelation technique is a widely-used technique in which calcium chloride is used as a cross linker to make the pre-gel of the alginate. The usage of calcium in this process result in the linkage of the

alginate monomers to each other making an egg-box-shaped structure in which the drug of interest can be captured (Wu et al., 2018; Zimet et al., 2018). Then, the coating of alginate which is an anionic polymer with chitosan which is cationic, results in alginate-chitosan nanoparticles. This type of coating presents a better coating because of the obtained polyelectrolyte complex with an increased stability (Paques et al., 2014). Since the phenolic acids that were used in this study are water soluble, alginate-chitosan nanoparticles were expected to provide a durable coat for better protection for these phenolic acids.

The important parameters of successful nanoparticle production are the homogeneity, physicochemical properties, size and shapes of the particles and the behavior. After the nanoparticle production, these properties can be characterized via some analyses (Bhattacharjee et al., 2016) such as dynamic light scattering (DLS), Fourier transform infrared spectrometry (FTIR) and scanning electron microscopy (SEM). Dynamic light scattering is a technique that measures the average hydrodynamic diameters of the particles (particle size) in a solution (Krausz et al., 2015; Bhattacharjee et al., 2016) and shows the uniformity of the tested sample. If the DLS result of a solution demonstrates a single peak, it can be concluded that the particles in that solution have a uniform nature (Mohammadi et al., 2016) while more than one peak of the same sample demonstrates the particles may not be homogeneous. In addition, the polydispersity index (PDI) values of the samples which are obtained from DLS data also give opinion about the homogeneity of the particles. The PDI value smaller than 1, displays that the particles in the solution show a narrow size distribution which leads to homogeneity in size (Liu et al., 2018; Qi et al., 2004). The FTIR measurements of the nanoparticle samples is useful to demonstrate that the produced nanoparticles display a unique spectrum as a unique compound. The spectra of the polymers and phenolic acids either individually and nanoparticle forms can be detected and compared for presenting the production of nanoparticles resulted in the eventual unique bonds (Mladenovska et al., 2007). Additionally, the exact shapes and diameters of the particles can be visualized under electron microscopy since DLS show only the average and hydrodynamic diameters.

The studies that focus on the antimicrobial agents loaded in chitosan nanoparticles or alginate-chitosan nanoparticles are increasing in the literature which present efficient results for the nanoparticles as antimicrobial agents. Liu et al. tested the

antimicrobial properties of ε-polylysine loaded alginate-chitosan nanoparticles on *E. coli*, *B. subtilis*, *S. aureus* and *M. luteus* (Liu et al., 2018) by agar diffusion and the results showed that ε-polylysine loaded alginate-chitosan nanoparticle showed high antimicrobial effects by producing distinct inhibition zones (Liu et al., 2018). In addition, the encapsulation of ε-polylysine displayed three-fold increase in antimicrobial activities than its free form on the same bacteria (Liu et al., 2018). In the study of Jamil et al., the chitosan nanoparticles loaded with kefzole, an antibiotic, and tested on multidrug resistant *Klebsiella pneumoniae* and *Pseudomonas aeruginosa* by agar diffusion (Jamil et al., 2016 (a)). It was demonstrated that the antibiotic alone did not produced zones of inhibition while encapsulated antibiotics showed antimicrobial effects in an increasing manner depending on the increasing concentrations of the antibiotics in the nanoparticles. This may demonstrate that the encapsulation of the drugs can enhance their antimicrobial properties (Jamil et al., 2016 (a)). In addition to agar diffusion studies, the bacterial growth studies also demonstrate the increased effects of the agents after encapsulation. Jamil et al. investigated the growth of MRSA and *E. coli* in the presence of cardamom essential oil and cardamom essential oil loaded chitosan nanoparticles individually (Jamil et al., 2016 (b)). The results demonstrated that cardamom essential oil caused no inhibition on the growth of both bacteria while both null nanoparticles and loaded nanoparticles resulted in growth control for the first 48 hours. After 48 hours, the complete inhibition was continued for only cardamom oil loaded chitosan nanoparticles until seven days. (Jamil et al., 2016 (b)). In another study, rosmarinic acid, protocatechuic acid and 2,5-dihydroxybenzoic acid were encapsulated into chitosan nanoparticles by using low and high molecular weights, individually and tested on the growth of various pathogens; *Bacillus cereus*, *Escherichia coli* O157, *Listeria innocua*, *Staphylococcus aureus*, *Salmonella typhimurium* and *Yersinia enterocolitica* (Madureira et al., 2015). These nanoparticles displayed high antimicrobial effects on the tested bacteria with higher than 70% inhibition of the growth with different inhibition percentages for each organism. Rosmarinic acid loaded nanoparticles presented the highest effect with more than 90% inhibition while protocatechuic acid loaded nanoparticles presented the lowest percent inhibition (Madureira et al., 2015). Thus, the phenolic compound loaded nanoparticles may show a strain-specific antimicrobial effect due to the type of loaded phenolic compound. Based on these knowledge, it was aimed to elucidate the effects of phenolic acids, 3-

HPAA and 4-HBA, on the growth of widely distributed, serious pathogenic bacteria, *P. aeruginosa*. Additionally, it was aimed to determine their effects on the whole proteome of the bacteria in order to show their antimicrobial effects at the molecular level. On the other hand, the investigations on the encapsulation of these phenolic acids in terms of production, characterization and antimicrobial effects on various pathogenic bacteria were also aimed. The main courses of the study are:

1. The determination of the growth behavior and morphological state of *P. aeruginosa* in the presence of water-soluble phenolic acids *in vitro*.
2. The determination of the changes in the total protein profile of *P. aeruginosa* in the presence of phenolic acids via LC-ESI-MS/MS and validation of the protein data at the transcriptomic level via real time quantitative PCR.
3. The production and demonstration of the potential usage route of alginate-chitosan nanoparticles loaded with water-soluble phenolic acids *in vitro*.

CHAPTER 2

EFFECTS OF THE PHENOLIC ACIDS ON GROWTH AND MORPHOLOGY OF *Pseudomonas aeruginosa*

2.1. Introduction

Pseudomonas aeruginosa, which can be isolated from various environments, is a health-threatening opportunistic pathogen. It causes various infections in humans worldwide. For instance, in nosocomial infections, *P. aeruginosa* is accepted as one of the most important pathogenic bacterium (Breidenstein et al., 2011). Although it is a rare resident of human microbiota, it may be found up to 50% of the microbial flora of the patients during the hospitalization period. It is difficult to cure the infections caused by these bacteria on the fact that they require an extensive antibiotic therapy. However, *P. aeruginosa* has resistance to many antimicrobials such as penicillins, cephalosporins, carbapenems, monobactams (Poole, 2011) and fluoroquinolones (Lister et al., 2009). Even if antibiotic resistance is not observed in some strains, they can gain resistance during the treatment (Potron et al., 2015). Besides their multidrug resistance (Strateva and Yordanov, 2009), the biofilm-formation property of these bacteria (Andonova and Urumova, 2013) make it difficult to combat. These properties make the infections of *P. aeruginosa* life-threatening with high mortality and morbidity rate (Aloush et al., 2006; Gill et al., 2018). Therefore, new antimicrobial agents are in search.

Phenolic compounds are naturally synthesized chemicals by almost all plants as secondary metabolites. (Hurtado-Fernandez et al., 2010). They have roles in plants for plant metabolisms in addition to protection against bacteria (Duthie et al., 2003). They have various beneficial properties for humans such as antimicrobial, anti-oxidant, anti-carcinogenic, cardio-protective and anti-inflammatory properties (Karaosmanoglu et al., 2010; Andjelkovic et al., 2006; Daglia, 2012; Gutiérrez-Larraínzar et al., 2012; Diaz-Gomez et al., 2013; Cueva et al.,2010). The common structure of simple phenolic compounds consist of a benzene ring with one or more hydroxyl groups and different functional groups (Hurtado-Fernandez et al., 2010). Hydroxybenzoic acids and

hydroxycinnamic acids are two main groups of phenolic acids. In hydroxycinnamic acids, carboxylic group is attached to benzene ring via an ethylene group. However, in hydroxybenzoic acids, carboxyl group is directly attached to the benzene ring (Andjelkovic et al., 2006). The phenolic acids that will be used in this study are 3-Hydroxyphenylacetic acid (3-HPAA) and 4-Hydroxybenzoic acid (4-HBA) which belong to hydroxycinnamic acids and hydroxybenzoic acids, respectively. They are simple phenolic acids with one phenol ring and they are water soluble.

The objectives of this study were to determine the minimum inhibitory concentrations (MIC) and minimum bacteriocidal concentrations (MBC) of 3-HPAA and 4-HBA on *P. aeruginosa* and to investigate morphological changes of the bacteria in the presence of subinhibitory concentrations of these phenolic acids.

2.2. Materials and Methods

The effects of phenolic acids on *P. aeruginosa* were investigated by spectrophotometric and enumeration methods prior to scanning electron microscopy.

2.2.1. Bacterial Strain and Culture Conditions

Pseudomonas aeruginosa (ATCC 27853) was grown in Mueller Hinton broth (MHB) and Mueller Hinton agar (MHA) media (Fluka) at 37^{o}C without shaking. Bacterial growth behavior was determined by plotting the growth curve of the bacteria during 24 hours (Appendix A). The bacteria were maintained on MHA at 4^{o}C which were refreshed every week or long term-stock cultures when necessary. The long term-stock cultures of the bacteria were kept at -80^{o}C in MHB containing 20% glycerol.

2.2.2. Antimicrobial Activities of Phenolic Acids

A single colony of *P. aeruginosa* was inoculated into 4 ml of MHB media and the bacteria were incubated at 37^{o}C for 18 hours (overnight). Spectrophotometric measurement was performed to determine the optical density (O.D.) of overnight bacterial culture at 600 nm. The phenolic acids (3-HPAA and 4-HBA) were obtained

commercially (Sigma-Aldrich). The solutions of 3-HPAA and 4-HBA were prepared freshly in the required concentrations in sterile double-distilled water (ddH_2O) and added to MHB at the time of each experiment. The final bacterial load of 10^6 cfu/ml from overnight culture was inoculated into phenolic acids containing MHB. Blanks of test group were the phenolic acid solution prepared in required concentration and MHB without addition of bacteria. Control group also had 10^6 cfu/ml final bacterial load from overnight culture into MHB without phenolic acid addition. Blank of control group was MHB. The O.D. of the treated and untreated cultures were measured at 600 nm at 0th and 24th time points of the growth. At the same time, the cell viabilities of the cultures grown for 24h were tested by enumeration method on MHA. The initial bacterial load was also confirmed by enumeration method in each experiment, throughout the study.

2.2.3. Determination of *P. aeruginosa* Morphology

The morphological properties of *P. aeruginosa* treated with/without phenolic acids were determined by scanning electron microscopy (SEM) and the colour changes of the bacterial cultures were clearly detected by naked eye. The bacterial cultures were prepared with the same protocol of antimicrobial studies (see Section 2.2.2). After 24 h of growth, the cells of each group was harvested by centrifugation at 14.000 x g for 2 minutes. The pellets were washed with 0.1% peptone twice and resuspended in 0.1% peptone. After placing 10 µl of these samples on aluminium (Al) foil, they were dried for 15 minutes at 37^{o}C. The prepared samples were placed on the carbon band containing, metal grids and covered with gold for 2 minutes. Then, these samples were examined under scanning electron microscope (Phillips XL-30S FEG) at İYTE-MAM.

To observe the color changes in the broth cultures, the samples were prepared as explaned in section 2.2.2. After 24 h of incubation, the cultures were photographed to demonstrate the colour differences between the control group and phenolic acid treated groups.

2.3. Results and Discussion

The investigated, water soluble phenolic acids (3-HPAA and 4-HBA) demonstrated strong antimicrobial activity against *P. aeruginosa*. The MIC and MBC

values were determined for both phenolic acids as well as their effects on the bacterial morphology and culture color.

2.3.1. Antimicrobial Effects of Phenolic Acids on *P. aeruginosa*

The antimicrobial effects of 3-HPAA and 4-HBA were determined on *P. aeruginosa* both spectrophotometric and viable cell count studies. The range of tested concentrations of 3-HPAA and 4-HBA were 1.7-2.3 mg/ml and 1.5-2.1 mg/ml, respectively. The growth curves of *P. aeruginosa* in the presence of 3-HPAA and 4-HBA with the indicated consantrations were presented in Figure 2.1a and b. The MIC values were determined as 2.1 mg/ml for 3-HPAA and 1.9 mg/ml for 4-HBA (Figure 2.1a and b). Since no survivors were detected in the presence of 2.3 mg/ml 3-HPAA and 2.1 mg/ml 4-HBA (Table 2.1), these concentrations were considered as MBC of the tested phenolic acids. The difference in concentration values for MIC and MBC arouse from the dose-dependent nature of antimicrobial effects of phenolic acids. Both phenolic acids demonstrated similar antimicrobial patterns. However, it could be concluded that 4-HBA has higher antimicrobial effect on *P. aeruginosa* than that of 3-HPAA, since the lower concentrations of 4-HBA showed the higher antimicrobial effect. For instance, 1.7 mg/ml 3-HPAA caused 31% inhibition while the same concentration of 4-HBA caused 71% inhibition (Table 2.1). This might be due to the structural differences between 3-HPAA and 4-HBA: Since, their carboxyl groups are attached to the benzene ring differently, they belong to different phenolic acid groups. While the carboxyl group of 3-HPAA (a member of hydroxycinnamic acid) is attached to benzene ring via an ethylene group, it is directly attached to the benzene ring in 4-HBA (a member of hydroxybenzoic acid) (Andjelkovic et al., 2006). Although they both contain one hydroxyl group attached, their positions on the benzene ring are different. These structural differences might be the reason for the slight variations of the antimicrobial effects of 3-HPAA and 4-HBA.

2.3.2. The Morphology of *P. aeruginosa*

The colour differences between bacterial cultures that were treated and untreated with 3-HPAA and 4-HBA were presented in Figure 2.2 a and b, respectively. The

culture of *P. aeruginosa* has a distinct greenish-blue colour as a result of the mixture of blue color from the bacteria and yellow color from the media (Rada and Leto, 2013). The pigment called pyocyanin produced by *P. aeruginosa* is the reason for the blue color (Rada and Leto, 2013). When the *P. aeruginosa* cultures were grown in the presence of 3-HPAA or 4-HBA, the blue color was not observed (Figure 2.2). The significatly distinct greenish blue color was observed in the control groups, after 24 hours of incubation without phenolic acids.

Our results were consistent with the study of Ugurlu et al. which presented that the the solutions of vanillic acid, caffeic acid, cinnamic acid and ferulic acid (phenolic acids) treatment reduced the pyocyanin production in *P. aeruginosa* (Ugurlu et al., 2016).

The morphological properties of untreated (Figure 2.3 a and b), 3-HPAA treated (Figure 2.3 c and d) and 4-HBA treated (Figure 2.3 e and f) *P. aeruginosa* were investigated by SEM analysis. It was clearly shown that the surface of the bacteria have a collapse line especially in 3-HPAA treatment. The collapse on the bacterial surfaces demonstrate that the phenolic acids might affect the envelope structure (characteristic structure of Gram negative bacteria made up of two membranes with a thin peptidoglycan layer in between) (Stinnett et al., 1973) of *P. aeruginosa*.

Table 2.1. Percent inhibitions and cell viabilities of phenolic acids for *P. aeruginosa*.

3-HPAA			**4-HBA**		
Phenolic Acid Concentrations (mg/ml)	**Percent Inhibitions**	**Cell Viability (cfu/ml)**	**Phenolic Acid Concentrations (mg/ml)**	**Percent Inhibitions**	**Cell Viability (cfu/ml)**
1.7	31	TMTC*	1.5	39	TMTC
1.9	58	TMTC	1.7	71	TMTC
2.1**	98	TMTC	1.9**	99	TMTC
2.3***	99	No survivors	2.1***	99	No survivors

*TMTC: Too many to count

** Minimum inhibitory concentration (MIC)

***Minimum bacteriocidal concentration (MBC)

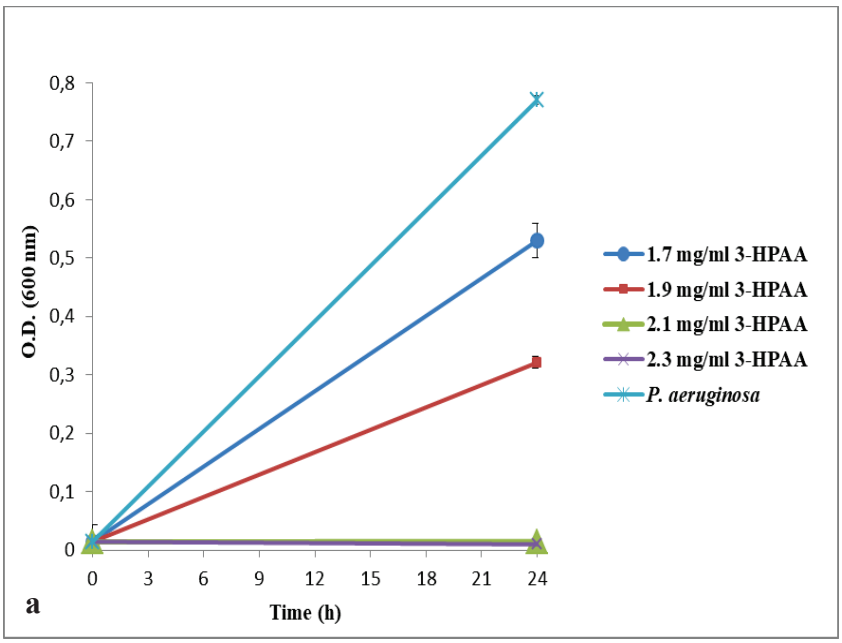

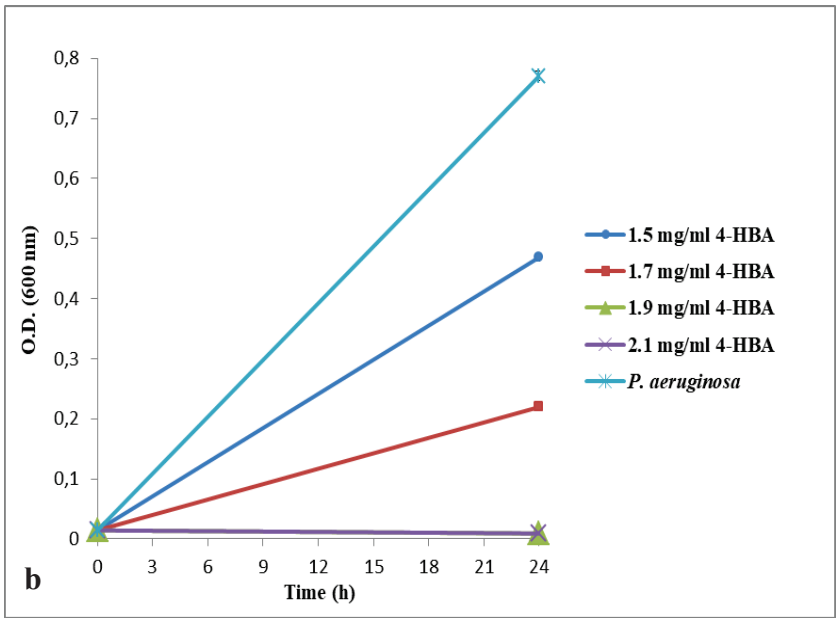

Figure 2.1. The growth of *P. aeruginosa* in the presence of phenolic acids. a) 3-HPAA b) 4-HBA

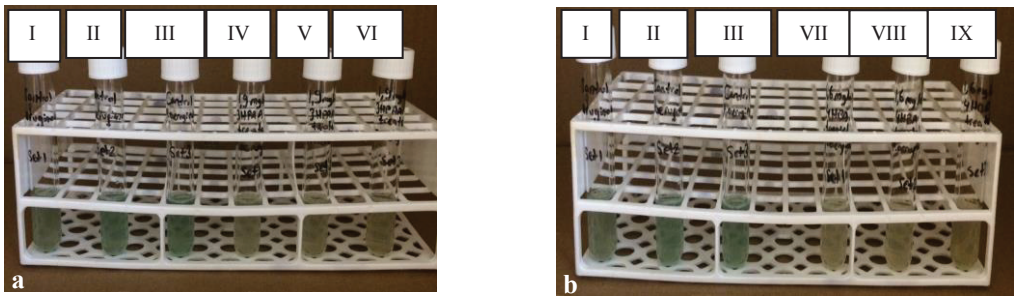

Figure 2.2. The comparison of colors of *P. aeruginosa* cultures after 24 hours of incubation. Control (a and b-I, II, III, 3 sets); 1.9 mg/ml 3-HPAA treated (a-IV, V, VI, 3 sets) 1.6 mg/ml 4-HBA treated (b-VII, VIII, IX, 3 sets) cultures.

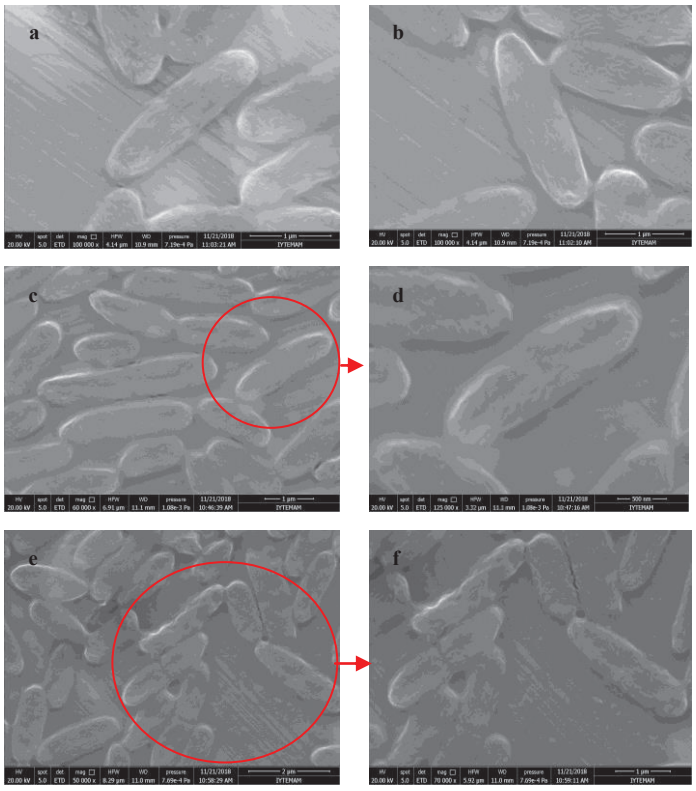

Figure 2.3. The morphology of *P. aeruginosa*. Control cells at 100,000x magnification (a,b); 3-HPAA treated cells at 60,000x magnification (c) and at 125,000x magnification (d); 4-HBA treated cells at 50,000x magnification (e) and at 70,000x magnification (f) at the 24th h of growth.

CHAPTER 3

MOLECULAR INVESTIGATION OF ANTIMICROBIAL EFFECTS OF THE PHENOLIC ACIDS ON *P. aeruginosa*

3.1. Introduction

Pseudomonas aeruginosa which is one of the most important pathogenic bacterium worldwide (Faure et al., 2013) has resistance to many antimicrobials such as penicillins, cephalosporins, carbapenems, monobactams (Poole, 2011) and fluoroquinolones (Lister et al., 2009). The infections of *P. aeruginosa* have a high mortality and morbidity rate (Gill et al., 2018). It is challenging to treat the infections caused by these bacteria since an extensive antibiotic therapy is required. (Zhou et al., 2015). Therefore, new antimicrobials other than antibiotics are in search (Mathieu et al., 2016). Phenolic compounds, which are naturally synthesized by almost all plants as secondary metabolites (Hurtado-Fernandez et al., 2010), are accepted as promising antimicrobial agents. Among their many beneficial properties (as antimicrobial, anti-oxidant, anti-carcinogenic, cardio-protective and anti-inflammatory) the antimicrobial effects of phenolic acids were presented in many studies (Karaosmanoglu et al., 2010; Andjelkovic et al., 2006; Daglia, 2012). However, these studies mostly focus on the antimicrobial effects of the phenolic acids without investigating the molecular mechanisms which is required for the development of new antimicrobial treatments.

The shot-gun proteomics is a reliable technique for presenting the molecular mechanisms (Wang et al., 2014) which includes a useful two step technique called LC-ESI-MS/MS. The usage of combination of two techniques allows the identification of more peptides than usage of one technique in peptide separation (Stapels et al., 2004). Since in the LC-ESI-MS/MS technique the peptide mixture is analyzed consecutively by liquid chromatography (LC) and electrospray ionization (ESI) coupled with mass spectrometry, it result in the identification of a large quantity of peptides. This technique includes these general steps: proteolytic digest, LC-ESI, MS/MS and data analysis (Walther and Mann, 2010). Briefly, in MS based shot-gun proteomics

technique, the protein samples undergo a proteolytic digest to obtain peptide samples which will be analyzed. The proteolytic digestion of the proteins can be performed either by in-gel digestion or in-solution digestion (Choksawangkarn et al., 2012). Following the proteolytic digestion the fractionation of the protein samples can be performed since the fractionation of the protein samples before LC-MS/MS analysis increases both the analytical dynamic range and proteome coverage (Yang et al., 2012). The first separation of peptides prior to tandem mass spectrometric analysis is carried out by liquid chromatography (The first HPLC step) either by strong cation exchange (SCX) chromatography which is charge based or (low or high) pH reversed-phase (RP) which depends on the hydrophobic interactions (Wang et al., 2011; Batth et al., 2014). However, the usage of high pH RP as the first separation rather than SCX or low pH RP results in more clean samples which eliminate the desalting step and an increase in the number of proteins identified (Yang et al., 2012). Therefore, usage of high pH RP gives better results since it decreases the samples loss and the process time while increasing the protein identification (Yang et al., 2012) and resolution (Batth et al, 2014). In the second HPLC step, coupled with electrospray ionization (ESI), low pH columns are used for the samples which become charged and transformed to gas form right before the HPLC by electrospraying (ESI). The gas phase allows the mass to charge ratio of the molecules can be determined in a static or dynamic electric field (Walther and Mann, 2010). Then the obtained data are processed by MASCOT (one of the widely used search engines) for protein identification which is followed by protein function search in online databases (i.e. UniProt, KEGG, SwissProt) (Walther and Mann, 2010).

The studies that focus on the investigation of protein profile of microorganisms by mass spectrometry exist in the literature either on the comparison of proteome of different strains (Carrera et al., 2017) or the comparison of toxic compound treated and untreated groups of the same strain (Kılıç et al., 2010).

In this study, the determination of protein profile of *P. aeruginosa* treated with or without phenolic acids were performed by LC-ESI-MS/MS. The phenolic acids which were used in this study were belong to two different groups of phenolic acids: hydroxycinnamic acids (3-HPAA) and hydroxybenzoic acids (4-HBA). The aim of this study was to present the changes in the protein profile of *P. aeruginosa* in the presence of 3-HPAA or 4-HBA which showed a dose-dependent antimicrobial activity on the bacteria (Chapter 2). We hypothesized that, if growth pattern of the bacteria changes in

the presence of phenolic acids, then; some changes in the proteome of the bacteria would be expected after the treatment with subinhibitory concentrations. The investigation of the proteomic changes of the bacteria after phenolic acid application would be the first step in the determination of the molecular action mechanism of phenolic acids by which the molecular targets of antimicrobial effects would be presented.

3.2. Materials and Methods

The changes in total protein profile of *P. aeruginosa* were investigated after treatments with subinhibitory concentrations of 3-HPAA (1.9 mg/ml) or 4-HBA (1.6 mg/ml) via LC-ESI-MS/MS analysis and MASCOT software by using reference database of *P. aeruginosa* in UniProt. The proteins that were undetected or newly detected after the treatment were grouped by Venn diagram analysis. The functions of the proteins were determined by UniProt and were grouped based on the biological processes according to which they were involved. The STRING database was used for the visualization of the interaction network of these group of proteins to suggest the effects of phenolic acids on *P. aeruginosa* at the proteomic level.

3.2.1. Bacterial Growth Conditions and Phenolic Acid Treatment

During the experiments; *Pseudomonas aeruginosa* (ATCC 27853) were maintained on MHA agar plates by inoculation of a single colony on fresh agar plate and overnight incubation at 37^{o}C, every week. The bacteria were kept in glycerol at -80^{o}C as stock culture.

To obtain the overnight cultures, the single colonies of *P. aeruginosa* were inoculated in 4 ml of MHB broth media individually and were incubated at 37^{o}C for 18 hours without shaking. The final bacterial load of 10^{6} cfu/ml from overnight culture was inoculated into 400 ml total volume of MHB containing 1.9 mg/ml 3-HPAA or 1.6 mg/ml 4-HBA. The same bacterial load from overnight culture was inoculated into 400 ml total volume of MHB without phenolic acid addition, for control group. All of these were incubated at 37^{o}C for 18 hours without shaking. The obtained cultures were used for total protein isolation.

3.2.2. Total Protein Isolation

Total proteins were isolated from control group and phenolic acid treated groups with the following protocol: The cells were harvested at 10,000 x g for 20 minutes at 4^{o}C. They were washed twice with 20 ml of 0.85% NaCl and centrifuged at 20,000 x g for 20 minutes at 4^{o}C. The pellet was dissolved in PBS (pH 7.4) buffer. Sonication was performed for 9 seconds with 9 seconds of intervals during 15 minutes for control group and 10 minutes for phenolic acid treated groups. The centrifugation was carried out at 20,000 x g for 20 minutes at 4^{o}C and the supernatant was transferred into lo-bind Eppendorf tubes. The samples were kept at -80^{o}C until further usage.

3.2.3. Preparation of Peptide Samples

The ice-cold acetone in 4 times volume of the samples was added on the protein samples and vortexed prior to keeping at -20^{o}C for overnight for acetone precipitation. Then, the protein concentrations were determined by Bradford assay. Since the proteins will be dissolved in resuspension buffer in the next step, bovine serum albumin (BSA) standard was prepared with resuspension buffer (7 M urea and 2 M thiourea in pH 7.8 0.1 M Tris-HCl) and graph was plotted based on the spectrophotometric values of solutions vs concentrations (Appendix C). Then the equation on the graph was used in protein amount determination (R^2>98). After Bradford assay, the concentrations of protein samples were adjusted to 0.4 mg for the LC-ESI-MS/MS analysis. Prior to trypsin addition, in solution digestion was applied to the protein samples as a three-step procedure: DTT (1st step), iodoacetamide (2nd step) and DTT (3rd step). The final concentrations of the reagents were used as 10 mM DTT, 20 mM iodoacetamide and 20 mM DTT in 50 mM Tris-HCl (pH 7.8). In each step, the samples were kept in dark at room temperature for 50 minutes. To clean up the samples, they were transferred into the pre-wetted (with ddH_2O) 10K cut-off filters centrifuge at 14,000 rpm for 30 minutes. After washing the samples with 50 mM Tris-HCl (pH 7.8), trypsin (in 50 mM Tris-HCl (pH 7.8)) was added in the final concentration of 0.04 µg/ml for each protein sample. The trypsin digestion was carried on overnight at 37^{o}C. The peptide samples were transferred into lo-bind Eppendorf tubes and the volumes of the samples were decreased below 100 µl with speed-vac centrifuge. They were kept at -20^{o}C.

3.2.4. LC-ESI-MS/MS (Liquid Chromatography-Electrospray Ionization-Tandem Mass Spectrometry)

High pH reversed-phase chromatography with fraction concatenation was applied to peptide samples as the first step. The volumes of the samples were adjusted to 100 µl by addition of phase A. The phases in fractionation are: Ammonium formate (10 mM) in ddH2O (phase A, pH 10) and acetonitrile (90%) and ammonium formate (10 mM) in ddH2O (phase B, pH 10). Fractionation of peptide samples were performed with HPLC with high-pH column by LC-solution programme and MALDI-Spotter. The samples were collected in 96-well plates by MALDI-Spotter with 0.05 ml/min flow rate and the fractions were transferred into Eppendorf tubes randomly.

The samples were completely dried by speed-vac centrifuge and zip-tip was applied to the samples before second step (low-pH HPLC) of the analysis. Zip-tip was performed according to the following protocol: 20 µl of Acetonitrile (ACN) (20%) and formic acid (FA) (0.1%) mixture in ddH2O was added on each fraction and mixed in ultrasonic bath (15 seconds) and vortexing (5 seconds) alternately for 3 times. The samples were centrifuged at 14,000 rpm for 10 minutes. Zip-tip column (C18) was conditioned by 10 µl of 100% ACN 5 times and 10 µl of 1% FA 5 times. Then the sample was zip-tipped for 10-15 cycles. The column was washed by 10 µl of 1% FA 5 times. The collection of the peptides in column was performed by 50% ACN twice and then by 75% ACN for one time. The collected samples was mixed with 25 µl of 0.1% FA and transferred into the insert tube. It was centrifuged immediately for 5-10 seconds and placed in a vial prior to place in well of HPLC instrument (15 cm low-pH column). The phases of HPLC were: 0.1 % FA in ddH2O (phase A) and 0.1 % FA in ACN (phase B). Chromeleon programme was used for HPLC step and after the ion trap electrospraying of these samples by use of Helium gas, the peaks of the samples were collected by LTQ Tune programme. The collected raw data were transferred into MGF format by Proteome Discoverer programme and the data of the fractions were merged by Mass Matrix MS Data File Conversion programme. The reference protein database of *P. aeruginosa* was downloaded from UniProt and saved in MASCOT MS/MS ions programme. MASCOT search of merged data was performed within Uniprot *P. aeruginosa* database. Conditions in MASCOT search were: In fixed modifications, Carbamidomethyl (C); in variable modifications, Oxidation (M); Peptide tolerance, +1.2

Da; MS/MS tolerance, +0.6 Da; peptide charge +2 and +3; instrument, ESI-TRAP; decoy checked. Two biological repeats were analyzed and the data of two independent experiments were combined. All the obtained protein data were compared in Draw Venn Diagram programme (http://bioinformatics.psb.ugent.be/webtools/Venn/) to determine the mutual and different proteins between control and phenolic acid treated groups. The functions of the proteins that were undetected or newly detected in the presence of phenolic acids were investigated in UniProt database by using UniProt Retrieve/ID Mapping with protein IDs. As a final step, these proteins were grouped in their functions based on the information in UniProt and the interaction network of the proteins of the groups were determined by STRING software version 10.5 (https://version-10-5.string-db.org/cgi/input.pl?sessionId =6mlAzREKIVnK&input _page_show_search=on).

3.2.5. Validation of Protein Data

The Real Time-Quantitative PCR (RT-qPCR) was performed for the validation of the protein data on the transcription level. The total RNA isolation of the bacterial cultures, which were subjected to the same conditions of protein isolation protocol, was performed and the total RNA converted to cDNA for RT-qPCR. The primers specific to the housekeeping gene and gene of interest were designed by Primer BLAST software.

3.2.5.1. Isolation of Total RNA and cDNA Preparation

The isolation of the total RNA from control and 1.9 mg/ml 3-HPAA or 1.4 mg/ml 4-HBA treated *P. aeruginosa* was carried out by GeneJET RNA purification kit (#K0732 Thermo Scientific) according to the manufacturer's instructions with the modifications in the numbers of the washing steps (two times with buffer 1 and three times for buffer 2). The isolated total RNA concentrations, and the 260/280 - 260/230 ratios of the samples were measured by nanodrop and they were kept at -80^{o}C until cDNA preparation.

The cDNA preparation was performed according to the manufacturer's instructions of the kit (# K1622 Thermo RevertAid First Strand cDNA Synthesis Kit). The PCR was carried out in the following conditions: 5 minutes at 25^{o}C; 60 minutes at

42°C and 5 minutes at 70°C. The produced cDNA samples were diluted for 8 times with nuclease free water immediately. They were aliquoted and kept at -20°C until usage.

3.2.5.2. Real Time-Quantitative PCR (RT-qPCR)

The primers which were used in RT-qPCR were designed for 30S ribosomal protein S15 and S12 encoded by rpsO and rpsL genes, respectively by using the Uniprot. Primer BLAST programme was used for designing the most suitable primers in Refseq database among Pseudomonadales with maximum target size of 200.

The PCR mixture was prepared based on the recommended protocol of SYBR green kit (LightCycler 480 SYBR Green I Master Mix, Roche) with half of the recommended volume. SYBR green master mix (5 µl) was mixed with primers (0.5 µl for each F and R primers from 10x primer solution) and nuclease free water up to 7.5 µl total volume. The mixture was transferred into the 96-well plate and 2.5 µl of appropriate cDNA (about 250 ng for each sample) was added on each wells. The 96-well plate of RT-qPCR was covered by sealing and centrifuged for 2 minutes at 1500 x g. RT-qPCR was performed in the Roche instrument based on the instructions in Roche catalog. The melting temperature was 50°C and the annealing cycles were 40 during the PCR process.

3.3. Results and Discussion

The bacteria require to adapt immediately to the environmental conditions for survival and regulate their cellular proteome under stress conditions (Langklotz et al., 2012). The treatment of *P. aeruginosa* with each phenolic acid result in various changes in the protein profile of the bacteria, as expected. However, besides the changes which might be attributed to the regulation of proteome for adaptation, various changes in the protein profile of vital mechanisms were also detected after phenolic acid treatment. All of these changes were discussed based on the functions of the undetected or newly detected proteins to be able to enlighten the targets of the phenolic acids for antimicrobial effects as well as regulation under stress conditions. Since the phenolic acids showed high antimicrobial effects on *P. aeruginosa*, these results were consistent with our hypothesis that “if growth pattern of the bacteria changes in the presence of

phenolic acids, then; some changes in the proteome of the bacteria would be expected after the treatment with subinhibitory concentrations of them".

The grouping of protein profiles of *P. aeruginosa* in the presence of 3-HPAA, 4-HBA or the untreated bacteria were presented in Figure 3.1 as a Venn diagram. There are 284 mutual proteins which remain the same in all groups (Figure 3.1, region VII). The names, protein IDs and gene names of these proteins could be found in Appendix D. Throughout the text, the proteins which were only detected in control group will be referred as "undetected proteins" whereas the proteins which were only detected in the phenolic acid treated groups as "newly detected proteins". The 108 proteins were not detected mutually (Figure 3.1, region V) and 55 mutual proteins were newly detected in the protein profile of *P. aeruginosa* in the presence of the phenolic acids (Figure 3.1, region II). The regions of the Venn diagram for each phenolic acid treatment represents the protein profiles in the following: Proteins that were mutual in control and 3-HPAA treated groups (regions VI and VII); undetected proteins in the presence of 3-HPAA (regions IV and V); newly detected proteins in the presence of 3-HPAA (regions I and II); mutual in control and 4-HBA treated groups (regions IV and VII); undetected proteins in the presence of 4-HBA (regions V and VI); newly detected proteins in the presence of 4-HBA (regions II and III).

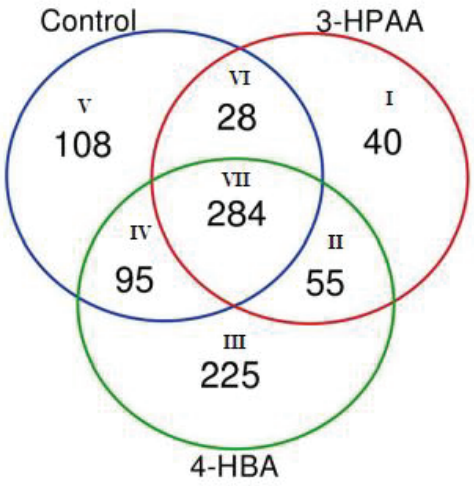

Figure 3.1. The Venn diagram representation of protein profile of *P. aeruginosa* in the presence of 3-HPAA or 4-HBA. The referring of the romen numbers were presented in the text.

3.3.1. The Protein Profile in the Presence of 3-HPAA

The results demonstrated that 312 proteins were mutual in control and 3-HPAA treated groups (Figure 3.1; regions VI and VII). On the other hand, 203 proteins were undetected (Figure 3.1; regions IV and V) and 95 proteins were newly detected (Figure 3.1; regions I and II) when the bacteria were treated with 3-HPAA. The proteins which were undetected or newly detected were divided into eight main groups according to their functions in UniProt database and the percentages of these groups were calculated (Figure 3.2). According to their functions, the protein groups were related with DNA; RNA; ribosomes and protein; cell wall and membrane; metabolism; redox and cell homeostasis; virulence and uncharacterized functioned proteins.

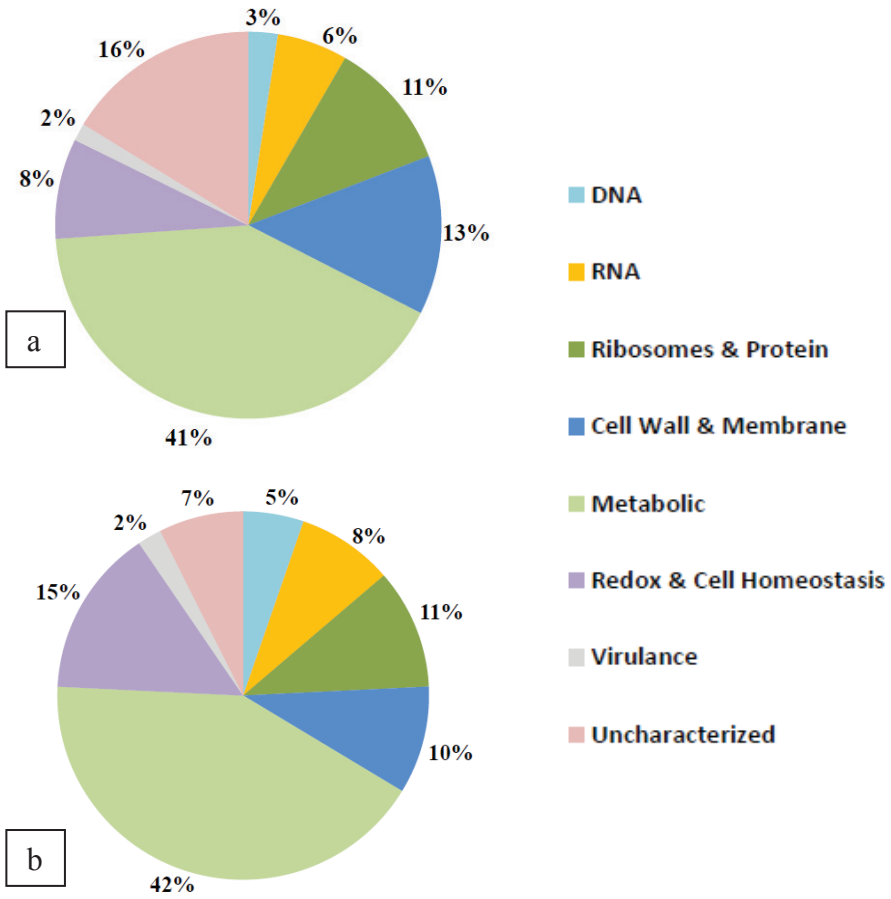

Figure 3.2. The percentages of proteins for each group of function in the presence of 3-HPAA. a) Undetected proteins b) Newly detected proteins

The percentages demonstrated that undetected proteins displayed 3%, 6%, 11%, 13%, 41%, 8%, 2% and 16% for DNA related, RNA related, ribosomes and protein related, cell wall and membrane related, metabolism related, redox and cell homeostasis related, virulence related and uncharacterized proteins, respectively (Figure 3.2 a). The newly detected proteins showed a similar percentage pattern for the groups of DNA related, RNA related, ribosomes and protein related, cell wall and membrane related, metabolism related, redox and cell homeostasis related, virulence related and uncharacterized proteins with 5%, 8%, 11%, 10%, 42%, 15%, 2% and 7%, respectively (Figure 3.2 b). These results indicated that metabolism related proteins comprised the highest percentages of protein profiles of 3-HPAA treatment. Since various proteins were in function in the general metabolism pathways, these highest percentages were expected. The lowest percentages were determined for the undetected and newly detected virulence-related proteins, which showed that 3-HPAA had a relatively small effect on virulence compared to the other groups of the functions.

3.3.1.1. DNA-Related Proteins of 3-HPAA Treatment

The interaction network of DNA related proteins were determined by STRING database via gene names for undetected proteins, newly detected proteins or both groups in Figures 3.3 a, 3.3 b and 3.3 c, respectively. The profile of DNA related proteins, which were undetected or newly detected, presented the changes in proteins functioned in DNA replication, recombination and DNA repair mechanisms (Tables 3.1 and 3.2).

According to these results, undetected proteins were functioned in DNA replication (DNA topoisomerase 4 subunit B and Vitamin B12-dependent ribonucleotide reductase) and DNA repair (UvrABC system protein A and DNA mismatch repair protein) (Table 3.1). On the other hand, one of the newly detected proteins were functioned in DNA repair (Exodeoxyribonuclease III) which might show the bacteria attempt to repair their DNA by Exodeoxyribonuclease III protein in default of the undetected ones.

When the STRING was applied to undetected and newly detected proteins together, it was demonstrated that the bacteria managed to survive by production of newly detected proteins which interact with undetected proteins, thus, maintaining the vital functions for DNA metabolism (Figure 3.3 c). The proper DNA replication and

repair mechanisms are required for cell survival. If some problems arise in these mechanisms, DNA recombination mechanisms are usually activated in bacteria for maintenance or DNA repair (Sidorenko et al., 2015). The treatment with 3-HPAA caused DNA replication and topological change related proteins as well as nucleotide excision repair and mismatch repair related proteins to be undetected. It might display that 3-HPAA result in DNA damage since these mechanisms had high importance for cell survival.

Three main DNA repair mechanisms exist in organisms which are base excision repair (BER), nucleotide excision repair (NER) and mismatch repair (MMR) (Tark et al., 2008). It could be seen that, the treatment with 3-HPAA might result in the destroy two of these mechanisms; NER and MMR (Table 3.1).

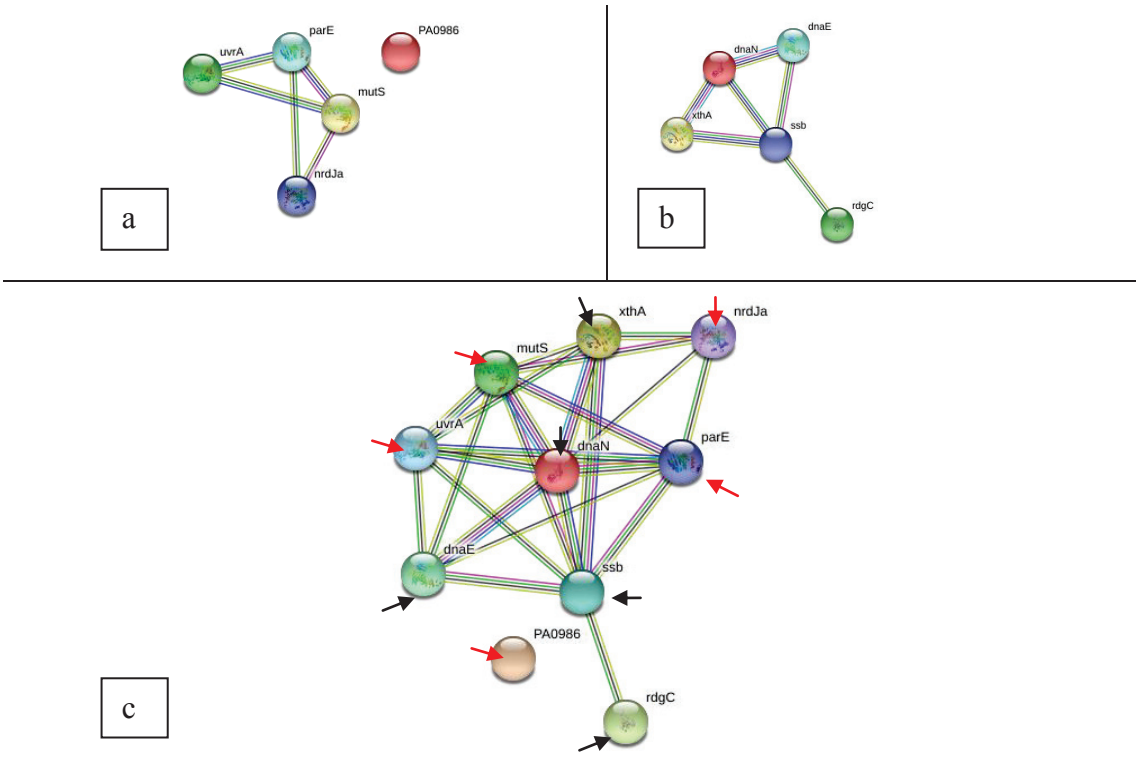

Figure 3.3. String representation of DNA-related proteins in the presence of 3-HPAA. a) Undetected proteins b) Newly detected proteins c) The both undetected and newly detected proteins. The proteins were indicated in arrows with different colors (Undetected proteins: red arrows and newly detected proteins: black arrows).

The UvrABC system protein A, which takes role in the initial steps of NER, was undetected after 3-HPAA treatment. The recognition of damaged region of DNA by UvrABC DNA repair mechanism requires the complex of proteins coded by uvrA, uvrB and uvrC. This complex is called UvrABC exonuclease and the initial assembly of it takes place by the binding of UvrA to UvrB. This initial complex searches for the lesion throughout the DNA for finding the damaged region to start the repair with NER (Tark et al., 2008). Since the UvrA protein was not detected in the presence of 3-HPAA, it might be speculated that NER mechanism of *P. aeruginosa* was negatively affected. Since the damage in the NER could be resulted in the accumulation of the mutations, 3-HPAA treatment might have caused the deterioration in the genome of *P. aeruginosa*, thus, inhibition of bacterial growth.

Table 3.1. The undetected proteins related to DNA in the presence of 3-HPAA.

Protein ID	Protein Name	Gene Name	Function
Q9HUJ8	DNA topoisomerase 4 subunit B	parE PA4967	DNA topological change
Q9HT76	Vitamin B12-dependent ribonucleotide reductase	nrdJa PA5497	DNA biosynthetic process, DNA replication
Q9HWG0	UvrABC system protein A	uvrA PA4234	Nucleotide excision repair, SOS response
Q9HY08	DNA mismatch repair protein MutS	mutS PA3620	Mismatch repair
Q9I4Y3	Uncharacterized protein	PA0986	Transposase activity, transposition

Table 3.2. The newly detected proteins related to DNA in the presence of 3-HPAA.

Protein ID	Protein Name	Gene Name	Function
Q9I0T9	Exodeoxyribonuclease III	xthA PA2545	Endonuclease activity, DNA repair
Q9HXZ1	DNA polymerase III subunit alpha	dnaE PA3640	DNA replication
Q9HYX7	Recombination-associated protein RdgC	rdgC PA3263	DNA recombination
Q9I7C4	Beta sliding clamp	dnaN PA0002	DNA strand elongation involved in DNA replication, 3'-5' exonuclease activity, DNA-directed DNA polymerase activity
P40947	Single-stranded DNA-binding protein	ssb PA4232	DNA recombination, DNA repair, DNA replication

Another important protein, MutS, which is a crucial protein functioned in the first steps of MMR mechanism (Monti et al., 2012) was also not detected after 3-HPAA treatment. MMR mechanism is one of the most important repair mechanism aids to maintain the genome integrity in DNA replication (Oliver et al., 2002). Initial recognition of the mismatch lesions in DNA is done by MutS protein after which the other components of the repair mechanism are recruited (Monti et al., 2012). The undetection of this protein in the presence of 3-HPAA might show that 3-HPAA damaged the mismatch repair mechanism of the bacteria. The incapacity of bacteria to repair mismatches may lead an increased mutation rate (Oliver et al., 2002) which might have been in the case of 3-HPAA treatment.

The newly detected proteins in the presence of 3-HPAA were mostly about DNA replication with which these proteins the bacteria attend to continue the proper DNA replication. Exodeoxyribonuclease III, DNA polymerase III subunit alpha, Single-stranded DNA-binding protein and Beta sliding clump not only function in replication, but also have DNA repairing properties. This might demonstrate that the DNA of *P. aeruginosa* was damaged with 3-HPAA application and the bacteria perform DNA repair as well as the replication. The replication machinery of bacteria requires DNA polymerase III holoenzyme for proper replication and proofreading. The holoenzyme has the catalytic DNA polymerase III (Pol III) alpha subunit in its structure and the binding of Pol III with beta sliding clump results in the process of proper replication (Rego et al., 2013). Since these proteins were newly detected, it could be speculated that the bacteria carried out the DNA replication simultaneously with the DNA repair after treated with 3-HPAA.

In addition, "Recombination-associated protein RdgC" was also newly detected. It might demonstrate that *P. aeruginosa* started to use recombination mechanism to protect its genome integrity. Additionally this might show that the bacteria managed to fix DNA damages since recombination also has role in DNA repair by working together with other repair systems (Sidorenko et al., 2014). Although the phenolic compounds are toxic to bacteria in a dose-dependent manner, some bacteria including *Pseudomonas* can consume them below the toxic concentrations (Ghaima et al., 2017). The bacteria may acquire the genes for the degradation of phenolic compounds by horizontal gene transfer via recombination (Tavita et al., 2012). Since the treatment of *P. aeruginosa* resulted in the new detection of "Recombination-associated protein RdgC", it might

attempt to handle with the damages on its DNA arouse from toxicity of 3-HPAA by recombination.

Therefore, the results indicated that the 3-HPAA treatment might lead serious damages in DNA replication and repair mechanisms which were managed to be fixed by new proteins of replication, repair and recombination mechanisms.

3.3.1.2. RNA-Related Proteins of 3-HPAA Treatment

The application of 3-HPAA resulted in changes in protein profile of *P. aeruginosa* by detection (Figure 3.4. a) and newly detection (Figure 3.4. b) of some RNA-related proteins. The undetected RNA related proteins were generally about the regulation of transcription, RNA polymerase core enzyme binding and tRNA processing (Table 3.3). The newly detected proteins were also functioned in transcriptional regulation in addition to transcription initiation and RNA polymerase transcription activation (Table 3.4). In addition, the interaction network of both groups were demonstrated in Figure 3.4. c which showed that the undetected and newly detected proteins had interactions.

The RNA polymerase sigma-54 factor (RpoN) was undetected while RNA polymerase sigma factor RpoD was newly detected. Although they are both important sigma factors functioned in the control of gene expression, their roles are different. The newly detection of RpoD (σ^{70}) might show that the bacteria manage to increase the transcription since σ^{70} is the major sigma factor for controlling the expression of many housekeeping genes (Potvin et al., 2008).

The RpoN (σ^{54}) was shown to have vital roles in motility, nutrient transport, quorum sensing, virulence, production of pilus and flagellum, adhesion and nitrogen assimilation (Potvin et al., 2008). In addition, σ^{54}-dependent promoters exist in *P. aeruginosa* (Buck et al., 2000) so that, the expression from these promoters cannot be made in the absence of σ^{54} (Potvin et al., 2008). Since σ^{54} was not detected when the bacteria was treated with 3-HPAA, the proteins which were expressed dependent to σ^{54} might be not expressed. Surprisingly, the major regulators of the catabolic systems of Pseudomonads for phenolic compounds, DmpR and XylR, are highly homologous to σ^{54}-dependent regulators with many similar structural and mechanistic properties, which activate the degradation of phenolic compounds (Sze et al., 2002). The undetection of

σ^{54} might lead to the elevated toxicity of 3-HPAA depending on the reduced function of phenolic catabolism pathways of *P. aeruginosa*. In addition, the reduction in nitrogen assimilation by undetection of σ^{54} as well as the undetection of DNA-binding transcriptional regulator NtrC functioned in nitrogen utilization (Table 3.3) also might cause nitrogen starvation and eventually bacterial growth inhibition.

The phenolic compounds are known to be metal chelators (Singh and Kumar, 2019; Andjelkovic et al., 2006). The treatment with 3-HPAA could result in the chelation of iron in the environment and the bacteria might be under stress because of iron starvation. Ferric uptake regulation protein (Fur) which was undetected in the presence of 3-HPAA (Table 3.3) was functioned in iron limitation and oxidative stress adaptations of bacteria (Pinochet-Barros and Helmann, 2018). The undetection of Fur protein indicated that 3-HPAA presented a change in iron homeostasis of *P. aeruginosa* accompanying with the oxidative stress. Fur proteins are accepted as promising targets of antimicrobial action since they are not found in eukaryotic cells and mandatory for bacterial cell survival and host infection. In addition, the studies which investigated the inactivation of fur genes of pathogenic bacteria including *P. aeruginosa,* resulted in reduced virulence in animal infection models (Mathieu et al., 2016). Since 3-HPAA caused Fur proteins to be undetected, the antimicrobial effect of it might be due to failure of bacteria to adapt iron starvation and oxidative stress.

The tRNA 2-selenouridine/geranyl-2-thiouridine synthase (SelU) which is the enzyme functioned in hydrophobic tRNA modification for geranylated tRNA formation (Wang et al., 2016), was undetected after 3-HPAA treatment. This hydrophobic modification of tRNA is a natural RNA modification and it was discovered in a few bacteria including *P. aeruginosa* (Wang et al., 2016). The geranylation occurs at the wobble position (U34) in the anticodon of lysine, glutamine and glutamic acid (Dumelin et al., 2012) and provides elevated codon recognition fidelity as well as reduced frameshift reading (Sierant et al., 2016). Furthermore, Ribonuclease T, which takes role in tRNA 3'-end processing, was also undetected. The processing of tRNA 3'-end is very important for tRNA biogenesis since it is used as editing and repairing of tRNAs (Rammelt and Rossmanith, 2016). These results indicated that 3-HPAA caused defects in tRNA biogenesis of the bacteria which might lead serious problems of RNA processes. The stringent starvation protein A, which is an important protein in stringent stress response, was undetected after 3-HPAA treatment. As a matter of fact, the

adaptation of bacteria to various conditions can be achieved by sigma factors since they are the key factors of RNA polymerase holoenzyme (Swiecilo and Zych-Wezyk., 2013). The stringent response proteins help functioning of the alternative sigma factors under stress conditions (Swiecilo and Zych-Wezyk., 2013). The undetection of stringent starvation protein A, might restrain the adaptation of bacteria to the environment containing 3-HPAA which aid the inhibition of bacterial growth.

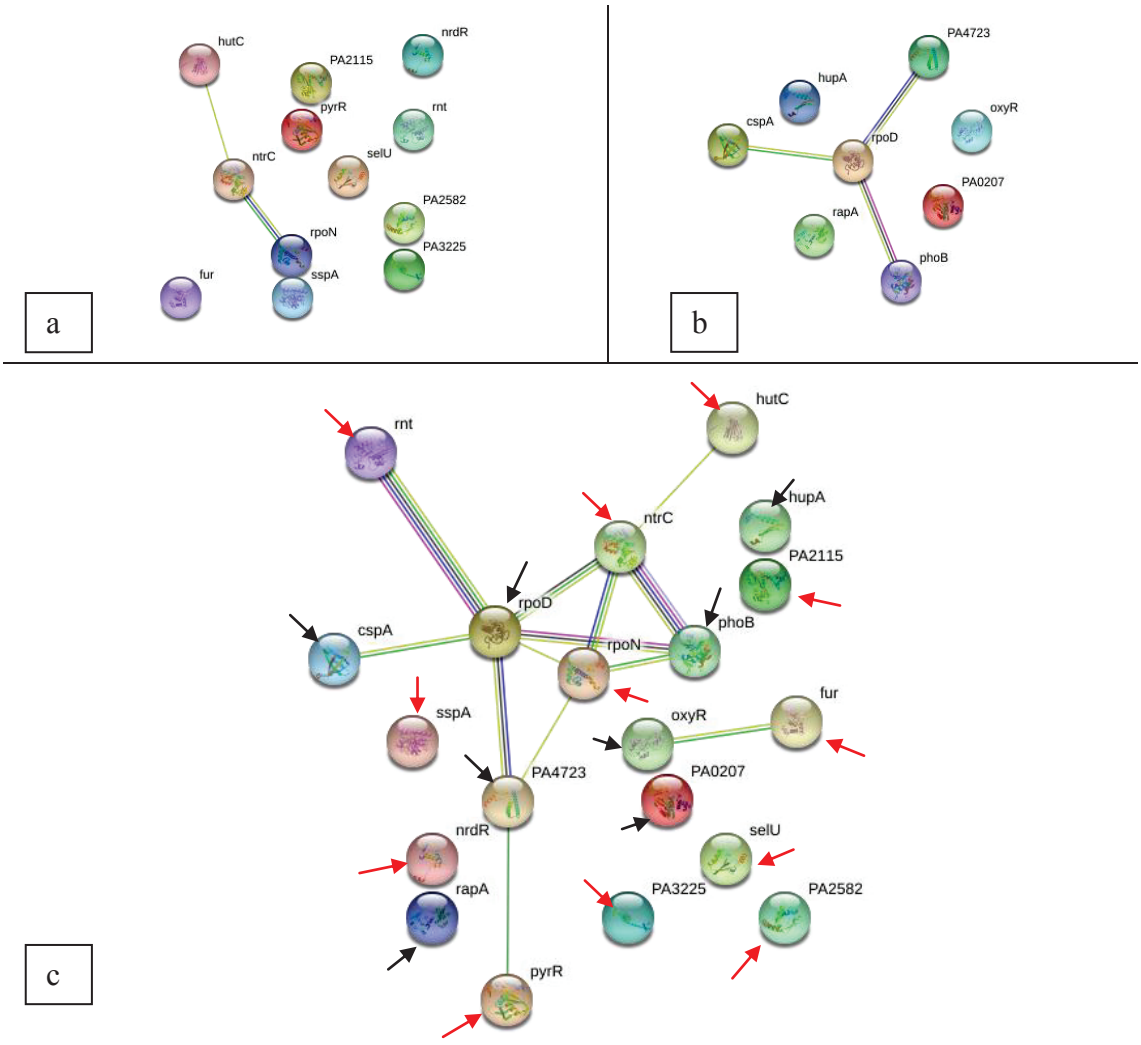

Figure 3.4. String representation of RNA-related proteins in the presence of 3-HPAA. a) Undetected proteins b) Newly detected proteins c) The both undetected and newly detected proteins. The proteins were indicated in arrows with different colors (Undetected proteins: red arrows and newly detected proteins: black arrows).

Table 3.3. The undetected proteins related to RNA in the presence of 3-HPAA.

Protein ID	Protein Name	Gene Name	Function
P49988	RNA polymerase sigma-54 factor	rpoN PA4462	Transcription initiation, sigma factor activity
Q9HVY7	Stringent starvation protein A	sspA PA4428	RNA-polymerase core enzyme binding
Q9X6W6	Bifunctional protein PyrR	pyrR PA0403	Nucleoside metabolic process, regulation of transcription
Q9I0Q4	RNA chaperone ProQ	PA2582	RNA strand exchange activity, RNA strand annealing activity, posttranscriptional regulation of gene expression
Q9I200	Probable transcriptional regulator	PA2115	Transcription
Q9HZ15	Probable transcriptional regulator	PA3225	Transcription
Q9I382	tRNA 2-selenouridine/geranyl-2-thiouridine synthase	selU PA1643	tRNA seleno modification
Q9HY82	Ribonuclease T	rnt PA3528	tRNA 3'-end processing
Q9HU78	Histidine utilization repressor	hutC PA5105	Negative regulation of transcription, histidine catabolic process
Q9HU59	DNA-binding transcriptional regulator NtrC	ntrC PA5125	Nitrogen fixation, regulation of nitrogen utilization, regulation of transcription
Q9HWX1	Transcriptional repressor NrdR	nrdR PA4057	Transcription, negative regulation of oxidoreductase activity,
Q03456	Ferric uptake regulation protein	fur PA4764	Negative regulation of transcription

The major cold shock protein CspA was newly detected which functions in the cell survival of the bacteria in sudden decrease of temperature (Table 3.4). It stabilizes the secondary structures on mRNA occurred by cold temperatures to fix the RNA functionality (Bisht et al., 2014). This might demonstrate that 3-HPAA resulted in the stress conditions as in the cold shock. Therefore *P. aeruginosa* might have used this protein for regaining proper RNA function under stress conditions. The phosphate regulon transcriptional regulatory protein PhoB which was newly detected after 3-HPAA treatment, which is a major protein functions in phosphate limitation of the bacteria (Faure et al., 2013). The regulation of virulence functions of *P. aeruginosa* is controlled by signal transduction pathway PUMA3 when inorganic phosphate limitation exist (Quesada et al., 2016). To be activated, PUMA3 requires not only the phosphate starvation but also PhoB transcription factor (Faure et al., 2013). Since PhoB is the only transcription factor that recognize the inorganic phosphate limitation and activate the other genes (VreA and VreR) of PUMA3 transduction pathway (Quesada et al., 2016),

the new detection of it might present that the bacteria experience the phosphate starvation in the presence of 3-HPAA.

Another stress condition that *P. aeruginosa* experienced under 3-HPAA treatment was the oxidative stress due to newly detection of OxyR. This protein is one of the key transcriptional regulators of oxidative stress defense (Kim et al., 2019). In addition to the oxidative stress response genes (katA, katB, ahpB and ahpCF), the oxyR gene also regulates the genes function in iron homeostasis, quorum sensing, protein synthesis and oxidative phosphorylation in *P. aeruginosa* (Wei et al., 2012). This might indicate that the bacteria showed various changes in metabolism dependent on the response to the oxidative stress caused by 3-HPAA.

Table 3.4. The newly detected proteins related to RNA in the presence of 3-HPAA.

Protein ID	Protein Name	Gene Name	Function
P95459	Major cold shock protein CspA	cspA PA3266	Regulation of transcription
Q9I6T1	Probable transcriptional regulator	PA0207	Transcription, DNA binding transcription factor activity
P23620	Phosphate regulon transcriptional regulatory protein PhoB	phoB PA5360	Flagellum-dependent swarming motility, phosphate ion transport positive regulation of cellular response to phosphate starvation, transcription
Q9HTL0	DNA-binding protein HU-alpha	hupA PA5348	Chromosome condensation, regulation of nucleic acid templated transcription
Q9HTL4	OxyR	oxyR PA5344	RNA polymerase transcription activator, transcription regulatory region DNA binding source, negative regulation of secondary metabolite biosynthetic process, cell motility, lipid biosynthesis, response to reactive oxygen species
Q9HYT6	RNA polymerase-associated protein RapA	rapA hepA, PA3308	Transcription, Helicase activity
G3XD14	RNA polymerase-binding transcription factor DksA	dksA PA4723	RNA polymerase binding, negative regulation of rRNA expression and positive regulation of several amino acid biosynthesis promoters
P26480	RNA polymerase sigma factor RpoD	rpoD rpoDA, PA0576	DNA binding transcription factor activity, sigma factor activity, transcription initiation

3.3.1.3. Ribosome and Protein-Related Proteins of 3-HPAA Treatment

The results of STRING for undetected and newly detected ribosomes and protein metabolism-related proteins were presented in Figure 3.5 a and b, respectively. The

interactions of all the proteins of these groups were also shown in Figure 3.6. According to these, various changes in t-RNA ligase profile occured after 3-HPAA treatment. For instance, Glutamine-tRNA ligase and Cysteine-tRNA ligase (Table 3.5) were undetected while Methionine-tRNA ligase, Glutamate-tRNA ligase, Tyrosine-tRNA ligase 2, Isoleucine-tRNA ligase, Phenylalanine-tRNA ligase beta subunit and Probable ATP-binding component of ABC transporter (Valine-tRNA ligase activity) were newly detected (Table 3.6). These show that 3-HPAA showed effect on tRNA ligases, thereby on bacterial protein synthesis. It is clear that tRNA ligases (Aminoacyl-tRNA synthetases; Source: https://www.uniprot.org/keywords/KW-0030) are crucial for protein translation in bacteria as they are crucial for translation of all organisms. They are the key components that carry aminoacids to the ribosomes to maintain the growth of peptide chain in translation (Ferro et al., 2018). Such that, the inhibition of processes of tRNA ligases is accepted as one of the important approaches for antimicrobial drug development recently (Ho et al., 2018; Lee et al., 2018). The mechanism of action of the topical antibiotic, which is in use, Mupirocin, depend on the inhibition of isoleucyl-tRNA reversibly in Gram positive bacteria (Parenti et al., 1987). Similarly, the antibiotic purpuromycin which inhibit bacterial translation by making complexes with tRNAs, acts by inhibiting the aminoacylation of tRNAs (Kirillov et al., 1997). Since the exposure of 3-HPAA caused some t-RNA ligases to be undetected, it might affect the growth of *P. aeruginosa* by affecting the tRNA ligase profile, thereby the bacterial protein synthesis.

The 30S ribosomal protein S15 which is crucial for bacterial ribosome structure and translation, was undetected (Table 3.5). Another 30S ribosomal protein, S18 was newly detected (Table 3.6) and according to STRING results, these proteins strongly interact each other (genes: rpsO and rpsL) (Figure 3.6). The prokaryotic ribosomes, on which the proteins are synthesized, consist of 30S small subunit and 50S large subunit which are made up of ribosomal RNAs and proteins (Aseev and Boni, 2011). The small subunit of the prokaryotic ribosome includes one rRNA (16S rRNA), large subunit includes two rRNA (23S and 5S rRNA) subunits and dozens of various ribosomal proteins (Aseev and Boni, 2011). These two main subunits make a complex via intersubunit bridges (Liu and Fredrick, 2016). The protein S15 which directly binds to mRNA (Shajani et al., 2011) is located in Bridge B4 of these bridges, which is required for proper ribosome assembly and translation (Liu and Fredrick, 2016). The binding of

the proteins S6, S18, S11 and S21 is dependent to the protein S15 *in vitro* (Shajani et al., 2011). However, in an *E. coli* strain, the deletion of rpsO which encodes for S15, did not prevent the binding of these proteins in vivo (Bubunenko et al., 2006). Thus, it could be speculated that even though S15 is a key component for small subunit assembly in vitro, there might be some other ribosomal assembly pathways that bacteria could use in the absence of S15 *in vivo* (Shajani et al., 2011). Since S18 protein was newly detected, the alternative assembly of the ribosome might be due to S18 protein. Another alternative of cell survival might be the assembly with the usage of S8 protein (Appendix D) rather than S15. Since S8 protein is another primary protein that binds to 16S rRNA in the same vicinity (Culver, 2003), bacteria might use this protein for proper ribosomal assembly in the absence of protein S15. Since Though Bubunenko et al. indicated that, the mutant bacteria had a diminished 70S ribosomal structure, it was compromised for growth and it had a cold-sensitive phenotype which shows that under non-optimal conditions S15 protein is vital for cell survival (Bubunenko et al., 2006). The undetection of protein S15 in the presence of 3-HPAA which caused an unideal condition might result in the detrimental effects on *P. aeruginosa* by damaging the ribosomal assembly. In addition, the cell survival of the bacteria might be due to the usage of subinhibitory concentrations of 3-HPAA for the protein isolation. It could be speculated that the bacteriocidal effect of higher concentration might be related to the bacteria not affording the proper ribosomal assembly in the absence of S15.

The antimicrobial effect of many antibiotics are due to targeting the ribosomal subunits. One of the main targets of antibiotics (i.e., gentamicin, kanamycin) is small ribosomal subunit of the bacteria (Sutcliffe, 2005). The 3-HPAA could be accepted as a promising antimicrobial agent since it displayed a change in small ribosomal subunit of *P. aeruginosa*.In addition to the effects on the small subunit structure, 3-HPAA also displayed effects on the large subunit assembly and RNA structure by undetection of ATP-dependent RNA helicase DeaD and Ribosomal RNA large subunit methyltransferase J. The large subunit is mainly related to production of polypeptide in translation (Aseev and Boni, 2011). Thus, 3-HPAA affected the translation by undetection of these large subunit proteins as well as the undetection of proteins related to translational initiation (Translation initiation factor IF-1), translational fidelity (Glutamyl-tRNA(Gln) amidotransferase subunit C) and rRNA (guanine-N7)-methylation (Ribosomal RNA small subunit methyltransferase G) (Table 3.5).

Besides these, the effect of 3-HPAA on protein metabolism could be noticed by undetection of proteins about homopolymerization and tetramerization, Chromosome partitioning protein Spo0J and Protein-export protein SecB, respectively (Table 3.5). Undetection of aminopeptidases, Cytosol aminopeptidase and Aminopeptidase N also showed the effect of 3-HPAA on protein metabolism (Table 3.5) and the STRING results showed that the Aminopeptidase N (gene pepN) were related with protein SecB (gene secB) (Figure 3.6). In addition, D-ala-D-ala-carboxypeptidase functioned in carboxypeptidase activity (gene dacC) was newly detected (Table 3.6). This might present the changes in metabolism of bacteria since aminopeptidase activity was diminished and carboxypeptidase activity occurred in the presence of 3-HPAA. Aminopeptidases are the enzymes that function in the cleavage of N-terminal of the peptides or proteins (Nandan and Nampoothri, 2017) which determine the structure and function them. A precursor protein which has an amino terminal signal sequence is recognized by the molecular chaperone SecB and it was determined that the inactivation of SecB caused defects in translocation of some precursor proteins and in growth of *E. coli* (Driessen, 2001). The undetection of SecB and Aminopeptidase N might lead the defects in process and translocation of the proteins with N-terminal signal sequence which might result in serious consequences in *P. aeruginosa* metabolism after treatment with 3-HPAA. On the other hand, the new detected protein, D-ala-D-ala-carboxypeptidase belongs to the carboxypeptidase enzymes. They are responsible for the removal of the terminal D-alanine from muramyl pentapeptide in the synthesis of peptidoglycan layer which is the protective component of bacterial cell wall (Ghosh et al., 2008; Meyer et al., 2018). An energy-saving property of the bacteria is the usage of the carboxypeptidases and endopeptidase together for recycling of the peptidoglycan subunits which were broken down or released in the media during the cell growth (Templin et al., 1999; Meyer et al., 2018).

Although in the rich media the bacteria build the peptidoglycan layer again (Meyer et al., 2018), it was shown that the blocking of this recycling could result in the autolysis of *E. coli* (Templin et al., 1999). New detection of D-ala-D-ala-carboxypeptidase might indicate that the bacteria manage to repair or reuse the peptidoglycan layer products which might be obtained from cell wall damage as well as the obligation of energy-saving in the media including 3-HPAA. All of these results demonstrated that the treatment of *P. aeruginosa* with 3-HPAA resulted in significant

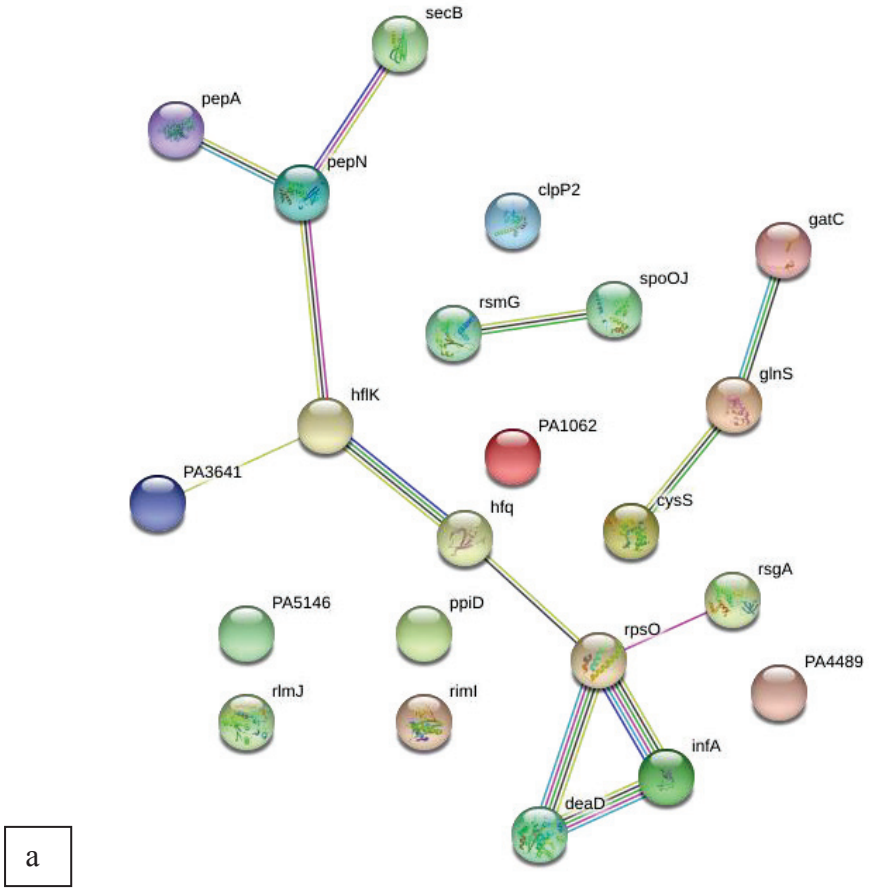

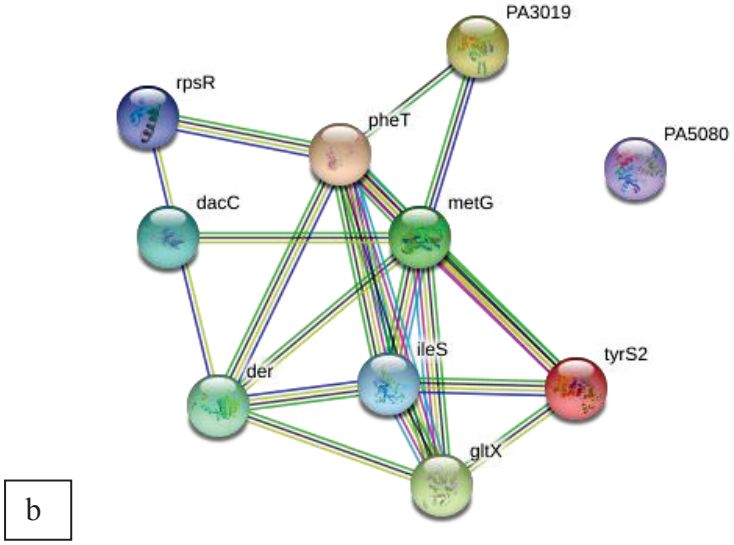

Figure 3.5. String representation of ribosome and protein-related proteins in the presence of 3-HPAA. a) Undetected proteins b) Newly detected proteins

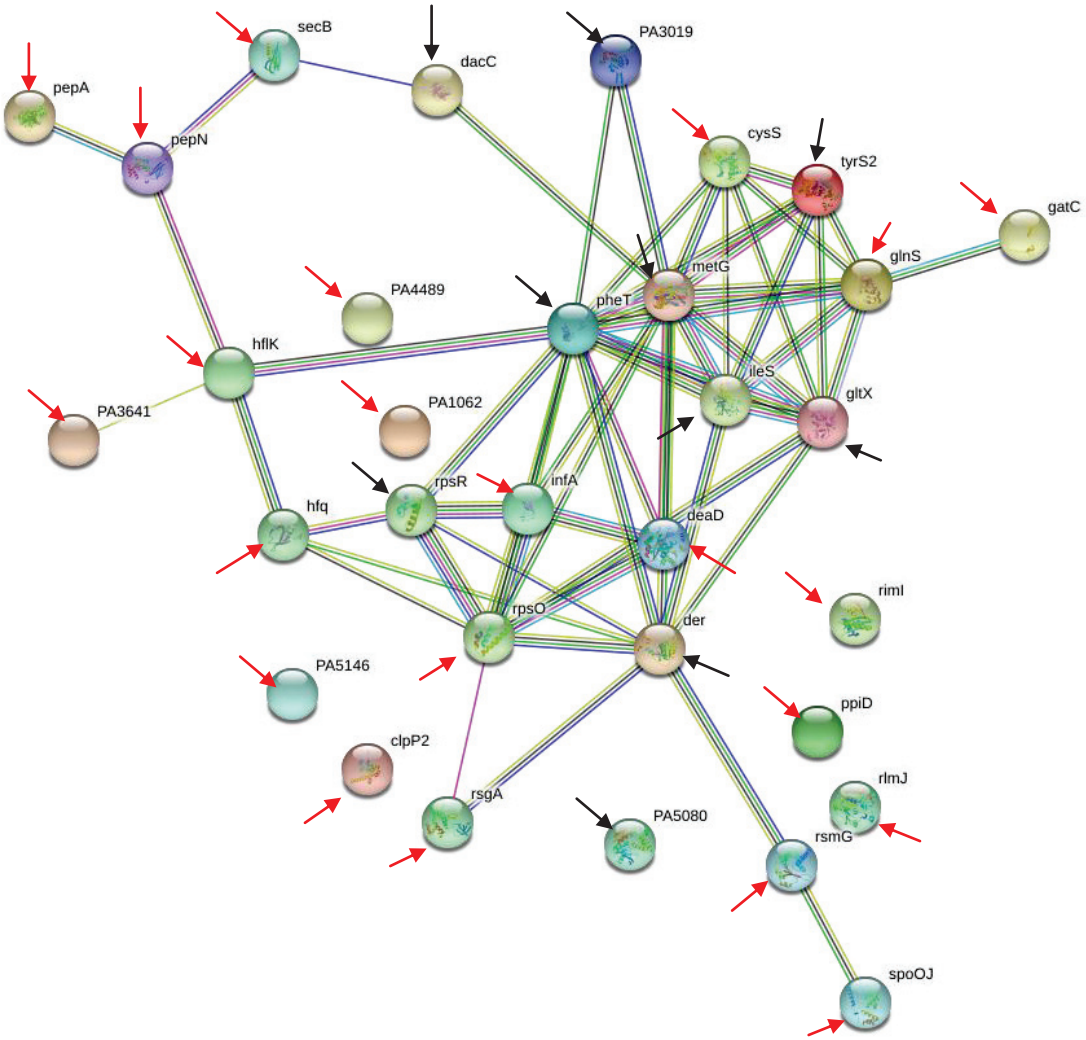

Figure 3.6. String representation of ribosome and protein-related undetected and newly detected proteins in the presence of 3-HPAA. The proteins were indicated in arrows with different colors (Undetected proteins: red arrows and newly detected proteins black arrows).

changes in ribosome structure, translation and protein metabolism in addition to clues for membrane damage of the bacteria. The undetection of mentioned proteins could result in the inhibition of the bacterial growth.

Table 3.5. The undetected proteins related to ribosome and protein in the presence of 3-HPAA.

Protein ID	Protein Name	Gene Name	Function
P65116	Translation initiation factor IF-1	infA PA2619	Ribosome binding, rRNA binding, translation initiation factor activity
Q9HVT9	Glutamyl-tRNA(Gln) amidotransferase subunit C	gatC PA4482	Regulation of translational fidelity, translation
Q9HUM0	RNA-binding protein Hfq	hfq PA4944	mRNA translational regulation
Q9HUL3	Small ribosomal subunit biogenesis GTPase RsgA	rsgA PA4952	Ribosome biogenesis
Q9HV58	30S ribosomal protein S15	rpsO PA4741	ribosome constituent, translation
Q9HT10	Ribosomal RNA small subunit methyltransferase G	rsmG PA5564	rRNA (guanine-N7)-methylation
Q9I003	ATP-dependent RNA helicase DeaD	deaD PA2840	ribosomal large subunit assembly, RNA catabolic process, RNA secondary structure unwinding
Q9HUF0	Ribosomal RNA large subunit methyltransferase J	rlmJ PA5019	rRNA base methylation
Q9I2U8	Glutamine--tRNA ligase	glnS PA1794	Glutamine--tRNA ligase activity
Q9I2U7	Cysteine--tRNA ligase	cysS PA1795	Cysteine--tRNA ligase activity
Q9I4R2	Uncharacterized protein	PA1062	Protein acetylation
Q9HVB7	Ribosomal-protein-alanine acetyltransferase	rimI PA4678	N-terminal protein amino acid acetylation
Q9I2T8	Peptidylprolyl isomerase	ppiD PA1805	peptidyl-prolyl cis-trans isomerase activity
Q9HT12	Chromosome partitioning protein Spo0J	spoOJ PA5562	Identical protein binding, protein homopolymerization
Q9HU56	Protein-export protein SecB	secB PA5128	Protein tetramerization, protein transport
O68822	Cytosol aminopeptidase	pepA phpA, PA3831	Release of an N-terminal amino acid, processing and regular turnover of intracellular proteins.
Q9HU38	Uncharacterized protein	PA5146	Regulation of protein targeting to membrane
Q9HXZ0	Probable amino acid permease	PA3641	Alanine:sodium symporter activity
Q9HYR9	ATP-dependent Clp protease proteolytic subunit 2	clpP2 PA3326	Endopeptidase activity
Q9HVT2	Alpha-2-macroglobulin homolog	PA4489	Endopeptidase inhibitor activity
Q9HUM2	Protein HflK	hflK PA4942	Peptidase activity
Q9HZC5	Aminopeptidase N	pepN PA3083	Peptide catabolic process, proteolysis

Table 3.6. The newly detected proteins related to ribosome and protein in the presence of 3-HPAA.

Protein ID	Protein Name	Gene Name	Function
Q9HYC7	Methionine--tRNA ligase	metG PA3482	Elongation of protein synthesis and initiation of all mRNA translation through initiator tRNA (fMet) aminoacylation.
Q9XCL6	Glutamate--tRNA ligase	gltX PA3134	Glutamate-tRNA ligase activity
Q9I5Q3	Tyrosine--tRNA ligase 2	tyrS2 PA0668	Tyrosine-tRNA ligase activity
Q9HVM4	Isoleucine--tRNA ligase	ileS PA4560	Isoleucine--tRNA ligase activity
Q9I0A4	Phenylalanine--tRNA ligase beta subunit	pheT PA2739	Phenylalanine--tRNA ligase activity
Q9HZI7	Probable ATP-binding component of ABC transporter	PA3019	Valine-tRNA ligase activity, ATPase activity
Q9HUA3	Proline iminopeptidase	PA5080	Aminopeptidase activity
Q9HXJ8	GTPase Der	der engA, PA3799	GTP binding, ribosome biogenesis
Q9HUN0	30S ribosomal protein S18	rpsR PA4934	Structural constituent of ribosome, translation
G3XD74	D-ala-D-ala-carboxypeptidase	dacC PA3999	Carboxypeptidase activity

3.3.1.4. Cell Wall and Membrane-Related Proteins of 3-HPAA Treatment

The application of 3-HPAA on *P. aeruginosa* resulted in the significant changes in the cell wall and membrane of the bacteria with the undetection (Figure 3.7 a) or newly detection (Figure 3.7 b) of important proteins interacted with each other (Figure 3.8). The undetected proteins were functioned in membrane composition and structure, cell division, Type IV-pilus biogenesis, flagellum and chemotaxis, and phosphorelay transduction system (Table 3.7). On the other hand, the newly detected proteins were related to cell envelope organization, cell division, flagellum and chemotaxis (Table 3.8). The cell envelope, which is characteristic to Gram negative bacteria, is the covering structure of bacterial cell that consists of two membranes with a thin peptidoglycan layer in between (Stinnett et al., 1973). It functions as the protective component (Meyer et al., 2018), basis for cell division, motility and signal transduction of bacterial cell. The detection of vital changes in the protein profile of this structure might indicate major changes in bacterial metabolism after 3-HPAA treatment.

The proteins about composition and structure of the membrane, Membrane protein insertase YidC, Signal recognition particle receptor FtsY, Rod shape-determining protein MreB and many other integral components of the membrane were undetected. The protein YidC is functioned in the insertion and integration of the small membrane proteins into the membrane by co-working with Sec proteins (Dalbey et al., 2011) as well as proteolytic degradation of membrane or cytoplasmic proteins (Kiefer and Kuhn, 2018). Another membrane related protein, FtsY, is one of the responsible proteins for the targeting of nascent polypeptide chains to the membrane which means it aids the transfer of the newly formed proteins to the cytoplasmic region of the membrane (Dalbey et al., 2011). Since these proteins were not detected after 3-HPAA exposure, the membrane protein targeting and insertion into the membrane in *P. aeruginosa* might be damaged because of 3-HPAA. The rod-shape of *P. aeruginosa* is regulated by MreB protein filaments which bind to the inner membrane and regulate the insertion of cell wall precursors (Shi et al., 2017). Surprisingly, the undetection of MreB was not resulted in the defect of rod shape of *P. aeruginosa* in SEM micrographs (Figure 2.3 c and d). Although MreB is accepted as an important component for rod shape of the bacteria, the bacteria might use an alternative way to overcome the undetection of MreB since the MreB function is adjustable and related mostly to its partner proteins, MreC, RodZ, FtsZ, RodA, PBPs, MurF, MraY, and MurG (Gurrola et al., 2017). Though, treatment of 3-HPAA forced *P. aeruginosa* to change the cell envelope structure for survival.

Besides this, outer membrane protein assembly factor BamD and Probable carboxyl-terminal protease, which are related to the cell envelope organization, and Cell division coordinator CpoB, which is functioned in FtsZ dependent cytokinesis, were newly detected. The lipoprotein BamD is one of the essential components of Bam complex which is vital for outer membrane biogenesis (Mori et al., 2012). Cell division coordinator CpoB is an important protein that controls peptidoglycan synthesis and outer membrane construction which result in the maintenance of integrity of cell envelope (Gray et al., 2015). It might show that the cell wall especially outer membrane was highly defected and repair was carried out by carboxyl-terminal protease and BamD for maintenance of proper cell division. In addition, the proteins which take vital roles in cell cycle and division, Tol-Pal system protein TolQ and ATP-dependent zinc metalloprotease FtsH were undetected. The Tol-Pal system is an important system of

Gram negative bacteria for outer membrane integrity continuance (Dubuisson et al., 2005). The Tol-Pal system, which is structurally conserved among Gram negative bacteria (Sturgis, 2001), consists of seven genes in *Pseudomonas*, orf1, tolQ, tolR, tolA, tolB, oprL and orf2 (Llamas et al., 2003) and the damages occur in the outer membrane if the mutations are generated in the genes of Tol-Pal system proteins (Dubuisson et al., 2005). Among these proteins, TolQ is undetected after 3-HPAA exposure which resulted in the defect in Tol-Pal system of *P. aeruginosa*, thereby the cell envelope integrity.

The undetection of another important protein, FtsH, might also result in the damage in the cell envelope structure and regulation of cell metabolism. FtsH is one of the proteases that control the regulation of the cell metabolism immediately in the presence of an environmental stress and it is universally conserved among prokaryotes (Langklotz et al., 2012). Although the proteases are found in cytoplasm, FtsH is the only one protease that is attached to the inner membrane (Narberhaus et al., 2009). It is responsible of quality control of the membrane proteins (Langklotz et al., 2012) and post-translation of transcription factors and enzymes (Narberhaus et al., 2009). As an example, the post translational regulation of RpoH (σ^{32}) is mostly carried out with FtsH (Langklotz et al., 2012) as well as the regulation of RpoN (σ^{54}) (Carmona and de Lorenzo, 1999) in *E. coli*. The undetection of FtsH might result in the problems in the regulation of these transcription factors, thus, transcription of *P. aeruginosa* might be defected. Since it was shown that RpoN was also undetected after 3-HPAA treatment (Table 3.3), it could be speculated that 3-HPAA treatment generated serious changes in the regulation of transcription in addition to the defects in the cell envelope structure of *P. aeruginosa*. The FtsH was presented to degrade FtsZ, which is the main protein functioned in the initiation of the septum formation in bacterial cell division, *in vitro* (Srinivasan et al., 2008). However, as far as we know, the studies which show the reason or result of this process *in vivo* are not exist. Though, it could be speculated that the undetection of FtsH resulted in the cell division changes in *P. aeruginosa* besides its aforementioned effects. Briefly, the cell envelope is a natural protection barrier against many unfavorable environmental conditions such as presence of antimicrobial agents and the undetection of some of the crucial proteins of cell envelope demonstrated that 3-HPAA affected the bacterial cell wall integrity and cell division as an antimicrobial agent. Relatedly, the invagination line in the surfaces of the bacteria in the presence of

3-HPAA, which were presented in SEM micrographs (Figure 2.3 c and d), might be due to the aforementioned undetected proteins.

The type4 pili components were also undetected in the presence of 3-HPAA. The type4 pili (fimbriae) flexible filaments found in the poles of *P. aeruginosa* (Kazmierczak et al., 2006) and one of the main virulence factors which aids the initiation and maintenance of the infections (Huang et al., 2003) and biofilm formation (Jain et al., 2017). The main functions of T4 pili were presented as the attachment to various surfaces such as metals, glass, plastics and various host tissues (Giltner et al., 2012) in a calcium dependent manner (Johnson et al., 2011) by twitching motility (Carter et al., 2017). Twitching motility, which is also crucial for biofilm formation, is a flagellum-independent type of motility and occurs by stretching and retractions of the pili (Huang et al., 2003; Carter et al., 2017). The T4 pili type that is found in *P. aeruginosa* is T4a pilus (T4aP) (Giltner et al., 2012). The protein PilY1, is a T4aP machinery protein (Carter et al., 2017) and is required for surface adherence and manipulation of the host (Giltner et al., 2012). PilQ, PilM (Carter et al., 2017; Jain et al., 2017) and PilG (Darzins, 1993) are another proteins of T4aP machinery which are functioned as the structural components of the pili. The protein FimX is functioned for proper twitching motility and required for biogenesis and assembly of type IV pili (Huang et al., 2003; Jain et al., 2017). On the other hand, B-type flagellin which is a virulence factor functioned in flagellum-dependent motility and flagellum organization (Bakht azad et al., 2018) was newly detected. This might show that the bacteria shifted the motility type from pilus-dependent to flagellum-dependent. The bacteria uses the flagellum not only in virulence (Bakht azad et al., 2018), but also for the movement in chemotaxis (Chaban et al., 2015) through which it can recognize the environmental conditions and decide their direction. The bacteria uses phosphorylated CheY protein in rotation of the flagellum in both cases of escaping form an environment or going towards an attractant (Chaban et al., 2015). Therefore, new detection of flagellin B protein might indicate that the bacteria manage to travel away because of 3-HPAA. However, undetection of CheY protein could either show that the flagellum-dependent motility of the bacteria is damaged or it used an alternative way rather than CheY usage. Another newly detected protein, Protein PilJ which is functioned in chemotaxis, also presented that the bacteria manage to escape from the inconvenient conditions of the environment in the presence of 3-HPAA.

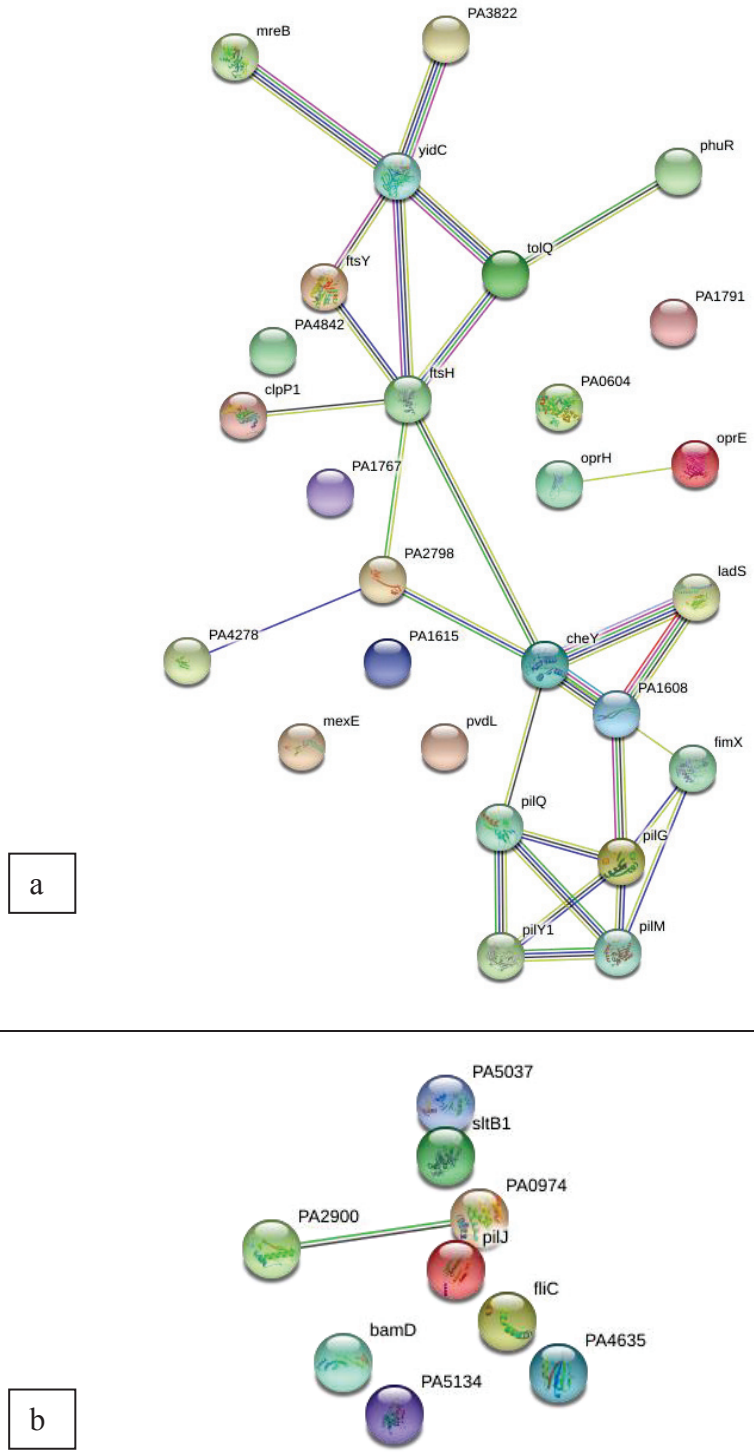

Figure 3.7. String representation of cell wall and membrane-related proteins in the presence of 3-HPAA. a) Undetected proteins b) Newly detected proteins

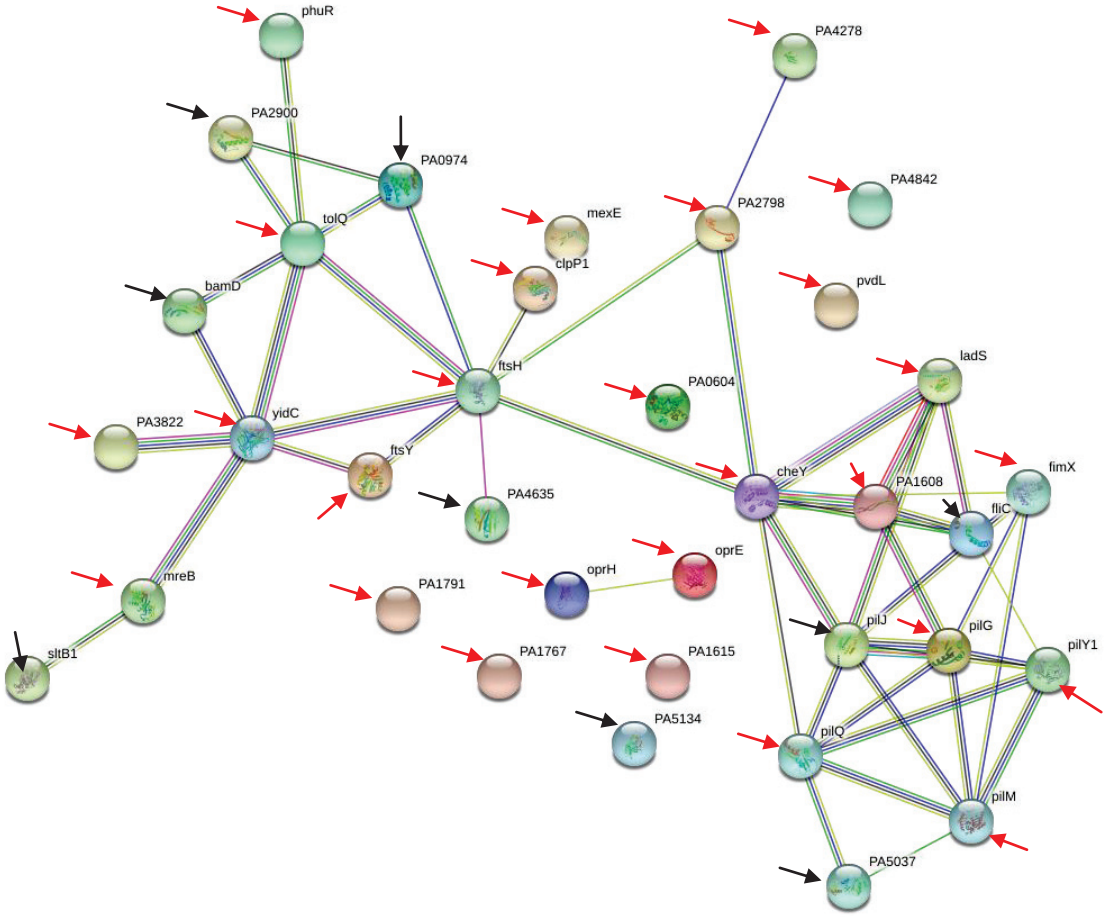

Figure 3.8. String representation of cell wall and membrane-related undetected and newly detected proteins in the presence of 3-HPAA. The proteins were indicated in arrows with different colors (Undetected proteins: red arrows and newly detected proteins black arrows).

In another point of view, it could be speculated that the disuse of Type 4 fimbrial motility (twitching) and usage of flagellar motility (planktonic, swimming) (Kazmierczak et al., 2015) under 3-HPAA applied conditions, might show the bacteria tried to produce flagella instead of the pili and planktonic motility is preferred as an adaptation process. In addition, since biofilm formation, which was related to higher virulence, was diminished by disuse of the pili, 3-HPAA might decrease the virulence of *P. aeruginosa*. Thus, the treatment of *P. aeruginosa* with 3-HPAA resulted in serious damages and changes in the cell wall and membrane structure and function which might lead the inhibition of bacterial growth.

Table 3.7. The undetected proteins in the presence of 3-HPAA functioned in cell wall and membrane.

Protein ID	Protein Name	Gene Name	Function
Q9HT06	Membrane protein insertase YidC	yidC PA5568	Membrane insertase activity, insertion and/or proper folding and/or complex formation of integral membrane proteins into the membrane
Q9I6C1	Signal recognition particle receptor FtsY	ftsY PA0373	Cotranslational protein targeting to membrane
Q9I157	PvdL	pvdL PA2424	Pyoverdine biosynthetic process
Q9HVM8	Type IV pilus biogenesis factor PilY1	pilY1 PA4554	Type IV-pilus dependent motility
P34750	Fimbrial assembly protein PilQ	pilQ PA5040	Type IV-pilus biogenesis
G3XD28	Type 4 fimbrial biogenesis protein PilM	pilM PA5044	Type IV pilus biogenesis, cell cycle,
P50598	Tol-Pal system protein TolQ	tolQ PA0969	Cell cycle, cell division, bacteriocin transport
Q9I0Y9	Resistance-Nodulation-Cell Division (RND) multidrug efflux membrane fusion protein MexE	mexE PA2493	Cell division, response to antibiotic
Q9HV48	ATP-dependent zinc metalloprotease FtsH	ftsH PA4751	Cell division, response to antibiotic
Q9HVU0	Rod shape-determining protein MreB	mreB PA4481	Cell morphogenesis
Q9HWC2	Uncharacterized protein	PA4278	Peptidoglycan binding
Q51455	Chemotaxis protein CheY	cheY PA1456	Flagellum dependent cell motility, chemotaxis, phosphorelay signal transduction system
Q9I2U1	ATP-dependent Clp protease proteolytic subunit 1	clpP1 PA1801	Flagellum dependent cell motility, single species biofilm formation, response to antibiotic
Q9I3B3	Probable chemotaxis transducer	PA1608	Chemotaxis
G3XDA5	Anaerobically-induced outer membrane porin OprE	oprE PA0291	Integral component of membrane
Q9I5T4	Probable binding protein component of ABC transporter	PA0604	Membrane transport
Q9I2X2	Uncharacterized protein	PA1767	Transmembrane component
Q9HUW8	Uncharacterized protein	PA4842	Integral component of membrane
Q9I3A7	Probable lipase	PA1615	Integral component of membrane
Q9HXI0	Uncharacterized protein	PA3822	Integral component of membrane
Q9I2V1	Uncharacterized protein	PA1791	Integral component of membrane
G3XD11	PhoP/Q and low Mg2+ inducible outer membrane protein H1	oprH PA1178	Integral component of membrane, cell outer membrane
Q9HV88	Heme/hemoglobin uptake outer membrane receptor PhuR	phuR PA4710	Integral component of membrane, response to iron ion, heme transport
P46384	Protein PilG	pilG PA0408	Phosphorelay signal transduction system, pilus biosynthesis and twitching motility
Q9I045	Probable two-component response regulator	PA2798	Phosphorelay transduction system
Q9HX42	Lost Adherence Sensor, LadS	ladS PA3974	Phosphorelay sensor kinase activity
Q9HUK6	FimX	fimX PA4959	Phosphorelay transduction system

Table 3.8. The newly detected proteins in the presence of 3-HPAA functioned in cell wall and membrane.

Protein ID	Protein Name	Gene Name	Function
Q9HX24	Soluble lytic transglycosylase B	sltB1 PA4001	Lytic transglycosylase activity
Q9HUD4	Uncharacterized protein	PA5037	Peptidoglycan binding
Q9HVF6	Uncharacterized protein	PA4635	Integral component of membrane
P42257	Protein PilJ	pilJ PA0411	Chemotaxis, transmembrane signaling receptor activity
P72151	B-type flagellin	fliC PA1092	Flagellum dependent cell motility, Flagellum organization
Q9HU50	Probable carboxyl-terminal protease	PA5134	Cell envelope organization, cell wall biogenesis, pathogenesis, endopeptidase activity
G3XDB2	Cell division coordinator CpoB	cpoB PA0974	FtsZ-dependent cytokinesis
Q9HZU7	Probable outer membrane protein	PA2900	Integral component of membrane, cell outer membrane
P33641	Outer membrane protein assembly factor BamD	bamD PA4545	Cell envelope organization, protein insertion into membrane

3.3.1.5. Metabolism-Related Proteins of 3-HPAA Treatment

The treatment with 3-HPAA resulted in various changes in the metabolism of *P. aeruginosa* at the proteomic level by which undetected or newly detected proteins (Figures 3.9, 3.10 and 3.11). Since the bacteria must adapt to the environment in the presence of non-optimal conditions such as the presence of a toxic substance (Langklotz et al., 2012), it could be speculated that the changes in the protein profile of the metabolic processes might aid the adaptation. Relatedly, the serious changes/adaptations in the particular metabolic systems of the bacteria after 3-HPAA exposure might give clues about the targets of its antimicrobial effect.

According to results of this study, various undetected and newly detected proteins functioned in amino acid biosynthesis were found (Tables 3.9 and 3.10). For

example, the proteins related to biosyntheses of alanine, lysine, leucine, cysteine and aromatic amino acid as well as arginine catabolic process were undetected and lysine, alanine, histidine, glutamine, serine and glycine metabolism related proteins were newly detected which indicate the regulations in the amino acid metabolism. In addition, Porin D, functioned in amino acid transport, and Aminopeptidase P were another undetected proteins related to amino acid biosynthesis. Aminopeptidase P (PepP) is a member of aminopeptidases P (APPro) family and functions in the removal of N-terminal residue of the polypeptides a second residue of proline (Peng et al., 2017). Since it is highly conserved among *Pseudomonads* and played role in the virulence of the bacteria, it is accepted as a promising antimicrobial target (Peng et al., 2017). The undetection of this protein indicates that it might be one of the targets for antimicrobial effect of 3-HPAA. Gram negative bacteria possess a resistance mechanism in which they decrease membrane permeability for antibiotic by reducing the porins (Serra et al., 2019). The undetected porin, Porin D, was presented as a channel protein for uptake of β-lactam antibiotics (Khatua et al., 2014). Thus, it might be speculated that *P. aeruginosa* did intentionally not express the Porin D to protect itself from 3-HPAA such in a way of resistance against β-lactam antibiotics. On the other hand, this might also show that there is a problem with the transport systems and outer membrane protein profile.

Nicotinate phosphoribosyltransferase 1, which is functioned in NAD biosynthesis, was not detected after 3-HPAA treatment, thus the NAD recycling of *P. aeruginosa* might be defected. Since NAD is the vital element of metabolic pathways of enzymes functioned in redox or non-redox processes, NAD depletion might cause a fatal result in the cell regardless of being prokaryotic or eukaryotic (Huang et al., 2009). The undetection of Nicotinate phosphoribosyltransferase 1 might indicate that the bacteria are under serious stress. Additionally, the problem in NAD biosynthesis might lead to serious damages in the energy metabolism of the bacteria. Howeveri the cell survival maintained in the presence of subinhibitory concentrations of 3-HPAA. Therefore, it could be speculated that *P. aeruginosa* handled the undetection of NAD 1 by using alternative partners of this protein for biosynthesis of NAD (Okon et al., 2017).

The 3-HPAA treatment resulted in the undetection of the proteins functioned in pyocyanin and phenazine biosyntheses. Many members of the genus *Pseudomonas* secrete extracellular pigments (El-fouyl et al., 2015). The *P. aeruginosa* culture

demonstrates a distinct greenish-blue color which arouse from the mixture of blue color of the bacteria and yellow color of the media (Rada and Leto, 2013). The pigment called pyocyanin produced by *P. aeruginosa* is the reason for the blue color (Rada and Leto, 2013). It synthesizes the pyocyanin pigment called phenazine, which is the water-soluble extracellular pigment possessing a heterocyclic structure, is capable of produce reactive oxygen species and toxic to other microorganisms for microbial competition as well as to eukaryotes (Dietrich et al., 2006; El-fouyl et al., 2015, Rada and Leto, 2013) Relatedly, the new antimicrobial agents arouse from phenazine were presented (Borrero et al., 2014). In addition, phenazine was presented as one of the three main molecules in quorum sensing mechanism of *P. aeruginosa* which is the system of bacteria to communicate and behave in a synchronized way as well as increasing the virulence (Dietrich et al., 2006, Ugurlu et al., 2016). Thus, quorum sensing targeted antimicrobial agents are accepted as promising new strategies against pathogenicity (Lu et al., 2018, Ugurlu et al., 2016) and the agents that inhibit the production of phenazine gets attention in this manner.

In our study, it was morphologically demonstrated that the greenish-blue color of the bacterial cultures disappeared when 3-HPAA was applied (Figure 2.2 a). At the proteomic level, this color decrease could be attributed to the undetection of the proteins which take role in phenazine production (5-methylphenazine-1-carboxylate 1-monooxygenase, Phenazine biosynthesis protein PhzB1, Phenazine biosynthesis protein PhzE). Thereby, it is clear 3-HPAA reduces the virulence of *P. aeruginosa* by preventing the phenazine production which makes it a favorable antimicrobial agent candidate.

The changes in the profile of lipid metabolism related proteins showed that the proteins functioned in fatty acid beta oxidation were undetected while lipid biosynthesis proteins as well as phosphate transport and phospholipase synthesis were newly detected. Thus, the treatment of *P. aeruginosa* with 3-HPAA resulted in elevated lipid biosynthesis and reduced fatty acid degradation which might indicate the effort of the bacteria to maintain the integrity of cell envelope in the presence of 3-HPAA.

All these changes in the metabolism-related proteins indicate that the bacteria not only attempt to adapt to the environmental conditions by changing the metabolic pathway preferences to survive, but also they were seriously affected via damages in virulence factors and quorum sensing components.

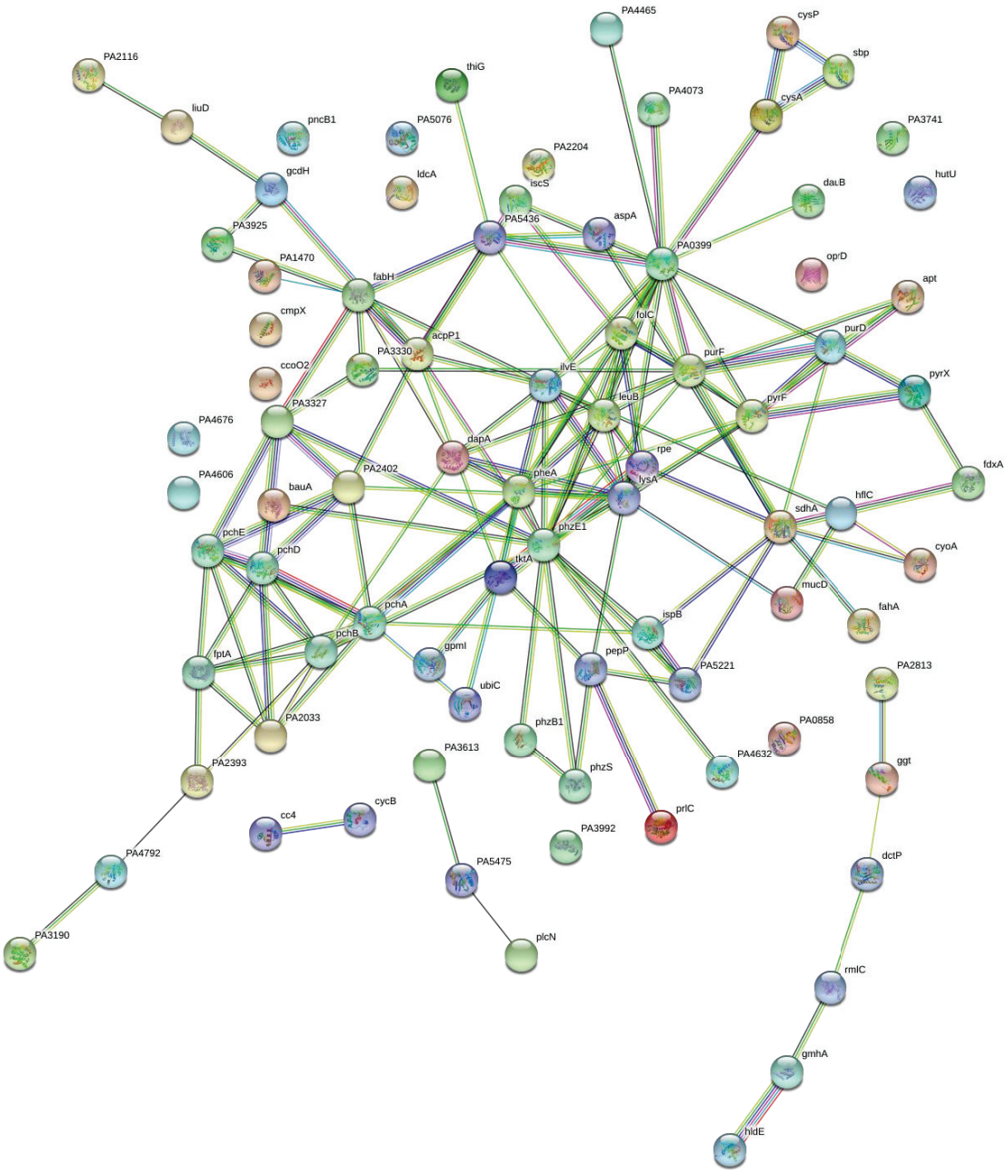

Figure 3.9. String representation of metabolism-related undetected proteins in the presence of 3-HPAA.

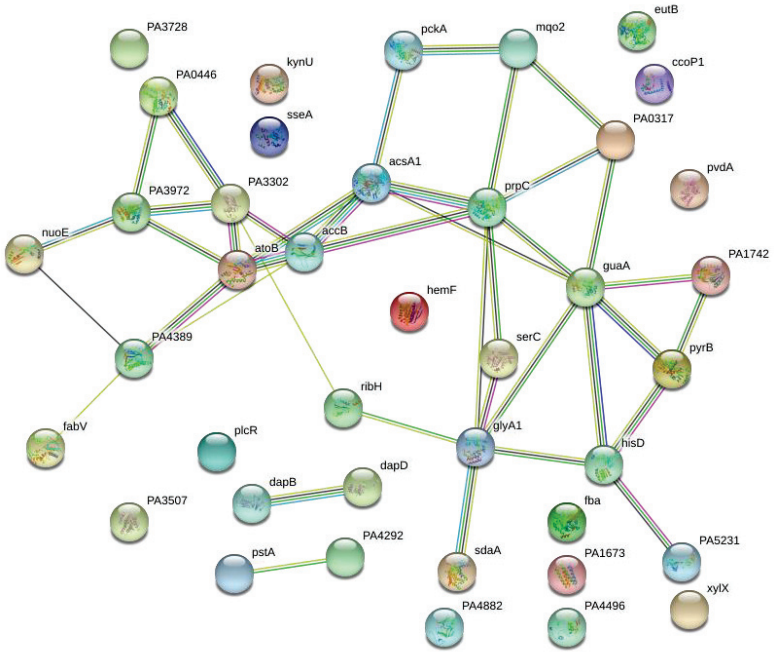

Figure 3.10. String representation of metabolism-related newly detected proteins in the presence of 3-HPAA.

Table 3.9. The undetected proteins in the presence of 3-HPAA functioned in metabolism.

Protein ID	Protein Name	Gene Name	Function
Q9I700	Beta-alanine--pyruvate aminotransferase	bauA PA0132	Beta-alanine biosynthetic process
Q9I2S7	Lysine-specific pyridoxal 5'-phosphate-dependent carboxylase, LdcA	ldcA PA1818	Amino acid metabolic process
Q9HTW6	Aminopeptidase P	pepP PA5224	Aminopeptidase activity
Q9I4W3	4-hydroxy-tetrahydrodipicolinate synthase	dapA PA1010	Diaminopimelate biosynthetic process, Lysine biosynthetic process
P19572	Diaminopimelate decarboxylase	lysA PA5277	Lysine biosynthetic process
Q51375	3-isopropylmalate dehydrogenase	leuB PA3118	Leucine biosynthetic process
O86428	Branched-chain-amino-acid aminotransferase	ilvE PA5013	Leucine biosynthetic process, Isoleucine biosynthetic process, valine biosynthetic process
Q9HXI8	Cysteine desulfurase IscS	iscS PA3814	Cysteine desulfurase activity
Q9I583	UPF0176 protein PA0858	PA0858	Cysteine persulfate intermediate

(cont. on next page)

Table 3.9. (continued)

Q9I6A1	Cystathionine beta-synthase	PA0399	Cysteine biosynthetic process
Q9HXE4	NAD(P)H-dependent anabolic L-arginine dehydrogenase DauB	dauB PA3862	Arginine catabolic process
Q9HZ67	Bifunctional chorismate mutase/prephenate dehydratase	pheA PA3166	L-phenylalanine biosynthesis, Prephenate biosynthesis
Q9HU83	Urocanate hydratase	hutU PA5100	Histidine catabolic process
Q9I2A2	Fumarylacetoacetase	fahA PA2008	Aromatic amino acid family metabolic process
P32722	Porin D	oprD PA0958	Amino acid transport
Q9HUP4	Nicotinate phosphoribosyltransferase 1	pncB1 PA4919	NAD biosynthetic process
Q9HTK1	Probable chorismate pyruvate-lyase	ubiC PA5357	Ubiquinone biosynthetic process
Q9HTW9	Probable FAD-dependent monooxygenase	PA5221	Ubiquinone biosynthetic process
Q9I187	Probable dipeptidase	PA2393	Biyoverdine biosynthetic process
Q51507	Isochorismate pyruvate lyase	pchB PA4230	Salicylate biosynthetic process
Q9HWG9	5-methylphenazine-1-carboxylate 1-monooxygenase	phzS PA4217	Pyocyanine biosynthetic process
Q9HU21	dTDP-4-dehydrorhamnose 3,5-epimerase	rmlC PA5164	Lipopolysaccharide biosynthesis, extracellular polysaccharide biosynthesis, dTDP-L-rhamnose biosynthesis
Q9I299	Methylcrotonyl-CoA carboxylase, alpha-subunit (Biotin-containing)	liuD PA2012	isoprenoid catabolic process, leucine catabolic process, terpene catabolic process
Q9I5T1	Ribulose-phosphate 3-epimerase	rpe PA0607	Carbohydrate metabolic process, pentose catabolic process
Q9I406	Glutathione hydrolase proenzyme	ggt PA1338	Glutathione catabolic process, glutathione biosynthetic process
Q9HVL5	Octaprenyl-diphosphate synthase	ispB PA4569	Isoprenoid biosynthetic process
Q9I282	Uncharacterized protein	PA2033	Iron assimilation
G3XD20	Periplasmic serine endoprotease DegP-like	mucD PA0766	Endopeptidase, signal transduction
O69753	Phenazine biosynthesis protein PhzB1	phzB1 PA4211	Phenazine biosynthetic process
Q9HWV5	Probable aldehyde dehydrogenase	PA4073	Phenylacetaldehyde dehydrogenase activity
Q04633	Adenine phosphoribosyltransferase	apt PA1543	Adenine salvage, AMP salvage, purine ribonucleoside salvage
Q51508	Salicylate biosynthesis isochorismate synthase	pchA PA4231	pyochelin biosynthetic process, salicylic acid biosynthetic process
Q9HWG3	Pyochelin biosynthesis protein PchD	pchD PA4228	Catalytic activity
Q9HUM3	Protein HflC	hflC PA4941	Peptidase activity

(cont. on next page)

Table 3.9. (continued)

Q9HVI3	Uncharacterized protein	PA4606	Cellular respose to nutrient levels, Starvation response
Q9I6K7	Sulfate-binding protein	sbp PA0283	Sulfate transmembrane transporter activity
Q9I765	Oligopeptidase A	prlC PA0067	Metal ion binding, signal peptide processing
Q9HUG9	Bifunctional protein HldE	hldE rfaE, PA4996	ADP-L-glycero-beta-D-manno-heptose biosynthesis, Carbohydrate phosphorylation, LPS core biosynthesis
Q9HUA7	Probable binding protein component of ABC transporter	PA5076	Ionotropic glutamate receptor
Q9HU18	C4-dicarboxylate-binding periplasmic protein DctP	dctP PA5167	C-4 dicarboxylate transport, transmembrane transport
Q9I3L9	Sulfate-binding protein of ABC transporter	cysP PA1493	Sulfate transmembrane transporter activity
Q9I1R3	Probable binding protein component of ABC transporter	PA2204	ionotropic glutamate receptor activity
Q9I6L0	Sulfate/thiosulfate import ATP-binding protein CysA	cysA PA0280	Sulfate transmembrane transporter activity
Q9HX28	Uncharacterized protein	PA3992	Metal ion binding
Q9HVF9	Uncharacterized protein	PA4632	Metallopeptidase activity
Q9HZ48	Probable binding protein component of ABC sugar transporter	PA3190	Carbohydrate transport
Q9HY13	Uncharacterized protein	PA3613	Carbohydrate metabolic process
Q9I427	Cytochrome bo(3) ubiquinol oxidase subunit 2	cyoA PA1317	ATP synthesis coupled electron transport, copper ion binding
Q9HVZ0	Phosphoheptose isomerase	gmhA PA4425	Carbohydrate biosynthesis, Lipopolysaccharide core region biosynthesis
Q9HU53	2,3-bisphosphoglycerate-independent phosphoglycerate mutase	gpmI pgm, PA5131	Glycolysis
Q9I3G1	Cytochrome c oxidase, cbb3-type, CcoO subunit	ccoO2 PA1556	Aerobic respiration, respiratory electron transport chain
Q9I3D5	Succinate dehydrogenase flavoprotein subunit	sdhA PA1583	Anaerobic respiration, Tricarboxylic acid cycle
Q9HTQ4	Cytochrome c5	cycB PA5300	Electron transfer activity, heme binding, iron ion binding
P00106	Cytochrome c4	cc4 PA5490	Electron transfer activity, heme binding, iron ion binding
Q9HTD7	Aspartate ammonia-lyase	aspA PA5429	Aspartate metabolic process, tricarboxylic acid cycle
Q7DC81	Phenazine biosynthesis protein PhzE	phzE1 phzE2, PA1903, PA4214	Glutamine metabolic process, tryptophan biosynthetic process, phenazine biosynthetic process

(cont. on next page)

Table 3.9. (continued)

Q51342	Amidophosphoribosyltransferase	purF PA3108	IMP biosynthetic process, Purine nucleobase biosynthetic process, Nucleoside metabolic process, Glutamine metabolic process,
Q9HXQ3	Uncharacterized protein	PA3741	acyl-CoA metabolic process, fatty acid metabolic process
P42512	Fe(3+)-pyochelin receptor	fptA PA4221	Iron transport, iron ion homeostasis, siderophore transport
Q9I6B4	Thiazole synthase	thiG PA0381	Transferase activity, thiamine diphosphate biosynthesis
Q9HVV3	Nucleotide-binding protein PA4465	PA4465	ATP binding, GTP binding
Q51551	Dihydroorotase-like protein	pyrC' pyrX, PA0401	Purine nucleobase catabolic process, Pyrimidine nucleotide biosynthetic process
Q59654	Orotidine 5'-phosphate decarboxylase	pyrF PA2876	Pyrimidine biosynthetic process
Q9HUV8	Phosphoribosylamine--glycine ligase	purD PA4855	Purine nucleobase biosynthetic process, IMP biosynthetic process
Q9I671	Glutaryl-CoA dehydrogenase	gcdH PA0447	Acyl-CoA dehydrogenase activity, flavin adenine dinucleotide binding
Q9I1Z9	Putative hydro-lyase PA2116	PA2116	Lyase activity
Q9HVB9	Carbonic anhydrase	PA4676	Carbon utilization
Q9I030	Probable glutathione S-transferase	PA2813	Transferase activity
Q9I5Y8	Transketolase	tktA PA0548	Transketolase activty
Q9HZA8	Folylpolyglutamate synthetase	folC PA3111	Dihydrofolate synthase activity, tetrahydrofolylpolyglutamate synthase activity
Q9HTD0	Probable biotin carboxylase subunit of a transcarboxylase	PA5436	Ligase activity
Q9HT95	Acetyltransferase PA5475	PA5475	Transferase activity
Q9HYR8	Probable non-ribosomal peptide synthetase	PA3327	Biosynthetic process
Q9HY07	Ferredoxin 1	fdxA PA3621	electron transfer activity, metal ion binding
G3XCV2	Dihydroaeruginoic acid synthetase	pchE PA4226	Metabolic process
Q9I179	Probable non-ribosomal peptidesynthetase	PA2402	Metabolic process
Q9I3P2	Probable short-chain dehydrogenase	PA1470	Dehydrogenase activity
Q9HYR5	Probable short chain dehydrogenase	PA3330	Dehydrogenase activity
Q9HV16	Uncharacterized protein	PA4792	Lipid metabolic process

(cont. on next page)

Table 3.9. (continued)

G3XD40	Probable acyl-CoA thiolase	PA3925	Fatty acid beta oxidation
Q9HYR2	3-oxoacyl-[acyl-carrier-protein] synthase 3	fabH PA3333	Fatty acid biosynthesis
P15713	Non-hemolytic phospholipase C	plcN PA3319	Lipid catabolic process, phosphatidylcholine phospholipase C activity
O54439	Acyl carrier protein 1	acpP1 acpP, PA2966	Lipid A Biosynthetic process
G3XCV6	Conserved cytoplasmic membraneprotein, CmpX protein	cmpX PA1775	Transmembrane transport

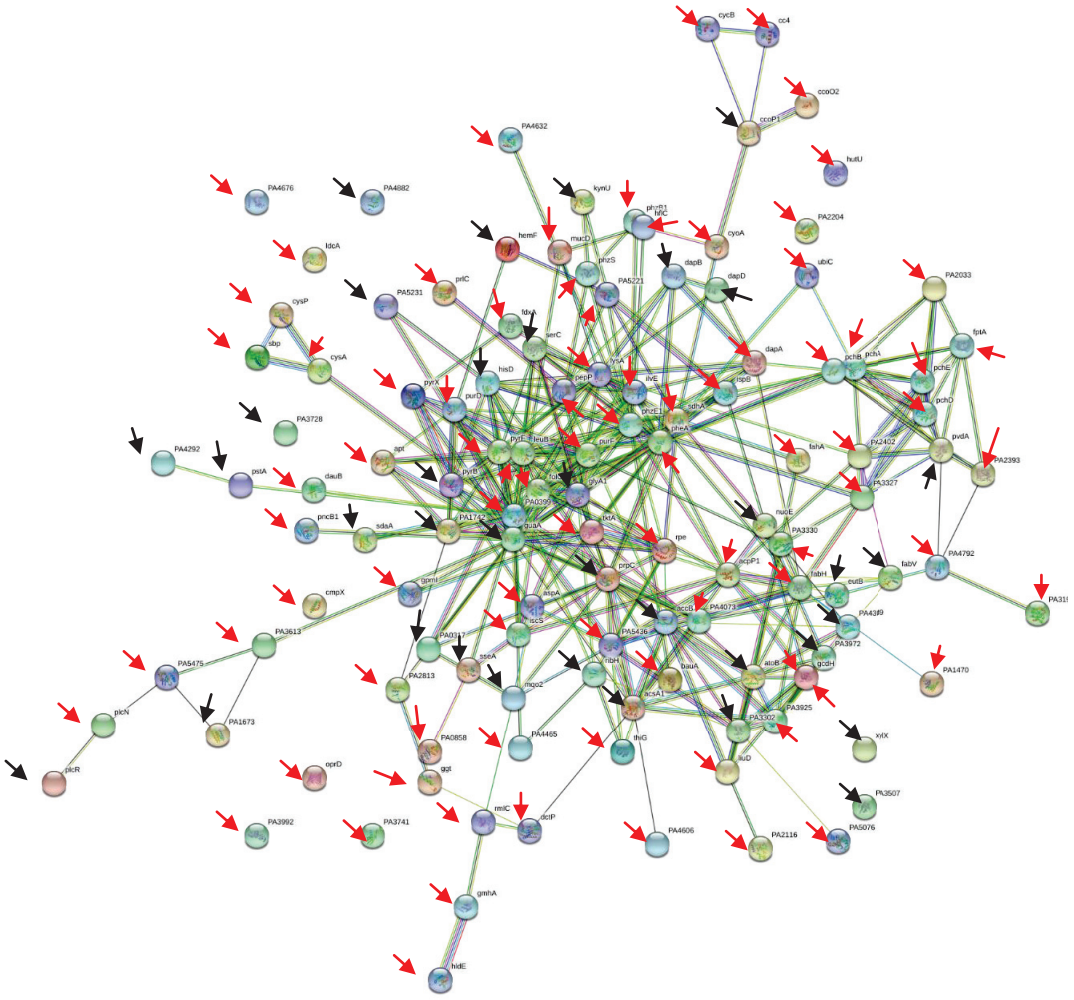

Figure 3.11. String representation of metabolism-related undetected and newly detected proteins in the presence of 3-HPAA. The proteins were indicated in arrows with different colors (Undetected proteins: red arrows and newly detected proteins: black arrows).

Table 3.10. The newly detected proteins related to metabolism in the presence of 3-HPAA.

Protein ID	Protein Name	Gene Name	Function
Q9HX03	Ethanolamine ammonia-lyase large subunit	eutB PA4024	Amino acid metabolic process
G3XD76	2,3,4,5-tetrahydropyridine-2,6-dicarboxylate N-succinyltransferase	dapD PA3666	Lysine biosynthetic process
Q59653	Aspartate carbamoyltransferase	pyrB PA0402	Amino acid metabolic process
P38103	4-hydroxy-tetrahydrodipicolinate reductase	dapB PA4759	Lysine biosynthetic process
Q9I235	Kynureninase	kynU PA2080	Alanine biosynthetic process
Q9HVW9	Histidinol dehydrogenase	hisD PA4448	Histidine biosynthetic process
Q9I2Z5	Probable amidotransferase	PA1742	Glutamine metabolic process
Q9HZ66	Phosphoserine aminotransferase	serC PA3167	Serine biosynthetic process
Q9HTE9	Serine hydroxymethyltransferase 1	glyA1 PA5415	Glycine biosynthetic process
Q9I452	Probable 3-mercaptopyruvate sulfurtransferase	sseA PA1292	Cysteine metabolic process
Q9I352	Bacteriohemerythrin	PA1673	Oxygen carrier activity
Q9HTV9	Probable ATP-binding/permease fusion ABC transporter	PA5231	ATPase activity
Q9HXR4	Uncharacterized protein	PA3728	ATPase activity
Q9HVS5	Probable binding protein component of ABC transporter	PA4496	Transmembrane transport
Q9I672	Uncharacterized protein	PA0446	Catalytic activity
Q9HTZ7	Phosphoenolpyruvate carboxykinase (ATP)	pckA PA5192	Gluconeogenesis
Q9I5Y1	Fructose-bisphosphate aldolase	fba fda, PA0555	Glycolysis
Q9I3G5	Cbb3-type cytochrome c oxidase subunit	ccoP1 PA1552	Oxidative phosphorylation
Q9I5E3	Citrate synthase	prpC PA0795	Tricarboxylic acid cycle
Q9I0J8	NADH-quinone oxidoreductase subunit E	nuoE PA2640	Respiratory electron transport chain
Q9I6H4	Uncharacterized protein	PA0317	Respiratory electron transport chain, lactate oxidation
Q9HVF1	Probable malate:quinone oxidoreductase 2	mqo2 mqoB, PA4640	Tricarboxylic acid cycle
Q9I139	L-serine dehydratase	sdaA PA2443	Gluconeogenesis
Q9HTJ5	Phosphate transport system permease protein PstA	pstA PA5367	Phosphate ion transmembrane transport
Q9HWA8	Phosphate transporter	PA4292	Phosphate ion transmembrane transport
P40695	Phospholipase C accessory protein PlcR	plcR PA0843	Regulation of synthesis of phospholipase C (possible)
Q9HW15	Probable short-chain dehydrogenase	speA PA4389	Fatty acid elongation
Q9HZP8	Enoyl-[acyl-carrier-protein] reductase [NADH]	fabV PA2950	Fatty acid biosynthesis

(cont. on next page)

Table 3.10. (continued)

P37799	Biotin carboxyl carrier protein of acetyl-CoA carboxylase	accB fabE, PA4847	Fatty acid biosynthesis
G3XD52	Uncharacterized protein	PA3302	Fatty acid synthase activity, Fatty acid biosynthesis
Q9I2A8	Acetyl-CoA acetyltransferase	atoB PA2001	Fatty acid beta oxidation
Q9HX44	Probable acyl-CoA dehydrogenase	PA3972	Flavin adenine dinucleotide binding
Q9I558	Acetyl-coenzyme A synthetase 1	acsA1 PA0887	Acetyl-Co A Biosynthetic process
Q9HYA2	Probable short-chain dehydrogenase	PA3507	Nucleotide binding
Q9HWX5	6,7-dimethyl-8-ribityllumazine synthase	ribH ribE, PA4053	Riboflavin biosynthesis
Q9HXM6	GMP synthase[glutamine-hydrolyzing]	guaA PA3769	GMP biosynthesis in purine metabolism
Q9HUT1	Uncharacterized protein	PA4882	Nitrate assimilation
P43898	Oxygen-dependent coproporphyrinogen-III oxidase	hemF PA0024	Protoporphyrin-IX biosynthesis
Q51548	L-ornithine N(5)-monooxygenase	pvdA pvd-1, PA2386	Pyoverdin biosynthesis, siderophore biosynthesis
Q9I0W4	Toluate 1,2-dioxygenase alpha subunit	xylX PA2518	Dioxygenase activity

3.3.1.6. Redox and Cell Homeostasis-Related Proteins of 3-HPAA Treatment

Superoxide and hydrogen peroxide are the examples of reactive oxygen species (ROS) which are required to be removed to maintain the cell homeostasis and survival (Kamariah et al., 2015). The redox and cell homeostasis related protein profile of *P. aeruginosa* presented various changes (Figure 3.12 a and b) related to each other (Figure 3.12 c) which indicated that 3-HPAA presence in the environment resulted in serious stress response. For example, the Lon protease, alkyl hydroperoxide reductase subunit F, glutathione reductase and superoxide dismutase [Mn] were the proteins, which are responsible for stress response, were undetected after 3-HPAA treatment (Table 3.11). On the other hand, glutathione peroxidase, organic hydroperoxide resistance protein, peptide methionine sulfoxide reductase MsrA and probable major facilitator superfamily (MFS) transporter which functioned in oxidoreductase activity were newly detected. Thus, 3-HPAA application resulted in serious oxidative stress on *P. aeruginosa*.

Lon protease is an intracellular protease that has roles in response to stress such as DNA damage, antibiotic resistance and virulence, swarming motility and biofilm

formation (Fernandez et al., 2016). In addition, the protein that regulate Lon protease, Hfq (Fernandez et al., 2016) (Table 3.5) was also undetected after 3-HPAA treatment. Thus, 3-HPAA result in not only damage of Lon protease mediated processes but also the regulation of Lon protease itself.

Alkyl hydroperoxide reductase is an enzyme functioned in reduction of peroxides (Kamariah et al., 2015) as well as superoxide dismutase [Mn] in superoxides (Iiyama et al., 2007). The superoxide and hydrogen peroxide are the toxic substances for the cell via damaging the DNA and membranes (Hassett et al., 1996). These proteins were undetected in the presence of 3-HPAA. In addition, Fur protein, which is related to proper superoxide dismutase activity (Hassett et al., 1996) and iron homeostasis, was also undetected (Table 3.3, Section 3.3.1.2). Thus, the redox and iron homeostasis might be damaged with 3-HPAA application.

Glutathione reductase was undetected while glutathione peroxidase was newly detected. Since both are functioned in oxidative stress response, it could be speculated that *P. aeruginosa* manage to respond the oxidative stress caused by 3-HPAA. Since the glutathione is a major response to oxidative stress and adaptation, the changes in the glutathione metabolism related proteins demonstrates that the bacteria regulated the adaptation for oxidative stress caused by 3-HPAA. Glutathione reductase is an evolutionary conserved protein and highly homologous in both prokaryotes and eukaryotes (Smirnova and Oktyabrsky, 2005) which functions in the reduction of highly toxic glutathione disulfide to glutathione by using NADPH to protect the cell from oxidative stress during the cell survival (Smirnova and Oktyabrsky, 2005). Thus, the undetection of this protein might affect the redox homeostasis regulation and led the new detection of Glutathione peroxidase which is another protein that takes role in reduction in hydroperoxides from glutathione (Atichartpongkul et al., 2016).

Peptide methionine sulfoxide reductase MsrA is one of the main enzymes which is induced in the stress caused by chemicals such as phenolic compounds (Tamburro et al., 2001). Under the oxidative stress conditions the reactive oxygen species cause oxidation of the methionine residues leading the reduction of the protein function. MsrA protein found in various tissues and organisms can repair these proteins by reducing the oxidized methionine back to methionine, thereby the function of these proteins are regained (Mintz et al., 2002, John et al., 2001). In addition, Spermidine/putrescine import ATP-binding protein PotA, biosynthetic arginine decarboxylase and polyamine

aminopropyltransferase 1 functioned in spermidine/putrescine metabolism were also newly detected after 3-HPAA treatment (Table 3.12). Spermidine and putrescine are main polyamines in bacteria which are functioned in cell viability, pathogenesis, antibiotic resistance and protecting the DNA from oxidative damage (Johnson et al., 2011). They also play roles in signaling and regulation against stress conditions caused by reactive oxygen species (ROS), heat, UV, acid and osmotic pressure as well as in production and function of porins in outer membrane (Bandounas et al., 2011). Therefore, the new detection of transport and biosynthesis proteins related to putrescine and spermidine might show that the bacteria give responses to stress conditions caused by 3-HPAA treatment in a similar way of oxidative stress.

Table 3.11. The undetected proteins in the presence of 3-HPAA functioned in redox and cell homeostasis.

Protein ID	Protein Name	Gene Name	Function
Q9I5F9	Lon protease	lon PA0779	Response to antibiotic, response to stress, nitric oxide metabolic process, peptidase activity
Q9I2T9	Lon protease	lon PA1803	Response to antibiotics, response to drug, response to stress, pathogenesis, protein quality control for misfolded or incompletely synthesized proteins, single species biofilm formation, type IV pilus dependent motility, flagellum dependent swarming motility
Q9HZI9	Universal stress protein	PA3017	Response to stress
Q9I2V3	Uncharacterized protein	PA1789	Response to stress
Q9HW73	Uncharacterized protein	PA4328	Response to stress
Q9HUK9	Thiosulfate sulfurtransferase	rhdA PA4956	Response to toxic substance (Contributes to P. aeruginosa survival under cyanogenic conditions)
Q9I6Z2	Alkyl hydroperoxide reductase subunit F	ahpF PA0140	Response to reactive oxygen species
P23189	Glutathione reductase	gor PA2025	Cell redox homeostasis, response to oxygen radical
P0C2B2	Thiol:disulfide interchange protein DsbA	dsbA PA5489	Cell redox homeostasis
Q9HYY4	Probable oxidoreductase	PA3256	Oxidoreductase activity
P53652	Superoxide dismutase [Mn]	sodA PA4468	Removal of superoxide radicals
Q9I1F8	Probable oxidoreductase	PA2317	Oxidoreductase activity

(cont. on next page)

Table 3.11. (continued)

Q9I067	Uncharacterized protein	PA2776	Oxidoreductase activity
Q9HVG5	Glycerate dehydrogenase	hprA PA4626	Oxidoreductase activity
Q9I0T4	Probable acyl-CoA dehydrogenase	PA2550	Oxidoreductase activity
Q9I5R7	S-adenosylmethionine decarboxylase proenzyme	speD PA0654	S-adenosylmethioninamine biosynthetic process, spermidine biosynthetic process

Table 3.12. The newly detected proteins in the presence of 3-HPAA functioned in redox and cell homeostasis.

Protein ID	Protein Name	Gene Name	Function
Q9I578	Probable oxidoreductase	PA0863	Oxidoreductase activity
Q9I0T0	Probable short-chain dehydrogenase	PA2554	Oxidoreductase activity
Q9HV44	Chaperone protein DnaJ	dnaJ PA4760	Response to hyperosmotic and heat shock
Q9I2C4	NAD+ dependent aldehyde dehydrogenase ExaC	exaC PA1984	Oxidoreductase activity
Q9I5A2	Glutathione peroxidase	PA0838	Response to oxidative stress
Q9HZZ3	Organic hydroperoxide resistance protein	ohr PA2850	Response to oxidative stress
Q9I2R2	Probable oxidoreductase	PA1833	Oxidoreductase activity
Q9HUF1	Peptide methionine sulfoxide reductase MsrA	msrA PA5018	Response to oxidative stress, response to hypochlorite
Q9HUQ6	Probable short-chain dehydrogenase	PA4907	Oxidoreductase activity
Q9I0Z1	Probable oxidoreductase	PA2491	Oxidoreductase activity, Negative regulation of secondary metabolite biosynthetic process
Q9HWP5	Probable major facilitator superfamily (MFS) transporter	PA4136	Drug transmembrane transporter activity
Q9I6I9	Spermidine/putrescine import ATP-binding protein PotA	spuF potA, PA0302	Spermidine transport, putrescine transport
Q9HUX1	Biosynthetic arginine decarboxylase	speA PA4839	Arginine catabolic process, putrescine biosynthetic process, spermidine biosynthetic process
Q9X6R0	Polyamine aminopropyltransferase 1	speE1 speE, PA1687	Spermidine biosynthetic process

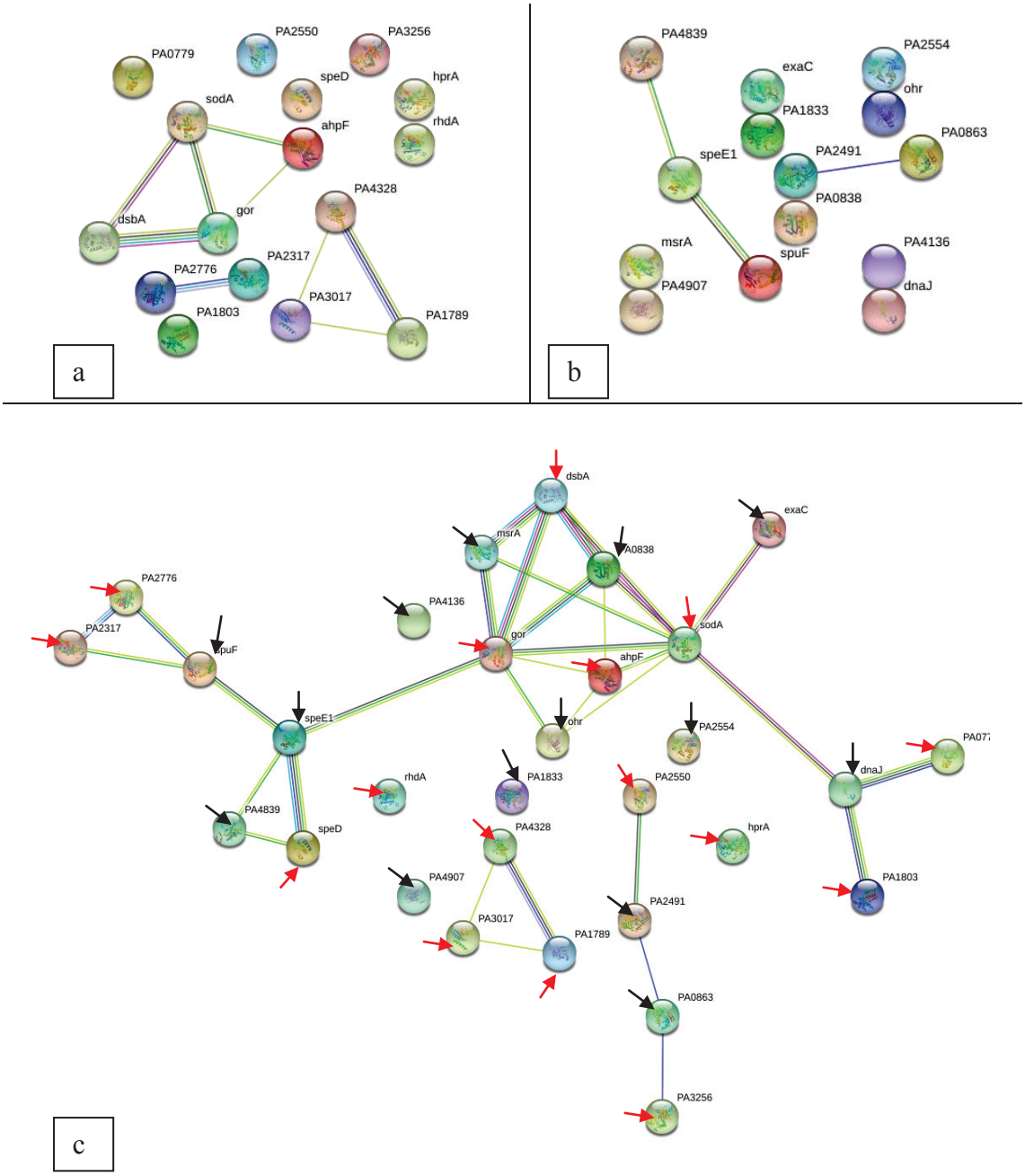

Figure 3.12. String representation of redox and cell homeostasis-related proteins in the presence of 3-HPAA. a) Undetected proteins b) Newly detected proteins c) The both undetected and newly detected proteins. The proteins were indicated in arrows with different colors (Undetected proteins: red arrows and newly detected proteins: black arrows).

3.3.1.7. Virulence-Related Proteins of 3-HPAA Treatment

The undetected proteins in the presence of 3-HPAA which were related to virulence were presented in Figure 3.13 a, while newly detected ones were in 3.13 b. They had no interactions as it could be seen in Figure 3.13 c.

Phosphomannomutase/phosphoglucomutase protein (Protein ID: P26276; Gene name: algC PA5322) was multi-functional with its roles in alginic acid biosynthetic process, GDP-alpha-D-mannose biosynthetic process, lipopolysaccharide core region biosynthetic process, O antigen biosynthetic process and pathogenicity. One of the results which is significant was undetection of this protein as it is functioned in alginate production in *P. aeruginosa* which is a exopolysaccharide layer aids the mucoid morphology by production of alginate layer (Darzins et al., 1985).

This layer acts as a protection for bacteria against host immune defenses and antibiotics as well as functioning in the attachment of the bacteria to the host cells (Glonti et al., 2010). Disappearance of these proteins after 3-HPAA application might cause a decrease in pathogenicity of *P. aeruginosa* by resulting a phenotype vulnerable to host immune system cells and antibiotics. On the other hand, the uncharacterized protein PA1579 (Protein ID: Q9I3D8; Gene name: PA1579) which might have a role in interaction of the bacterium with animal cells was newly detected as well as other uncharacterized protein (Protein ID: Q9HVG7; Gene name: PA4624) which functioned in single-species biofilm formation. These results might indicate that the bacteria manage to maintain the virulence properties in the absence of the undetected phosphomannomutase/phosphoglucomutase protein.

The other undetected proteins, cyclic AMP receptor-like protein (Protein ID: P55222; gene name: vfr PA0652) and uncharacterized PhzA/B-like protein PA3332 (Protein ID: Q9HYR3; Gene name: PA3332) were functioned in pathogenesis and antibiotic biosynthesis, respectively. The undetection of these proteins suggest that the virulence of *P.* aeruginosa could be decreased with 3-HPAA treatment.

3.3.1.8. Uncharacterized Proteins of 3-HPAA Treatment

Various uncharacterized proteins were presented in Figure 3.14 a and b. The most significant profile change for these proteins were the undetection of PA0083,

PA0084 and PA0086 which were strongly interacted each other (Figure 3.14 c). According to the protein BLAST results, these proteins might be Type VI secretion system contractile sheath small subunit, Type VI secretion system contractile sheath large subunit and tetratricopeptide repeat protein for PA0083, PA0084 and PA0086, respectively (Table 3.13). The bacteria possess various mechanisms to interact each other in their niche in a contact-dependent manner to communicate or compete (Basler et al., 2013). Type VI secretion system (T6SS) is one of the widely presented mechanism for the competition of the Gram negative bacteria by secretion of the proteins in adjacent cell.

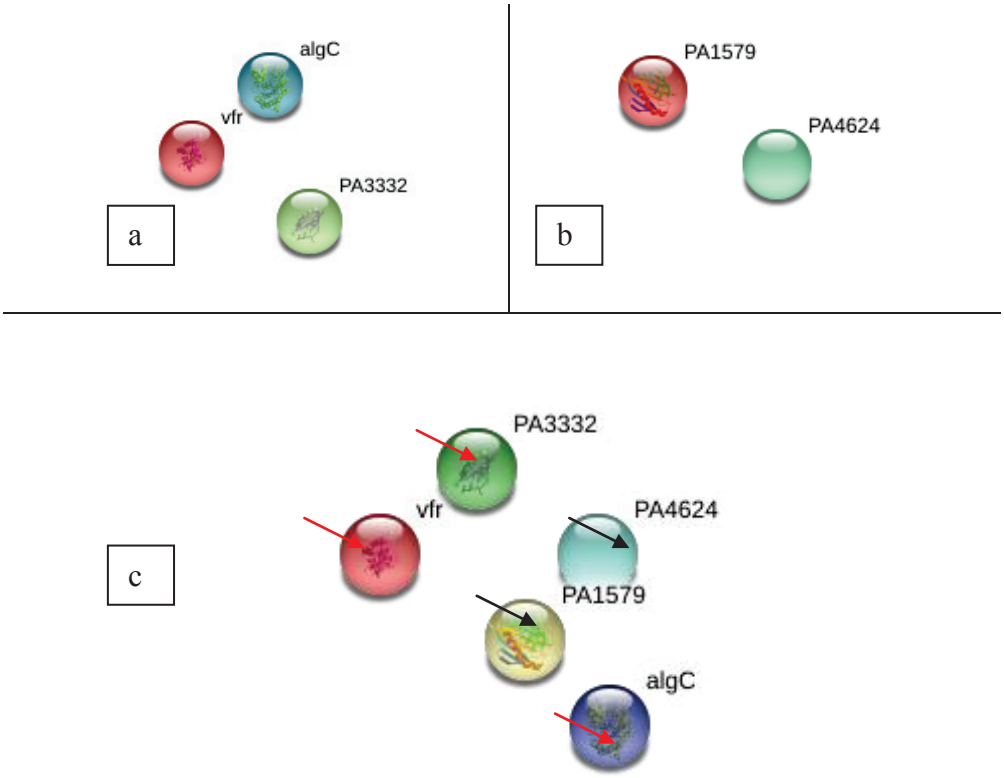

Figure 3.13. String representation of virulence-related proteins in the presence of 3-HPAA. a) Undetected proteins b) Newly detected proteins c) The both undetected and newly detected proteins. The proteins were indicated in arrows with different colors (Undetected proteins: red arrows and newly detected proteins: black arrows).

A contractile sheath similar to T4 phage, but in an inverted structure, is used by the bacteria (Russel et al., 2012; Salih et al., 2018). This system is not only used for dispelling the bacteria in vicinity but also used for secretion of toxic effector proteins into eukaryotic cells. Thus, it is has a virulence
related property for Gram negative pathogenic bacteria including *P. aeruginosa* and may be a promising target for new antimicrobial agents (Salomon and Orth, 2015; Salih et al., 2018). The most striking function of this system was presented as its role in horizontal gene transfer. This system secretes nucleases, pore-forming toxins and hydrolyses to the target bacterial cell and after the death of this cell, the genes of the dead bacteria are taken by the bacteria which secreted the T6SS effector proteins in the first place (Salomon and Orth, 2015). The bacteria which possess T6SS target, lyse and kill the other bacteria possessing T6SS regardless of their species to gain new genes from those (Ringel et al., 2017). However, *P. aeruginosa* do not kill the bacteria which do not contain T6SS. This might indicate that *P. aeruginosa* compete with the ones which could be dangerous to them. In addition, since these bacteria are strong enough to survive in the environment with their "useful" genes than the bacteria without T6SS, they prefer to gain new genes from T6SS positive bacteria (Ringel et al., 2017). The apparatus of T6SS consists of three parts: the membrane complex, the baseplate, and the sheath-tube complex (Ringel et al., 2017). Since the activity of T6SS mostly depends upon the assembly and contraction of sheath part (Salih et al., 2018), the undetection of large and small subunit proteins of contractile sheath might result in the defect of T6SS. Other undetected protein, tetratricopeptide repeat protein, was important for the stability of exporting process of secretions from cell membrane (Whitney and Howell, 2013; Mejias et al., 2019). Thus, the bacterial virulence, competing property and horizontal gene transfer properties of *P. aeruginosa* were diminished by 3-HPAA treatment.

RidA family protein PA5303 was undetected while RidA family protein PA5339 was newly detected which have interaction to each other. RidA, which was named as YjgF previously, is an important protein for metabolite damage repair and presented as an imine diaminase that protect certain enzymes from damage such as repairing specifically inactivation of pyridoxal 5' phosphate dependent enzymes (Hogde-Hanson and Downs, 2017; de Crecy-Lagard et al., 2018). The changes in the members of this family demonstrated that *P. aeruginosa* manage to fix the enzyme damages caused by 3-HPAA.

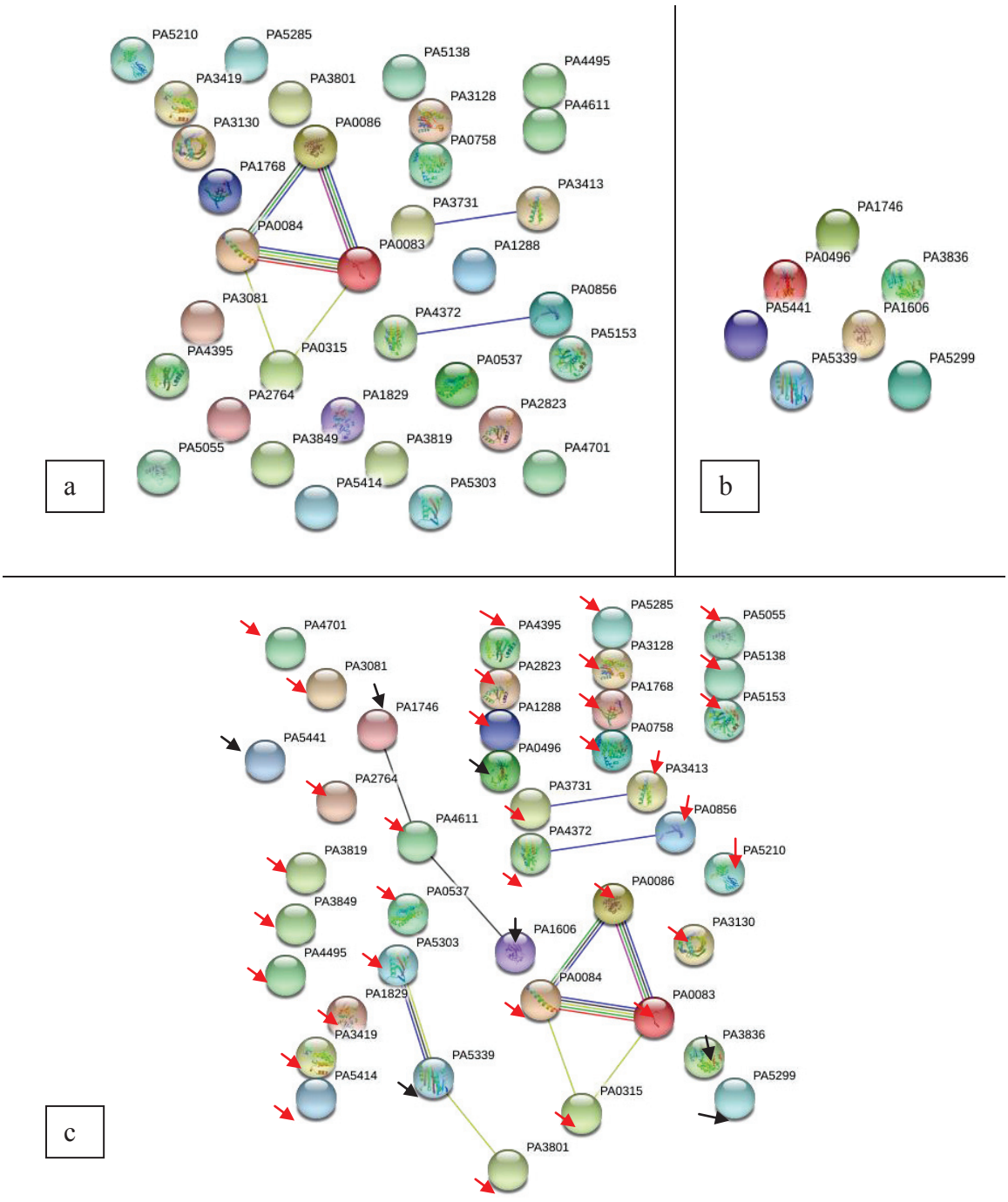

Figure 3.14. String representation of uncharacterized proteins in the presence of 3-HPAA. a) Undetected proteins b) Newly detected proteins c) The both undetected and newly detected proteins. The proteins were indicated in arrows with different colors (Undetected proteins: red arrows and newly detected proteins: black arrows).

Table 3.13. The undetected proteins in the presence of 3-HPAA which are uncharacterized.

Protein ID	Protein Name	Gene Name	Function	Protein Blast Results
Q9HW11	UPF0234 protein PA4395	PA4395	Uncharacterized	YajQ family cyclic di-GMP-binding protein
Q9HTF0	Uncharacterized protein	PA5414	Uncharacterized	Hypothetical protein
Q9HZC7	Uncharacterized protein	PA3081	Uncharacterized	DUF1329 domain-containing protein
Q9I748	Uncharacterized protein	PA0084	Uncharacterized	Type VI secretion system contractile sheath large subunit
Q9HTQ1	Uncharacterized protein	PA5303	Uncharacterized	RidA Family protein
Q9I5H1	Uncharacterized protein	PA0758	Uncharacterized	HDOD domain-containing protein
Q9I456	Probable outer membrane protein	PA1288	Uncharacterized	Hypothetical protein, Long-chain fatty acid transport protein
Q9HXI3	Uncharacterized protein	PA3819	Uncharacterized	Glycine zipper 2TM domain-containing protein
Q9I079	Uncharacterized protein	PA2764	Uncharacterized	Alpha/beta hydrolase
Q9I746	Uncharacterized protein	PA0086	Uncharacterized	Tetratricopeptide repeat protein
Q9I2X1	Uncharacterized protein	PA1768	Uncharacterized	ATP-dependent zinc protease
Q9I6H6	Uncharacterized protein	PA0315	Uncharacterized	DUF4399 domain-containing protein
Q9HVH9	Uncharacterized protein	PA4611	Uncharacterized	DUF465 domain-containing protein
Q9HW30	Uncharacterized protein	PA4372	Uncharacterized	Imelysin
Q9HVS6	Uncharacterized protein	PA4495	Uncharacterized	DUF541 domain-containing protein
Q9I5Z9	Uncharacterized protein	PA0537	Uncharacterized	LemA family protein
Q9HXJ6	Uncharacterized protein	PA3801	Uncharacterized	Tetratricopeptide repeat protein
Q9HYI6	UPF0162 protein PA3419	PA3419	Uncharacterized	Transglut_core2 superfamily hypothetical protein
Q9HU46	Uncharacterized protein	PA5138	Uncharacterized	ABC transporter substrate-binding protein
Q9HYJ2	Uncharacterized protein	PA3413	Uncharacterized	YebG superfamily hypothetical protein
Q9HXR1	Uncharacterized protein	PA3731	Uncharacterized	PspA/IM30 family protein
Q9HU31	Amino acid (Lysine/arginine/ornithine/histidine/octopine) ABC transporter periplasmic binding protein	PA5153	Uncharacterized	Amino acid ABC transporter substrate-binding protein
G3XD27	Uncharacterized protein	PA5055	Uncharacterized	DUF971 domain-containing protein
Q9HV96	Uncharacterized protein	PA4701	Uncharacterized	COG2187 and AA_33 superfamilies hypothetical protein
Q9HTR9	Uncharacterized protein	PA5285	Uncharacterized	Hypothetical protein
Q9I020	Uncharacterized protein	PA2823	Uncharacterized	ATP-binding protein

(cont. on next page)

Table 3.13. (continued)

Q9HTY0	Probable secretion pathway ATPase	PA5210	Uncharacterized	Type II/IV secretion system protein
Q9I585	Uncharacterized protein	PA0856	Uncharacterized	DUF2059 domain-containing protein
Q9I749	Uncharacterized protein	PA0083	Uncharacterized	Type VI secretion system contractile sheath small subunit
Q9HZ94	Uncharacterized protein	PA3130	Uncharacterized	Acyl-CoA thioesterase
Q9I2R6	Uncharacterized protein	PA1829	Uncharacterized	Phosphotransferase family protein
Q9HXF7	Nucleoid-associated protein PA3849	PA3849	Uncharacterized	Nucleoid-associated protein YejK
Q9HZ96	Probable short-chain dehydrogenase	PA3128	Uncharacterized	SDR family oxidoreductase

Table 3.14. The newly detected proteins in the presence of 3-HPAA which are uncharacterized.

Protein ID	Protein Name	Gene Name	Function	Protein Blast Results
Q9HTL9	Uncharacterized protein	PA5339	Uncharacterized	RidA Family protein
Q9I622	Uncharacterized protein	PA0496	Uncharacterized	Biotin-dependent carboxyltransferase family protein
Q9HXG8	Uncharacterized protein	PA3836	Uncharacterized	ABC transporter substrate binding protein
Q9HTQ5	Uncharacterized protein	PA5299	Uncharacterized	Acetyl-CoA hydrolase, putative
Q9I3B5	Uncharacterized protein	PA1606	Uncharacterized	DUF3859 Domain containing protein, protein of unknown function
Q9HTC5	Uncharacterized protein	PA5441	Uncharacterized	Hypothetical protein, Outer membrane assembly lipoprotein YfiO
Q9I2Z1	Uncharacterized protein	PA1746	Uncharacterized	Hypothetical protein, Appr-1-p processing protein

3.3.2. The Protein Profile in the Presence of 4-HBA

The results showed that 379 proteins were mutual in control and 4-HBA treated groups (Figure 3.1; regions IV and VII). Number of undetected proteins were 136 (Figure 3.1; regions V and VI) and number of newly detected proteins were 280 (Figure 3.1; regions II and III) after the treatment with 4-HBA.

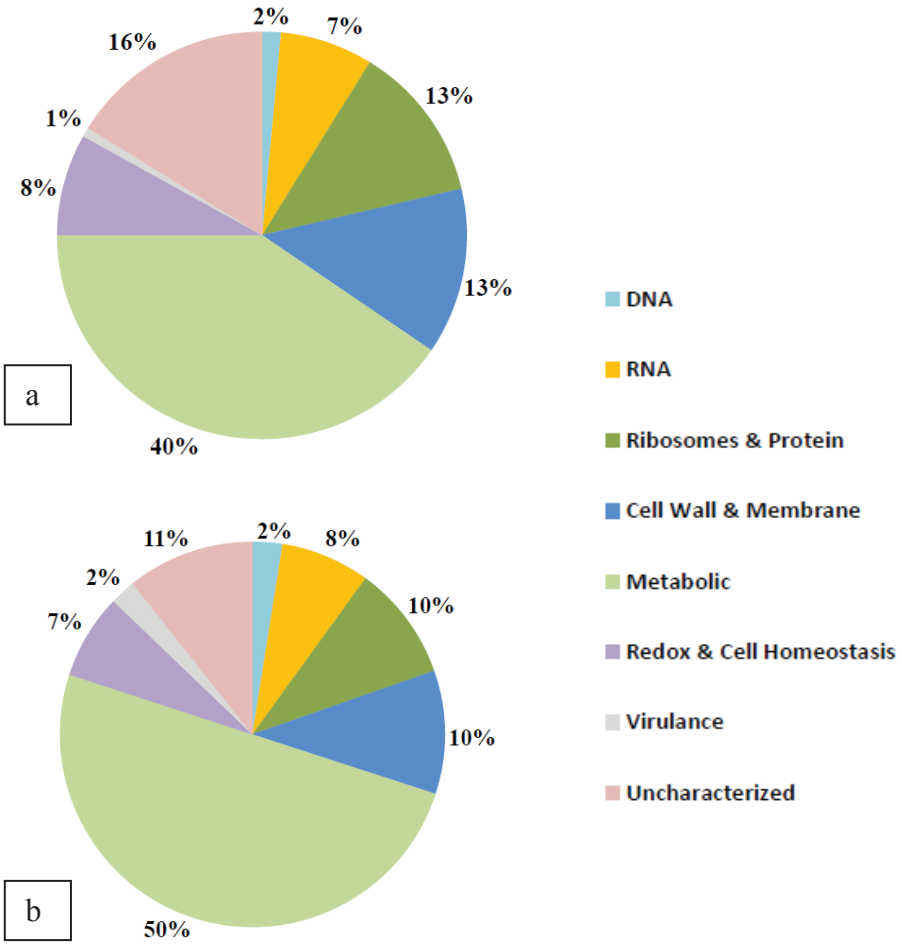

Figure 3.15. The percentages of proteins for each group of function in the presence of 4-HBA. a) Undetected proteins b) Newly detected proteins

The undetected and newly detected proteins were separated according to their functions in UniProt database into eight main groups and their percentages were calculated (Figure 3.20). The protein groups were related with DNA; RNA; ribosomes and protein; cell wall and membrane; metabolism; redox and cell homeostasis; virulence and uncharacterized functioned proteins based on their functions. The undetected proteins in groups of DNA, RNA, ribosomes and protein, cell wall and membrane, metabolism, redox and cell homeostasis, virulence related and uncharacterized proteins showed 2%, 7%, 13%, 13%, 40%, 8%, 1% and 16%, respectively (Figure 3.15 a). The same order of groups, DNA, RNA, ribosomes and protein, cell wall and membrane,

metabolism, redox and cell homeostasis, virulence related and uncharacterized proteins, displayed 2%, 8%, 10%, 10%, 50%, 7%, 2% and 11% for newly detected proteins (Figure 3.15 b). According to these, the metabolism related proteins showed the highest percentages in both undetected and newly detected protein groups. The percentage of newly detected metabolism related proteins percentage was 50% while the undetected proteins' was 40% which showed that 4-HBA treatment result in the production of new proteins more than undetection.

Though, metabolism related proteins show the highest percentage since the general metabolism pathways include various proteins. The virulence related proteins displayed the lowest percentages for both undetected and newly detected proteins. Thus, it could be speculated that the virulence of the bacteria was seldomly affected by 4-HBA treatment.

3.3.2.1. DNA-Related Proteins of 4-HBA Treatment

The STRING database was used to visualize the interaction network of DNA related proteins via gene names. The network of undetected proteins were presented in Figure 3.16 a and of newly detected proteins were in Figure 3.16 b. The complete interaction network of these proteins were demonstrated in Figure 3.16 c in means of undetection and newly detection. In addition, the functions of the undetected proteins and newly detected proteins were shown in Tables 3.15 and 3.16, respectively.

The results demonstrated that the only two proteins related to DNA were undetected after 4-HBA treatment. The most significant result was the undetection of DNA polymerase I which is a key component in DNA replication and repair (Table 3.15). This enzyme is one of the vital enzymes for DNA replication. Since the bacteria survived, the undetection of it might be due to the limitation of LC-ESI-MS/MS method which might detect the proteins up to a level based on ESI conditions. Still, the undetection of this enzyme might demonstrate a significant decrease of it and might show serious defect in DNA replication and repair of the bacteria. DNA polymerase I protein was found in interaction with the proteins related to DNA replication, repair and recombination which were among the newly detected ones (Figure 3.16 and Table 3.16). This might show that the bacteria manage to maintain the DNA replication and repair with these proteins in the absence of DNA polymerase I enzyme. The replication

and repair mechanisms are vital for cell survival, it could be discussed that 4-HBA resulted in important changes in processes related to DNA metabolism. Recombination related proteins, recombination-associated protein RdgC, integration host factor subunit alpha, integration host factor subunit beta and single-stranded DNA-binding protein were newly detected (Figure 3.16 and Table 3.16). Since the bacteria start to activate the DNA recombination mechanisms when replication and repair mechanisms had problems (Sidorenko et al., 2015), *P. aeruginosa* could newly produce these proteins to start recombination for proper replication and repair of DNA. Additionally, bacteria can use recombination for horizontal gene transfer to deal with the toxicity of phenolic compounds (Tavita et al., 2012). The newly detected recombination associated proteins might demonstrate that the bacteria attempt to protect the DNA from damage caused by 4-HBA by recombination. Therefore, the results indicated that the 4-HBA application might lead the changes in DNA replication and cause problems in DNA metabolism of *P. aeruginosa*. The problems arose from undetected proteins might be overcame with the newly detected proteins function in replication, repair and recombination mechanisms.

Table 3.15. The undetected proteins in the presence of 4-HBA related to DNA.

Protein ID	Protein Name	Gene Name	Function
Q9HT80	DNA polymerase I	polA PA5493	DNA-dependent DNA replication, DNA repair
Q9I4Y3	Uncharacterized protein	PA0986	Transposase activity, transposition

Table 3.16. The newly detected proteins in the presence of 4-HBA related to DNA.

Protein ID	Protein Name	Gene Name	Function
Q9HYX7	Recombination-associated protein RdgC	rdgC PA3263	DNA recombination
Q9I7C5	Chromosomal replication initiator protein DnaA	dnaA PA0001	DNA replication initiation, Regulation of DNA replication

(cont. on next page)

Table 3.16. (continued)

Q9I7C4	Beta sliding clamp	dnaN PA0002	DNA strand elongation involved in DNA replication, 3'-5' exonuclease activity, DNA-directed DNA polymerase activity
Q9HZK3	Transcription-repair-coupling factor	mfd PA3002	Transcription-coupled nucleotide-excision repair, DNA damage recognition
Q51473	Integration host factor subunit beta	ihfB himD, PA3161	DNA recombination, regulation transcription, regulation of translation
P40947	Single-stranded DNA-binding protein	ssb PA4232	DNA recombination, DNA repair, DNA replication
Q51472	Integration host factor subunit alpha	ihfA himA, PA2738	DNA recombination, positive regulation of transcription, regulation of translation

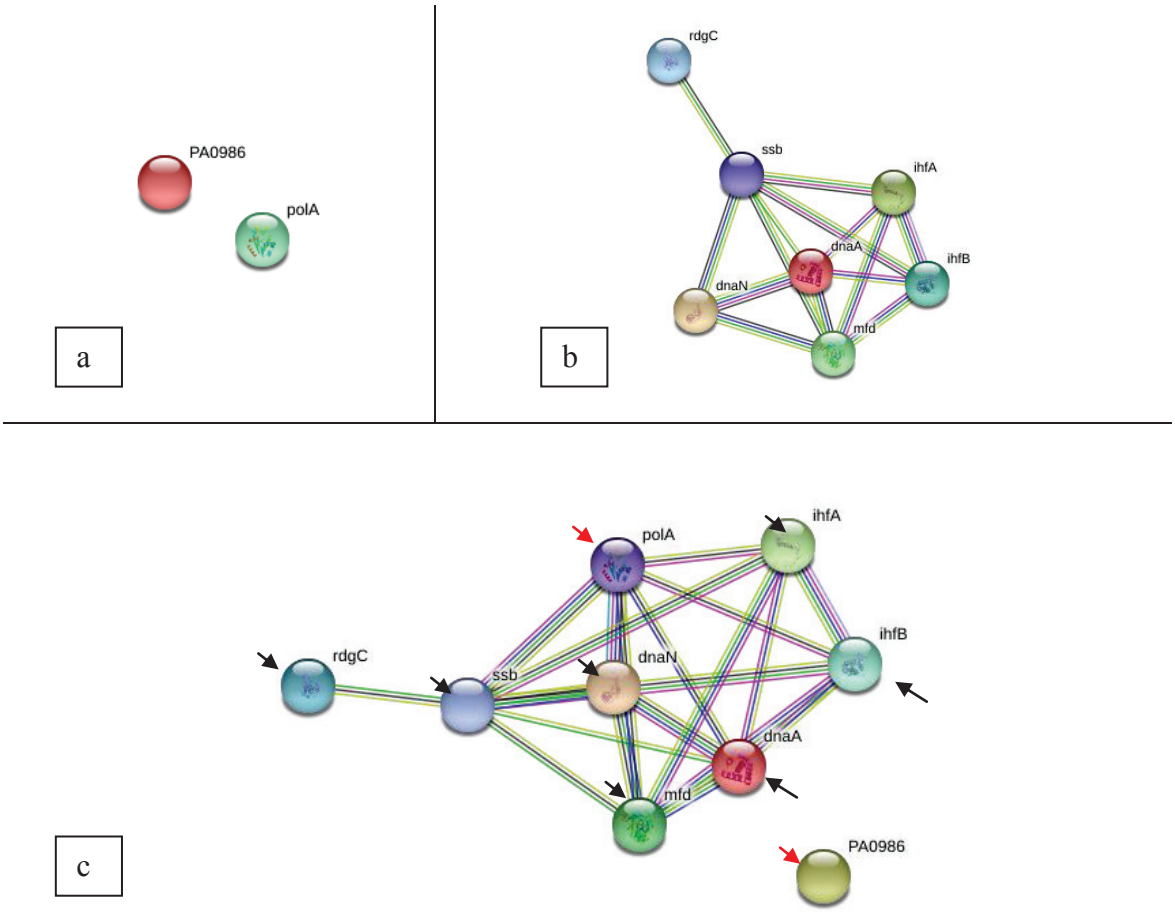

Figure 3.16. String representation of DNA-related proteins in the presence of 4-HBA. a) Undetected proteins b) Newly detected proteins c) The both undetected and newly detected proteins. The proteins were indicated in arrows with different colors (Undetected proteins: red arrows and newly detected proteins: black arrows).

3.3.2.2. RNA-Related Proteins of 4-HBA Treatment

The interaction network of undetected proteins (Figure 3.17 a), newly detected proteins (Figure 3.17 b) and the interaction of those to each other (Figure 3. 18) were determined by STRING. These results showed that, tRNA-specific 2-thiouridylase MnmA protein was undetected while Poly(A) polymerase I and tRNA(Ile)-lysidine synthase were newly detected which have strong interactions. The tRNA-specific 2-thiouridylase MnmA protein is functioned in tRNA wobble position uridine thiolation and tRNA binding. This protein is a thiouridylase for uridine modification in bacteria which senses sulfur atom and combine with it *in vivo* for the modification of tRNAs (Shigi, 2018). It is conserved in evolutionary process and functions specifically on lysine, glutamic acid and glycine tRNAs (Armengod et al., 2014). Since this protein is vital for the thiouridine modification in bacteria (Black and Santos, 2015) and the posttranslational modifications of tRNAs are crucial for the precise translation, the undetection of MnmA protein might result in defects in translation. Hence, the thiouridylation of tRNAs were diminished in the absence of MnmA leading the unrecognition of proper codon by tRNA. The newly detected proteins related to tRNA processing might be used for the maintenance of the translation by carrying out the tRNA modification processes. For example, the protein tRNA(Ile)-lysidine synthase has strong interactions with MnmA protein and it functioned in the modification of tRNA (Ile) by ligating lysedine nucleoside to the cytidine at the wobble position (Numata, 2015) for the production of isoleucine specific tRNA (Nakanishi et al., 2009). The bacteria might manage to continue the translation by fixing the problems that arouse during the tRNA processing by newly detected proteins for compensating the conformation of the subsequent protein. The Poly(A) polymerase I which was also newly detected, is functioned in mRNA polyadenylation as well as rRNA and tRNA processing. Although the Poly(A) polymerase I was partially purified and characterized in 1962, the polyadenylation of RNA in prokaryotes was underestimated. Nowadays, the importance of polyadenylation in prokaryotes are presented in RNA turnover (recycling of RNA) since the polyadenylated mRNAs are protected from exonucleotic degradation. Additionally, it is speculated that the Poly(A) polymerase I has a role in quality-control of target defective tRNAs to exonuclease processes (Hajnsdorf and

Kaberdin, 2018). Thus, new detection of Poly(A) polymerase I might be due to quality control of tRNAs to determine the defective ones caused by 4-HBA exposure.

In addition, stringent starvation protein A was undetected and ribosome-binding ATPase YchF, which has intearction with this protein, was newly detected. Stringent stress response is functioned in the usage of alternative sigma factors in RNA polymerase holoenzyme for the adaptation to stress conditions (Swiecilo and Zych-Wezyk., 2013). Thus, the adaptation control of the bacteria in stress conditions might be diminished in the presence of 4-HBA since stringent starvation protein A was not detected. The newly detected ribosome-binding ATPase YchF is functioned in virulence, various cellular processes and stress responses including DNA repair and oxidative stress response (Hannemann et al., 2016). It could be speculated that the bacteria experienced a significant stress in the presence of 4-HBA. They manage to fight against DNA damage and especially the oxidative stress.

The new detection of the phosphate regulon transcriptional regulatory protein PhoB might show that 4-HBA application might result in the phosphate starvation in *P. aeruginosa*. This protein has a vital role in phosphate limitation responses of the bacteria (Faure et al., 2013). The genes of signal transduction pathway PUMA3 (VreA and VreR) which is used in limited phosphate conditions, is activated by PhoB (Quesada et al., 2016; Faure et al., 2013). In addition to phosphate starvation, the bacteria might also have nitrogen starvation, since the DNA-binding transcriptional regulator NtrC functioned in nitrogen utilization was undetected (Table 3.17).

OxyR, which is one of the main transcriptional regulators of oxidative stress response (Kim et al., 2019), was newly detected after 4-HBA treatment. Thus, it could be speculated that 4-HBA activated the oxidative stress response of *P. aeruginosa*. Since OxyR has roles in iron homeostasis, quorum sensing, protein synthesis and oxidative phosphorylation (Wei et al., 2012), the new detection of OxyR showed that various changes occurred in *P. aeruginosa* metabolism with 4-HBA application. To handle these nutrient limiting and stress conditions, the bacteria might manage to maintain the transcription by newly detection of RpoD (σ^{70}) as well as many other proteins (Table 3.18). Since RpoD is the main sigma factor controlling various housekeeping genes (Potvin et al., 2008) bacteria might try to adapt and survive to the stress conditions arouse by 4-HBA application by increasing the transcription of these housekeeping genes.

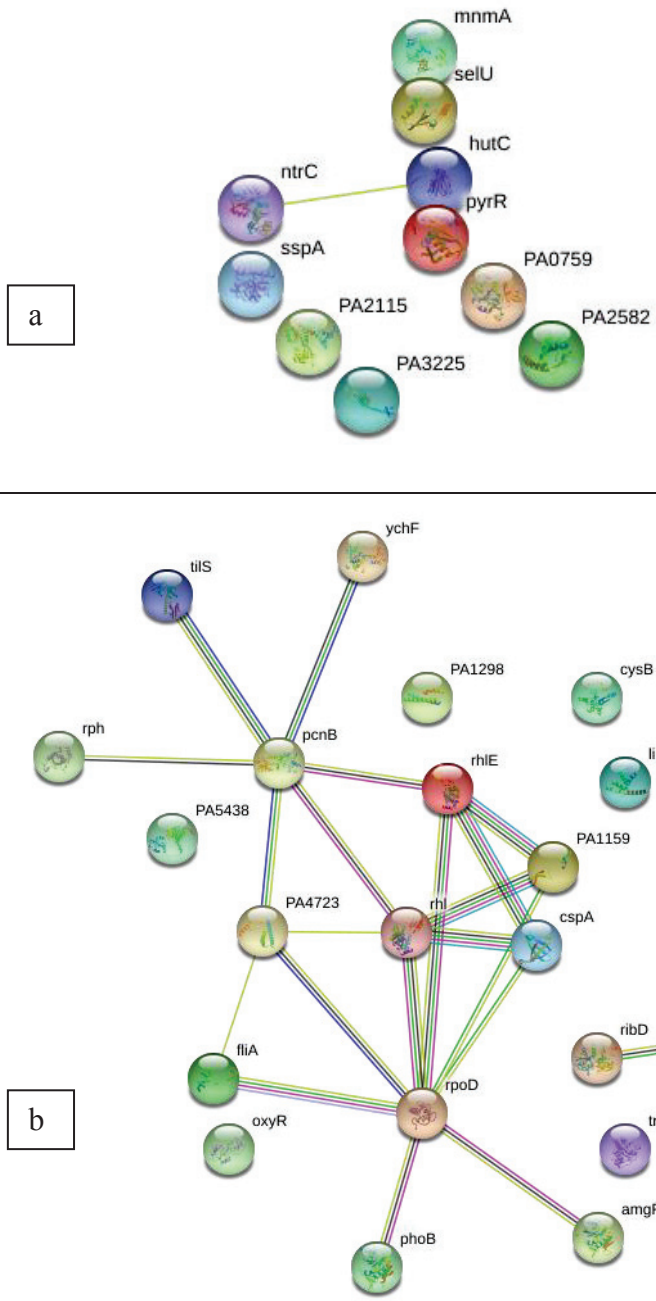

Figure 3.17. String representation of RNA-related proteins in the presence of 4-HBA. a) Undetected proteins b) Newly detected proteins

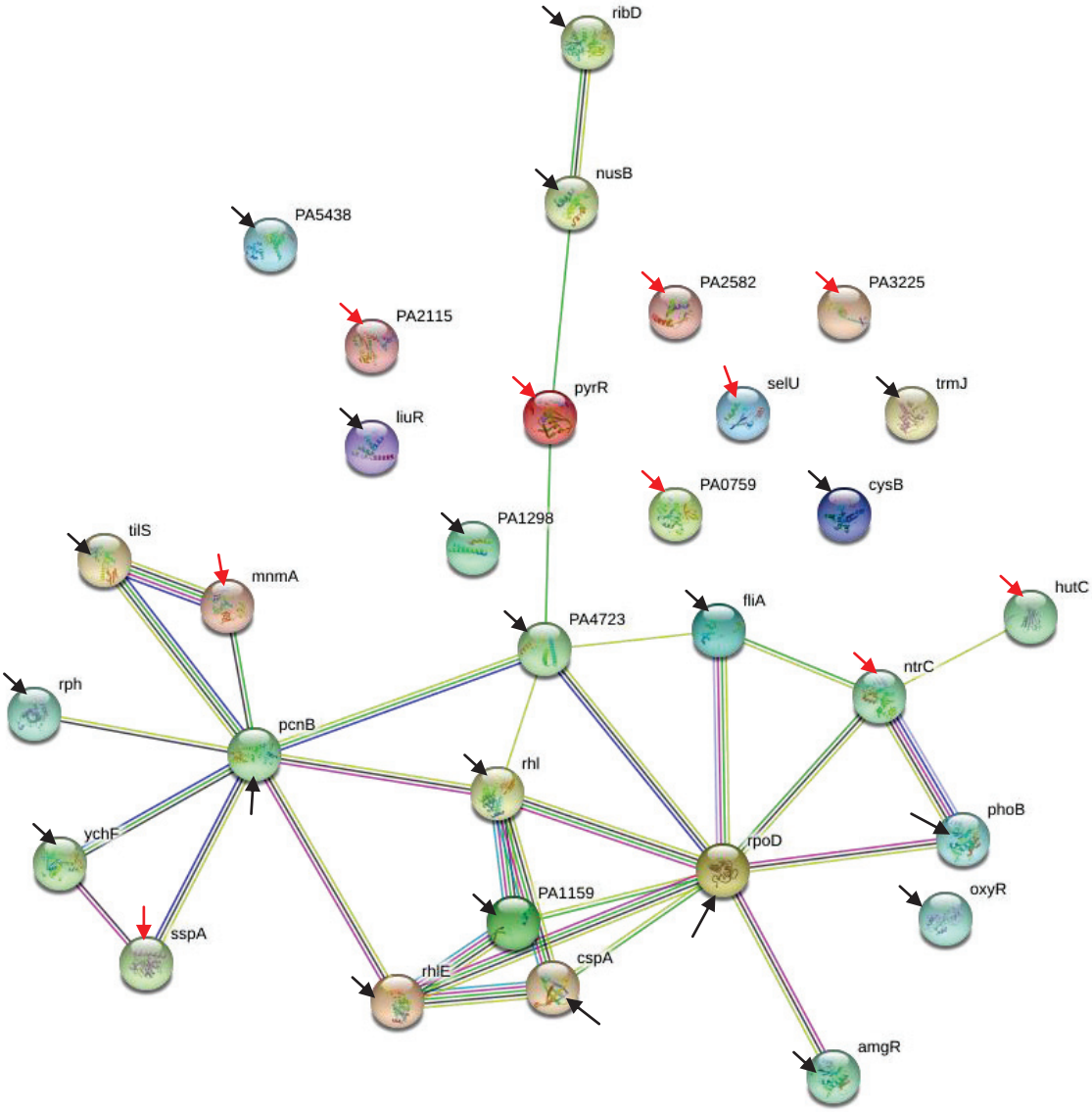

Figure 3.18. String representation of RNA-related undetected and newly detected proteins in the presence of 4-HBA. The significant proteins were indicated in arrows with different colors (Undetected proteins: red arrows and newly detected proteins: black arrows).

Table 3.17. The undetected proteins in the presence of 4-HBA related to RNA.

Protein ID	Protein Name	Gene Name	Function
Q9I0L2	tRNA-specific 2-thiouridylase MnmA	mnmA trmU, PA2626	tRNA wobble position uridine thiolation, tRNA binding
Q9HU78	Histidine utilization repressor	hutC PA5105	Negative regulation of transcription, histidine catabolic process
Q9HVY7	Stringent starvation protein A	sspA PA4428	RNA polymerase core enzyme binding
Q9X6W6	Bifunctional protein PyrR	pyrR PA0403	Nucleoside metabolic process, regulation of transcription
Q9I0Q4	RNA chaperone ProQ	PA2582	Posttranscriptional regulation of gene expression
Q9I200	Probable transcriptional regulator	PA2115	Transcription factor activity, transcription
Q9HU59	DNA-binding transcriptional regulator NtrC	ntrC PA5125	Nitrogen fixation, regulation of nitrogen utilization, regulation of transcription
Q9I5H0	tRNA-modifying protein YgfZ	PA0759	tRNA processing
Q9I382	tRNA 2-selenouridine/geranyl-2-thiouridine synthase	selU PA1643	tRNA-seleno modification
Q9HZ15	Probable transcriptional regulator	PA3225	Transcription factor activity, transcription

Table 3.18. The newly detected proteins in the presence of 4-HBA related to RNA.

Protein ID	Protein Name	Gene Name	Function
Q9HTY9	AmgR	amgR PA5200	Transcription, Transcription regulation, Phosphorelay signal transduction system, proteolysis, transport
Q9HTL4	OxyR	oxyR PA5344	RNA polymerase transcription activator, transcription regulatory region DNA binding source, negative regulation of secondary metabolite biosynthetic process, cell motility, lipid biosynthesis, response to reactive oxygen species
P23620	Phosphate regulon transcriptional regulatory protein PhoB	phoB PA5360	Flagellum-dependent swarming motility, phosphate ion transport positive regulation of cellular response to phosphate starvation, transcription
Q9HV72	Poly(A) polymerase I	pcnB PA4727	mRNA polyadenylation, transcription
P50597	Ribonuclease PH	rph PA5334	rRNA catabolic process, rRNA processing, tRNA processing
P95459	Major cold shock protein CspA	cspA PA3266	Regulation of transcription

(cont. on next page)

Table 3.18. (continued)

G3XD14	RNA polymerase-binding transcription factor DksA	dksA PA4723	Negative regulation of proteolysis, negative regulation of lipid biosynthetic process, negative regulation of transcription, Positive regulation of cellular respiration, positive regulation of transcription regulatory region DNA binding
Q9HXI5	tRNA (cytidine/uridine-2'-O-)-methyltransferase TrmJ	trmJ PA3817	tRNA processing, RNA methyltransferase activity
P26480	RNA polymerase sigma factor RpoD	rpoD rpoDA, PA0576	DNA binding transcription factor activity, sigma factor activity, transcription initiation
Q9I295	Regulator of liu genes	liuR PA2016	Regulation of transcription, isoprenoid catabolic process
Q9I446	Uncharacterized protein	PA1298	Regulation of transcription, DNA binding, metal ion binding
Q9HXE5	ATP-dependent RNA helicase RhlB	rhlB rhl, PA3861	Helicase activity, RNA secondary structure unwinding
Q9HWX2	Riboflavin biosynthesis protein RibD	ribD PA4056	Riboflavin biosynthetic process, RNA modification
Q9HVC2	Ribosome-binding ATPase YchF	ychF PA4673	ATPase activity, ATP binding, ribosomal large subunit binding, ribosome binding
Q9I4H8	Probable cold-shock protein	PA1159	Regulation of transcription
Q9I689	ATP-dependent RNA helicase RhlE	rhlE PA0428	Bacterial-type flagellum-dependent swarming motility, ribosome assembly, RNA secondary structure unwinding, single-species biofilm formation
P29248	RNA polymerase sigma factor FliA	fliA rpoF, PA1455	Transcription initiation, positive regulation of cell motility
Q9HXZ3	tRNA(Ile)-lysidine synthase	tilS PA3638	Ligase activity, tRNA processing
G3XCU6	Transcriptional regulator CysB	cysB PA1754	RNA polymerase transcriptional activator activity, positive regulation of transcription, cysteine biosynthetic process
Q9HWX6	Transcription antitermination protein NusB	nusB PA4052	Transcription, transcription antitermination
Q9HTC8	Probable transcriptional regulator	PA5438	Glucose 6-phosphate metabolic process, regulation of transcription

3.3.2.3. Ribosome and Protein-Related Proteins of 4-HBA Treatment

The 4-HBA treatment showed undetection (Figure 3.19 a) and newly detection protein profiles (Table 3.19 b) whose interactions were demonstrated in Figure 3.20. The undetection or new detection of t-RNA ligases were presented after 4-HBA treatment: Phenylalanine-tRNA ligase alpha subunit and glycine-tRNA ligase alpha subunit were undetected (Table 3.19) while methionine-tRNA ligase, valine-tRNA ligase, histidine-tRNA ligase, glutamate-tRNA ligase, tyrosine-tRNA ligase 2,

threonine-tRNA ligase, phenylalanine-tRNA ligase beta subunit and isoleucine-tRNA ligase were newly detected (Table 3.20). The changes of tRNA ligases after 4-HBA exposure indicated the bacteria make modifications in their protein translation since the transport of amino acids to the ribosomes are carried out mainly by tRNA ligases (Ferro et al., 2018). In addition, the approach of targeting tRNA ligases is a compelling concept in the antimicrobial agent development (Ho et al., 2018; Lee et al., 2018). Thus, the undetection of some tRNA ligases might show that one of the targets of 4-HBA for antimicrobial effect, might be tRNA ligases.

Another important point was the undetection of many small or large subunit components of ribosome after 4-HBA exposure (Table 3.19 and 3.20). Since in 3-HPAA treatment only led the undetection of one small subunit (S15) (Table 3.5) and new detection of one small subunit (S18) (Table 3.6), it might be speculated that 4-HBA resulted in more detrimental defects on ribosome structure and assembly than 3-HPAA did. The undetected ribosome-related proteins were; 30S ribosomal proteins S15, S11, S2, small ribosomal subunit biogenesis GTPase RsgA, ribosomal RNA small subunit methyltransferase G, ribosomal RNA large subunit methyltransferase J and ATP-dependent RNA helicase DeaD (has functions in ribosomal large subunit assembly).

On the other hand, 30S ribosomal protein S18, ribosomal RNA small subunit methyltransferase H, 50S ribosomal protein L23, ribRibosomal RNA large subunit methyltransferase K/L and ribosomal large subunit pseudouridine synthase D were newly detected.

According to these results, it is clear that 4-HBA mostly targeted the small subunit components and the bacteria began to produce different small and large subunit components to compensate the defects in the ribosome structure and assembly to maintain proper translation. Thus, 4-HBA affected the protein translation via damaging the ribosome not only by changing the small and large subunit components but also by changing the proteins related to translational initiation such as the undetection of translation initiation factor IF-1 and methyltransferases.

Since the aminopeptidases determine the structure and function of the proteins by cleaving the N-terminal (Nandan and Nampoothri, 2017), the changes in these proteins might indicate the significant changes in the protein structure and function, thereby the whole metabolism. SecB which was undetected while SecA was newly detected after 4-HBA treatment.

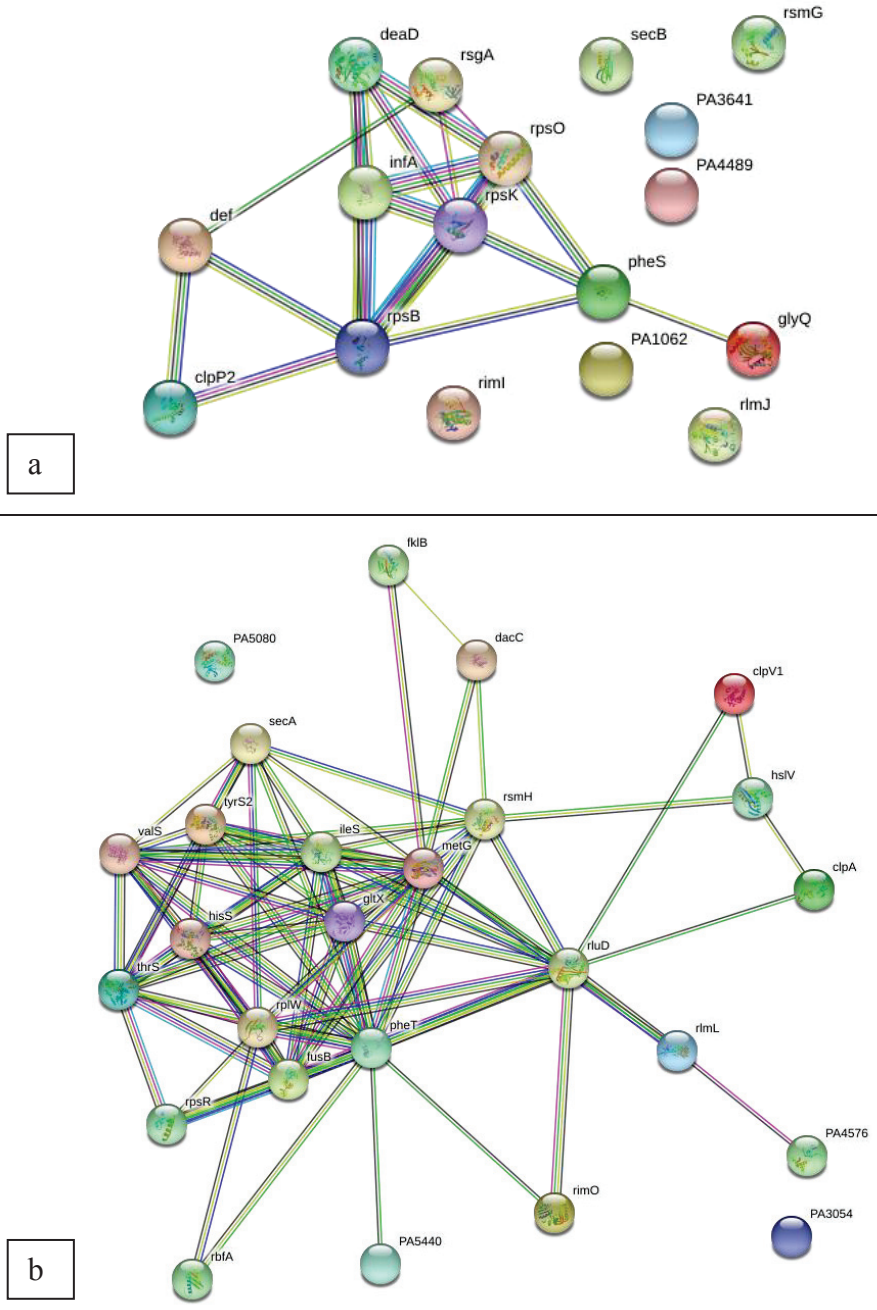

Figure 3.19. String representation of ribosomes and protein-related proteins in the presence of 4-HBA. a) Undetected proteins b) Newly detected proteins

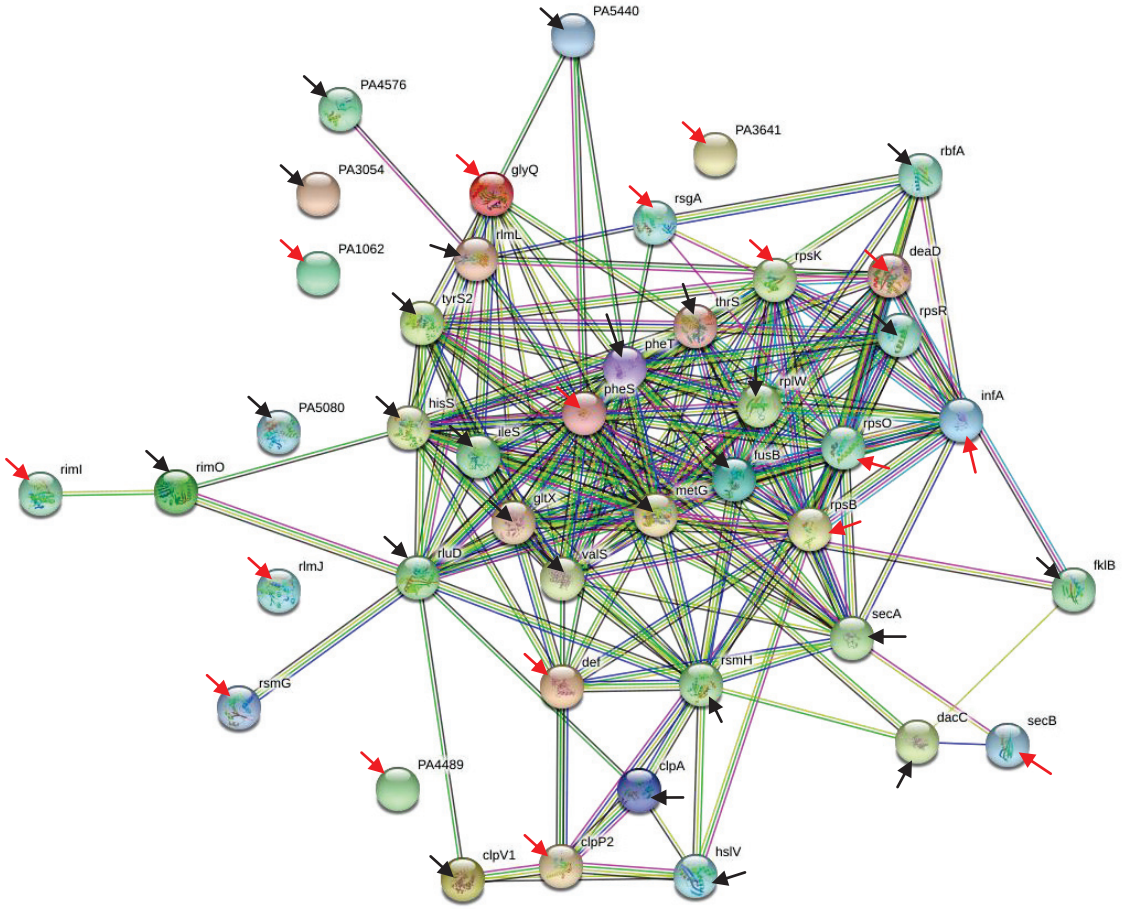

Figure 3.20. String representation of ribosomes and protein-related undetected and newly detected proteins in the presence of 4-HBA. The proteins were indicated in arrows with different colors (Undetected proteins: red arrows and newly detected proteins: black arrows).

The translocation of preproteins with N-terminal signal across the cell membrane is performed by Sec complex (Krishnan et al., 2009). SecA is the ATPase unit of the translocation complex while SecB is the soluble cytosolic protein which recognizes the N-terminal signal of preproteins to direct them to SecA (Driessen et al., 2001). The undetection of SecB indicated a serious damage on the Sec complex which might lead detrimental defects in bacterial protein metabolism.

Various endopeptidases and carboxypeptidases were newly detected while endopeptidase inhibitor Alpha-2-macroglobulin homolog was undetected after 4-HBA treatment similarly to the results of 3-HPAA treatment. The bacteria uses

carboxypeptidases and endopeptidase together for peptidoglycan units recycling as energy-saving rather than producing them from the scratch (Templin et al., 1999; Meyer et al., 2018). The recycling is crucial for the cell viability, such that, inhibition of this process results in autolysis of *E. coli* (Templin et al., 1999). The undetection of endopeptidase inhibitor and new detection of various endopeptidases were noticed in the presence of 4-HBA. In addition, the D-ala-D-ala-carboxypeptidase that cleaves the terminal D-alanine from muramyl pentapeptide was also newly detected which functions in the production of peptidoglycan layer of the bacteria (Ghosh et al., 2008; Meyer et al., 2018). These results might indicate a serious damage in the cell envelope and the bacteria increased the recycling process to repair the peptidoglycan layer by reusing the peptidoglycan units came from membrane damage. This stress might result in the reduction of the bacterial growth in the case of 4-HBA exposure.

3.3.2.4. Cell Wall and Membrane-Related Proteins of 4-HBA Treatment

The undetected proteins in the presence of 4-HBA were demonstrated in Figure 3.21 a and newly detected ones were in 3.21 b. According to interaction network of these proteins (Figure 3.22), the undetected protein CheY which is functioned in flagellum-dependent cell motility, chemotaxis and positive regulation of single-species biofilm formation was undetected (Table 3.21) while B-type flagellin (FliC) functioned in flagellum-dependent cell motility, bacterial-type flagellum organization was newly detected (Table 3.22).

Since both interacted proteins had roles in flagellum-dependent motility, the undetection of CheY might demonstrate a defect in this system. This protein is used for flagellum rotations in motility for the escape from the undesirable environmental conditions (Chaban et al., 2015). The newly detected protein B-type flagellin is also functioned in flagellum-dependent motility and flagellum organization (Bakht azad et al., 2018). Hence, the bacteria managed to escape the toxic conditions caused by 4-HBA by continuing the flagellum-dependent motility. Although the protein Type IV pilus biogenesis factor PilY1 was undetected, other proteins related to pilus formation, PilV and PilF, which were functioned in pilus assembly, were newly detected. This might

show that 4-HBA resulted in the damage in pilus formation and the bacteria maintained this process by other related proteins.

Table 3.19. The undetected proteins in the presence of 4-HBA related to ribosome and protein.

Protein ID	Protein Name	Gene Name	Function
P65116	Translation initiation factor IF-1	infA PA2619	Ribosome binding, rRNA binding, translation initiation factor activity
Q9HVT2	Alpha-2-macroglobulin homolog	PA4489	Endopeptidase inhibitor activity
Q9HYR9	ATP-dependent Clp protease proteolytic subunit 2	clpP2 PA3326	Endopeptidase activity
Q9HXZ0	Probable amino acid permease	PA3641	Alanine:sodium symporter activity
Q9HU56	Protein-export protein SecB	secB PA5128	Protein tetramerization, protein transport
Q9HUL3	Small ribosomal subunit biogenesis GTPase RsgA	rsgA PA4952	Ribosome biogenesis
Q9HV58	30S ribosomal protein S15	rpsO PA4741	ribosome constituent, translation
Q9HWF8	30S ribosomal protein S11	rpsK PA4240	Maturation of SSU-rRNA from tricistronic rRNA transcript, ribosomal small subunit assembly, translation
Q9I003	ATP-dependent RNA helicase DeaD	deaD PA2840	ribosomal large subunit assembly, RNA catabolic process, RNA secondary structure unwinding
Q9I0A3	Phenylalanine--tRNA ligase alpha subunit	pheS PA2740	Phenylalanine--tRNA ligase activity
Q9HVB7	Ribosomal-protein-alanine acetyltransferase	rimI PA4678	N-terminal protein amino acid acetylation
Q9I7A8	Peptide deformylase	def PA0019	Co-translational protein modification, N-terminal protein amino acid modification, peptidyl-methionine modification, translation
Q9I4R2	Uncharacterized protein	PA1062	Protein acetylation
Q9HT10	Ribosomal RNA small subunit methyltransferase G	rsmG PA5564	rRNA (guanine-N7)-methylation
Q9I7B7	Glycine--tRNA ligase alpha subunit	glyQ PA0009	Glycine--tRNA ligase activity
Q9HUF0	Ribosomal RNA large subunit methyltransferase J	rlmJ PA5019	rRNA base methylation
O82850	30S ribosomal protein S2	rpsB PA3656	Structural constituent of ribosome, translation

Table 3.20. The newly formed proteins in the presence of 4-HBA related to ribosome and protein.

Protein ID	Protein Name	Gene Name	Function
Q9HYC7	Methionine--tRNA ligase	metG PA3482	Methionine--tRNA ligase activity
Q9HXH0	Valine--tRNA ligase	valS PA3834	Valine--tRNA ligase activity
Q9HXJ5	Histidine--tRNA ligase	hisS PA3802	Histidine--tRNA ligase activity
Q9HUA3	Proline iminopeptidase	PA5080	Aminopeptidase activity
G3XD74	D-ala-D-ala-carboxypeptidase	dacC PA3999	Endopeptidase activity, D-ala-D-ala-carboxypeptidase activity
Q9HWD7	50S ribosomal protein L23	rplW PA4261	Ribosomal large subunit assembly, translation
Q9HZG0	RibRibosomal RNA large subunit methyltransferase K/L	rlmL PA3048	23S rRNA (guanine(2445)-N(2))-methyltransferase activity, rRNA (guanine-N2-)-methyltransferase activity, RNA binding,
Q9XCL6	Glutamate--tRNA ligase	gltX PA3134	Glutamate--tRNA ligase activity
Q9HV56	Ribosome-binding factor A	rbfA PA4743	Ribosome biosynthesis
Q9I742	Protein ClpV1	clpV1 PA0090	Protein metabolic process, ATP binding
Q9I0L8	ATP-binding protease component ClpA	clpA PA2620	Protein unfolding, peptidase activity
Q9HVL2	Peptidyl-prolyl cis-trans isomerase	fklB PA4572	Peptidyl-prolyl cis-trans isomerase activity, protein folding
Q9HUC6	ATP-dependent protease subunit HslV	hslV PA5053	Endopeptidase activity, protein catabolic process
Q9I5Q3	Tyrosine--tRNA ligase 2	tyrS2 PA0668	Tyrosine--tRNA ligase activity
Q9I099	Threonine--tRNA ligase	thrS PA2744	Threonine--tRNA ligase activity
Q9I0A4	Phenylalanine--tRNA ligase beta subunit	pheT PA2739	Phenylalanine--tRNA ligase activity
Q9HUN0	30S ribosomal protein S18	rpsR PA4934	rRNA binding, structural constituent of ribosome, translation
E1JGJ8	Peptide chain release factor 2	prfB PA3701	Translation release factor activity, codon specific
Q9HVZ5	Ribosomal RNA small subunit methyltransferase H	rsmH mraW, PA4420	rRNA base methylation

(cont. on next page)

Table 3.20. (continued)

Q9I244	Elongation factor G 2	fusB fusA2, PA2071	GTP binding, translation elongation factor activity
P33640	Ribosomal large subunit pseudouridine synthase D	rluD PA4544	Enzyme-directed rRNA pseudouridine synthesis
Q9HVM4	Isoleucine--tRNA ligase	ileS PA4560	Isoleucine--tRNA ligase activity
Q9HVK8	Endopeptidase La	PA4576	Endopeptidase activity, protein catabolic process
Q9HTC6	Probable peptidase	PA5440	Peptidase activity
Q9HZF4	Uncharacterized protein	PA3054	Metallocarboxypeptidase activity, zinc ion binding
Q9LCT3	Protein translocase subunit SecA	secA PA4403	Protein import, Protein targeting, protein transport by Sec complex, Part of the Sec protein translocase complex.
Q9I541	Ribosomal protein S12 methylthiotransferase RimO	rimO PA0916	Peptidyl-L-beta-methylthioaspartic acid biosynthetic process from peptidyl-aspartic acid, tRNA modification

The profile of main proteins for cell division, Fts proteins, was changed in the presence of 4-HBA. The proteins FtsH and FtsY were undetected while FtsZ was newly detected.

The FtsZ protein is the main protein in the cell division process of the bacteria since it is functioned in the initiation of the septum (Srinivasan et al., 2008). The new detection of it might be due to the bacteria intent to maintain the cell division in the undetection of FtsH and FtsY. Among these proteins, FtsH is functioned in the regulation of the cell metabolism after an environmental stress, quality control of the membrane proteins (Langklotz et al., 2012) as well as posttranslation of various transcription factors and enzymes (Narberhaus et al., 2009).

Another crucial process, targeting the nascent polypeptide chains to the membrane for transferring the new proteins across the membrane is achieved by FtsY (Dalbey et al., 2011) which was also undetected as well as YidC protein which takes roles in the small protein insertion into the membrane in coordination with Sec proteins (Dalbey et al., 2011) and proteolytic cleavage of the membrane or cytoplasmic proteins (Kiefer and Kuhn, 2018). The undetection of these proteins might show that 4-HBA application resulted in serious defects in the bacterial cell membrane structure and integrity which would lead to bacterial death, eventually.

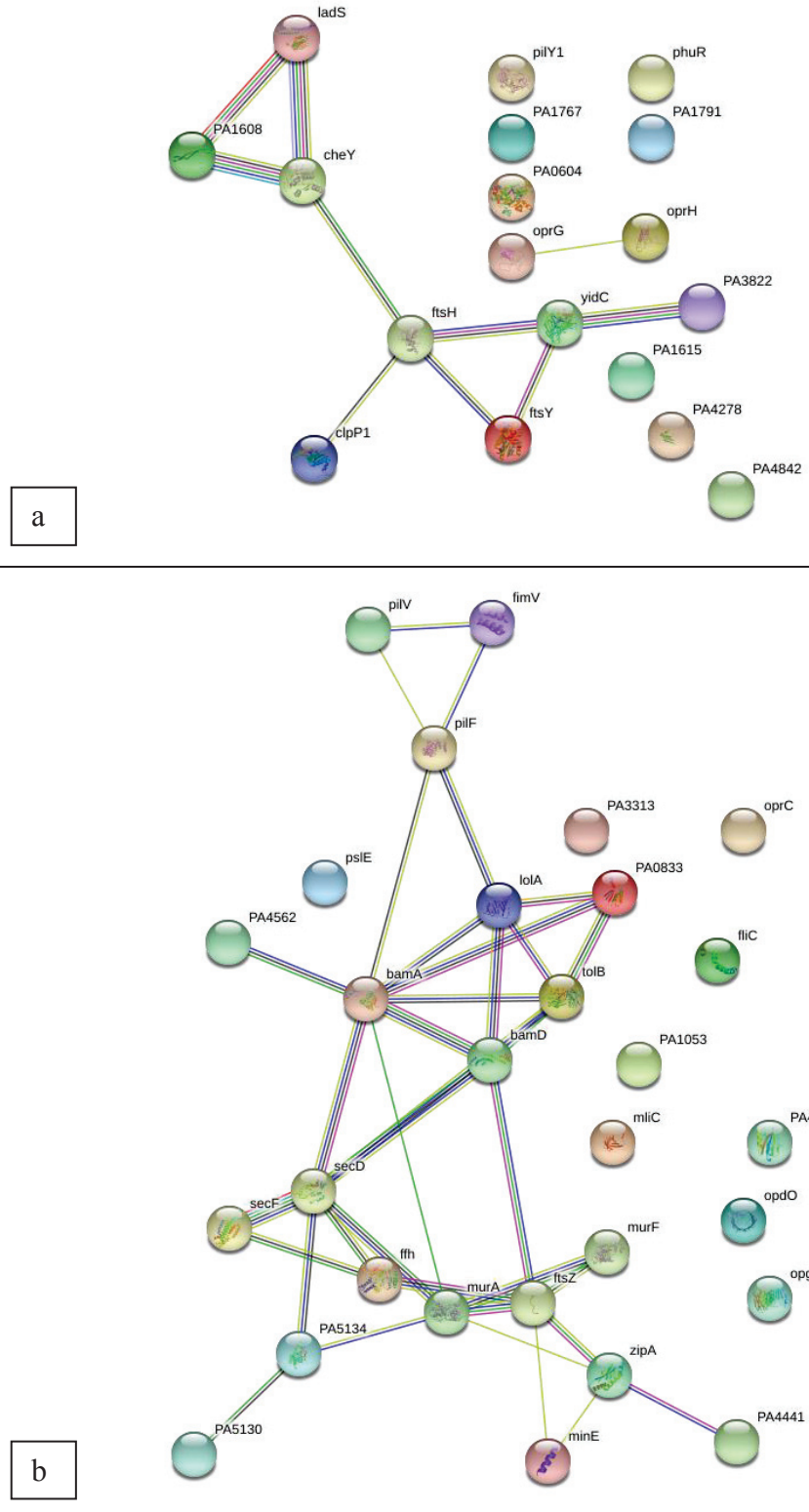

Figure 3.21. String representation of cell wall and membrane-related proteins in the presence of 4-HBA. a) Undetected proteins b) Newly detected proteins

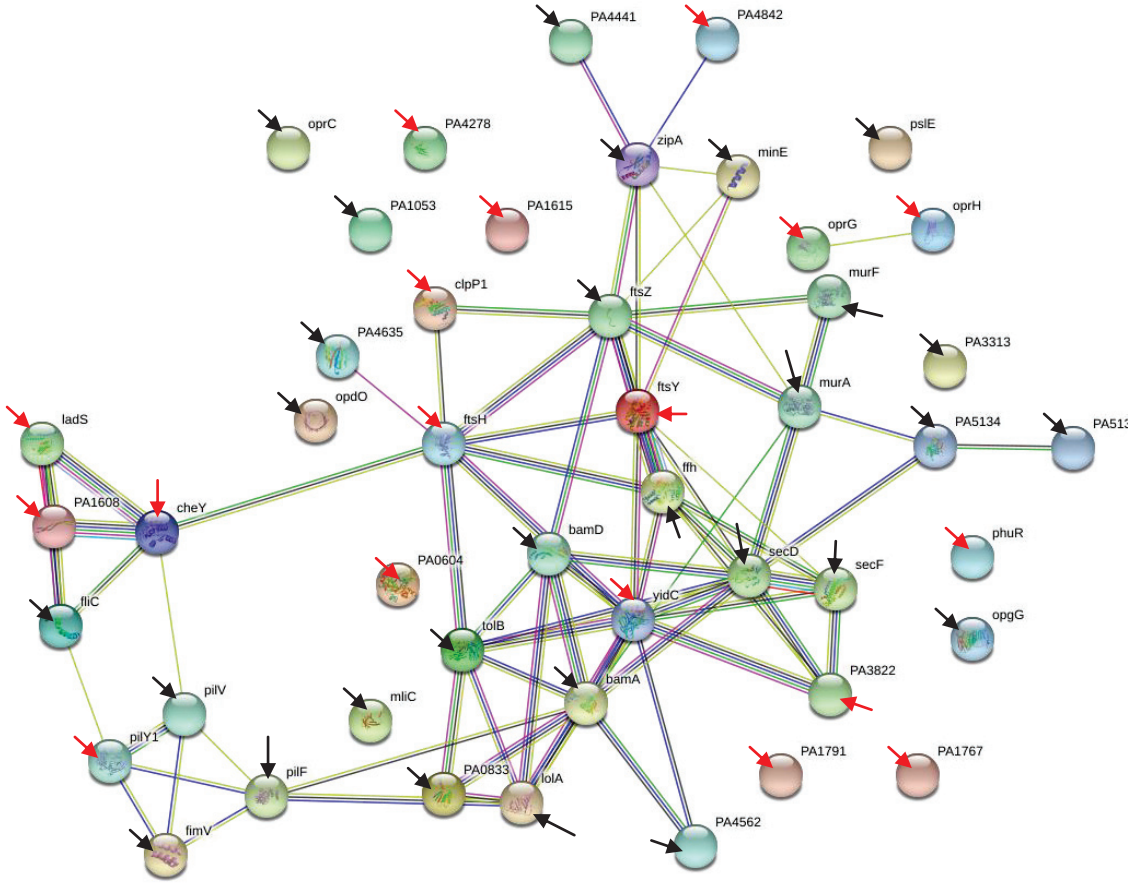

Figure 3.22. String representation of cell wall and membrane-related undetected and newly detected proteins in the presence of 4-HBA. The proteins were indicated in arrows with different colors (Undetected proteins: red arrows and newly detected proteins: black arrows).

Table 3.21. The undetected proteins in the presence of 4-HBA functioned in cell wall and membrane.

Protein ID	Protein Name	Gene Name	Function
Q9HT06	Membrane protein insertase YidC	yidC PA5568	Membrane insertase activity
Q9I5T4	Probable binding protein component of ABC transporter	PA0604	Membrane transport
Q51455	Chemotaxis protein CheY	cheY PA1456	Flagellum-dependent cell motility, chemotaxis, phosphorelay signal transduction system, positive regulation of single-species biofilm formation
Q9I2U1	ATP-dependent Clp protease proteolytic subunit 1	clpP1 PA1801	Flagellum dependent cell motility, single species biofilm formation, response to antibiotic
Q9HVM8	Type IV pilus biogenesis factor PilY1	pilY1 PA4554	Type IV pilus-dependent motility
Q9HUW8	Uncharacterized protein	PA4842	Transmembrane protein
Q9I3A7	Probable lipase	PA1615	Integral component of membrane
Q9HV88	Heme/hemoglobin uptake outer membrane receptor PhuR	phuR PA4710	Response to iron ion, heme transport
Q9HXI0	Uncharacterized protein	PA3822	Integral component of membrane
Q9HV48	ATP-dependent zinc metalloprotease FtsH	ftsH PA4751	Cell division, cellular response to antibiotic, protein catabolic process, proteolysis
Q9HWC2	Uncharacterized protein	PA4278	Peptidoglycan binding
Q9I6C1	Signal recognition particle receptor FtsY	ftsY PA0373	SRP-dependent cotranslational protein targeting to membrane
Q9I2V1	Uncharacterized protein	PA1791	Transmembrane protein
G3XD11	PhoP/Q and low Mg2+ inducible outer membrane protein H1	oprH PA1178	Integral component of membrane
Q9I3B3	Probable chemotaxis transducer	PA1608	Transmembrane signaling receptor activity, chemotaxis
Q9HWW1	Outer membrane protein OprG	oprG PA4067	Transmembrane transport
Q9HX42	Lost Adherence Sensor, LadS	ladS PA3974	Phosphorelay sensor kinase activity
Q9I2X2	Uncharacterized protein	PA1767	Transmembrane protein

On the other hand, SecD, SecF, BamA, BamD TolA and TolB, which had interactions with YidC were newly detected. Sec complex is functioned in the transfer of preproteins possessing N-terminal signal through the membrane (Krishnan et al., 2009). SecDFyajC complex is one of the complexes that is involved in the Sec complex and is required for the proper insertion of new proteins into the membrane (Dalbey et al., 2011) and Tol-Pal complex, which includes TolA and TolB, is required for outer membrane integrity of Gram negative bacteria (Dubuisson et al., 2005). Similarly, BamA and BamD proteins had roles in cell envelope organization and cell assembly. Thus, new detection of these proteins might be due to continue the cell wall integrity

and structure caused by 4-HBA. Thus, protein targetting, membrane insertion, cell division and membrane integrity of *P. aeruginosa* were seriously affected by 4-HBA exposure. In addition, these damaged were determined in SEM images of the bacteria as a collapse line on the bacteria surfaces after 4-HBA treatment (Figure 2.3 e and f) which visually demonstrated the serious damage of 4-HBA on cell envelope.

Table 3.22. The newly detected proteins in the presence of 4-HBA functioned in cell wall and membrane.

Protein ID	Protein Name	Gene Name	Function
Q9HUA5	Glucans biosynthesis protein G	opgG PA5078	Beta-Glucan biosynthetic process, osmoregulated periplasmic glucan (OPG) biosynthesis (Glycan metabolism)
Q9I0M4	Outer-membrane lipoprotein carrier protein	lolA PA2614	Lipoprotein transporter activity, Lipoprotein localization to outer membrane, chaperone-mediated protein transport across periplasmic space
Q9I5A7	Uncharacterized protein	PA0833	Cell outer membrane, integral component of membrane
Q9HYZ5	Cell division topological specificity factor	minE PA3245	Cell cycle, cell division, regulation of division septum assembly
Q9HVM2	Probable lipid II flippase MurJ	murJ PA4562	Peptidoglycan biosynthetic process, cell wall organization, lipid translocation, regulation of cell shape
Q9HXJ2	Type 4 fimbrial biogenesis protein PilF	pilF PA3805	TPR domain binding, pilus assembly, type IV pilus biogenesis type IV pilus-dependent motility
Q9HXI2	Protein translocase subunit SecF	secF PA3820	Intracellular protein transport
Q9HXP8	Signal recognition particle protein	ffh PA3746	SRP-dependent cotranslational protein targeting to membrane, 7S RNA binding, GTPase activity
Q9I574	Membrane-bound lysozyme inhibitor of C-type lysozyme	mliC PA0867	Cell outer membrane
G3XD84	Type 4 fimbrial biogenesis protein PilV	pilV PA4551	Pilus assembly, type IV pilus biogenesis, type IV pilus-dependent motility
Q9I1N4	PslE	pslE PA2235	Extracellular polysaccharide biosynthetic process, single-species biofilm formation
G3XD89	Putative copper transport outer membrane porin OprC	oprC PA3790	Receptor, cell outer membrane component
Q9I202	Pyroglutatmate porin OpdO	opdO PA2113	Integral component of membrane

(cont. on next page)

Table 3.22. (continued)

Q9HYT1	Uncharacterized protein	PA3313	Transporter activity, transmembrane transport
Q9HU54	Uncharacterized protein	PA5130	Integral component of membrane
Q9I4S1	Uncharacterized protein	PA1053	Outer membrane component
Q9HVF6	Uncharacterized protein	PA4635	Integral component of membrane
Q9HVW7	UDP-N-acetylglucosamine 1-carboxyvinyltransferase	murA PA4450	Peptidoglycan biosynthetic process, cell cycle, cell division, cell wall organization regulation of cell shape, UDP-N-acetylgalactosamine biosynthetic process
P50601	Tol-Pal system protein TolB	tolB PA0972	Cell cycle, cell division, protein import
Q9HVX4	Uncharacterized protein	PA4441	Integral component of membrane
P72151	B-type flagellin	fliC PA1092	Flagellum-dependent cell motility, bacterial-type flagellum organization
Q9HXI1	Protein translocase subunit SecD	secD PA3821	Protein transport, intracellular protein transport
Q9HU50	Probable carboxyl-terminal protease	PA5134	Cell envelope organization, cell wall biogenesis, pathogenesis, signal transduction
P33641	Outer membrane protein assembly factor BamD	bamD PA4545	Cell envelope organization, protein insertion into membrane
Q9HZA6	Motility protein FimV	fimV PA3115	Peptidoglycan binding
Q9I3I5	Cell division protein ZipA	zipA PA1528	Cell septum assembly
Q9HXY4	Outer membrane protein assembly factor BamA	opr86 bamA, PA3648	Gram-negative-bacterium-type cell outer membrane assembly, protein insertion into membrane
P47204	Cell division protein FtsZ	ftsZ PA4407	Cell cycle, cell division
Q9HVZ7	UDP-N-acetylmuramoyl-tripeptide--D-alanyl-D-alanine ligase	murF PA4416	Peptidoglycan biosynthetic process, Cell cycle, cell division, cell wall organization, peptidoglycan biosynthetic process, regulation of cell shape

3.3.2.5. Metabolism-Related Proteins of 4-HBA Treatment

The 4-HBA exposure resulted in various metabolic changes. Since the bacteria are in the adaptation period to environmental conditions, the undetection of proteins (Figure 3.23) and newly detected ones (Figure 3.24) with various interactions (Figure 3.25) were expected. In addition, these changes might indicate the potential targets of 4-HBA for the antimicrobial effect. For instance, the proteins functioned in lipid

metabolism as fatty acid metabolic process and lipid catabolic processes were presented as undetected (Table 3.23) while fatty acid biosynthetic process proteins were newly detected (Table 3.24). This might be due to the usage of fatty acids in the repair process of defects of the cell membrane resulted by 4-HBA as well as cell wall maintenance. The changes in energy metabolisms were presented such as undetection of quinolinate synthase A functioned in NAD biosynthetic process and newly detection of NH(3)-dependent NAD(+) synthetase which is vital for the survival. Besides these, the proteins of phenazine biosynthesis process, Phenazine biosynthesis protein PhzB1 and 5-methylphenazine-1-carboxylate 1-monooxygenase were undetected. Since phenazine is the soluble blue pigment with virulence properties (Dietrich et al., 2006, Ugurlu et al., 2016), 4-HBA treatment might led to reduced virulence. The color differences in the bacterial cultures which were 4-HBA treated or untreated (Figure 2.2. b) might be explained by the undetection of these proteins.Another important result was the undetection of proteins related to iron transport, iron assimilation and sulfate homeostasis, FptA PA4221, PA2033 and CysP PA1493, CysA PA0280, Sbp PA0283, respectively. The new detection of sulfite reductase (CysI PA1838) functioned in response to sulfate starvation and new detection of probable metal-transporting P-type ATPase might also show the sulfate and iron starvation.

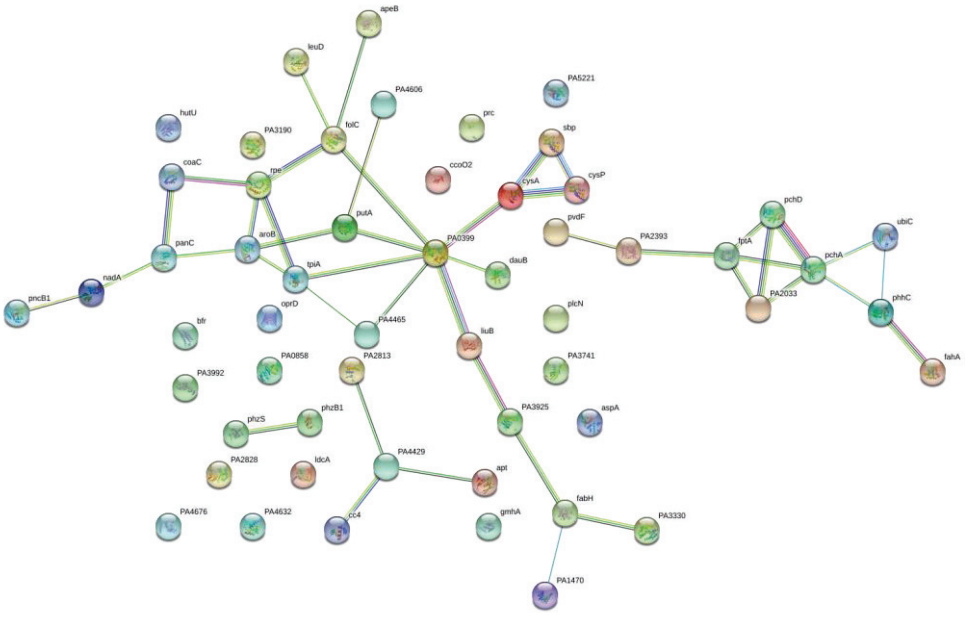

Figure 3.23. String representation of metabolism-related undetected proteins in the presence of 4-HBA.

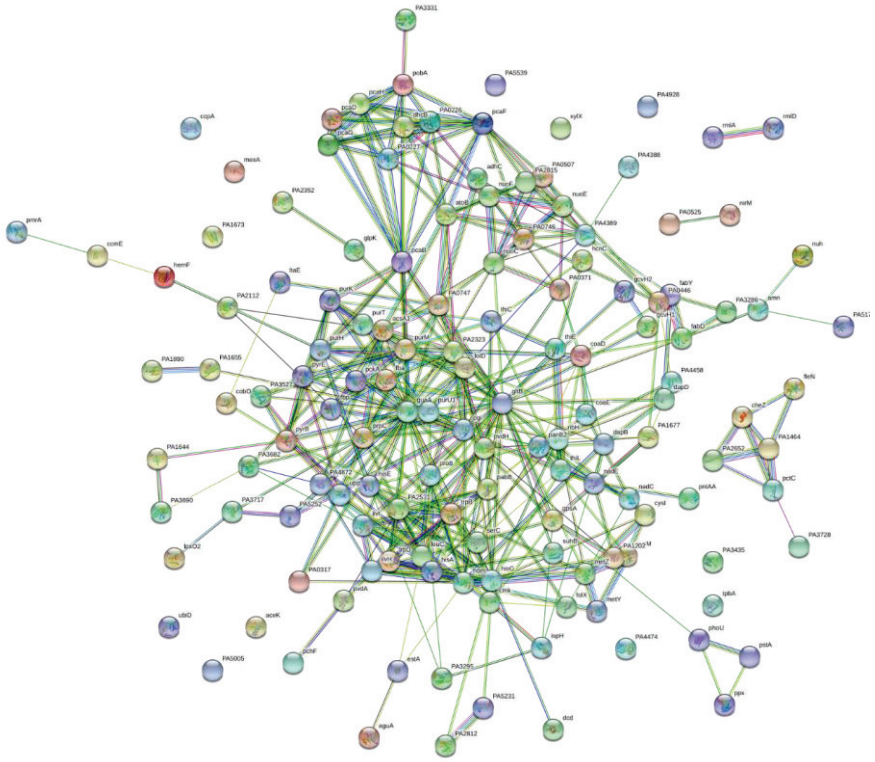

Figure 3.24. String representation of metabolism-related newly detected proteins in the presence of 4-HBA.

The pyoverdine proteins (Pvd) were demonstrated to have important roles in iron uptake (Drehe et al., 2018) and showed a changing profile in the presence of 4-HBA which might be due to iron limitations. Since iron and sulfate are crucial for cell survival, it might be speculated that 4-HBA exposure resulted in iron and sulfate starvation which might be lethal for bacteria in higher degrees. In addition, the p-hydroxybenzoate hydroxylase which is functioned in benzoate catabolic process and protocatechuate 3,4-dioxygenase alpha subunit and protocatechuate 3,4-dioxygenase beta subunit which are functioned in 3,4-dihydroxybenzoate catabolic process were newly detected. Since these proteins are used in the degradation of benzoate, it might be speculated that the bacteria started to consume 4-HBA up to a point to be able to handle the toxic effects. It might be speculated that, the bacteria could not be able to consume all 4-HBA since phenolic acids have a dose-dependent antimicrobial property. Thus, 4-HBA resulted in serious stress conditions which led to activate this mechanism for survival. The flagellum-dependent motility proteins exopolyphosphatase, esterase EstA

and protein phosphatase CheZ exist among the new detected proteins. Flagellum is required for both virulence (Bakht azad et al., 2018) and bacterial movement in chemotaxis (Chaban et al., 2015) which aid bacteria to decide the movement according to environmental conditions. These proteins suggested that *P. aeruginosa* increases the motility and/or virulence under inconvenient environmental conditions of 4-HBA.

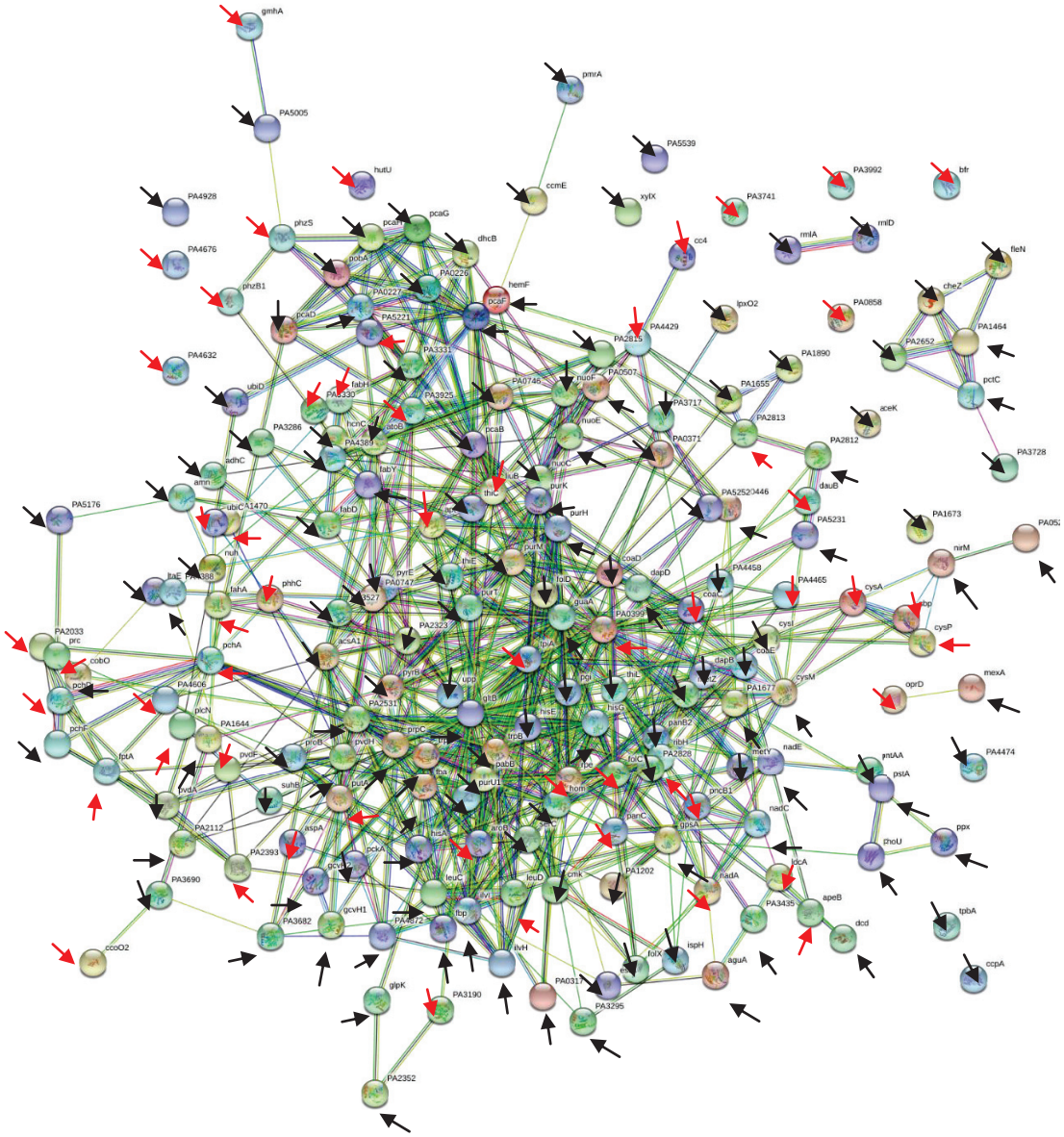

Figure 3.25. String representation of metabolism-related undetected and newly detected proteins in the presence of 4-HBA. The proteins were indicated in arrows with different colors (Undetected proteins: red arrows and newly detected proteins: black arrows).

Table 3.23. The undetected proteins related to metabolism in the presence of 4-HBA.

Protein ID	Protein Name	Gene Name	Function
Q9HX28	Uncharacterized protein	PA3992	Metal ion binding
Q9HYR5	Probable short chain dehydrogenase	PA3330	Dehydrogenase activity
Q9I3P2	Probable short-chain dehydrogenase	PA1470	Dehydrogenase activity
O69753	Phenazine biosynthesis protein PhzB1	phzB1 PA4211	Phenazine biosynthetic process
Q9HWG9	5-methylphenazine-1-carboxylate 1-monooxygenase	phzS PA4217	Pyocyanine biosynthetic process
Q9HTW9	Probable FAD-dependent monooxygenase	PA5221	Oxidoreductase activity, ubiquinone biosynthetic process
P42512	Fe(3+)-pyochelin receptor	fptA PA4221	Ion transport, iron ion homeostasis, siderophore transport
Q9I3L9	Sulfate-binding protein of ABC transporter	cysP PA1493	Sulfate transmembrane transporter activity
P00106	Cytochrome c4	cc4 PA5490	Electron transfer activity, iron ion binding
Q9HZ48	Probable binding protein component of ABC sugar transporter	PA3190	Carbohydrate transport
P32722	Porin D	oprD PA0958	Porin activity, peptidase activity, basic amino acid transport
Q9I4W9	Quinolinate synthase A	nadA PA1004	NAD biosynthetic process from aspartate
Q9HVZ0	Phosphoheptose isomerase	gmhA PA4425	D-glycero-D-manno-heptose 7-phosphate biosynthetic process, LPS core biosynthetic process
Q9HVB9	Carbonic anhydrase	PA4676	Carbon utilization
Q9I583	UPF0176 protein PA0858	PA0858	Cysteine persulfide intermediate active site
G3XD40	Probable acyl-CoA thiolase	PA3925	Fatty acid beta oxidation
Q9HTK1	Probable chorismate pyruvate-lyase	ubiC PA5357	Ubiquinone biosynthetic process
P34002	3-dehydroquinate synthase	aroB PA5038	Chorismate biosynthetic process, aromatic amino acid family biosynthetic process
Q9I030	Probable glutathione S-transferase	PA2813	Transferase activity
Q9HZA4	3-isopropylmalate dehydratase small subunit	leuD PA3120	Leucine biosynthetic process
Q9I187	Probable dipeptidase	PA2393	Dipeptidase activity, pyoverdine biosynthetic process
Q9HZA8	Folylpolyglutamate synthetase	folC PA3111	Dihydrofolate synthase activity, tetrahydrofolylpolyglutamate synthase activity
Q9HYR2	3-oxoacyl-[acyl-carrier-protein] synthase 3	fabH PA3333	Fatty acid biosynthetic process, fatty acid metabolic process

(cont. on next page)

Table 3.23. (continued)

Q9HWF9	Bacterioferritin	bfr bfrA, PA4235	Intracellular sequestering of iron ion, iron ion transport
P15713	Non-hemolytic phospholipase C	plcN PA3319	Lipid catabolic process, protein secretion, protein transport
Q9I3G1	Cyt Cytochrome c oxidase, cbb3-type, CcoO subunit	ccoO2 PA1556	Aerobic respiration, respiratory electron transport chain
Q9I5F6	Bifunctional protein PutA	putA PA0782	Proline catabolic process to glutamate, proline biosynthetic process
Q9HV51	Triosephosphate isomerase	tpiA PA4748	Gluconeogenesis, Glycolysis, Glycerol catabolic process
Q9HTN4	Coenzyme A biosynthesis bifunctional protein CoaBC	coaC PA5320	Coenzyme A biosynthetic process, pantothenate catabolic process
Q9HTD7	Aspartate ammonia-lyase	aspA PA5429	Aspartate metabolic process, tricarboxylic acid cycle
Q9HVY6	Probable cytochrome c1	PA4429	ATP synthesis coupled electron transport
Q9I297	Methylcrotonyl-CoA carboxylase, beta-subunit	liuB PA2014	Isoprenoid catabolic process
Q9HWG3	Pyochelin biosynthesis protein PchD	pchD PA4228	Catalytic activity, metabolic process
Q9HUP4	Nicotinate phosphoribosyltransferase	pncB1 PA4919	NAD biosynthetic process, nicotinate nucleotide biosynthetic process
Q9I184	Pyoverdine synthetase F	pvdF PA2396	Pyoverdine biosynthetic process
Q9I2S7	Lysine-specific pyridoxal 5'-phosphate-dependent carboxylase, LdcA	ldcA PA1818	Amino acid metabolic process
Q9HV69	Pantothenate synthetase	panC PA4730	Pantothenate biosynthetic process
Q9HU83	Urocanate hydratase	hutU PA5100	Histidine catabolic process to glutamate
Q9HYY3	Periplasmic tail-specific protease	prc PA3257	Endopeptidase activity, signal transduction
Q9HVF9	Uncharacterized protein	PA4632	Metallopeptidase activity
Q9HXE4	NAD(P)H-dependent anabolic L-arginine dehydrogenase DauB	dauB PA3862	Arginine catabolic process, arginine metabolic process
Q9I5T1	Ribulose-phosphate 3-epimerase	rpe PA0607	Cellular carbohydrate metabolic process, pentose catabolic process, pentose-phosphate shunt
Q9I282	Uncharacterized protein	PA2033	Iron assimilation
Q04633	Adenine phosphoribosyltransferase	apt PA1543	Adenine salvage, AMP salvage, purine ribonucleoside salvage
Q51508	Salicylate biosynthesis isochorismate synthase	pchA PA4231	Pyochelin biosynthetic process, salicylic acid biosynthetic process
Q9I6A1	Cystathionine beta-synthase	PA0399	Cysteine biosynthetic process from serine

(cont. on next page)

Table 3.23. (continued)

Q9HVI3	Uncharacterized protein	PA4606	Response to nutrient levels, response to starvation
Q9I6L0	Sulfate/thiosulfate import ATP-binding protein CysA	cysA PA0280	Sulfate transmembrane transporter activity
Q9I6K7	Sulfate-binding protein	sbp PA0283	Sulfate transmembrane transporter activity, sulfur compound binding
Q9HXQ3	Uncharacterized protein	PA3741	Acyl-CoA metabolic process, fatty acid metabolic process
Q9HYZ3	Probable M18 family aminopeptidase 2	apeB PA3247	Peptide metabolic process
P43336	Aromatic-amino-acid aminotransferase	phhC PA0870	Phenylalanine biosynthetic process, tyrosine catabolic process
Q9HVV3	Nucleotide-binding protein PA4465	PA4465	ATPase activity, GTPase activity
Q9I015	Probable aminotransferase	PA2828	Biosynthetic process
Q9I2A2	Fumarylacetoacetase	fahA PA2008	Aromatic amino acid family metabolic process

Table 3.24. The newly detected proteins related to metabolism in the presence of 4-HBA.

Protein ID	Protein Name	Gene Name	Function
Q9HYU8	Probable HIT family protein	PA3295	Catalytic activity
Q9I0J8	NADH-quinone oxidoreductase subunit E	nuoE PA2640	Respiratory electron transport chain
Q9I6H4	Uncharacterized protein	PA0317	Lactate oxidation, respiratory electron transport chain
Q9HTJ5	Phosphate transport system permease protein PstA	pstA PA5367	Phosphate ion transmembrane transport
Q9HTV9	Probable ATP-binding/permease fusion ABC transporter	PA5231	Transmembrane transport
Q9I611	Probable acyl-CoA dehydrogenase	PA0507	Flavin adenine dinucleotide binding, oxidoreductase activity
Q9HXI4	Inositol-1-monophosphatase	suhB PA3818	Inositol metabolic process
Q9HW16	Uncharacterized protein	PA4388	Cofactor binding
Q9I6X9	Protocatechuate 3,4-dioxygenase, beta subunit	pcaH PA0153	3,4-dihydroxybenzoate catabolic process
Q9I370	Probable glutathione S-transferase	PA1655	Transferase activity
Q9HYR4	Cytochrome P450	PA3331	Iron binding, Monooxygenase activity, Oxidoreductase activity
Q9I168	L-2,4-diaminobutyrate:2-ketoglutarate 4-aminotransferase, PvdH	pvdH PA2413	Pyoverdine biosynthetic process, transaminase activity
Q9I348	Uncharacterized protein	PA1677	Catalytic activity, metabolic process
Q9I5I2	Probable aldehyde dehydrogenase	PA0747	Methylmalonate-semialdehyde dehydrogenase (acylating) activity
Q9I136	Glycine cleavage system H protein 1	gcvH1 PA2446	Glycine decarboxylation

(cont. on next page)

Table 3.24. (continued)

Q9HXR4	Uncharacterized protein	PA3728	ATPase activity, ATP binding
Q9HWX7	Thiamine-monophosphate kinase	thiL PA4051	Thiamine diphosphate biosynthetic process
Q9HU43	1-(5-phosphoribosyl)-5-[(5-phosphoribosylamino)methylidene amino] imidazole-4-carboxamide isomerase	hisA PA5141	Histidine biosynthetic process, tryptophan biosynthetic process
Q9HUU1	Oxaloacetate decarboxylase	PA4872	Oxaloacetate decarboxylase activity, metal ion binding
Q9I672	Uncharacterized protein	PA0446	Catalytic activity
Q9HVV9	3-deoxy-D-manno-octulosonate 8-phosphate phosphatase KdsC	PA4458	Lipopolysaccharide biosynthetic process
Q9HXS4	Peptidyl-prolyl cis-trans isomerase	PA3717	Peptidyl-prolyl cis-trans isomerase activity
Q14T74	Putative NAD(P) transhydrogenase, subunit alpha part 1	pntAA PA0195	NADPH regeneration
Q9HZA3	3-isopropylmalate dehydratase large subunit	leuC PA3121	Leucine biosynthetic process
Q9I2Q7	Sulfite reductase	cysI PA1838	Response to sulfate starvation, sulfate reduction
P00099	Cytochrome c-551	nirM PA0518	Electron transfer activity, iron ion binding,
Q9HT35	GTP cyclohydrolase FolE2	folE2 PA5539	7,8-dihydroneopterin triphosphate biosynthetic process, GTP cyclohydrolase I activity
Q9I6Q7	Beta-ketoadipate enol-lactone hydrolase	pcaD PA0231	Beta-ketoadipate pathway, 3-oxoadipate enol-lactonase activity
Q9I472	Cob(I)yrinic acid a,c-diamide adenosyltransferase	cobO PA1272	Adenosylcobalamin biosynthesis, cobalamin biosynthetic process, porphyrin-containing compound biosynthetic process
G3XD76	2,3,4,5-tetrahydropyridine-2,6-dicarboxylate N-succinyltransferase	dapD PA3666	Diaminopimelate biosynthetic process, Lysine biosynthetic process via diaminopimelate
Q59653	Aspartate carbamoyltransferase	pyrB PA0402	UMP biosynthetic process, Amino acid metabolic process, pyrimidine ribonucleotide biosynthetic process
P38103	4-hydroxy-tetrahydrodipicolinate reductase	dapB PA4759	Diaminopimelate biosynthetic process, Lysine biosynthetic process via diaminopimelate
Q9HVP8	Dephospho-CoA kinase	coaE PA4529	Coenzyme A biosynthetic process
G3XD64	Site-determining protein	fleN PA1454	ATP binding
Q9I5I3	Probable acyl-CoA dehydrogenase	PA0746	Acyl-CoA Dehydrogenase activity, lipid metabolic process
Q9HUG0	Probable carbamoyl transferase	PA5005	Transferase activity, biosynthetic process
Q9HVE6	Uracil phosphoribosyltransferase	upp PA4646	UMP biosynthetic process, pyrimidine nucleoside salvage, UMP salvage
Q9HW15	Probable short-chain dehydrogenase	speA PA4389	Dehydrogenase activity
Q9HTX6	Glycine cleavage system H protein 2	gcvH2 PA5214	Glycine decarboxylation
Q9I0V2	Probable aminotransferase	PA2531	Transaminase activity, biosynthetic process
Q9HTZ7	Phosphoenolpyruvate carboxykinase (ATP)	pckA PA5192	Gluconeogenesis
Q9I2K7	Probable glutathione S-transferase	PA1890	Transferase activity

(cont. on next page)

Table 3.24. (continued)

Q9HW87	Formyltetrahydrofolate deformylase	purU1 purU, PA4314	IMP biosynthetic process, purine metabolism, one carbon metabolic process
Q9I522	Lipopolysaccharide biosynthetic protein LpxO2	lpxO2 PA0936	Peptidyl-aspartic acid hydroxylation
Q9HV67	Glucose-6-phosphate isomerase	pgi PA4732	Glycolysis
Q9I6C3	Uncharacterized protein	PA0371	Catalytic activity, metal ion binding
Q9HWG4	Pyochelin synthetase	pchF PA4225	Hydrolase activity acting on ester bonds, biosynthetic process
Q9HUP3	NH(3)-dependent NAD(+) synthetase	nadE PA4920	NAD(+) biosynthetic process
Q9HYV7	Beta-ketodecanoyl-[acyl-carrier-protein] synthase	PA3286	Fatty acid biosynthesis
Q9HXV8	Uncharacterized protein	PA3682	Catalytic activity
G3XCZ6	Malonyl CoA-acyl carrier protein transacylase	fabD PA2968	Fatty acid biosynthetic process
P43898	Oxygen-dependent coproporphyrinogen-III oxidase	hemF PA0024	Protoporphyrin-IX biosynthetic process
P50587	Orotate phosphoribosyltransferase	pyrE PA5331	UMP biosynthetic process, pyrimidine nucleotide biosynthetic process,
Q9I2A8	Acetyl-CoA acetyltransferase	atoB PA2001	(R)-mevalonate biosynthetic process, Acetyl-CoA C-acetyltransferase activity, Fatty acid beta oxidation
Q9I2U6	Bifunctional protein FolD	folD PA1796	Tetrahydrofolate interconversion, one carbon metaboolism, hisitidine biosynthetic process, methionine biosynthetic process
P72170	Dihydroorotase	pyrC PA3527	UMP biosynthetic process, pyrimidine nucleotide biosynthetic process
Q9I4D6	Probable hydrolase	PA1202	Hydrolase activity, metabolic process,
P14532	Cytochrome c551 peroxidase	ccpA PA4587	Cytochrome-c peroxidase activity, electron transfer activity, metal ion binding
G3XD72	Probable purine-binding chemotaxis protein	PA1464	Chemotaxis, signal transduction
Q9HTF1	Low specificity L-threonine aldolase	ltaE PA5413	Threonine aldolase activity
Q9HVU7	Uncharacterized protein	PA4474	Metallopeptidase activity
Q9I6X8	Protocatechuate 3,4-dioxygenase, alpha subunit	pcaG PA0154	Aromatic compound catabolic process, protocatechuate 3,4-dioxygenase activity
Q9HU73	Fructose-1,6-bisphosphatase class 1	fbp PA5110	Gluconeogenesis
Q51548	L-ornithine N(5)-monooxygenase	pvdA pvd-1, PA2386	Pyoverdin biosynthesis, siderophore biosynthesis
Q51390	Glycerol kinase 2	glpK2 glpK, glpK1, PA3582	Glycerol catabolic process, glycerol metabolic process,
P30819	Nicotinate-nucleotide pyrophosphorylase [carboxylating]	nadC PA4524	NAD(+) biosynthetic process
Q9I6R0	Beta-ketoadipyl-CoA thiolase	pcaF PA0228	3,4-dihydroxybenzoate catabolic process, beta-ketoadipate pathway
Q9HUN6	UPF0313 protein PA4928	PA4928	Catalytic activity, metal ion binding
Q9HY01	S-(hydroxymethyl)glutathione dehydrogenase	adhC PA3629	Ethanol oxidation, formaldehyde catabolic process

(cont. on next page)

Table 3.24. (continued)

Q9HYG7	D-erythro-7,8-dihydroneopterin triphosphate epimerase	folX PA3439	Folic acid-containing compound metabolic process, tetrahydrobiopterin biosynthetic process
Q9I2A9	DhcB, dehydrocarnitine CoA transferase, subunit B	dhcB PA2000	Carnitine catabolic process, CoA transferase activity
P20586	p-hydroxybenzoate hydroxylase	pobA PA0247	Benzoate catabolic process, FAD binding
Q51547	Phosphate-specific transport system accessory protein PhoU homolog	phoU PA5365	Cell chemotaxis, cellular phosphate ion homeostasis, negative regulation of phosphate metabolic process, negative regulation of phosphate transmembrane transport, phosphate ion transport
Q9HXC7	Protein tyrosine phosphatase TpbA	tpbA PA3885	Protein tyrosine phosphatase activity
Q9HVA1	Acetolactate synthase isozyme III small subunit	ilvH PA4695	Acetolactate synthase activity, isoleucine biosynthetic process, valine biosynthetic process
Q9HZ66	Phosphoserine aminotransferase	serC PA3167	Serine biosynthetic process, pyridoxine 5'-phosphate biosynthetic activity
Q9I513	Phosphoribosylformylglycinamidine cyclo-ligase	purM PA0945	IMP biosynthetic process
Q9I5Y1	Fructose-bisphosphate aldolase	fba fda, PA0555	Glycolysis
Q9I1F5	Probable glyceraldehyde-3-phosphate dehydrogenase	PA2323	Gamma-aminobutyric acid catabolic process, glutamate decarboxylation to succinate
Q9HX46	AMP nucleosidase	amn PA3970	AMP salvage, nucleoside metabolic process
Q9I0J9	NADH-quinone oxidoreductase subunit C/D	nuoC nuoCD, nuoD, PA2639	NAD binding, NADH dehydrogenase (ubiquinone) activity, quinone binding
Q9I3A8	Glycerol-3-phosphate dehydrogenase [NAD(P)+]	gpsA PA1614	Glycerophospholipid metabolic process, glycerol-3-phosphate catabolic process, carbohydrate metabolic process, phospholipid biosynthetic process
Q9I381	Uncharacterized protein	PA1644	FMN binding
Q9I203	5-oxoprolinase subunit A 2	pxpA2 PA2112	Carbohydrate metabolic process
G3XD12	Hydrogen cyanide synthase subunit HcnC	hcnC PA2195	Glycine dehydrogenase (cyanide-forming) activity, oxidoreductase activity
P29365	Homoserine dehydrogenase	hom PA3736	Methionine biosynthetic process, threonine biosynthetic process, isoleucine biosynthesis process
Q9HVM7	4-hydroxy-3-methylbut-2-enyl diphosphate reductase	spH lytB, PA4557	Dimethylallyl diphosphate biosynthetic process, isopentenyl diphosphate biosynthetic process
Q9HV70	3-methyl-2-oxobutanoate hydroxymethyltransferase 2	panB2 PA4729	Pantothenate biosynthetic process
P07345	Tryptophan synthase beta chain	trpB PA0036	Tryptophan biosynthetic process
Q9I6R2	Probable CoA transferase, subunit A	PA0226	CoA transferase activity, metabolic process
Q9I6D1	Phosphopantetheine adenylyltransferase	coaD PA0363	Coenzyme A biosynthetic process
Q9HX40	Thiamine-phosphate synthase	thiE PA3976	Thiamine diphosphate biosynthetic process, thiamine biosynthetic process

(cont. on next page)

Table 3.24. (continued)

Q9HUE4	Homocysteine synthase	metY PA5025	Methionine biosynthetic process
Q9I526	Cysteine synthase B	cysM PA0932	Cysteine biosynthetic process
Q9I0J7	NADH-quinone oxidoreductase subunit F	nuoF PA2641	FMN binding, NAD binding, quinone binding, NADH dehydrogenase (ubiquinone) activity
Q9I5E3	Citrate synthase	prpC PA0795	Tricarboxylic acid cycle, Citrate synthase activity
Q9I6R1	Probable CoA transferase, subunit B	PA0227	CoA-transferase activity, metabolic process
Q9I1C6	Probable glycerophosphoryl diester phosphodiesterase	PA2352	Lipid metabolic process
Q9HU23	dTDP-4-dehydrorhamnose reductase	rmlD PA5162	dTDP-L-rhamnose biosynthetic process, lipopolysaccharide core region biosynthetic process
Q9I6Q8	3-carboxy-cis,cis-muconate cycloisomerase	pcaB PA0230	Beta-ketoadipate pathway, 3,4-dihydroxybenzoate catabolic process
Q9HWX5	6,7-dimethyl-8-ribityllumazine synthase	ribH ribE, PA4053	Riboflavin biosynthetic process
Q9HVW8	ATP phosphoribosyltransferase	hisG PA4449	Histidine biosynthetic process
Q9HYH1	Uncharacterized protein PA3435	PA3435	FMN binding, oxidation-reduction process
Q9HYC9	dCTP deaminase	dcd PA3480	dUMP biosynthetic process, dUTP biosynthetic process
Q51484	Uncharacterized protein PA0525	PA0525	Denitrification process
Q9I2Y1	Para-aminobenzoate synthase component I	pabB PA1758	Tetrahydrofolate biosynthetic process
Q9HZ70	Cytidylate kinase	cmk PA3163	Nucleotide phosphorylation, pantothenate biosynthetic process from valine
Q9HVA0	Acetolactate synthase	ilvI PA4696	Isoleucine biosynthetic process, valine biosynthetic process
Q9HUV9	Bifunctional purine biosynthesis protein PurH	purH PA4854	IMP biosynthetic process
Q9HXP3	Formate-dependent phosphoribosylglycinamide formyltransferase	purT PA3751	IMP biosynthetic process
Q9HUB6	Phosphoribosyl-ATP pyrophosphatase	hisE PA5067	Histidine biosynthetic process
Q9HU13	Uncharacterized protein	PA5176	Hydrolase activity
Q9I6Y9	Nonspecific ribonucleoside hydrolase	nuh PA0143	Purine nucleotide metabolic process, purine nucleoside catabolic process
P20574	Anthranilate phosphoribosyltransferase	trpD PA0650	Tryptophan biosynthetic process
P55218	O-succinylhomoserine sulfhydrylase	metZ PA3107	Methionine biosynthetic process
Q9I6J9	Agmatine deiminase	aguA PA0292	Putrescine biosynthetic pathway
Q9HU15	Beta-ketoacyl-[acyl-carrier-protein] synthase FabY	fabY PA5174	Fatty acid biosynthetic process
Q9I3W8	Isocitrate dehydrogenase kinase/phosphatase	aceK PA1376	Glucose metabolic process, glyoxylate cycle, peptidyl-serine phosphorylation, regulation of catalytic activity, tricarboxylic acid cycle
Q9HXM6	GMP synthase [glutamine-hydrolyzing]	guaA PA3769	Glutamine metabolic process, GMP biosynthetic process

(cont. on next page)

Table 3.24. (continued)

Q9HU22	Glucose-1-phosphate thymidylyltransferase	rmlA PA5163	dTDP-rhamnose biosynthetic process, extracellular polysaccharide biosynthetic process, lipopolysaccharide core region biosynthetic process
Q9HUJ2	Phosphomethylpyrimidine synthase	thiC PA4973	Thiamine diphosphate biosynthetic process, thiamine biosynthetic process
Q9I0W4	Toluate 1,2-dioxygenase alpha subunit	xylX PA2518	Cellular metabolic process
Q9HVL9	Glutamate 5-kinase	proB PA4565	Proline biosynthetic process
Q9I028	Probable acyl-CoA dehydrogenase	PA2815	Acyl-CoA dehydrogenase activity, fatty acid beta-oxidation using acyl-CoA dehydrogenase
Q9ZN70	Exopolyphosphatase	ppx PA5241	Flagellum-dependent swimming motility, flagellum-dependent swarming motility, response to nitrogen starvation, response to phosphate starvation, glycolipid biosynthetic process, pathogenesis, polyphosphate catabolic process, quorum sensing, single-species biofilm formation
Q9I558	Acetyl-coenzyme A synthetase 1	acsA1 PA0887	Acetyl-CoA biosynthetic process from acetate
P72158	N5-carboxyaminoimidazole ribonucleotide synthase	purK PA5425	IMP biosynthetic process
O33407	Esterase EstA	estA papA, PA5112	Flagellum-dependent cell motility, flagellum-dependent swarming motility, cell motility, glycolipid biosynthetic process, lipid biosynthetic process, single-species biofilm formation
Q9HTV3	3-octaprenyl-4-hydroxybenzoate carboxy-lyase	ubiD PA5237	Ubiquinone biosynthetic process
Q9I352	Bacteriohemerythrin	PA1673	Oxygen carrier activity
Q9HUD5	Glutamate synthase large chain	gltB PA5036	Ammonia assimilation cycle, glutamate biosynthetic process
Q9HV32	PmrA: two-component regulator system response regulator PmrA	pmrA PA4776	Phosphorelay signal transduction system, regulation of transcription
Q9I0I6	Methyl-accepting chemotaxis protein PA2652	PA2652	Chemotaxis, response to organic substances,integral component of membrane
Q9HTU2	Probable ATP-binding component of ABC transporter	PA5252	ATPase activity, ATP binding
Q9HW93	Methyl-accepting chemotaxis protein PctC	pctC PA4307	Chemotaxis, response to amino acid
Q9I031	Probable ATP-binding component of ABC transporter	PA2812	ATPase activity, ATP binding
Q9HXV0	Probable metal-transporting P-type ATPase	PA3690	Metal ion transport
Q9I3N3	Cytochrome c-type biogenesis protein CcmE	ccmE cycJ, PA1479	Cytochrome complex assembly, protein-heme linkage
P52477	Multidrug resistance protein MexA	mexA PA0425	Drug transmembrane transporter activity, response to antibiotic, protein homooligomerization
Q51434	Protein phosphatase CheZ	cheZ PA1457	Flagellum-dependent swarming motility, chemotaxis, regulation of chemotaxis

3.3.2.6. Redox and Cell Homeostasis-Related Proteins of 4-HBA Treatment

The undetected (Figure 3.26 a) and newly detected proteins (Figure 3.26 b) were determined with their interaction network (Figure 3.27) related to redox and cell homeostasis in the presence of 4-HBA. According to results, various proteins functioned in oxidative stress response such as quinone oxidoreductase, superoxide dismutase [Mn] and thiol:disulfide interchange protein DsbA were undetected. On the other hand, iron-sulfur cluster assembly scaffold protein IscU functioned in iron-ion homeostasis, peptide methionine sulfoxide reductase MsrA functioned in oxidative stress response, polyamine aminopropyltransferase 1 and spermidine/putrescine import ATP-binding protein PotA functioned in spermidine biosynthesis were newly detected. In the presence of superoxide and hydrogen peroxide the DNA and membranes of the cell are seriously damaged (Hassett et al., 1996) and the bacteria require the ROS to be reduced for survival. The changes in the proteins related to response to these toxic substances demonstrated that the 4-HBA treatment resulted in the oxidative stress in *P. aeruginosa*. Relatedly, 4-HBA presented changes in the spermidine metabolism. The detection of changes in proteins of spermidine and putrescine biosynthesis, might show that the bacteria manage to handle the toxic effects of 4-HBA by these polyamines. Since they are the main polyamines in bacteria for cell viability, pathogenesis, antibiotic resistance and protecting the DNA from oxidative damage (Johnson et al., 2011) and have functions in signaling and regulation against stress conditions caused by ROS, heat, UV, acid and osmotic pressure (Bandounas et al., 2011), it could be speculated that 4-HBA showed significant stress conditions in the environment in which *P. aeruginosa* survived.

The new detection of iron-sulfur cluster assembly scaffold protein IscU which has roles in iron-ion homeostasis might demonstrate that 4-HBA caused defects in iron metabolism. Iron is the essential nutrient for cell survival regardless of being prokaryote or eukaryote (Drehe et al., 2018). It is accepted that the phenolic compounds have iron chelation properties (Singh and Kumar, 2019; Andjelkovic et al., 2006). Thus, it could be speculated that 4-HBA might chelate the iron ion in the environment which led to iron starvation of *P. aeruginosa*. Additionally, pyoverdine proteins (Pvd), which have vital roles in iron uptake (Drehe et al., 2018), were also demonstrated with a changed

protein profile in metabolism section (Table 3.23 and 3.24). Therefore, 4-HBA might show its damaging effects not only by oxidative stress but also by iron limitation for the bacteria.

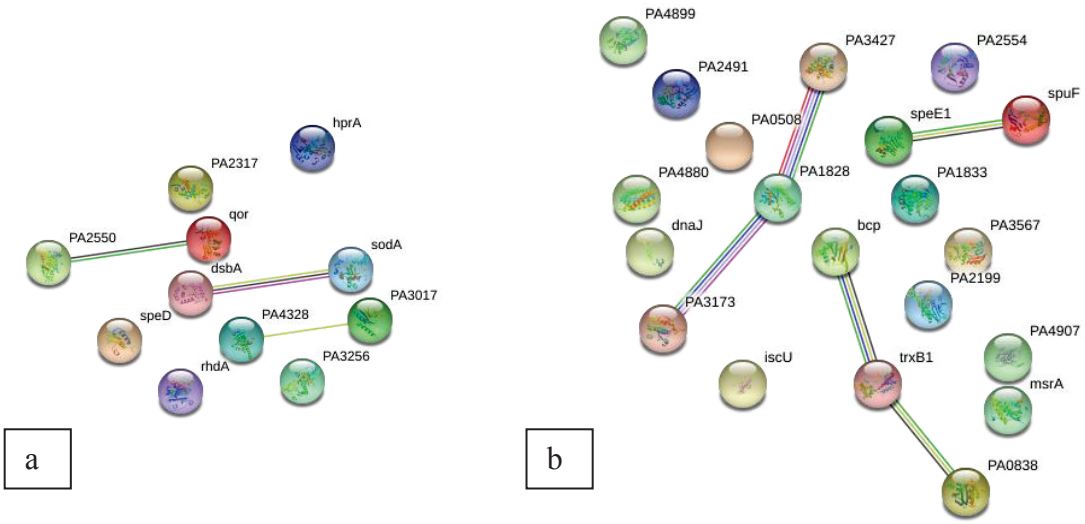

Figure 3.26. String representation of redox and cell homeostasis-related proteins in the presence of 4-HBA. a) Undetected proteins b) Newly detected proteins

Table 3.25. The undetected proteins in the presence of 4-HBA functioned in redox and cell homeostasis.

Protein ID	Protein Name	Gene Name	Function
Q9HW73	Uncharacterized protein	PA4328	Response to stress
Q9HZI9	Universal stress protein	PA3017	Response to stress
Q9I0T4	Probable acyl-CoA dehydrogenase	PA2550	FAD binding, oxidoreductase activity
Q9HUK9	Thiosulfate sulfurtransferase	rhdA PA4956	Thiosulfate sulfurtransferase activity, Response to toxic substance
P43903	Quinone oxidoreductase	qor PA0023	Response to oxidative stress

(cont. on next page)

Table 3.25. (continued)

P0C2B2	Thiol:disulfide interchange protein DsbA	dsbA PA5489	Cell redox homeostasis
Q9HYY4	Probable oxidoreductase	PA3256	Oxidoreductase activity
Q9HVG5	Glycerate dehydrogenase	hprA PA4626	Oxidoreductase activity
P53652	Superoxide dismutase [Mn]	sodA PA4468	Removal of superoxide radicals
Q9I1F8	Probable oxidoreductase	PA2317	Oxidoreductase activity
Q9I5R7	S-adenosylmethionine decarboxylase proenzyme	speD PA0654	Adenosylmethioninamine biosynthetic process, spermidine biosynthetic process

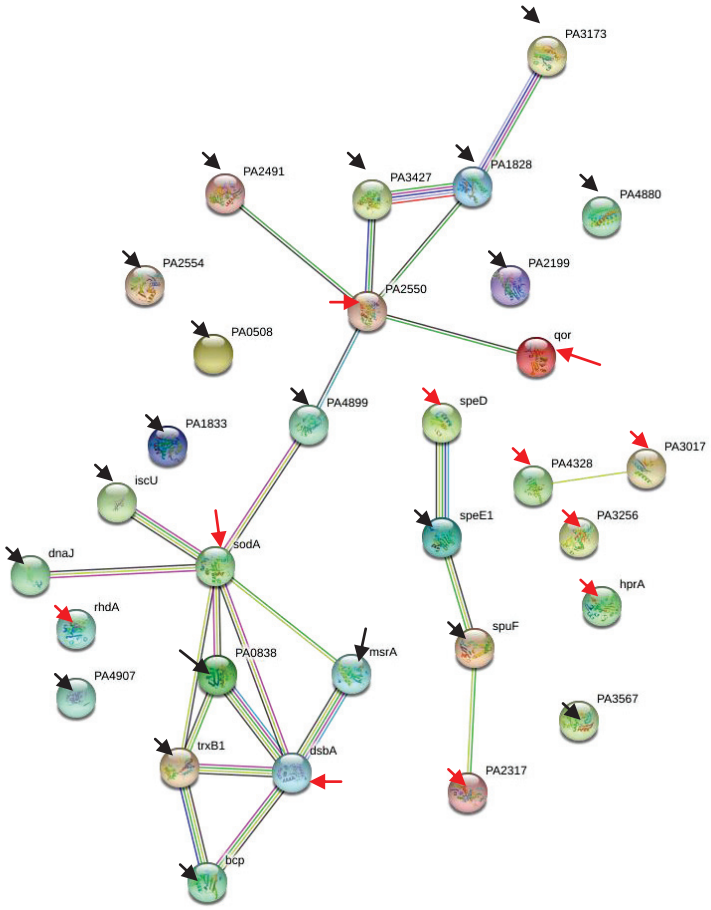

Figure 3.27. String representation of redox and cell homeostasis-related undetected and newly detected proteins in the presence of 4-HBA. The significant proteins were indicated in arrows with different colors (Undetected proteins: red arrows and newly detected proteins: black arrows).

Table 3.26. The newly detected proteins in the presence of 4-HBA functioned in redox and cell homeostasis.

Protein ID	Protein Name	Gene Name	Function
Q9I0T0	Probable short-chain dehydrogenase	PA2554	Oxidoreductase activity
Q9I0Z1	Probable oxidoreductase	PA2491	Negative regulation of protein secretion, negative regulation of secondary metabolite biosynthetic process, negative regulation of transmembrane transport
Q9HV44	Chaperone protein DnaJ	dnaJ PA4760	Response to hyperosmotic and heat shock
Q9HZ61	Probable short-chain dehydrogenase	PA3173	Oxidoreductase activity, organic substance catabolic process
Q9HY50	Zinc-type alcohol dehydrogenase-like protein	PA3567	Oxidoreductase activity, zinc ion binding
Q9I2R7	Probable short-chain dehydrogenase	PA1828	Oxidoreductase activity
Q9HUR4	Probable aldehyde dehydrogenase	PA4899	Oxidoreductase activity
Q9HUT3	Probable bacterioferritin	PA4880	Cellular iron ion homeostasis, iron ion transport, ferric ion binding
Q9I1R8	Probable dehydrogenase	PA2199	NAD binding, NADP binding,oxidoreductase activity
Q9I610	Probable acyl-CoA dehydrogenase	PA0508	Oxidoreductase activity
Q9I4W5	Bacterioferritin comigratory protein	bcp PA1008	Antioxidant activity, oxidoreductase activity, cell redox homeostasis
Q9I2R2	Probable oxidoreductase	PA1833	Oxidoreductase activity
Q9HUF1	Peptide methionine sulfoxide reductase MsrA	msrA PA5018	Cellular response to oxidative stres, pathogenesis, response to hypochlorite
Q9HUQ6	Probable short-chain dehydrogenase	PA4907	Oxidoreductase activity
Q9I0M2	Thioredoxin reductase	trxB1 PA2616	Thioredoxin-disulfide reductase activity, removal of superoxide radicals
Q9I5A2	Glutathione peroxidase	PA0838	Response to oxidative stress
Q9HYH8	Probable short-chain dehydrogenase	PA3427	Oxidoreductase activty
Q9X6R0	Polyamine aminopropyltransferase 1	speE1 speE, PA1687	Spermidine biosynthetic process
Q9I6I9	Spermidine/putrescine import ATP-binding protein PotA	spuF potA, PA0302	Spermidine transport, putrescine transport
Q9HXI9	Iron-sulfur cluster assembly scaffold protein IscU	iscU PA3813	Cellular iron ion homeostasis, iron ion homeostasis, iron-sulfur cluster assembly

3.3.2.7. Virulence-Related Proteins of 4-HBA Treatment

The protein 2-heptyl-4(1H)-quinolone synthase subunit PqsC (Protein ID: Q9I4X1; Gene name: pqsC PA0998) was undetected after 4-HBA treatment. This protein is a soluble signal which functioned in quorum sensing of *P. aeruginosa* leading the elevated virulence (Dulcey et al., 2013). The undetection of this protein demonstrated that 4-HBA exposure resulted in the decrease in the virulence of *P. aeruginosa* by diminishing the quorum sensing.

However, the bacteria maintained their virulence by newly detected proteins such as exoenzyme T and response regulator GacA (Table 3.27). In addition, they manage to handle the toxic effects of 4-HBA by aminoglycoside 3'-phosphotransferase type Iıb and regulatory protein TypA. Since these proteins have roles in the cellular response to antibiotics, it might be speculated that 4-HBA led the bacteria to protect themselves as they were exposed to antibiotics.

Table 3.27. The newly detected proteins in the presence of 4-HBA functioned in virulence.

Protein ID	Protein Name	Gene Name	Function
Q9I788	Exoenzyme T	exoT PA0044	Pathogenesis
Q9I3D8	Uncharacterized protein PA1579	PA1579	Lipid binding
Q9HWR2	Aminoglycoside 3'-phosphotransferase type Iıb	aph PA4119	Response to antibiotic
G3XDB0	Catabolite repression control protein	crc PA5332	Base-excision repair, pathogenesis, quorum sensing, regulation of carbon utilization, regulation of single-species biofilm formation
Q51373	Response regulator GacA	gacA PA2586	Pathogenesis, phosphorelay signal transduction system, positive regulation of single-species biofilm formation on inanimate substrate, regulation of transcription,
Q9HU67	Regulatory protein TypA	typA PA5117	Cellular response to antibiotic, Flagellum-dependent swarming motility, cell adhesion involved in single-species biofilm formation, , positive regulation of protein secretion

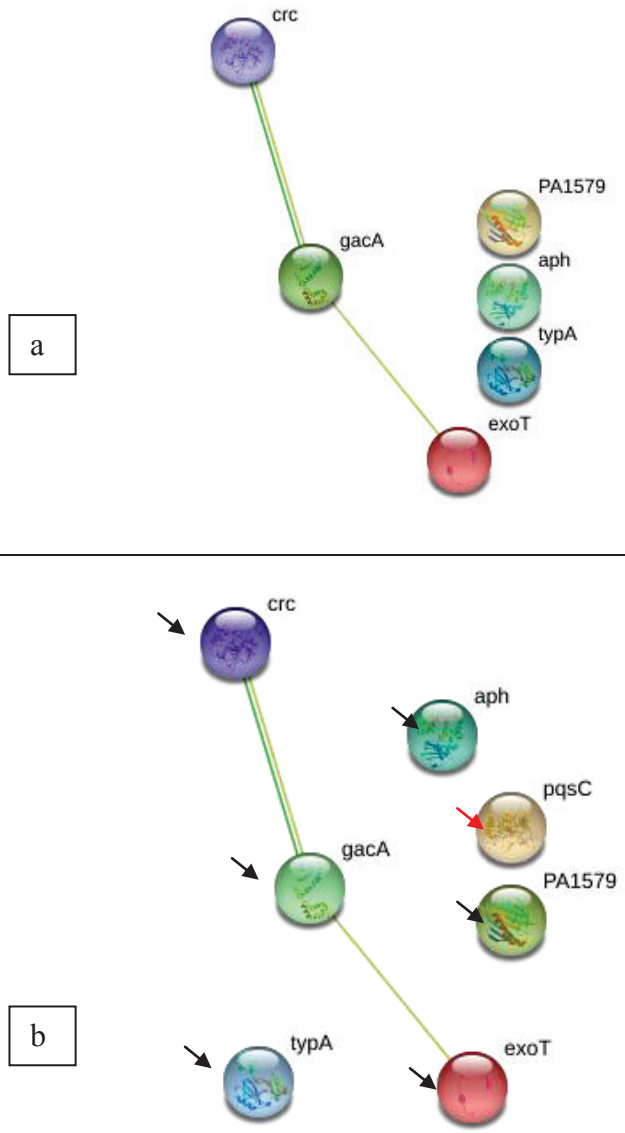

Figure 3.28. String representation of virulence-related proteins in the presence of 4-HBA. a) Newly detected proteins b) The both undetected and newly detected proteins. The proteins were indicated in arrows with different colors (Undetected proteins: red arrows and newly detected proteins: black arrows).

3.3.2.8. Uncharacterized Proteins of 4-HBA Treatment

Various undetected (Figure 3.29 a) and newly detected (Figure 3.29 b) proteins were shown which were uncharacterized in Uniprot. The STRING results demonstrated the interaction network of these undetected and newly detected proteins (Figure 3.30).

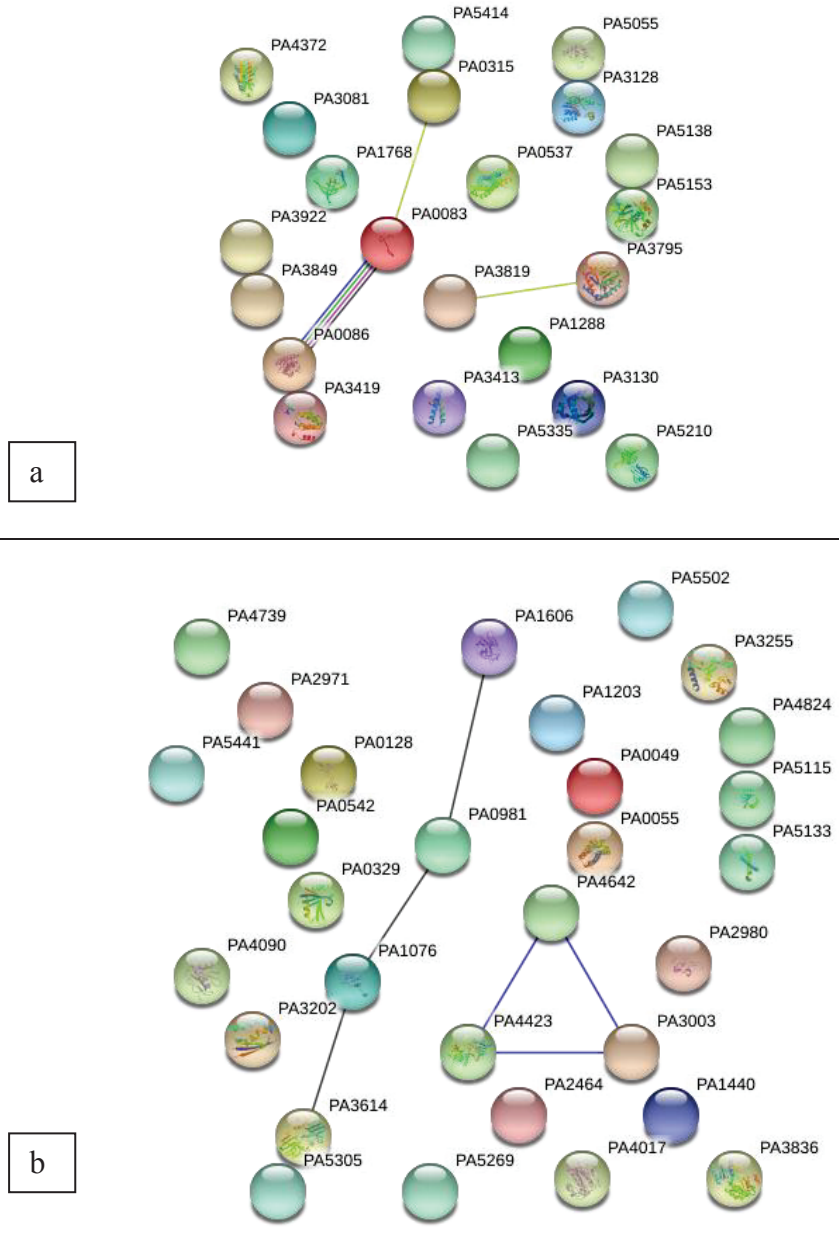

Figure 3.29. String representation of uncharacterized proteins in the presence of 4-HBA. a) Undetected proteins b) Newly detected proteins

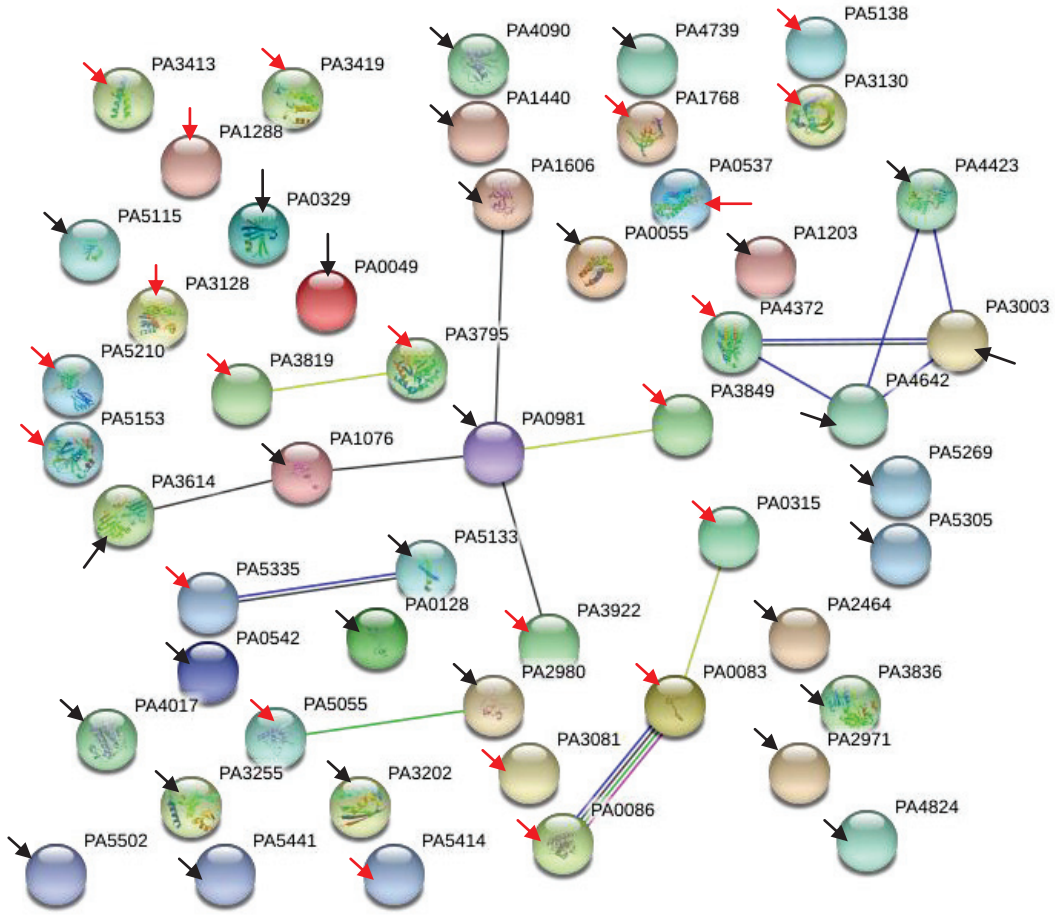

Figure 3.30. String representation of uncharacterized undetected and newly detected proteins in the presence of 4-HBA. The significant proteins were indicated in arrows with different colors (Undetected proteins: red arrows and newly detected proteins: black arrows).

The protein BLAST results showed that the uncharacterized proteins were mostly hypothetical proteins and the proteins belonging to transport systems, virulence and oxidative stress response proteins as well as structural components of various proteins (Table 3.28 and 3.29). The strongly interacted PA0086 and PA0083 were undetected after 4-HBA exposure which were functioned as tetratricopeptide repeat protein and Type VI secretion system contractile sheath small subunit, respectively (table 3.28). Type VI secretion system has a role in the competition of Gram negative bacteria with which toxic effector proteins are released into adjacent prokaryotic cell or

into eukaryotic cells by using a contractile sheath (Russel et al., 2012; Salih et al., 2018). Being virulence related, the proteins of this mechanism may be good targets of new antimicrobial agents (Salomon and Orth, 2015; Salih et al., 2018). In addition, Type VI secretion system also functions in horizontal gene transfer from lysed cells which were killed by Type VI secretion system possessing bacteria (Salomon and Orth, 2015) to obtain new genes from killed bacteria in the vicinity (Ringel et al., 2017). The undetection of these proteins might show that the treatment with 4-HBA demonstrated reduced virulence and competition properties of *P. aeruginosa*.

Another point was undetection of PA5335 which might be YicC family protein according to protein BLAST. Since it was presented as related to the DNA damage associated protein, YicC protein might be functioned in repair mechanisms. The undetection of YicC might show the DNA damage arouse from 4-HBA treatment.

Table 3.28. The undetected proteins in the presence of 4-HBA which are uncharacterized.

Protein ID	Protein Name	Gene Name	Function	Protein Blast Results
Q9HTF0	Uncharacterized protein	PA5414	Uncharacterized	Hypothetical protein
Q9HXI3	Uncharacterized protein	PA3819	Uncharacterized	Glycine zipper 2TM domain-containing protein
Q9HXF7	Nucleoid-associated protein PA3849	PA3849	Uncharacterized	Nucleoid-associated protein YejK
Q9HZC7	Uncharacterized protein	PA3081	Uncharacterized	DUF1329 domain-containing protein
Q9I456	Probable outer membrane protein	PA1288	Uncharacterized	Long-chain fatty acid transport protein
Q9I746	Uncharacterized protein	PA0086	Uncharacterized	tetratricopeptide repeat protein
Q9I2X1	Uncharacterized protein	PA1768	Uncharacterized	ATP-dependent zinc protease
Q9I6H6	Uncharacterized protein	PA0315	Uncharacterized	DUF4399 domain-containing protein
Q9HTM3	Uncharacterized protein	PA5335	Uncharacterized	YicC family protein
Q9HXK2	Probable oxidoreductase	PA3795	Uncharacterized	Aldo/keto reductase
Q9HW30	Uncharacterized protein	PA4372	Uncharacterized	Imelysin
Q9I5Z9	Uncharacterized protein	PA0537	Uncharacterized	LemA family protein

(cont. on next page)

Table 3.28. (continued)

Q9HYI6	UPF0162 protein PA3419	PA3419	Uncharacterized	Transglut_core2 superfamily hypothetical protein
Q9HU46	Uncharacterized protein	PA5138	Uncharacterized	ABC transporter substrate-binding protein
Q9HYJ2	Uncharacterized protein	PA3413	Uncharacterized	YebG superfamily hypothetical protein
Q9HX91	Uncharacterized protein PA3922	PA3922	Uncharacterized	DUF1329 domain-containing protein
Q9HZ96	Probable short-chain dehydrogenase	PA3128	Uncharacterized	SDR family oxidoreductase
Q9HU31	Amino acid (Lysine/arginine/ornithine /histidine/octopine) ABC transporter periplasmic binding protein	PA5153	Uncharacterized	Amino acid ABC transporter substrate-binding protein
G3XD27	Uncharacterized protein	PA5055	Uncharacterized	DUF971 domain-containing protein
Q9HTY0	Probable secretion pathway ATPase	PA5210	Uncharacterized	Type II/IV secretion system protein
Q9I749	Uncharacterized protein	PA0083	Uncharacterized	Type VI secretion system contractile sheath small subunit
Q9HZ94	Uncharacterized protein	PA3130	Uncharacterized	Acyl-CoA thioesterase

Table 3.29. The newly detected proteins in the presence of 4-HBA which are uncharacterized.

Protein ID	Protein Name	Gene Name	Function	Protein Blast Results
Q9HUY6	Uncharacterized protein	PA4824	Uncharacterized	Hypothetical protein
Q9I777	Uncharacterized protein	PA0055	Uncharacterized	DUF1993 family protein
Q9HZN3	Uncharacterized protein	PA2971	Uncharacterized	DUF177 domain-containing protein
Q9HY12	Uncharacterized protein	PA3614	Uncharacterized	MBL fold metallo-hydrolase
Q9HTT1	Uncharacterized protein	PA5269	Uncharacterized	Hypothetical protein
Q9I4Q3	Uncharacterized protein	PA1076	Uncharacterized	DUF5064 family protein
Q9I3Q7	Uncharacterized protein	PA1440	Uncharacterized	YecA family protein
Q9I6G2	UPF0339 protein PA0329	PA0329	Uncharacterized	DUF1508 domain-containing protein

(cont. on next page)

Table 3.29. (continued)

Q9HU69	Uncharacterized protein	PA5115	Uncharacterized	Class I SAM-dependent methyltransferase
Q9HV60	Uncharacterized protein	PA4739	Uncharacterized	BON domain-containing protein
Q9HZ38	Uncharacterized protein	PA3202	Uncharacterized	YciI family protein
Q9HX10	Uncharacterized protein	PA4017	Uncharacterized	Oxidoreductase
Q9I5Z4	Uncharacterized protein	PA0542	Uncharacterized	DUF1090 domain-containing protein
Q9HU51	Uncharacterized protein	PA5133	Uncharacterized	Peptidase M23
Q9HXG8	Uncharacterized protein	PA3836	Uncharacterized	ABC transporter substrate-binding protein
Q9I4Y8	Uncharacterized protein	PA0981	Uncharacterized	Hypothetical protein
Q9HWT8	Uncharacterized protein	PA4090	Uncharacterized	DUF2218 domain-containing protein
Q9I4D5	Uncharacterized protein	PA1203	Uncharacterized	OsmC family peroxiredoxin
Q9HTP9	Uncharacterized protein	PA5305	Uncharacterized	DUF1318 domain-containing protein
Q9HVZ2	Uncharacterized protein	PA4423	Uncharacterized	Penicillin-binding protein activator
Q9HZM4	UPF0434 protein PA2980	PA2980	Uncharacterized	Trm112 family protein
Q9I118	Uncharacterized protein	PA2464	Uncharacterized	Hypothetical protein
Q9HYY5	Uncharacterized protein	PA3255	Uncharacterized	HAD-IB family hydrolase
Q9HTC5	Uncharacterized protein	PA5441	Uncharacterized	Outer membrane assembly lipoprotein YfiO
Q9HVF0	Uncharacterized protein	PA4642	Uncharacterized	Hypothetical protein
Q9I783	Uncharacterized protein PA0049	PA0049	Uncharacterized	Hypothetical protein
Q9I3B5	Uncharacterized protein	PA1606	Uncharacterized	DUF3859 domain-containing protein
Q9I704	Uncharacterized protein	PA0128	Uncharacterized	Alkylphosphonate utilization protein
Q9HZK2	Uncharacterized protein	PA3003	Uncharacterized	CsiV superfamily hypothetical protein
Q9HT71	Uncharacterized protein	PA5502	Uncharacterized	Hypothetical protein

3.3.3. Comparison of Mutual Protein Profiles of 3-HPAA and 4-HBA

Although the water soluble phenolic acids 3-HPAA and 4-HBA are included in two different groups of the phenolic acids (Andjelkovic et al., 2006), the treatment of *P. aeruginosa* with each of them was resulted in various mutual proteins. This might present that the antimicrobial effects of phenolic acids are due to targetting similar biochemical pathways of *P. aeruginosa*. According to Venn diagram results which

were constructed by protein IDs of the proteins, 55 mutual proteins were newly detected for 3-HPAA and 4-HBA treatments (Figure 3.1, region II), while 108 mutual proteins were undetected (Figure 3.1, region V). Besides, 284 mutual proteins were found as mutual for control, 3-HPAA and 4-HBA treated groups (Figure 3.1, region VII). These mutual protein of phenolic acid treated groups contain proteins which were separated into groups related to their functions as DNA, RNA, ribosomes and protein, cell wall and membrane, metabolism, redox and cell homeostasis, virulence and uncharacterized. The percentages of these groups were presented in Figure 3.31 a and b for the undetected and newly detected proteins, respectively.

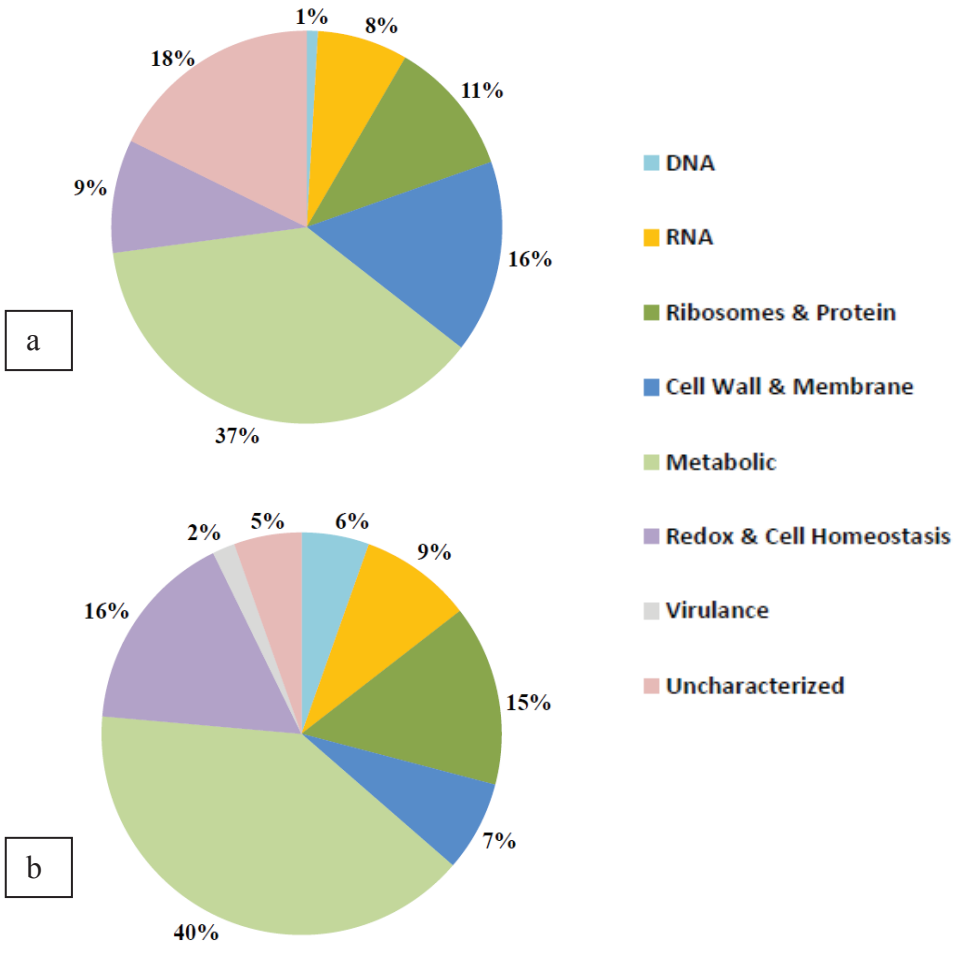

Figure 3.31. The percentages of mutual proteins for each group of function in the presence of 3-HPAA and 4-HBA. a) Undetected proteins b) Newly detected proteins

. According to the results, there were no mutual virulence related proteins for each phenolic acid group which were undetected and only 2% of the newly detected mutual proteins were related to virulence. It might be speculated that the common antimicrobial effect of phenolic acids did not occur based on changes in the virulence. The changes in metabolism presented the highest percentages for both undetected and newly detected mutual proteins which indicates that the treatment with phenolic acids resulted in various metabolic changes depending on the adaptation to new environmental conditions. The most significant results were high percentage (16%) of the undetection of cell wall and membrane related mutual proteins. This might indicate that the phenolic acids mostly target cell wall and membrane proteins which led the defects in cell envelope structure and integrity. Additionally, ribosome and protein related mutual proteins showed a high undetection rate with 11% which might indicate that the other targets of the phenolic acids for antimicrobial effect are ribosome integrity and protein metabolism. On the other hand, the presence of the phenolic acids resulted in new detection of the proteins related to redox and cell homeostasis in high percentage (16%) demonstrating the high oxidative stress response of the bacteria against phenolic acid treatment.

3.3.3.1. DNA-Related Mutual Proteins of 3-HPAA and 4-HBA

The treatment of *P. aeruginosa* with 3-HPAA or 4-HBA resulted in the undetection of the uncharacterized protein PA0986 which has transposase activity (Figure 3.32; Table 3.1 and 3.15). On the other hand, the recombination-associated protein RdgC, single-stranded DNA-binding protein (Ssb) and beta sliding clamp (DnaN) were newly detected, mutually (Figure 3.32). The proteins RdgC was functioned in DNA recombination as well as protein Ssb functioned in DNA recombination and repair (Table 3.2 and 3.16).

Additionally, the DnaN protein has role in DNA replication and 3'-5' exonuclease activity (Table 3.2 and 3.16). These results could be concluded as the phenolic acid treatment resulted in the damage of the bacterial genome and *P. aeruginosa* activated the DNA repair and recombination mechanisms. It is known that some bacteria including *Pseudomonas* could degrade phenolic compounds up to a point in subinhibitory concentrations (Ghaima et al., 2017). The recombination in bacteria

allow to obtain the genes with horizontal gene transfer for degradation of phenolic compounds (Tavita et al., 2012) and it aids the DNA repair systems to fix the DNA (Sidorenko et al., 2014). Therefore, *P. aeruginosa* might attempt not only to repair the defects in its genome but also attempt to protect itself by gaining new genes to adapt the new environment involving phenolic acid toxicity. Thus, one of the antimicrobial action mechanisms of phenolic acids might be due to the DNA damage of *P. aeruginosa*.

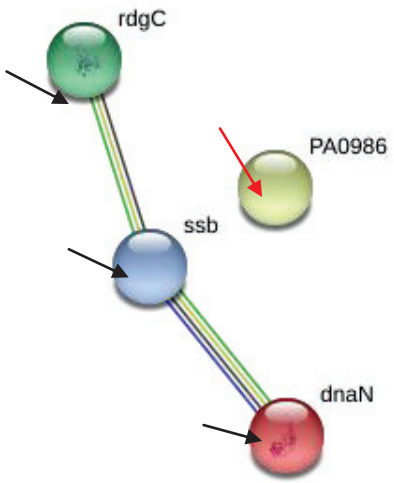

Figure 3.32. String representation of DNA-related undetected and newly detected mutual proteins in the presence of phenolic acids. The significant proteins were indicated in arrows with different colors (Undetected proteins: red arrows and newly detected proteins: black arrows).

3.3.3.2. RNA-Related Mutual Proteins of 3-HPAA and 4-HBA

The undetected and newly detected proteins functioned in transcriptional regulation of various metabolisms and RNA structure were mutual for 3-HPAA and 4-HBA displaying interactions (Figure 3.33). Bifunctional protein PyrR, DNA-binding transcriptional regulator NtrC, tRNA 2-selenouridine/geranyl-2-thiouridine synthase SelU and stringent starvation protein A (SspA) were undetected. Major cold shock

protein CspA, RNA polymerase sigma factor RpoD, phosphate regulon transcriptional regulatory protein PhoB and oxyR were newly detected after phenolic acid treatment.

Bifunctional protein PyrR is functioned in nucleoside metabolic process (Table 3.3 and 3.17) and the undetection of it might demonstrate the defects in the synthesis of nucleosides which are the subunits of nucleic acids. Thus, phenolic acids might show their effects by targetting the nucleic acid production process. DNA-binding transcriptional regulator NtrC takes role in the transcriptional regulation of nitrogen utilization (Table 3.3 and 3.17). The undetection of this protein demonstrated that the bacteria might undergo nitrogen starvation by phenolic acid treatment which led to the bacterial growth inhibition. The enzyme tRNA 2-selenouridine/geranyl-2-thiouridine synthase (protein SelU) carries out the tRNA seleno-modification (Table 3.3 and 3.17). It shows function in the formation of geranylation, a natural hydrophobic modification of tRNA, which is found in a few bacterial species involving *P. aeruginosa* (Wang et al., 2016). This modification which enhances the codon recognition fidelity and decreases the frameshift reading (Sierant et al., 2016), takes place at the wobble position of anticodons of lysine, glutamine and glutamic acid (Dumelin et al., 2012). Since the modification of tRNAs is a crucial step in tRNA biogenesis, the undetection of this protein might result in the defects in tRNA metabolism and eventually in the proper translation of proteins possessing the lysine, glutamine and glutamic acid. The sigma factors, which are important components of RNA polymerase holoenzyme, lead the adaptation and the proteins of stringent response aid the alternative sigma factors to function under stress conditions (Swiecilo and Zych-Wezyk., 2013). Therefore, the undetection of the stringent starvation protein A (SspA) might reduce the adaptation of the bacteria which might led the conclusion that the phenolic acids resulted in the defects in the stress response control of *P. aeruginosa* in their antimicrobial effect processes.

On the other hand, the newly detected major cold shock protein CspA is functioned in the repair of mRNA by stabilizing the secondary structures caused by cold stress (Bisht et al., 2014). Thus, phenolic acid treatment resulted in serious stress similar to the stress after sudden decrease of temperature and the bacteria attempt to fix the RNA function for survival by CspA protein. In addition, *P. aeruginosa* might encounter the phosphate starvation since the newly detected protein PhoB is the transcription regulator functioned in the stress response regulation under phosphate limitation (Faure

et al., 2013; Quesada et al., 2016). In the presence of phenolic acids, another vital stress response protein, OxyR was also newly detected. In addition to being one of the main transcriptional regulator of oxidative stress response (Kim et al., 2019), OxyR has also roles in iron homeostasis, quorum sensing, protein synthesis and oxidative phosphorylation (Wei et al., 2012). Therefore, when treated with phenolic acids, *P. aeruginosa* undergo serious metabolic changes to overcome the damaging effects of these stress conditions. The new detection of RpoD (σ^{70}) which is the main sigma factor regulating various housekeeping genes (Potvin et al., 2008) also demonstrate the effort of the bacteria during these changes for cell survival and adaptation.

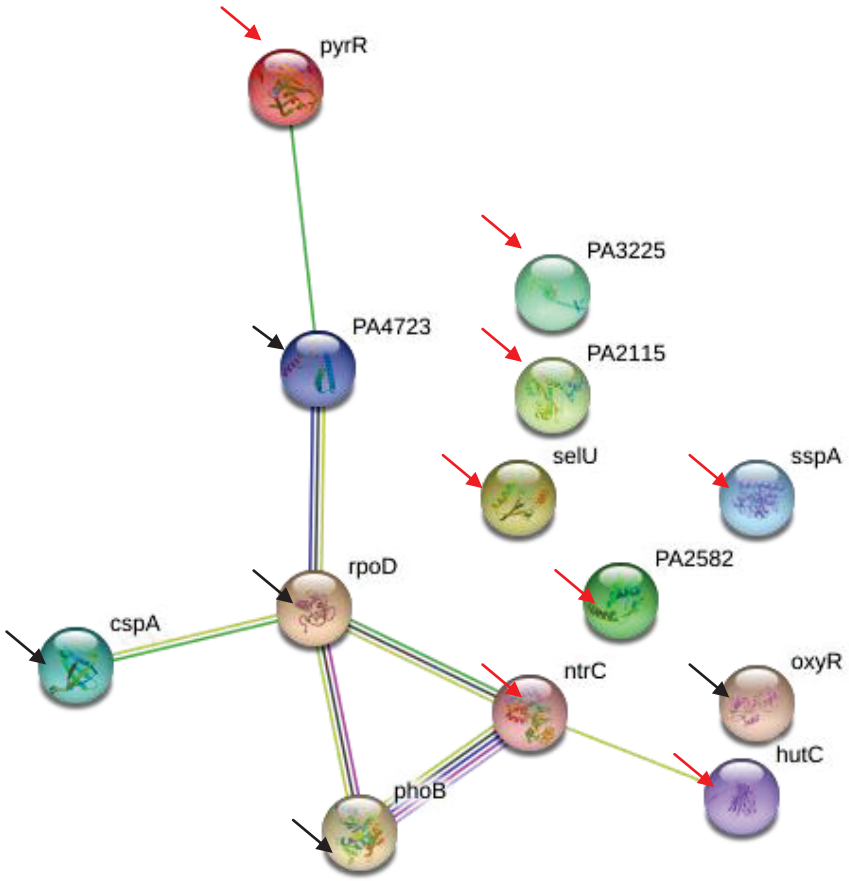

Figure 3.33. String representation of RNA-related undetected and newly detected mutual proteins in the presence of phenolic acids. The significant proteins were indicated in arrows with different colors (Undetected proteins: red arrows and newly detected proteins: black arrows).

3.3.3.3. Ribosome and Protein- Related Mutual Proteins of 3-HPAA and 4-HBA

The treatment with phenolic acids resulted in the problems in ribosome structure and assembly. For instance, small ribosomal subunit biogenesis GTPase RsgA and 30S ribosomal protein S15 rpsO were undetected. The protein S15 is one of the main ribosomal proteins functioned in the assembly of the ribosomal small subunit (Shajani et al., 2011; Liu and Fredrick, 2016) and RsgA is an important enzyme functioned in the small subunit assembly. In addition, ATP-dependent RNA helicase DeaD and ribosomal RNA large subunit methyltransferase J (rimJ) which are functioned in ribosomal large subunit assembly were also undetected. These might indicate that phenolic acids block the proper ribosomal structure and assembly process. Since the large subunit is the major part of the ribosome for the polypeptide translation (Aseev and Boni, 2011), undetection of these proteins eventually affected the protein translation by damaging the ribosome structure and assembly. Since 30S ribosomal protein S18 (rpsR) was newly detected, it might show that the bacteria managed to continue the maintained ribosomal small subunit assembly. Translational initiation was also damaged by phenolic acids since Translation initiation factor IF-1(infA) functioned in ribosome binding, rRNA binding and translation initiation was undetected. Besides the effects on ribosome and translation, protein metabolism was defected by undetection of Protein-export protein SecB. This protein is a molecular chaperone which recognizes the N-terminal signal sequence of some precursor proteins and and functions in the translocation of them for proper protein production. Since SecB was undetected, it might be concluded that serious changes occured in the protein metabolism including the defects in the process of the proteins with N-terminal signal sequences (Driessen, 2001).

D-ala-D-ala-carboxypeptidase (DacC) was newly detected which is functioned in the synthesis of peptidoglycan layer, the main component of the bacterial cell wall wall (Ghosh et al., 2008; Meyer et al., 2018). The bacteria use this enzyme in the recycling of the peptidoglycan layer subunits which were released into media (Templin et al., 1999; Meyer et al., 2018). This could demonstrate that the bacterial cell wall was damaged and *P. aeruginosa* attempted to fix it by using carboxypeptidase. The t-RNA ligases such as IleS, TyrS2, GltX and MetG were newly detected after phenolic acid exposure which presented that the phenolic acids resulted in an increase for some

tRNAs for the metabolism changes for adaptation. Since t-RNAs are the main components for aminoacids transfer to the ribosomes to maintain the growth of peptide chain in translation (Ferro et al., 2018), it could be concluded that the phenolic acids affected the protein synthesis profile of *P. aeruginosa*.

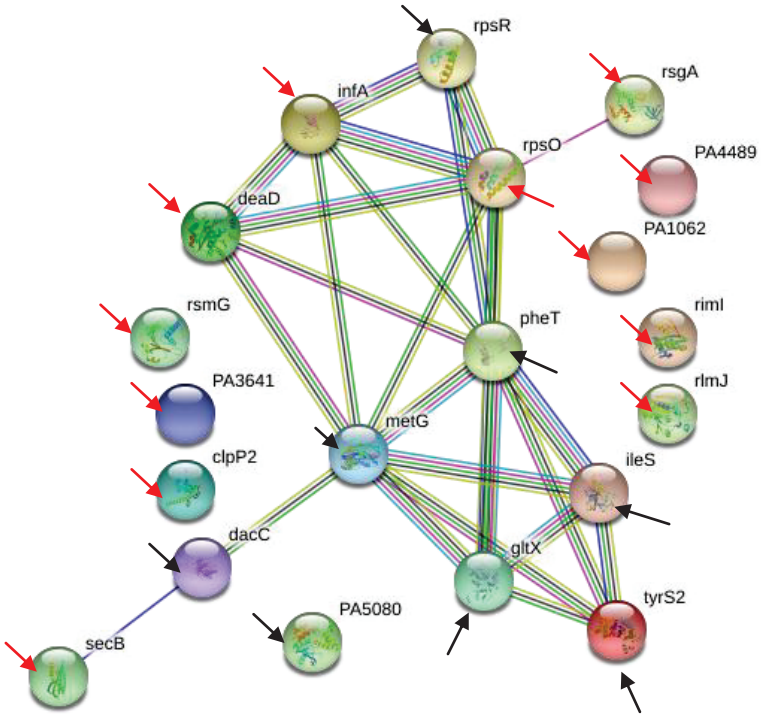

Figure 3.34. String representation of ribosome and protein-related undetected and newly detected mutual proteins in the presence of phenolic acids. The significant proteins were indicated in arrows with different colors (Undetected proteins: red arrows and newly detected proteins: black arrows).

3.3.3.4. Cell Wall and Membrane- Related Mutual Proteins of 3-HPAA and 4-HBA

The undetected proteins share many mutual proteins in the treatments with 3-HPAA and 4-HBA (Table 3.7 and 3.21). Therefore, the effect of 4-HBA and 3-HPAA

might be carried out by damaging similar cell wall structures. YidC is one of the important proteins for the insertion and integration of small membrane proteins into the membrane (Dalbey et al., 2011; Kiefer and Kuhn, 2018). The protein FtsY has a role in the targetting of nascent polypeptide chains to the membrane for the transfer of them to the cytoplasmic region of the membrane (Dalbey et al., 2011). Hence, the undetection of YidC and FtsY demonstrated the phenolic acids blocked the targetting and insertion of new proteins into the membrane which might lead the antimicrobial effect due to defects in the cell wall structure. Additionally, another vital protein for cell wall integrity and cell metabolism, FtsH, was undetected. This protein is conserved among prokaryotes and functioned in the regulation control of the cell metabolism in the case of an environmental stress (Langklotz et al., 2012). It is a protease attached to the inner membrane (Narberhaus et al., 2009) and has roles in quality control of the membrane proteins (Langklotz et al., 2012) as well as posttranslational modifications of transcription factors and enzymes (Narberhaus et al., 2009). The undetection of this protein might point out another target for the phenolic acids for their antimicrobial effects

Another meaningful result of the antimicrobial effects of phenolic acids might be presented with the undetection of the proteins related to flagellum and type IV pili. The bacteria can sense the environmental changes and use chemotaxis for either going towards desirable or escape from the undesirable environments. Since the motility for chemotaxis might be carried out by flagellum, the changes in their proteins might be considered as a bacterial attempt to adapt the new conditions. For instance, B-type flagellin (FliC) which has a role in the flagellum organization and motility (Bakht azad et al., 2018) was newly detected while CheY protein functioned in rotation of the flagellum (Chaban et al., 2015) was undetected. These situations might show both the adaptation and the damage in the chemotaxis process. The flagellum has important roles in the virulence and the movement for chemotaxis (Bakht azad et al., 2018; Chaban et al., 2015). Therefore it could be speculated that the B-type flagellin (FliC) was produced for the flagellum synthesis for increased motility or virulence due to phenolic acids. However, since the CheY protein was undetected, the movement with flagellum was defected. This might present that phenolic acids resulted in the damage in the chemotaxis and diminished the swimming motility with the flagellum which could cause the antimicrobial effect. The proteins related to another mechanism, the type4 pili,

was also undetected. The type4 pili are the filaments found in the poles of *P. aeruginosa* which are flexible (Kazmierczak et al., 2006). These structures are serious virulence factors that aid the initiation of the infections (Huang et al., 2003) as well as the biofilm formation (Jain et al., 2017). The type4 pili is functioned in the twitching motility which is a flagellum-independent motility of the bacteria (Huang et al., 2003; Carter et al., 2017). The protein PilY1 is one of the proteins of type4a pilus (Carter et al., 2017) which is the type4 pili found in *P. aeruginosa* (Giltner et al., 2012). The undetection of PilY1 protein may suggest that the phenolic acids caused defects in the twitching motility and biofilm formation of *P. aeruginosa*. Thus, the motility of the bacteria was seriously affected by the phenolic acid treatments.

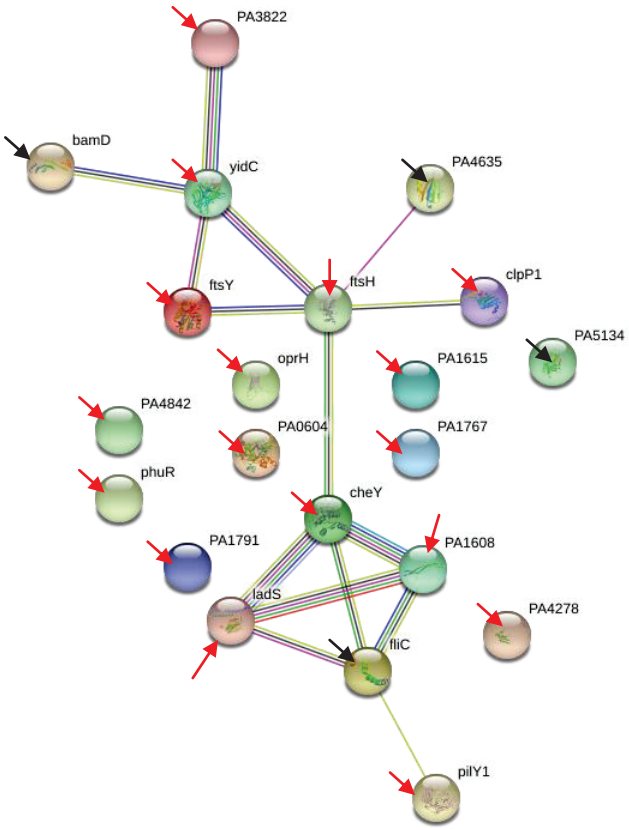

Figure 3.35. String representation of cell wall and membrane-related undetected and newly detected mutual proteins in the presence of phenolic acids. The significant proteins were indicated in arrows with different colors (Undetected proteins: red arrows and newly detected proteins: black arrows).

The outer membrane protein assembly factor BamD and probable carboxyl-terminal protease PA5134 which have roles in the cell envelope biogenesis (Mori et al., 2012) were newly detected after phenolic acid treatments. It demonstrated that the phenolic acids might damage the cell envelope, especially the outer membrane of *P. aeruginosa* which was attempted to be fixed by BamD and carboxyl-terminal protease for maintained cell wall integrity.

3.3.3.5. Metabolism- Related Mutual Proteins of 3-HPAA and 4-HBA

Many mutual proteins related to various metabolic processes were presented after phenolic acid exposures. The changes in the protein profiles of the bacteria related to energy metabolism (i.e. undetection of Rpe functioned in carbohydrate metabolic process), amino acid metabolism (i.e. undetection of Apt functioned in purine ribonucleoside salvage and new detection of GuaA functioned in GMP biosynthesis in purine metabolism) and lipid metabolism (i.e. new detection of AtoB functioned in fatty acid beta oxidation) (Table 3.23 and 3.24) showed that the bacteria undergo many metabolic changes to adapt the environment containing phenolic acids for a maintained metabolism. Besides these expected changes originated from the adaptation processes, some changes were also demonstrated which might aid the antimicrobial effect of the phenolic acids. The sulfate transport of *P. aeruginosa* was diminished since sulfate/thiosulfate import ATP-binding protein CysA, sulfate-binding protein of ABC transporter (CysP) and sulfate-binding protein (Sbp) were undetected. Therefore phenolic acids resulted in the sulfate limitation which might led the growth inhibition of the bacteria. The iron starvation might be another result of the presence of phenolic acids since the protein Fe(3+)-pyochelin receptor (FptA) was mutual in the undetected proteins related to iron homeostasis. Since the phenolic compounds are metal chelators (Singh and Kumar, 2019; Andjelkovic et al., 2006), the environment containing phenolic acids might result in the non-utilizable iron which caused the inhibition of the bacterial growth under iron limitation stress. Besides these, the phenolic acids showed reduced virulence with the undetection of proteins related to phenazine production of *P. aeruginosa*. Since phenazine biosynthesis protein PhzB1 and 5-methylphenazine-1-carboxylate 1-monooxygenase proteins were undetected, phenolic acids damaged the in phenazine biosynthetic process, reducing the virulance.

Thus, it could be concluded that the phenolic acids essentially showed their negative effects on bacterial metabolism by limiting the basic nutrients which lead the starvation and growth inhibition of the bacteria.

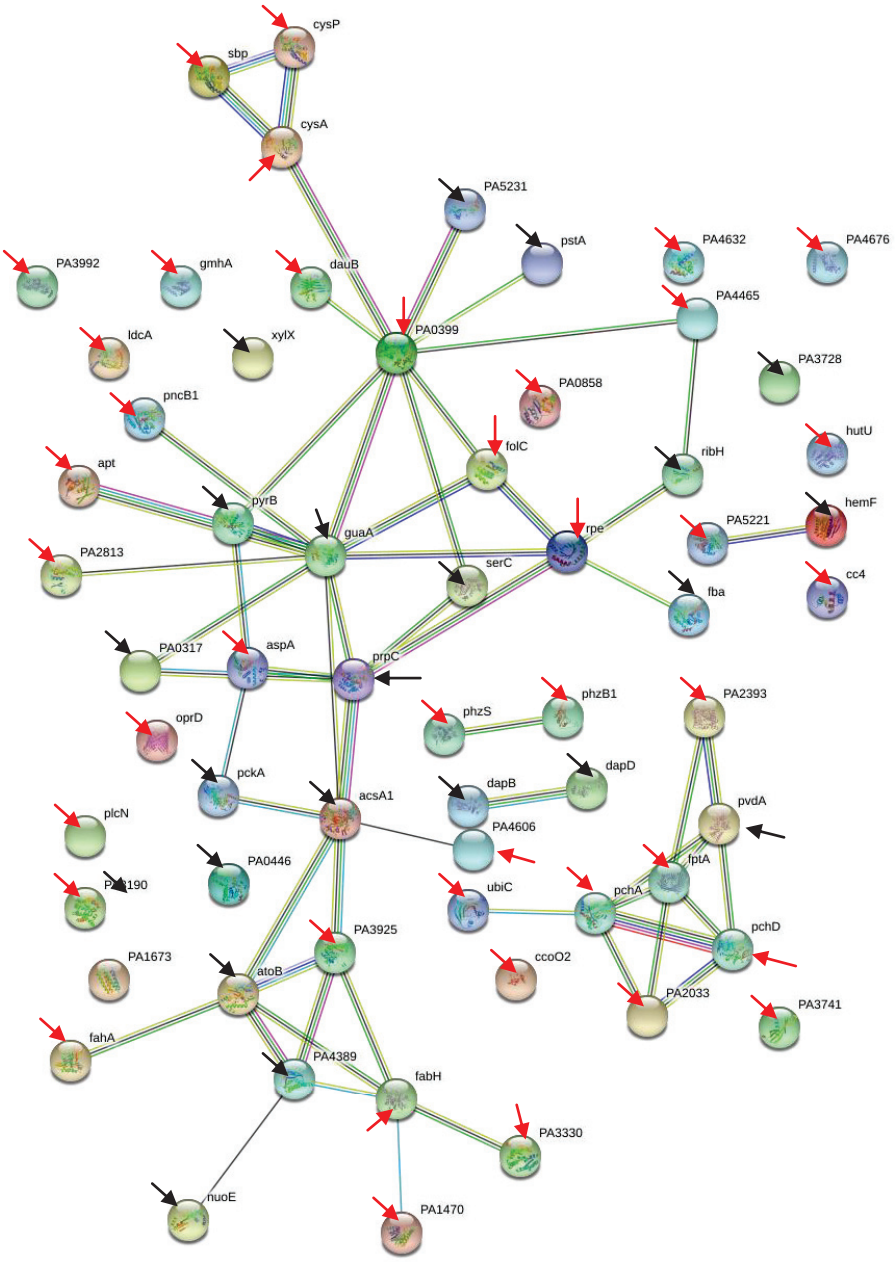

Figure 3.36. String representation of metabolism-related undetected and newly detected mutual proteins in the presence of phenolic acids. The significant proteins were indicated in arrows with different colors (Undetected proteins: red arrows and newly detected proteins: black arrows).

3.3.3.6. Redox and Cell Homeostasis- Related Mutual Proteins of 3-HPAA and 4-HBA

The phenolic acid treatment resulted in the mutual changes in the protein profile related to redox and cell homeostasis which indicates that both phenolic acids caused oxidative stress on *P. aeruginosa*. Additionally, the undetection of the proteins functioned in oxidative stress response might show that the phenolic acids led the reducing of the redox homeostasis for the antimicrobial effect. For instance, Superoxide dismutase [Mn] (SodA) and thiol:disulfide interchange protein DsbA were undetected. Superoxide dismutase [Mn] is functioned in removal of superoxide radicals (Table 3.11 and 3.25) (Iiyama et al., 2007) while DsbA in cell redox homeostasis. The protein thiosulfate sulfurtransferase (RhdA) which takes role in response to toxic substance and aids to survival of *P. aeruginosa* under stress conditions was also undetected. Since the redox homeostasis and removal of superoxides are required to protect the DNA from the damage in the DNA and membranes (Hassett et al., 1996), the undetection of these proteins showed the enhanced oxidative stress due to diminished oxidative stress response. On the other hand, S-adenosylmethionine decarboxylase proenzyme speD was undetected whereas SpeE1 and SpuF were newly detected. These proteins are functioned in the spermidine biosynthesis and transport processes. Spermidine is a polyamine which functions in the cell viability, pathogenesis, antibiotic resistance and signaling and regulation against stress conditions caused by reactive oxygen species (ROS), heat, UV, acid and osmotic pressure (Johnson et al., 2011; Bandounas et al., 2011). The undetection of SpeD might be compensated by the new detection of SpeE1and SpuF to continue the spermidine biosynthesis. Other newly detected proteins, Chaperone protein DnaJ and Glutathione peroxidase PA0838 are functioned in the response to hyperosmotic and heat shock and Response to oxidative stress, respectively. One of the main enzymes which takes role in the stress caused by chemicals such as phenolic compounds (Tamburro et al., 2001), Peptide methionine sulfoxide reductase MsrA was also newly detected. This protein is vital for the repairing the proteins which become unfunctional by oxidative stress damage (Mintz et al., 2002, John et al., 2001). Thus, it is clear that phenolic acids degrade the cell homeostasis of *P. aeruginosa* by causing serious oxidative stress.

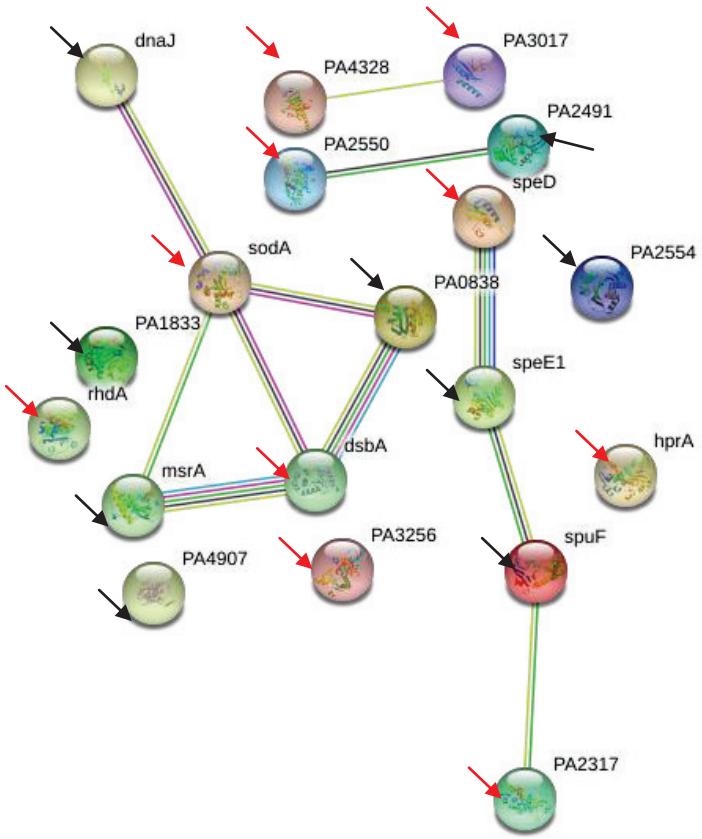

Figure 3.37. String representation of redox and cell homeostasis-related undetected and newly detected mutual proteins in the presence of phenolic acids. The significant proteins were indicated in arrows with different colors (Undetected proteins: red arrows and newly detected proteins: black arrows).

3.3.3.7. Virulence- Related Mutual Proteins of 3-HPAA and 4-HBA

The Uncharacterized protein PA1579 (Protein ID: Q9I3D8; Gene Name: PA1579) functioned in lipid binding (Table 3.27) was the only mutual newly detected protein for 3-HPAA and 4-HBA and no undetected proteins exist related to virulence. It might be concluded that, although the phenolic acids resulted in the changes in the virulence of *P. aeruginosa* individually, their effects related to virulence was not via the same protein profile.

3.3.3.8. Uncharacterized Mutual Proteins of 3-HPAA and 4-HBA

The most notable change in the uncharacterized protein profile were the undetection of PA0086 and PA0083 which showed strong interactions. These proteins were suggested as Tetratricopeptide repeat protein (PA0086) and Type VI secretion system contractile sheath small subunit (PA0083) in the protein BLAST.

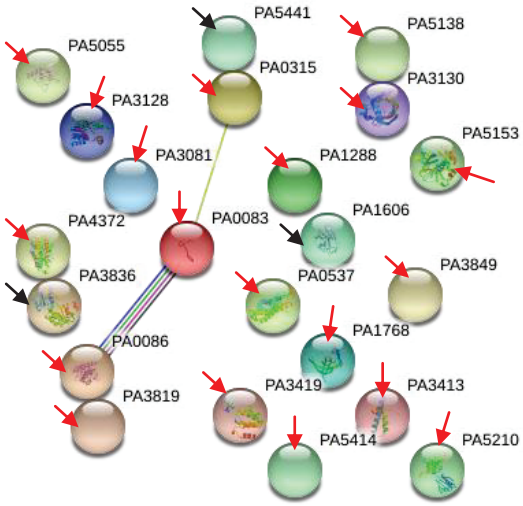

Figure 3.38. String representation of uncharacterized, undetected and newly detected mutual proteins in the presence of phenolic acids. The significant proteins were indicated in arrows with different colors (Undetected proteins: red arrows and newly detected proteins: black arrows).

Type VI secretion system (T6SS) is an important mechanism of Gram negative bacteria to compete to each other and functions to secrete effector proteins in adjacent bacteria by its contractile sheath part (Russel et al., 2012; Salih et al., 2018). The most notable function of this system is its role in horizontal gene transfer. The bacteria use this mechanism to lyse the other bacteria in the vicinity with T6SS system to gain the new genes (Salomon and Orth, 2015). It is also a virulence factor and it is accepted as a good target for new antimicrobials (Salomon and Orth, 2015; Salih et al., 2018). The

undetection of small subunit of contractile sheath resulted in the defect of this system of *P. aeruginosa*. Relatedly, tetratricopeptide repeat protein which is functioned in the exporting the secretions from cell membrane (Whitney and Howell, 2013; Mejias et al., 2019) was also undetected. Therefore, the phenolic acids might target T6SS mechanism of *P. aeruginosa* for their antimicrobial effects which led the decreasing in virulence, competing property and horizontal gene transfer.

To conclude; tested water soluble, simple phenolic acids, 3-HPAA and 4-HBA could be presented as "multi-target antimicrobial agents" since they resulted in the changes in various metabolic processes of *P. aeruginosa*, such as DNA, RNA, ribosomes, proteins and cell envelope as well as cell homeostasis and virulence at the proteomic level. The most notable targets for tested phenolic acids could be presented as their effects on the cell wall and membrane integrity as well as their damages from serious oxidative stress. Other vital systems, ribosome structure, assembly and protein metabolism were also highly affected in the presence of phenolic acids. It is known that many antibiotics show their antimicrobial effects on one system of the bacteria which might lead to the immediate drug resistance development of bacteria. Thus, phenolic acids could be more useful antimicrobial agents since they have more than one targets in bacterial metabolism and there are any known resistance mechanism of the bacteria against them. They showed not only the bacteriocidal effects on *P. aeruginosa* but also diminished probability of resistance by targetting many metabolic pathways. Thus, the phenolic acids could be considered as promising antimicrobial agents against serious pathogenic bacteria.

3.3.4. Validation of Protein Data by RT-qPCR

The protein data was validated at the transcription level by real time quantitative polymerase chain reaction (RT-qPCR). Since protein data was obtained from the 18 hours cultures which was the very beginning of the stationary phase, total RNA samples were isolated from the 18 hour cultures of *P. aeruginosa*. Since the ribosomal rpsL gene, which encodes the S12 protein of 16S rRNA, was shown in the mutual proteins for control, 3-HPAA or 4-HBA treated bacteria and it was presented as the housekeeping (reference) gene for *P. aeruginosa* in RT-qPCR in the literature (Dumas et al., 2006; Llanes et al., 2004), it was chosen as reference gene in RT-qPCR. In the

protein data, S15 protein of 16S rRNA was undetected in the presence of each phenolic acid. S15 protein is one of the important constituents of small subunit of prokaryotic ribosome (Aseev and Boni, 2011). It was demonstrated that it is required for ribosome assembly and it provides an important bridge between small and large subunits *in vitro* (Serganov et al., 2003; Geissmann et al., 2009) and it was required for the proper ribosome assembly in the stress conditions *in vivo* (Bubunenko et al., 2006). Hence, the rpsO gene which encodes the S15 ribosomal protein, was determined to be validated by RT-qPCR to show the decreased expression of it. The primers specific to these genes were designed for these genes by Primer BLAST database were shown in Table 3.30.

Table 3.30. The primers used in RT-qPCR.

Genes	F Primer	R Primer
rpsL	CGTACATCGGTGGTGAAGGT	CGACCCTGCTTACGGTCTTT
rpsO	TACAAGCAAGCTGAAGGCGA	CCATACGGATCAGACCACGG

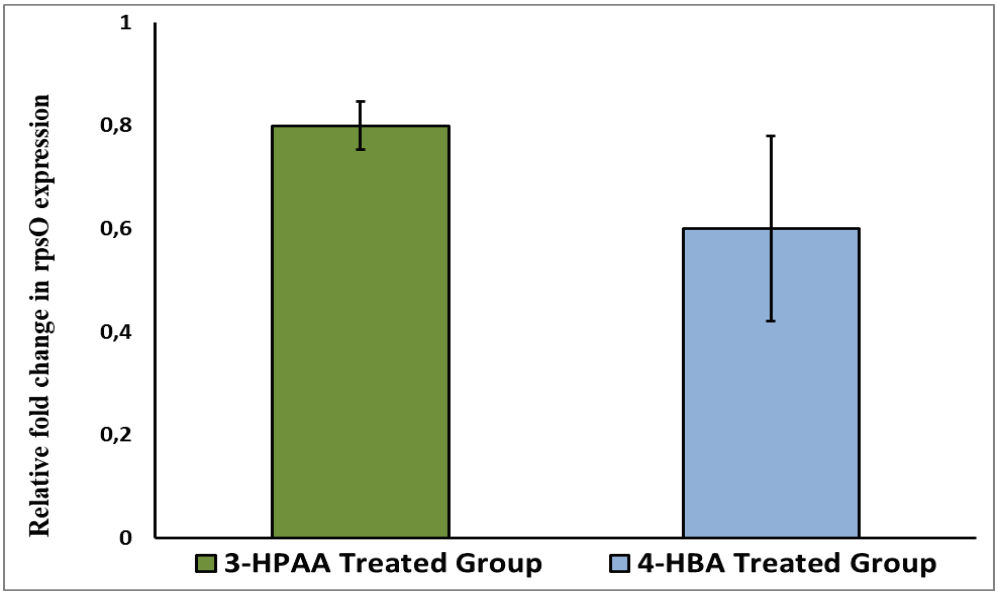

Figure 3.39. Relative fold change in the expression of rpsO gene. Average fold change of control group is 1.0. Normalization was performed based on rpsL gene expression and untreated group.

According to the calculations based on delta Ct method, the results of three biological samples and three technical repeats were found. The average fold change in Ct values of mRNA expression of rpsO gene was 0.8 (±0.04) for 3-HPAA treated cells while it was 0.6 (±0.2) for 4-HBA treated cells. The normalization was performed for the mRNA expression of housekeeping gene and untreated group (as 1.0 in fold change). These results showed that 3-HPAA treatment resulted in a 1.3 fold decrease and 4-HBA treatment resulted in a 1.7 fold decrease in the expression of rpsO gene which is consistent with the protein data (Figure 3.39).

CHAPTER 4

THE ANTIMICROBIAL EFFECTS OF PHENOLIC ACID LOADED ALGINATE-CHITOSAN NANOPARTICLES ON PATHOGENIC BACTERIA

4.1. Introduction

Pathogenic bacteria are serious treats for human health since they result in serious infections in humans, worldwide. Nosocomial pathogens (i.e. *Pseudomonas aeruginosa*, *Staphylococcus epidermidis*, methicillin resistant *Staphylococcus aureus*, methicillin susceptible *Staphylococcus aureus*, *Acinetobacter haemolyticus*) and food-borne pathogens (i.e. *Escherichia coli* O157H:7, *Salmonella* Enteritidis and *Listeria monocytogenes*) are well-known pathogenic bacteria which cause high morbidity and mortality. The treatments of the infections caused by these bacteria are carried out by antibiotics in use. However, these bacteria have resistance against many of the antibiotics as well as they can develop resistance during the treatment. Thus, it is a challenge to combat these bacteria. Therefore, bioactive compounds are in search as new antimicrobial agents all over the world.

The phenolic acids, which are synthesized as secondary metabolites by almost all plants (Hurtado-Fernandez et al., 2010), are accepted as promising candidates of new antimcirobial agents. Their stuructures consist of the benzene ring with one or more hydroxyl groups and sometimes additional radical groups (Hurtado-Fernandez et al., 2010). The phenolic acids and the plant extracts that contain phenolic compounds were shown in many studies for their antimicrobial properties (Karaosmanoglu et al., 2010; Gutiérrez-Larraínzar et al., 2012; Díaz-Gómez et al., 2013; Cueva et al.,2010; Albanoa et al., 2019). However, they are sensitive to environmental conditions which may result in decreasing or fluctuating antimicrobial effects. Encapsulation of bioactive compounds, which catches attention in the studies of biomedical field, may facilitate the long term stability and preserved therapeutic effects (Krausz et al, 2015). Structural durability of phenolic acids by encapsulation are achieved by decreasing the oxidation

and/or degradation of them (Li et al., 2015). Nowadays, there are many studies which show the antimicrobial effects of encapsulated antimicrobial agents in an increasing manner (Khan et al.,2019; MubarakAli et al., 2018; Liu et al., 2018; Wu et al., 2018; Ananda et al., 2019; Wintachai et al., 2019). The results of these studies indicate efficient results to combat pathogenic bacteria with encapsulated agents.

The phenolic acids used in this study, 3-hydroxyphenylacetic acid (3-HPAA) and 4-hydroxybenzoic acid, are water-soluble, simple phenolic acids with dose-dependent antimicrobial activities which were determined in our previous studies (chapter 2). In the current study, it was aimed to show the antimicrobial effects of encapsulated 3-HPAA and 4-HBA in the solution form on nosocomial and food-borne pathogens.

The encapsulation of bioactive compounds could be achieved by using polymers such as chitosan and alginate. Since these materials are both biocompatible and biodegradible with easy-to-use natures, they are frequently used for this purpose (Paques et al., 2014). Cationic polymer, chitosan, is obtained from chitin and it has antimicrobial properties (Jayakumar et al., 2010). It can be used to make effective substances by combining with vitamins, minerals, oils, proteins and biologically active natural compounds (Tang et al., 2013; Azevedo et al., 2014; Budnyak et al., 2016; Deka et al., 2016; Wu et al., 2018; Moschona and Liakopoulou-Kyriakides, 2018). Alginate, which is also a polymer, is obtained from algea. It is water soluble and has anionic nature (Paques et al., 2014). Since it can be used to synthesize hydrogels in the presence of divalent cations, it is an important encapsulation material (Yang et al., 2011).

In our study, encapsulations of 3-HPAA and 4-HBA into alginate- chitosan nanoparticles were achieved via ion gelation technique. In the first step, the complexes of alginate with 3-HPAA or 4-HBA were produced by calcium chloride ($CaCl_2$) which was used as a cross-linker. Then these pre-gels were covered with chitosan as the outermost layer of the nanoparticles. Coating of the anionic polymer, alginate, with a cationic polmer, chitosan, produces the alginate-chitosan nanoparticles by electrostatic interactions (Liu et al., 2018) with enduring coat and high structural stability (Paques et al., 2014).

Herein we report the synthesis, physco-chemical characterization and *in vitro* antimicrobial effects of alginate-chitosan nanoparticles on various pathogenic bacteria. The alginate chitosan nanoparticles loaded with 3-HPAA (3-HPAA-Alg-Chi) or 4-HBA

(4-HBA-Alg-Chi) were investigated in comparison to their unloaded alginate-chitosan nanoparticles (null nanoparticles).

4.2. Materials and Methods

All of the materials; low molecular weight chitosan, low viscosity alginic acid sodium salt, calcium chloride dihydrate, sodium hydroxide, hydrochloric acid, acetic acid, 3-hydroxyphenylacetic acid, 4-hydroxybenzoic acid, ethanol, agar were purchased from Sigma-Aldrich while tryptic soy broth was purchased from Merck. Ion gelation technique was used in the production of nanoparticles. Null nanoparticles (without any antimicrobial agents) and phenolic acid loaded nanoparticles (3-HPAA-Alg-Chi and 4-HBA-Alg-Chi) were produced under aseptic conditions with sterile equipments and solutions.

4.2.1. Preparation of Alginate-Chitosan Nanoparticles

Alginate-Chitosan nanoparticles were prepared based on the protocol of Azevedo et al. with the modification of increasing in the concentration of $CaCl_2$ (Azevedo et al., 2014).

The alginate solution was prepared by dissolving sodium alginate (0.63 mg/ml) in double distilled water (ddH_2O). The pH of the alginate solution was adjusted to pH 4.9 by 1 M hydrochloric acid (HCl). This solution was used in null nanoparticle production. Besides that, in phenolic acid loaded nanoparticle productions, the alginate solutions with additions of 3-HPAA (3mg/ml or 25 mg/ml) or 4-HBA (2.8 mg/ml) were used. Chitosan solution was prepared by dissolving the chitosan (low molecular weight) (0.4 mg/ml) in sterile 1% acetic acid (in ddH_2O, v/v). The pH of chitosan solution was adjusted to pH 4.6 by 1 M sodium hydroxide (NaOH).

The stock solution of calcium chloride ($CaCl_2$) in 25 mM was prepared by dissolving calcium chloride dihydrate in ddH_2O and autoclaving before usage. This solution was used as cross-linker by addition in 7.5 ml into alginate solution on ice with 0.125 ml/min flow rate for each type of nanoparticle. During this step, Ultra-Turrax was used to have continuous 20.000 rpm stirring for homogenization. Prepared chitosan solution was added onto alginate-$CaCl_2$ pre-gel (for null nanoparticles) and onto

alginate-phenolic acid-$CaCl_2$ pre-gel (for phenolic acid loaded nanoparticles) with 0.278 ml/min flow rate for each with 600 rpm continuous stirring. Alginate and chitosan were used in the 5:1 volume ratio (alginate:chitosan) for each nanoparticle solution. Prepared nanoparticle solutions were allowed to stir 20 more minutes and they were kept at 4°C until usage.

In each study, required volumes of the nanoparticle solutions were vortexed for 30 seconds and sonicated for 30 minutes at 4°C before usage. Sonication bath was kept cold by using ice cubes during sonication.

4.2.2. Characterization of Nanoparticles

The prepared nanoparticles were investigated via Dynamic Light Scattering (DLS), Fouirer Transfrom Infrared Spectrometry (FT-IR) and Scanning Electron Microscopy (SEM).

4.2.2.1. Dynamic Light Scattering (DLS)

The determination of size distributions (by number distribution) and polydispersity indexes (PDI) of nanoparticles were performed by dynamic light scattering (DLS) by Zetasizer (Nanoplus 3 Zeta/nano particle analyzer, Micromeritics) with Nanoplus version 5.22/3 software. Analyses were performed at a scattering angle of 165°, refractive index of 1.3, repetition of 2 and temperature of 25°C.

Each sample in 3 ml volume was investigated in disposable DLS cuvettes immediately after sonication. Average and standart deviation calculations were done by Microsoft Excel software.

4.2.2.2. Fouirer Transform Infrared Spectrometry (FT-IR)

The infrared spectra measurements were performed by FT-IR spectrometer (PerkinElmer Spectrum 2) equipped with a deuterated tri-glycine sulphate (DTGS) detector and a horizontal attenuated total reflectance (HATR) sampling accessory (ZnSe crystal). The spectra were recorded in the mid-infrared (4000-650 cm^{-1} wavenumber)

range by transmittance (T%) values at room temperature with the number of scans of 20 and resolution of 4 cm^{-1}. Each nanoparticle solution was liyophilized for 24 hours (Labconco-Freezone) before FT-IR measurements. After collecting the background spectra prior to measurements, the nanoparticles (null, 3-HPAA-Alg-Chi and 4-HBA-Al-Chi), chitosan, alginate, 3-HPAA and 4-HBA were placed on the crystal region of the instrument individually and compressed by metal arm until a stable force gauge value was achieved. The data were collected by Spectrum software (Version 10.4.3). In between each measurement ZnSe crystal was cleaned by isopropyl alcohol.

4.2.2.3. Scanning Electron Microscopy (SEM)

Sonicated samples were centrifuged at 18,000 x g at 4^{o}C for 30 minutes. They were diluted by dissolving the pellet in ddH_2O with 2-fold of the original solution volume. Diluted nanoparticle solutions were vortexed and sonicated for 5 minutes. Then, 10 µl of the samples were placed on aluminum foil and allowed to dry at 37^{o}C for 30 minutes. These samples were placed on double-sided carbon bands on metal grids. They were covered by gold for 2 minutes and investigated under SEM (Philips XL 30). Micrographs of the nanoparticles were taken with different magnifications.

4.2.3. Encapsulation Percentages of Phenolic Acids

The encapsulation percentages of phenolic acids into Alg-Chi nanoparticles were determined by UV-visible spectrophotometer (Thermo Multiscan) measurements.

4.2.3.1. UV-Visible Peaks of Phenolic Acids

Stock solutions of 3-HPAA and 4-HBA were dissolved in ddH_2O (1 mg/ml) individually. To see the peak of the solution clearly, the dilutions of 10-fold, 50-fold, 100-fold and 500-fold of each stock solution were prepared in ddH_2O and were subjected to UV-Spectrum scanning. The measurements were performed in the range of 200-400 nm wavelenght by using quartz cuvettes in 1ml volume. The wavelenghts that show significant peaks were chosen for each phenolic acids for further studies.

4.2.3.2. Standard Graphs of Phenolic Acids

The stock solutions of 3-HPAA and 4-HBA were prepared (1mg/ml) in ddH_2O. The dilutions in 0.001 mg/ml, 0.002 mg/ml, 0.005 mg/ml, 0.01 mg/ml and 0.02 mg/ml concentrations were prepared and measured spectrophotometrically in UV-Vis spectrum by using quartz cuvettes (1 ml). The wavelengths which were pre-determined in UV-Spectrum scanning analyses were used for each phenolic acid. The standart curves were plotted by absorbance values (nm) of each dilution versus concentration (mg/ml) of the dilutions (Microsoft Excel). Slope equations and R^2 values were indicated to use in calculations in further steps.

4.2.3.3. Calculation of Encapsulation Percentages

The encapsulation percentages of phenolic acids into Alg-Chi nanoparticles were calculated by using the concentrations of the phenolic acids in the supernatant of nanoparticles. For this purpose, phenolic acid loaded nanoparticle solutions were vortexed for 30 seconds and sonicated for 30 minutes. The solutions were centrifuged at 18000 x g for 30 minutes. The supernatants were measured spectrophotometrically by using quartz cuvettes in 1 ml volume at pre-determined wavelengths. According to equations of the standard curves of each phenolic acid, the concentrations of phenolic acids were calculated in mg/ml by using the absorbance values. These concentration values were called “supernatant phenolic acid concentration” in the calculation of percentages (equation 4.1). The encapsulation percentage for each phenolic acid was calculated according to the equation 4.1 below. In the equation, “total phenolic acid concentration” indicates the total phenolic acid amount that was used in nanoparticle preparation. The measurements and the calculations were performed in duplicates.

$$(\text{Encapsulation \%}) = 100 - ((\text{Supernatant phenolic acid conc.} / \text{Total phenolic acid conc.}) \times 100) \quad (4.1)$$

4.2.4. Antimicrobial Effects of Nanoparticles

During all antimicrobial experiments; bacteria were maintained on tyrptic soy agar (TSA) plates by inoculation of a single colony on fresh agar plate every week. The bacteria were grown overnight at 37^{o}C. The bacteria were maintained in TSB containing 20% glycerol and kept at -80^{o}C for long term storage.

4.2.4.1. Agar Diffusion Method

The bacteria which were used in agar diffusion studies were *Pseudomonas aeruginosa*, *Acinetobacter haemolyticus*, *Escherichia coli* O157:H7, *Salmonella* Enteritidis, *Staphylococcus epidermidis*, Methicillin Resistant *Staphylococcus aureus* (MRSA), Methicillin Susceptible *Staphylococcus aureus* (MSSA), and *Listeria monocytogenes.* In all agar diffusion experiments, the bacterial lawn was prepared according to the protocol below:

A single colony of the bacteria was inoculated into 4 ml of TSB media and incubated at 37^{o}C for 18 hours to obtain overnight cultures. A 100 µl of the overnight culture was spreaded onto TSA media and allowed to dry for 1 hour at room temperature for agar diffusion tests.

To determine the antimicrobial effects, 15 µl of each solution (3 mg/ml-3-HPAA-Alg-Chi or 2.8 mg/ml-4-HBA-Alg-Chi and the respective phenolic acids solutions (in ddH_2O) in the same concentrations) were tested by direct application on the agar plate. Nanoparticles and phenolic acid solutions were tested after treating with 1% (v/v) acetic acid in ddH_2O for 24 hours at +4^{o}C before application or without acetic acid treatment.

In addition, the higher concentrations of 3-HPAA were tested to determine the most effective concentration on bacteria by agar diffusion. According to these results, 25 mg/ml 3-HPAA loaded nanoparticles were produced with the aforementioned nanoparticle production protocol, and were tested on bacteria in 15 µl volume on agar directly. The nanoparticles were treated with 1% acetic acid in ddH_2O, incubated for 24 hours and 72 hours at +4^{o}C before application (for 25 mg/ml 3-HPAA-Alg-Chi solution).

4.2.4.2. The Effect of the Nanoparticles on Bacterial Growth

The bacteria which were used in these studies were *Pseudomonas aeruginosa*, *Staphylococcus epidermidis*, Methicillin Resistant *Staphylococcus aureus* (MRSA), and Methicillin Susceptible *Staphylococcus aureus* (MSSA). A single colony of the bacteria was inoculated into 4 ml of TSB and incubated at 37^{o}C for 18 hours. The tubes containing 4 ml of total volume of the mixture of TSB, Alg-Chi nanoparticle solutions (null or 3-HPAA-Alg-Chi) with 10% or 20% (v/v) final concentrations and 1% (v/v) acetic acid (final concentration) were inoculated with 10^6 cfu/ml final bacterial load. The effect of 1% (v/v) acetic acid (final concentration) was simultaneously tested with the same concentrations with addition of ddH_2O instead of nanoparticle solution. The optical density (O.D.) of the cultures were measured spectrophotometrically at 600 nm at the time of inoculation (hour 0) and at the end of the incubation period (hour 24). The cell viabilities of these cultures were also determined by enumeration studies.

4.3. Results and Discussion

To investigate the possible application route of encapsulated phenolic acid solutions in the microbiological point of view, the alginate-chitosan nanoparticles (null or phenolic acid loaded) were produced, characterized and antimicrobially tested on various pathogenic bacteria *in vitro*.

4.3.1. Investigation of Properties of Nanoparticles

The polydispersity indexes (PDI), average diameters and distributions of number of all Alg-Chi nanoparticles were investigated by dynamic light scattering (DLS). The infrared spectra of the compounds were determined by Fouirer Transform Infrared Spectroscopy (FT-IR) for comparison of physco-chemical properties of alginate, chitosan, 3-HPAA, 4-HBA, null Alg-Chi, 3-HPAA-Alg-Chi (3 mg/ml or 25 mg/ml 3-HPAA loaded) and 4-HBA-Alg-Chi (2.8 mg/ml 4-HBA loaded). To visualize the morphologies of null Alg-Chi, 3-HPAA-Alg-Chi (3 mg/ml or 25 mg/ml 3-HPAA loaded) and 4-HBA-Alg-Chi (2.8 mg/ml 4-HBA loaded), scanning electron microscopy (SEM) was used.

4.3.1.1. Dynamic Light Scattering of Alg-Chi Nanoparticles

The results of DLS indicated the increase in the average size of Alg-Chi nanoparticles which indicates the successful encapsulation of 3-HPAA and 4-HBA. The size distributions of 3 mg/ml or 25 mg/ml 3-HPAA-Alg-Chi indicated the shift of the peaks of 3-HPAA-Alg-Chi were further to the right than null nanoparticles (Figures 4.1 a and b) while a minor shift of the peak was determined for 4-HBA-Alg-Chi compared to null nanoparticles (Figure 4.1 c). This might contributed to different physco-chemical properties of 3-HPAA and 4-HBA. Consequently, phenolic acid loaded nanoparticles have bigger average sizes than those of null ones. Since a single peak occurred for each solution, particle sizes had a high uniformity (Mohammadi et al., 2016).

Related to that, the average sizes of null nanoparticles were shown to be smaller than these of phenolic acid loaded nanoparticles (Table 4.1). For instance, 25 mg/ml 3-HPAA-Alg-Chi were determined as 278.8 ± 12.4 nm and 361.0 ± 69.8 nm for null and 3-HPAA-Alg-Chi, respectively (Table 4.1). Additionally, 3 mg/ml 3-HPAA-Alg-Chi had 291.1±0.5 nm and 4-HBA-Alg-Chi had 316.0 ±3.8 nm while null nanoparticles had 255.8 ±2.3 nm average diameters (Table 4.1). According to these results, the loading of 3-HPAA or 4-HBA into nanoparticles considered as successful. The loading the lower concentrations of phenolic acids resulted in the narrowest size distribution: the standart deviation was ±0.5 for 3 mg/ml 3-HPAA while it was ±69.8 when 25 mg/ml 3-HPAA was loaded (Table 4.1).

In addition, the distribution of size of null nanoparticles and phenolic acid nanoparticles were narrow (Table 4.1). Null nanoparticles had smaller diameters than 25 mg/ml 3-HPAA-Alg-Chi with narrower size distribution: ±12.4 standart deviation for null and ±69.8 for 25 mg/ml 3-HPAA-Alg-Chi (Table 4.1). It might be speculated that the protocol of nanoparticle production supported the homogeneous particles. However, loading with phenolic acids caused the homogeneity of the particles to decrease slightly depending on the concentration of loading compound used.

Additionally, it could be recognized that the average diameters of the nanoparticles were determnined higher than 100 nm in DLS. Since the hydrodynamic diameters of the particles are measured in DLS technique (Krausz et al., 2015) and these values are the distribution in sizes, these higher diameters were expected. To be able to

determine exact diameters, the measurement of the diameters of particles in scanning electron microscopy could be examined.

Table 4.1. Comparison of average diameters (nm) and PDI values of null and phenolic acid loaded Alg-Chi nanoparticles via DLS.

Sample Name	PDI	Average Diameter (nm)
Null Nanoparticles	0.25	255.8 ±2.3
3-HPAA-Alg-Chi (3mg/ml)	0.27	291.1±0.5
Null Nanoparticles	0.22	278.8±12.4
3-HPAA-Alg-Chi (25 mg/ml)	0.23	361.0±69.8
Null Nanoparticles	0.25	255.8 ±2.3
4-HBA-Alg-Chi (2.8 mg/ml)	0.29	316.0 ±3.8

The polydispersity index (PDI) is another important parameter of size distribution. A decreased PDI value indicates an increase in the particle size homogeneity. Small PDI values (PDI <1) shows narrow size distributions (Liu et al., 2018; Qi et al., 2004).

In addition, PDI values must be below 0.7 for a nanoparticle sample to be suitable for DLS analysis (Dynamic Light Scattering Common Terms Defined, Malvern Instruments Manual; www. malvern.com). Since the PDI values of nanoparticles were about 0.2 for each nanoparticle solution (Table 4.1), all nanoparticle solutions were suitable for DLS analysis and it could be accepted that nanoparticle solutions were homogenous with similar homogeneity patterns.

4.3.1.2. SEM Images of Alg-Chi Nanoparticles

According to the scanning electron micrographs, the produced null nanoparticles (Figure 4.2) were spherical. Also the same spherical structures were observed in the nanoparticles which were loaded with 3 mg/ml, 25 mg/ml 3-HPAA and 2.8 mg/ml 4-HBA (Figures 4.5, 4.6 and 4.7, respectively). The agglutinations of nanoparticles in the figures were expected based on the natural properties of chitosan based particles to produce agglomerates (Jamil et al., 2016 (b)).

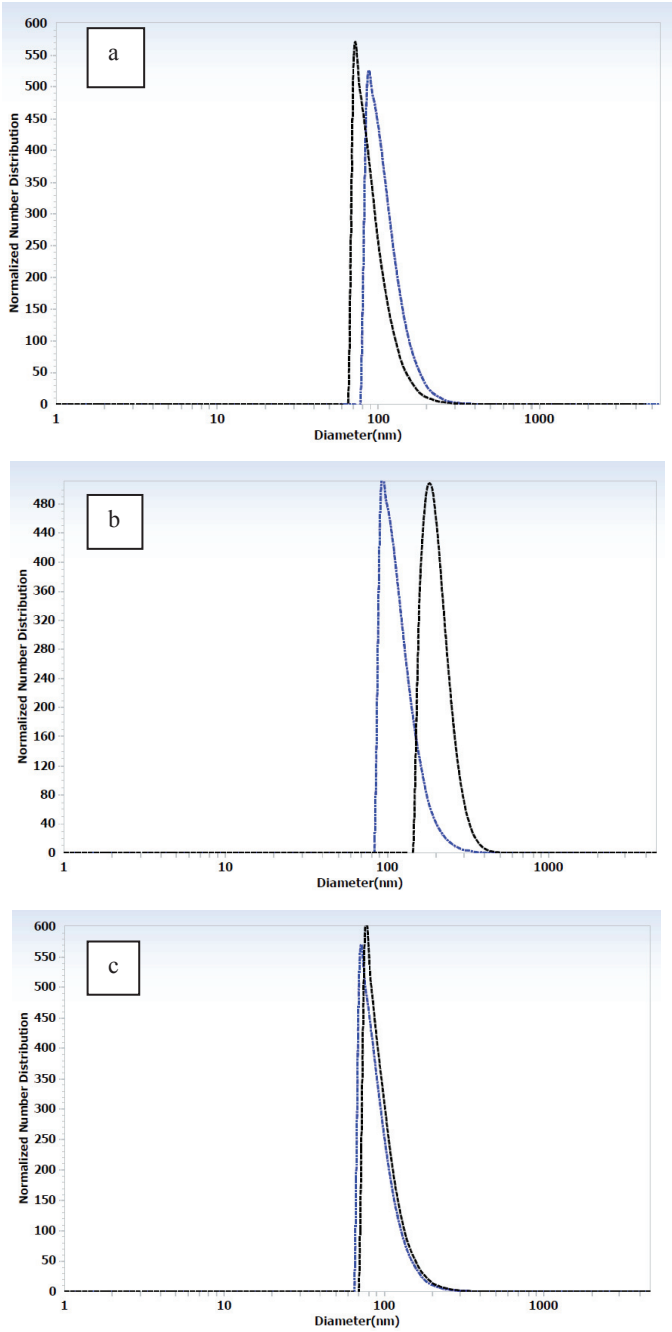

Figure 4.1. Normalized number distribution graphs of null and phenolic acid loaded Alg-Chi. a) 3 mg/ml 3-HPAA-Alg-Chi (Black peak: Null nanoparticles, Blue peak: 3-HPAA-Alg-Chi); b) 25 mg/ml 3-HPAA-Alg-Chi (Black peak: 3-HPAA-Alg-Chi, Blue peak: Null Nanoparticles); c) 4-HBA-Alg-Chi (Black peak: 4-HBA-Alg-Chi, Blue peak: Null Nanoparticles)

The chitosan nanoparticles are inclined to agglomerate depending on the domination of van der Walls attractive forces over repulsive forces (Jamil et al., 2016 (b)). According to the SEM images, the nanoparticles display homogenous sizes. In addition, the measurements of the diameters that were carried out at the time of SEM analyses via SEM instrument presented that the particles have diameters in a range of 25-40 nm for null, 3 mg/ml 3-HPAA-Alg-Chi and 2.8 mg/ml 4-HBA-Alg-Chi while 40-70 nm for 25 mg/ml 3-HPAA-Alg-Chi. Our results were consistent with the results of Azevedo et al. of which the production protocol of nanoparticles was used, since they also presented that the shapes of the nanoparticles they produced were spherical (Azevedo et al., 2014). However, the nanoparticles they produced were not homogeneous in sizes under TEM analysis. Since the particles of ours seem to display more homogeneous sizes under SEM, it could be speculated that the usage of increased molarity of $CaCl_2$ in the production process might result in the production of more homogeneous nanoparticles.

4.3.1.3. FTIR Analysis of Alg-Chi Nanoparticles

The FT-IR results were shown in the Figures 4.8 and 4.9 for 25mg/ml- or 3 mg/ml-3-HPAA-Alg-Chi and 4-HBA-Alg-Chi, respectively. When the spectra were investigated, the differences in the wavelengths of the peaks could be recognized for each loaded naoparticle type in comparison to null nanoparticles, chitosan, alginate and phenolic acid spectra. The differences in wavenumbers of peaks occured especially in the region below 1500 cm^{-1} which is the fingerprint region of FT-IR spectrum (Hynes et al., 2005).

These differences show that the compounds tested have different structures because of the new bond formations in the null or phenolic acid loaded nanoparticles productions. In addition, the spectra of 3-HPAA-Alg-Chi were the same regardless of the loaded concentrations of 3-HPAA and their spectra differ from that of 4-HBA-Alg-Chi. Since each compound had a unique FT-IR spectra, successful productions of nanoparticles as well as successful loading of phenolic acids into nanoparticles were achieved. The discussions about the structural changes were performed by comparing the peak wavelenghts of the aforementioned samples obtained from Spectrum programme to the similar studies in the literature.

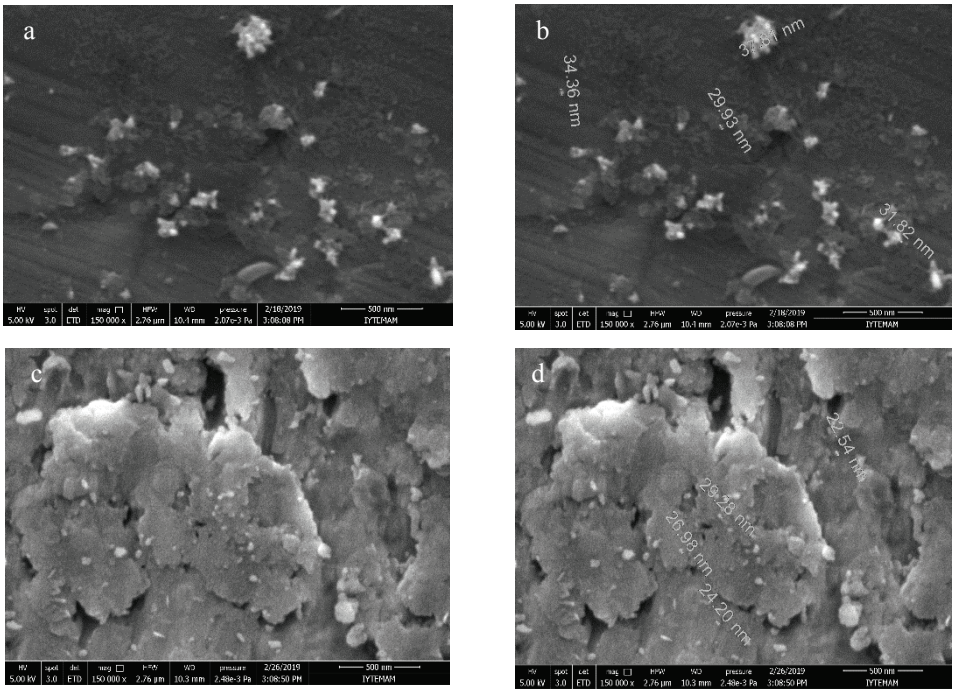

Figure 4.2. Morphologies of null Alg-Chi. a,b) The null nanoparticles which were produced in the study of 3 mg/ml 3-HPAA-Alg-Chi or 2.8 mg/ml 4-HBA-Alg-Chi; c, d) The null nanoparticles which were produced in the study of 25 mg/ml 3-HPAA-Alg-Chi at 150,000 x magnification. The diameters of the particles were determined at the time of SEM analysis.

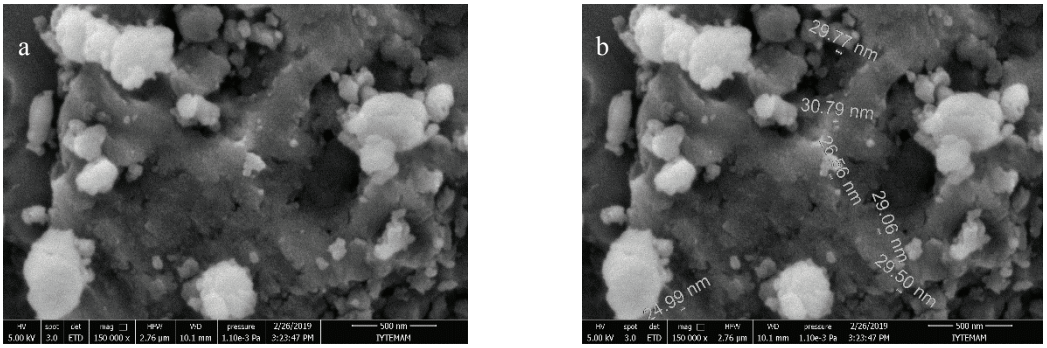

Figure 4.3. Morphologies of 3 mg/ml-3-HPAA-Alg-Chi (a) and the diameters of the particles (b) at 150,000 x magnification. The diameters were determined at the time of SEM analysis.

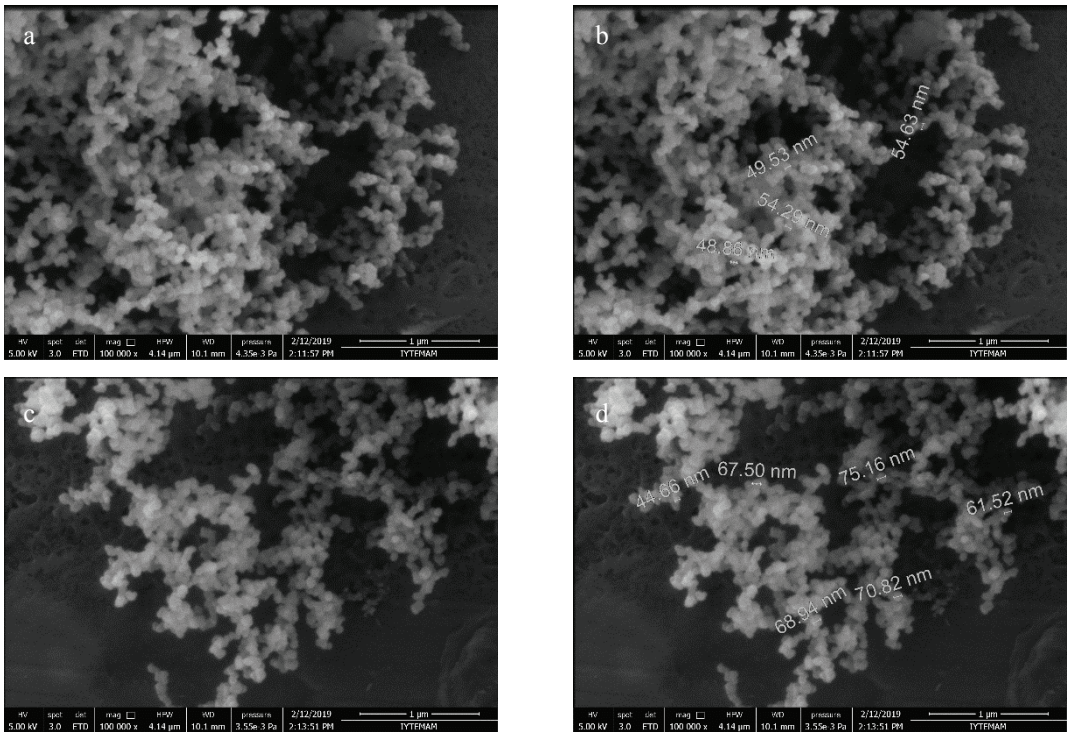

Figure 4.4. Morphologies of 25 mg/ml-3-HPAA-Alg-Chi (a and c) and the diameters of the particles (b and d) at 100,000 x magnification. The diameters were determined at the time of SEM analysis.

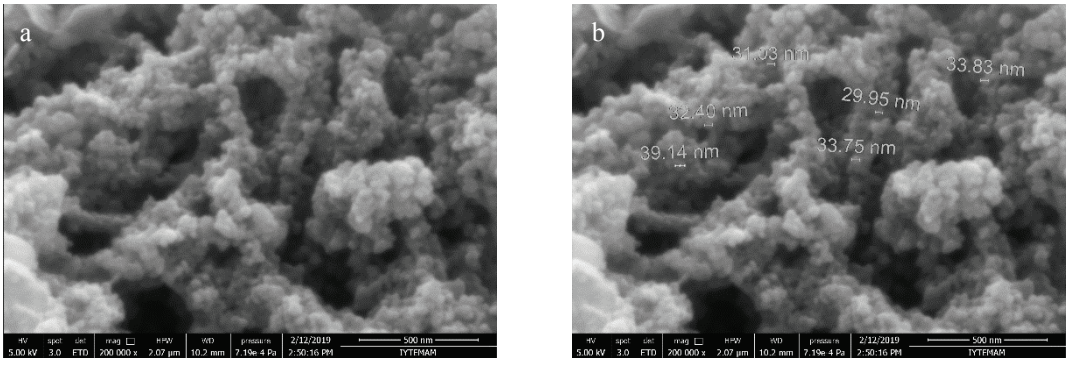

Figure 4.5. Morphologies of 2.8 mg/ml 4-HBA-Alg-Chi (a) and the diameters of the particles (b) at 200,000 x magnification. The diameters were determined at the time of SEM analysis.

The peaks of loaded nanoparticles at 3196 cm^{-1} (Figure 4.6. a), 3241 cm^{-1} (Figure 4.6. b), and 3376 cm^{-1} (Figure 4.6. c), and null nanoparticles at 3264 cm^{-1} (Figure 4.6. a and b), and 3265 cm^{-1} (Figure 4.6. c), nanoparticles contain hydroxyl groups. These were caused from oxial O-H and N-H stretching of Chi at 3288 cm^{-1} (Figure 4.6. a and b) and 3289 cm^{-1} (Figure 4.6. c) and O-H stretching of Alg at 3240 cm^{-1} (Figure 4.6. a and b) and 3241 cm^{-1} (Figure 4.6. c) (Wu et al., 2018).

Additionally, the peak of null nanoparticles at 3264 cm^{-1} (Figure 4.6. a and b) shifted to lower wavenumbers in 3-HPAA-Alg-Chi: 3196 $cm^{-}1$ for 3 mg/ml 3-HPAA-Alg-Chi, 3241$cm^{-}1$ for 25 mg/ml 3-HPAA-Alg-Chi (Figure 4.6). Differently from 3-HPAA, in 4-HBA-Alg-Chi the wavenumber of null nanoparticles at 3265 $cm^{-}1$ was shifted to higher wavenumber 3376 cm^{-1} because of different physco-chemical properties of these nanoparticles (Figure 4.7). These shifts in wavenumbers of peaks presented the successful loading of phenolic acids into alginate-chitosan nanoparticles (Wu et al., 2018). Another indicator of loading of 3-HPAA could be accepted as the disappearence of CH stretching of 3-HPAA compound at 2965 cm^{-1} (Barrera-Necha et al., 2018) in 3-HPAA-Alg-Chi (Figure 4.6).

In Figure 4.6, the shifting of the peaks at 1558 cm^{-1} in null nanoparticles could be seen towards the higher wavenumbers, 1696 cm^{-1} and 1698 cm^{-1} for 3 mg- and 25 mg/ml-3-HPAA-Alg-Chi, respectively. Similarly, in the 4-HBA-Alg-Chi spectra (Figure 4.7), the same peak at 1558 cm^{-1} in null nanoparticles was shifted to 1673 cm^{-1}. This was arised from electrostatic interactions which occur between the amine group of chitosan at 1648 cm^{-1} and carboxylate group of alginate at 1597 cm^{-1} (Figures 4.8 and 4.9) (Wu et al., 2018).

According to Wu et al., the peak at 1404 cm^{-1} in null alginate-chitosan nanoparticles was caused from the symmetric stretching in carboxylic acid groups of alginate and chitosan (Wu et al.,2018). In our study, this peak was seen at 1407 cm^{-1} in null nanoparticles (Figures 4.8 and 4.9) and its shift was obtained towards 1386 cm^{-1} (Figure 4.6 a) 1385 cm^{-1} (Figure 4.6 b) and 1412 cm^{-1} (Figure 4.7) in 3 mg/ml-3-HPAA-Alg-Chi, 25 mg/ml-3-HPAA-Alg-Chi and 4-HBA-Alg-Chi. This shifting showed the loading of 3-HPAA or 4-HBA into the alginate-chitosan nanoparticles since they differ from null nanoparticles. Depending on the stretching vibrations of C-O-C of the polysaccharide structure, the peaks were obtained at 1027 cm^{-1} and 1026 cm^{-1} for chitosan and alginate, respectively (Liu et al., 2018).

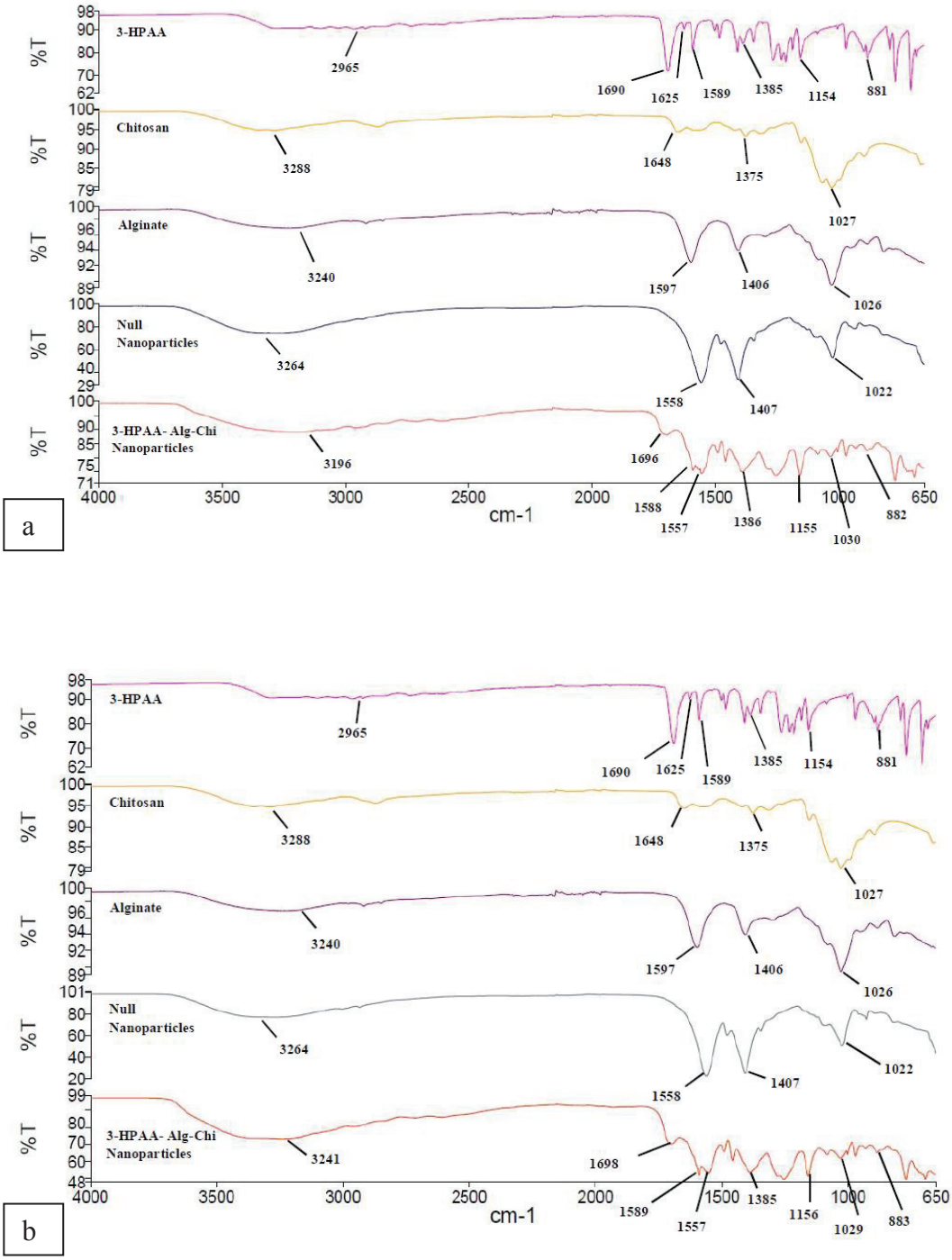

Figure 4.6. Comparison of the FT-IR spectra of the compounds in mid-IR region for 3 mg/ml (a) and 25 mg/ml (b) 3-HPAA-Alg-Chi. Different colors were used for the spectrum of each compound: 3-Hydroxyphenylacetic Acid (3-HPAA) (pink); Chitosan (yellow); Alginate (purple); Null Nanoparticles (grey) and 3-HPAA-Alg-Chi (orange)

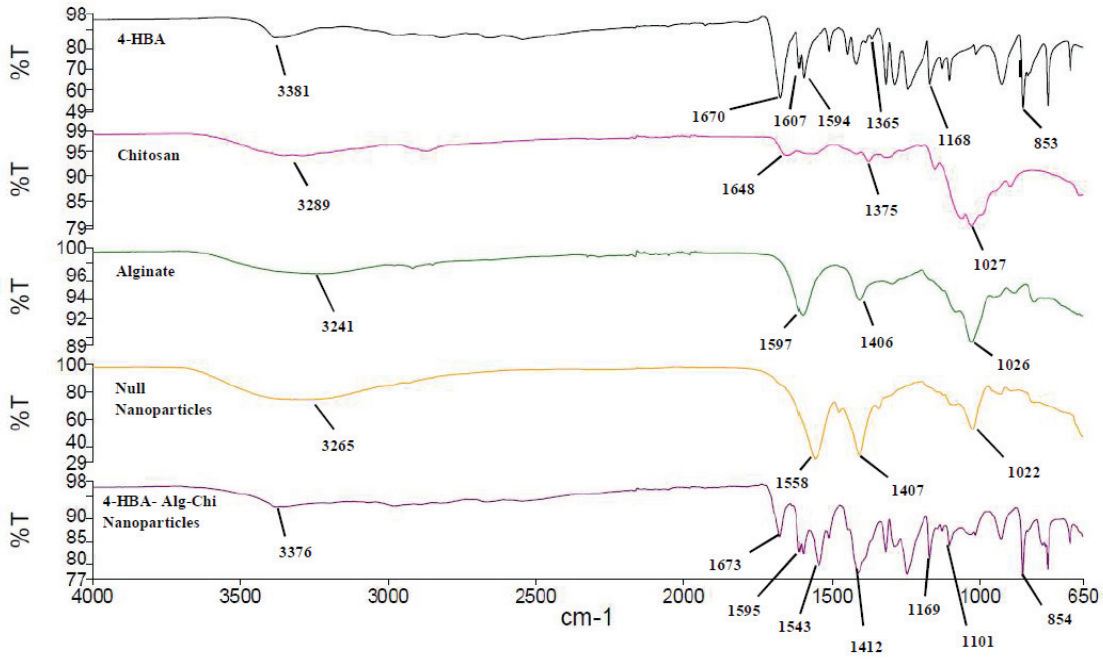

Figure 4.7. Comparison of the FT-IR spectra of the compounds in mid-IR region for 4-HBA-Alg-Chi. Different colors were used for the spectrum of each compound: 4-Hydroxybenzoic Acid (4-HBA) (grey); Chitosan (pink); Alginate (green); Null Nanoparticles (yellow) and 4-HBA -Alg-Chi (purple)

The peak which was related to C-O-C stretching was observed at 1022 cm^{-1} in null nanoparticles and it was obtained at higher wavenumbers in phenolic acid loaded nanoparticles: 1030 cm^{-1}, 1029 cm^{-1} and 1101 cm^{-1} for 3 mg/ml-3-HPAA-Alg-Chi, 25 mg/ml-3-HPAA-Alg-Chi and 4-HBA-Alg-Chi, respectively (Figures 4.8 a, b and 4.9). This might show the bondings and chemical structure of each nanoparticle differentiated from each other and from alginate and chitosan.

Additionally, the peak at 1154 cm^{-1} in 3-HPAA and at 1168 in 4-HBA corresponds to the asymmetric stretching of C-O-C bridge (Mladenovska et al., 2007). Since these peaks exist and slightly shifted to 1155 cm^{-1} in 3 mg/ml 3-HPAA-Alg-Chi, to 1156 cm^{-1} in 25 mg/ml 3-HPAA-Alg-Chi and to 1169 cm^{-1} in 4-HBA-Alg-Chi, phenolic acid loading was successfully obtained (Figures 4.8 and 4.9).

Likewise, the peaks at 881 cm^{-1} in 3-HPAA and at 853 cm^{-1} in 4-HBA, which might demonstrate the aromatic ring (Barrera-Necha et al., 2018), were shifted to

slightly higher wavenumbers. These peaks were seen at 882 cm^{-1} and 883 cm^{-1} for 3 mg/ml 3-HPAA-Alg-Chi and 25 mg/ml 3-HPAA-Alg-Chi (Figures 4.8 a and b) and 854 cm^{-1} for 4-HBA-Alg-Chi (Figure 4.7).

All in all, the comparison of the FT-IR spectra of null nanoparticles, phenolic acid loaded nanoparticles, phenolic acids, chitosan and alginate, indicated the successful production of null and phenolic acid loaded nanoparticles which show unique physco-chemical properties.

4.4. Determination of Encapsulation Percentages

After the specific wavelengths and standart graphs of phenolic acids were determined spectrophotometrically, the standart graphs were plotted and used in the encapsulation percentage calculations.

4.4.1. Determination of UV-Visible Peaks of Phenolic Acids

The wavelengths of the phenolic acids were determined based on the UV-Spectrum scanning of the diluted samples of phenolic acids. The spectrums of the phenolic acids were achieved in the range of 200-400 nm wavelengths in spectrophotometer.

The UV-Vis wavelength was demonstrated with 10-fold diluted 1 mg/ml stock solution of 3-HPAA (Figure 4.8 a). Since this phenolic acid had a significant peak at 270 nm, the wavelength for studies which were carried out with 3-HPAA was determined as 270 nm.

In the case of 4-HBA, the UV-Vis wavelength was demonstrated with 100-fold diluted 4-HBA stock solution (1 mg/ml) as demonstrated in Figure 4.8 b. The specific peak of this phenolic acid was observed at 250 nm. Thus, 250 nm was chosen as the wavelength for the studies of 4-HBA.

4.4.2. The Standart Graphs of Phenolic Acids

In the Figure.4.11 a and b, the standard curves of 3-HPAA and 4-HBA were shown, respectively. The graph of 3-HPAA has a R^2 value of 0.9962 while that of 4-

HBA was 1 (Figure 4.9 a and b).The equations of these graphs, Equation 4.2 for 3-HPAA and Equation 4.3 for 4-HBA, were used for encapsulation percentage calculations of the phenolic acids.

The y value in these equations was the average absorbance value of supernatant while the x value show the concentration of phenolic acid in the supernatant at specific wavelength of each phenolic acid (Figure 4.9 a and b). The equations of the standart graphs were found as below:

$$y = 10.665x-0.005 \quad (4.2)$$

$$y = 87.098x-0.0057 \quad (4.3)$$

4.4.3. Determination of Encapsulation Percentages

The encapsulation percentages of 3-HPAA-Alg-Chi or 4-HBA-Alg-Chi were calculated based on the equations of standart graphs of the phenolic acids.

Centrifugation was performed prior to measurements to harvest the nanoparticles and to get rid of the impurities. Thus, the supernatant has the amount of phenolic acid that could not been encapsulated into nanoparticles.Table 4.2 demonstrates the average encapsulation percentages of 3-HPAA and 4-HBA into nanoparticles. As it is seen in Table 4.2, 3-HPAA or 4-HBA were loaded into nanoparticles with more than 99% encapsulation. Therefore, it was decided to test the nanoparticles in solution forms in the antimicrobial studies. The cross-linker, $CaCl_2$, is one of the important parameters for the loading percentage, size and homogeneity of nanoparticles. The usage of higher concentrations of $CaCl_2$ in the nanoparticle production process results in the increased encapsulation percentage as well as the decreased average sizes and PDI values (Wu et al., 2018). Wu et al. demonstrated that higher encapsulation percentage, lower average size and PDI were obtained in the usage of 5 mM $CaCl_2$ when compared to those of 1 mM and 3 mM $CaCl_2$ usage in encapsulation of lysozyme into alginate-chitosan nanoparticles.

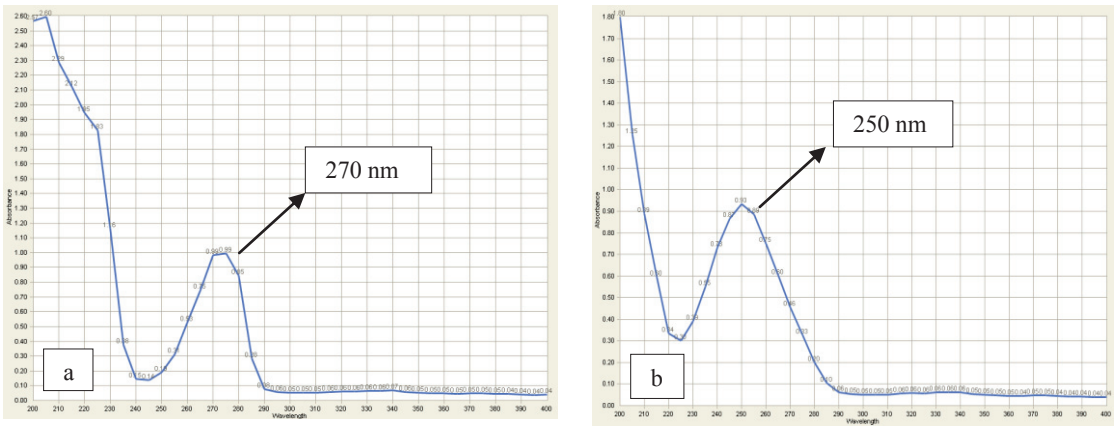

Figure 4.8. Graph of UV-spectrum scanning of phenolic acids. a) 3-HPAA (10-fold diluted from 1mg/ml stock solution in ddH_2O) b) 4-HBA (100-fold diluted from 1mg/ml stock solution in ddH_2O) (y axis: Absorbance, x axis: Wavelength).

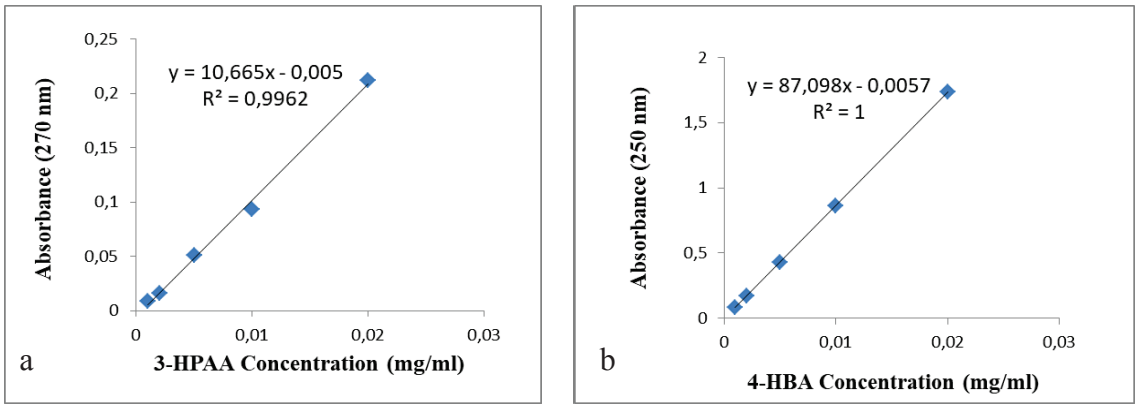

Figure 4.9. Standard graphs of phenolic acids. a) 3-HPAA b) 4-HBA

Table 4.2. The average encapsulation percentages of phenolic acids.

Sample	Concentration of Phenolic Acid in Supernatant (mg/ml)	Encapsulation Percentage (%)
3-HPAA-Alg-Chi (3 mg/ml)	0.23±0.002	99.6±0.31
3-HPAA-Alg-Chi (25 mg/ml)	0.28±0.017	99.9±0.04
4-HBA-Alg-Chi (2.8 mg/ml)	0.27±0.005	99.5±0.39

It was suggested that the increased concentration of $CaCl_2$ leads the increased cross-linking properties which result in fine pores and compact gelation of the polymers (Wu et al., 2018). In our study, the concentration of $CaCl_2$ was 25 mM. Thus, it could be concluded that, the obtained small and homogeneous alginate-chitosan nanoparticles with very high encapsulation percentages might be due to the usage of $CaCl_2$ in high concentration.

In the study of Madureira et al., phenolic acids (rosmarinic acid, protocatechuic acid or 2,5-dihydroxybenzoic acid) were encapsulated into chitosan nanoparticles with both high and low molecular weight chitosan (Madureira et al.,2015). Their results of low molecular weight chitosan are comparable to ours. They presented that the encapsulation percentages were in between 60-90% whereas it was found to be 99% in our study for each type of nanopaticles (Table 4.2). The usage of alginate for entrapping phenolic acids before covering with chitosan might enhance the encapsulation percentage in our study. In addition the cross-linker type (CaCl2 in our study and tripolyphosphate in theirs) might cause the change in entrapment conditions. In addition to that, the simpler structure and different physico-chemical properties of 3-HPAA than those of rosmarinic acid, protocatechuic acid or 2,5-dihydroxybenzoic acid could cause higher encapsulation percentages in our study.

4.4.4. Antimicrobial Tests of Nanoparticle Solutions

The antimicrobial tests of nanoparticle solutions loaded with 3 mg/ml 3-HPAA or 2.8 mg/ml 4-HBA were performed with the comparison of free phenolic acid solutions in ddH_2O with the same phenolic acid concentrations by agar diffusion (Figure 4.10 and 4.13). All solutions that contain acetic acid were applied after 24 hours of treatment with 1% acetic acid. These concentrations of phenolic acids were determined according to the antimicrobial studies of phenolic acids on *P. aeruginosa* which were performed previously (Appendix E).

The phenolic acid solutions without acetic acid treatment displayed no inhibition zones for tested Gram negative bacteria (Figure 4.10 a, c, e, g, regions III and V). When 1% acetic acid treated 4-HBA solution was tested, small and turbid inhibition zones for *P. aeruginosa*, *E.coli* O157:H7 and *S.* Enteritids (Figure 4.10 a, e, g, region VI) and clear inhibition zone for *A. haemolyticus* (Figure 4.10 c, region VI) were observed. The

similar small and turbid inhibiton zones were detected for 1% acetic acid treated 4-HBA loaded nanoparticle solution for the same aforementioned bacteria (Figure 4.10 b, f, h, region X) and a similar clear inhibition zone was observed for *A. haemolyticus* (Figure 4.10 d, region X). Therefore, 4-HBA loaded nanoparticles showed very slight effect on Gram negative bacteria except *A. haemolyticus*. Both 1% acetic acid and 1% acetic acid treated 4-HBA solutions (both free and nanoparticle) showed similar inhibition zones for this bacterium. The antimicrobial effect on *A. haemolyticus* might be due to the synergistic effect of acetic acid and tested solutions.

The 3-HPAA solution treated with 1% acetic acid did not produce any zones on Gram negative bacteria except *A. haemolyticus* (Figure 4.10 a, c, e, g, region IV). When the inhibition zones were compared in *A. haemolyticus* 1% acetic acid treated 3-HPAA-Alg-Chi solution (Figure 4.10 d, region IX) displayed bigger inhibition zones than that of 1% acetic acid treated 3-HPAA solution. However, the zones for phenolic acid loaded nanoparticle solutions as well as null nanoparticle solution were bigger and more clear (Figure 4.10 d, region VIII, IX, X). Thus, it might be concluded that nanoparticle solutions with 1% acetic acid treatment showed higher antimicrobial effect on *A. haemolyticus*. However, 3-HPAA-Alg-Chi solution treated with 1% acetic acid results in production of inhibition zones for other tested Gram negative bacteria. A better effect of this nanoparticle solution was detected for *S.* Enteritidis when compared to free 3-HPAA solution with 1% acetic acid (Figure 4.10 g, region IV and h, region IX). It could be concluded that, 3-HPAA-Alg-Chi solution treated with 1% acetic acid demonstrated slight antimicrobial effect on *P. aeruginosa* and *E. coli* O157:H7 while it showed higher antimicrobial effect on *A. haemolyticus* and *S.* Enteritidis. These results suggest that: The antimicrobial effect is depending on the type of the phenolic acid tested. The cell wall properties of the bacteria doesn't play any role in the antimicrobial effect of tested phenolic acids.

When the antimicrobial effects of all tested solutions were considered for Gram positive bacteria, it was clear that none of these solutions were effective on them. The application of the phenolic acids treated or untreated with 1% acetic acid and the nanoparticle solutions treated with 1% acetic acid result in no inhibition zones for *S. epidermidis*, MRSA, MSSA and *L. monocytogenes* as well as 1% acetic acid (Figure 4.11). Briefly, 3 mg/ml-3-HPAA-Alg-Chi and 4-HBA-Alg-Chi were slightly effective on some of the tested Gram negative bacteria while they have no inhibition effect on the

tested Gram positive bacteria. Treatment with 1% acetic acid increases the antimicrobial activity of the nanoparticle solutions depending on the pH change in Gram negative bacteria.

In addition, inside the inhibition zone of 70% ethanol, a ring-like growth of *Staphylococci* was observed. A further study was performed to test the effects of higher concentrations of ethanol on *Staphylococci* to determine the most effective ethanol concentration on these bacteria (Appendix F).

The increase in phenolic acid concentration could be useful for producing nanoparticle solutions with higher antimicrobial effects. Therefore, it was decided to use higher concentrations of phenolic acids in the production of loaded alginate chitosan nanoparticles. However, since the higher concentrations of 4-HBA was not dissolved properly in water, only 3-HPAA could be used in higher concentrations. The concentration of 3-HPAA which could produce inhibition zones on bacterial lawn was determined by agar diffusion experiment of 3-HPAA solutions (in ddH_2O). The concentrations of 5, 10, 15, 20, 25 mg/ml of 3-HPAA were tested on each bacteria. Among Gram negative bacteria, the highest antimicrobial effect of 3-HPAA concentration range was observed for *A. haemolyticus*. The ihibition zones were clear for 20 and 25 mg/ml 3-HPAA while they were small and turbid for 10 and 15 mg/ml (Figure 4.12 b1 and b2, regions III, IV, V, VI). In the cases of *P. aeruginosa* and *S.* Enteritidis, 20 mg/ml 3-HPAA result in turbid zones and 25 mg/ml showed clear inhibition zones (Figure 4.12 a1, a2, d1, d2, regions V and VI). *E. coli* O157:H7 demonstrated turbid zones only with 25 mg/ml 3-HPAA (Figure 4.12 c1, c2, region VI). Thus, 25 mg/ml was the common concentration of 3-HPAA which show high antimicrobial effect among tested Gram negative bacteria. Among tested concentrations of 3-HPAA, only 25 mg/ml showed slight antimicrobial effect on *S. epidermidis* and *L. monocytogenes* (Figure 4.13 a1, a2, d1, d2, region VI). MRSA and MSSA could not be inhibited with any of the tested concentrations of 3-HPAA. As expected, phenolic acids demonstrated strain-specific and dose-dependent nature of antimicrobial effect in this study. Since the most effective concentration was determined as 25 mg/ml for most of the tested bacteria, it was chosen as the concentration of 3-HPAA for nanoparticle production.

The antimicrobial effects of 25 mg/ml-3-HPAA-Alg-Chi solution were demonstrated as well as null nanoparticle solution on Gram negative and Gram positive

bacteria in Figures 4.14 and 4.15, respectively. The effect of 1% acetic acid was also investigated because of its usage for dissolution of nanoparticles. The 1% acetic acid solution and null nanoparticle solutions with or without acetic acid tretament did not result in any inhibition zones for each bacterium (Figure 4.14 and 4.17, regions II, III, IV). However, both 1% acetic acid treated and untreated 25 mg/ml-3-HPAA-Alg-Chi solutions presented clear inhibition zones for the bacteria except MRSA and MSSA (Figures 4.16 and 4.17, regions V and VI). Smaller, clear inhibition zones of MRSA and MSSA were detected only in 1% acetic acid treated 25 mg/ml-3-HPAA-Alg-Chi solution applied regions (Figure 4.15 c, d, e, f, region VI).

According to these results, it could be concluded that the obtained antimicrobial effect might be due to the 3-HPAA existence in the nanoparticle solution, not to the alginate-chitosan or acetic acid. This emphasized antimicrobial effect of 3-HPAA-Alg-Chi could be related to the interactions of 3-HPAA with alginate and chitosan. In addition, in *P. aeruginosa*, *E. coli* O157:H7, S. Enteritidis and *S. epidermidis*, bigger and clearer inhibition zones were detected for 1% acetic acid treated 3-HPAA-Alg-Chi than those of untreated one. Since acetic acid provide the required pH change for dissolution of nanoparticles, higher antimicrobial effect of the solution was an expected consequence.

The observation of the inhibition zones only for 1% acetic acid treated 3-HPAA-Alg-Chi in both MRSA and MSSA indicates the enhancement of the antimicrobial effect of 3-HPAA via encapsulation. Previously, it was determined that 25 mg/ml 3-HPAA was not effective on MRSA and MSSA (Figure 4.13 b1, b2, c1, c2, region VI). However after encapsulation and 1% acetic acid treatment, the inhibition zones were detected for MRSA and MSSA (Figure 4.15, c, d, e, f, region VI) which demonstrate the elevated antimicrobial effect of bioactive compounds after encapsulation. Consistent with our results, in the two studies of Jamil et al. in 2016, and the study of Liu et al in 2018, the increase of antimicrobial effect by encapsulation was clearly shown (Jamil et al., 2016 (a); Jamil et al., 2016 (b), Liu et al., 2018). The kefzole loaded chitosan nanoparticles showed larger inhibition zones for *Klebsiella pneumoniae* and *Pseudomonas aeruginosa* with the increasing concentrations of drugs in nanoparticles while no inhibition zones were detected in the application of the antibiotics alone (Jamil et al., 2016 (a)). Jamil et al. also examined the increased antimicrobial effect of chitosan nanoparticles loaded with cardamom essential oil on growth of MRSA and *E. coli* (Jamil et al., 2016 (b)).

Although the bacterial growth inhibition was not observed in the presence of cardamom essential oil, the application of cardamom essential oil loaded chitosan nanoparticles result in the complete inhibition of growth of both MRSA and *E. coli*.

Likewise, Liu et al. demonstrated a three-fold increase in the antimicrobial effect of the alginate-chitosan nanoparticles loaded with ε-polylysine than that of free ε-polylysine on *E. coli*, *B. subtilis*, *S. aureus* and *M. luteus* (Liu et al., 2018). Our study was also showed the enhancement of the antimicrobial effects of bioactive compounds after encapsulation. In the study of Liu et al. in which the antimicrobial effects of null alginate-chitosan nanoparticles and ε-polylysine loaded alginate-chitosan nanoparticles were tested on *E. coli*, *B. subtilis*, *S. aureus* and *M. luteus* (Liu et al., 2018). They indicated that in the application of ε-polylysine loaded alginate-chitosan nanoparticles, significant inhibition zones were observed while in unloaded alginate-chitosan nanoparticle application no inhibition zones were observed similar to our results.

Another important point was the maintained antimicrobial effect of 3-HPAA-Alg-Chi after 24 hours or 72 hours of 1% acetic acid treatment. When the inhibiton zones were compared for 24 hours and 72 hours of treatment with 1% acetic acid, a similar pattern was determined for each tested bacterium. Thus, it was concluded that the antimicrobial effect of 3-HPAA-Alg-Chi could be obtained after 24 hours of 1% acetic acid treatment. In addition, its antimicrobial properties were carried on even after 72 hours subsequent to treatment with 1% acetic acid (Figures 4.16 a,c,e,f and 4.17 b, d, f, g, region VI).

The growths of tested bacteria in the presence of nanoparticle solutions treated with 1% acetic acid were demonstrated in Figure 4.16. All tested solutions with the 10% (v/v) applications, inhibited the *P. aeruginosa* growth (Figure 4.16 a) with higher than 95% inhibitions (Table 4.3). However, the cell viability studies presented that the only solution which showed bacteriocidal effect (no survivors) on *P. aeruginosa* among the solutions tested in 10% (v/v) application was 3-HPAA-Alg-Chi (Table 4.3). In the case of *S. epidermidis*, the inhibition was observed only with the presence of 3-HPAA-Alg-Chi solution with 10% (v/v) concentration (Figure 4.16 b) as well as being bacteriocidal (Table 4.3). On the other hand, the application of 10% (v/v) concentration of 3-HPAA-Alg-Chi showed the highest antimicrobial effect among all the tested solutions with higher than 93% growth inhibition in MRSA and MSSA. These results were demonstrated in Table 4.3.

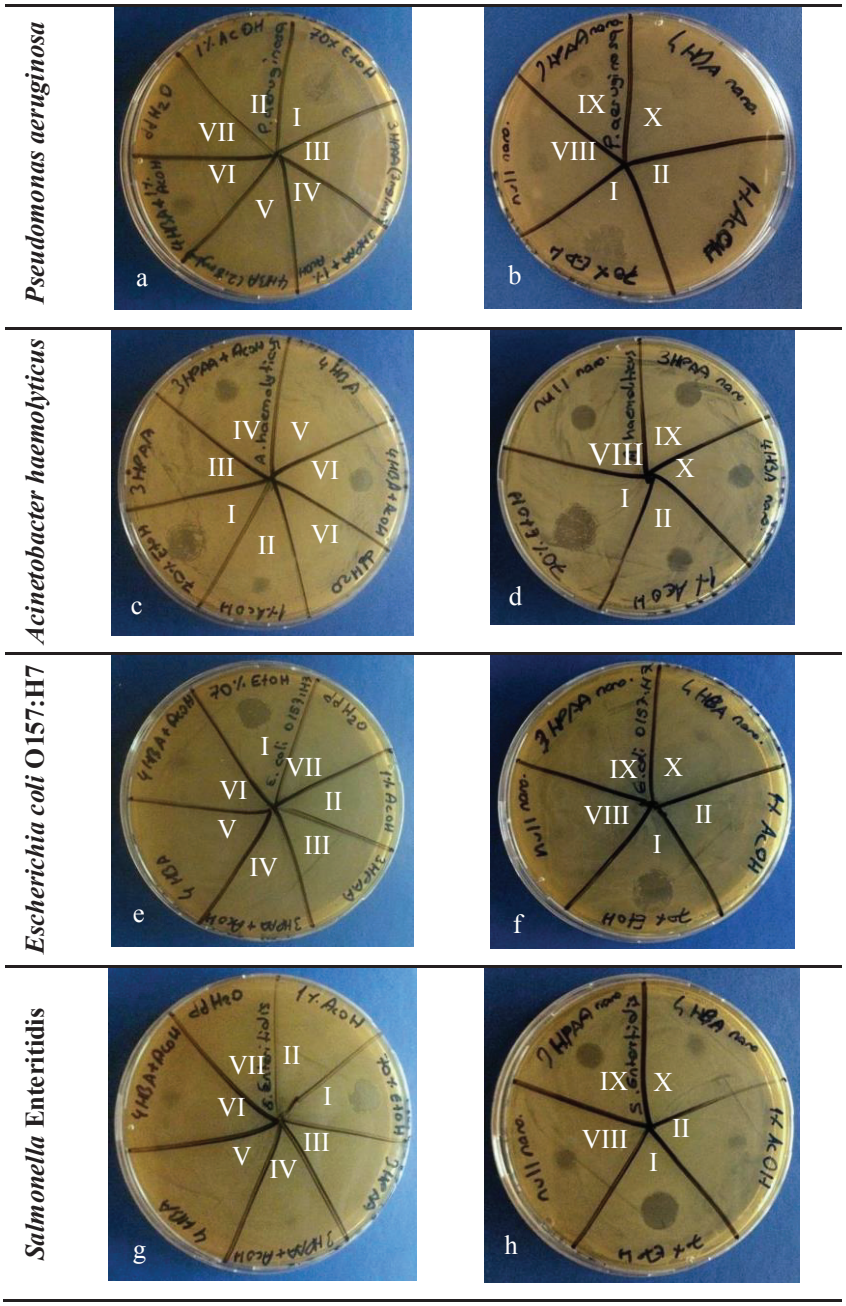

Figure 4.10. The effects of phenolic acid solutions (a, c, e, g) and phenolic acid loaded nanoparticle solutions (b, d, f, h) on Gram negative bacteria. *P. seruginosa* (a, b); *A. haemolyticus* (c, d); *E. coli* O157H:7 (e,f); *S.* Enteritidis (g, h). Each solution was indicated in a roman number as folllowing: 70% Ethanol (I); 1% Acetic acid (II); 3-HPAA in ddH_2O (3mg/ml) (III); 3-HPAA in 1% acetic acid (3mg/ml) (IV); 4-HBA in ddH_2O (2.8 mg/ml) (V); 4-HBA in 1% acetic acid (2.8 mg/ml) (VI); ddH_2O (VII); Null nanoparticle solution (VIII); 3 mg/ml 3-HPAA-Alg-Chi solution (IX); 2.8 mg/ml 4-HBA-Alg-Chi solution (X).

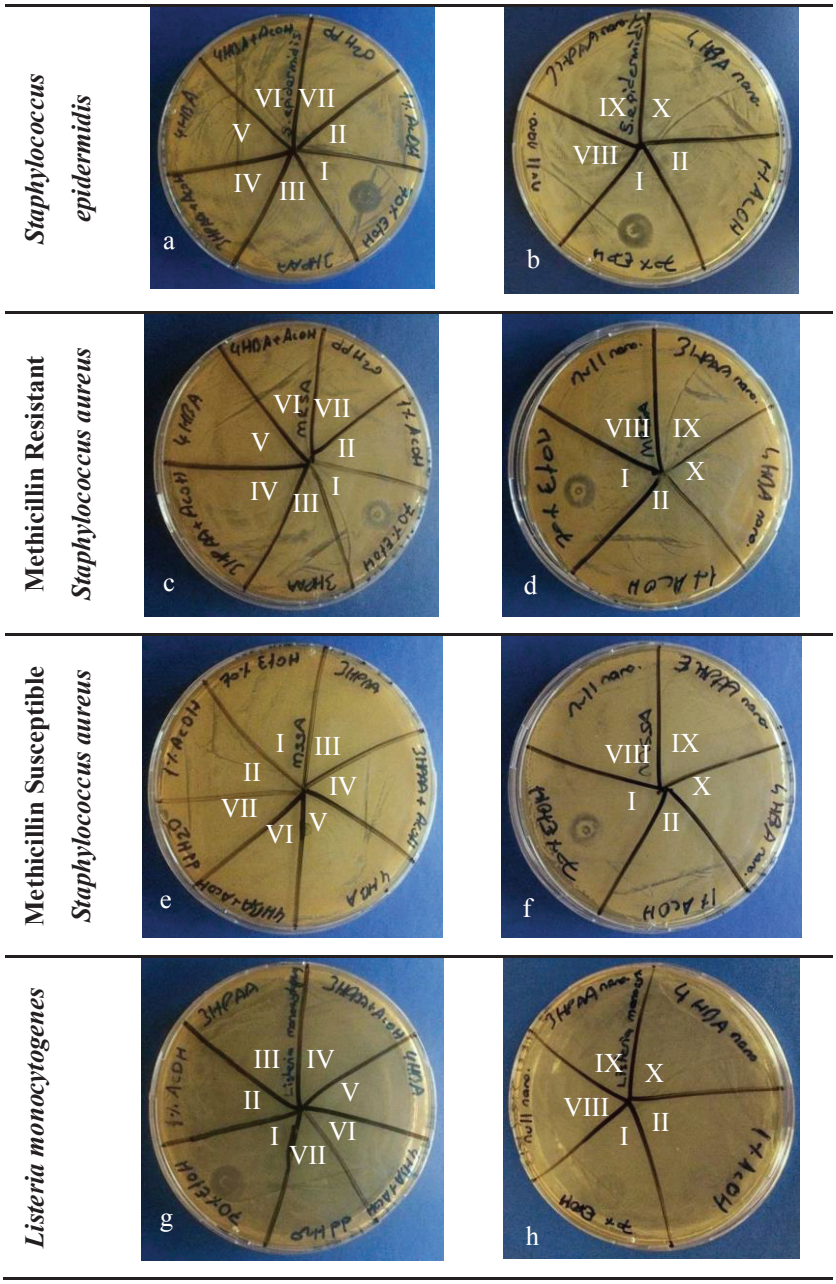

Figure 4.11. The effects of phenolic acid solutions (a, c, e, g) and phenolic acid loaded nanoparticle solutions (b, d, f, h) on Gram positive bacteria. *S. epidermidis* (a, b); MRSA (c, d); MSSA (e,f); *L. monocytogenes* (g, h). Each solution was indicated in a roman number as folllowing: 70% Ethanol (I); 1% Acetic acid (II); 3-HPAA in ddH_2O (3mg/ml) (III); 3-HPAA in 1% acetic acid (3mg/ml) (IV); 4-HBA in ddH_2O (2.8 mg/ml) (V); 4-HBA in 1% acetic acid (2.8 mg/ml) (VI); ddH_2O (VII); Null nanoparticle solution (VIII); 3 mg/ml 3-HPAA-Alg-Chi solution (IX); 2.8 mg/ml 4-HBA-Alg-Chi solution (X).

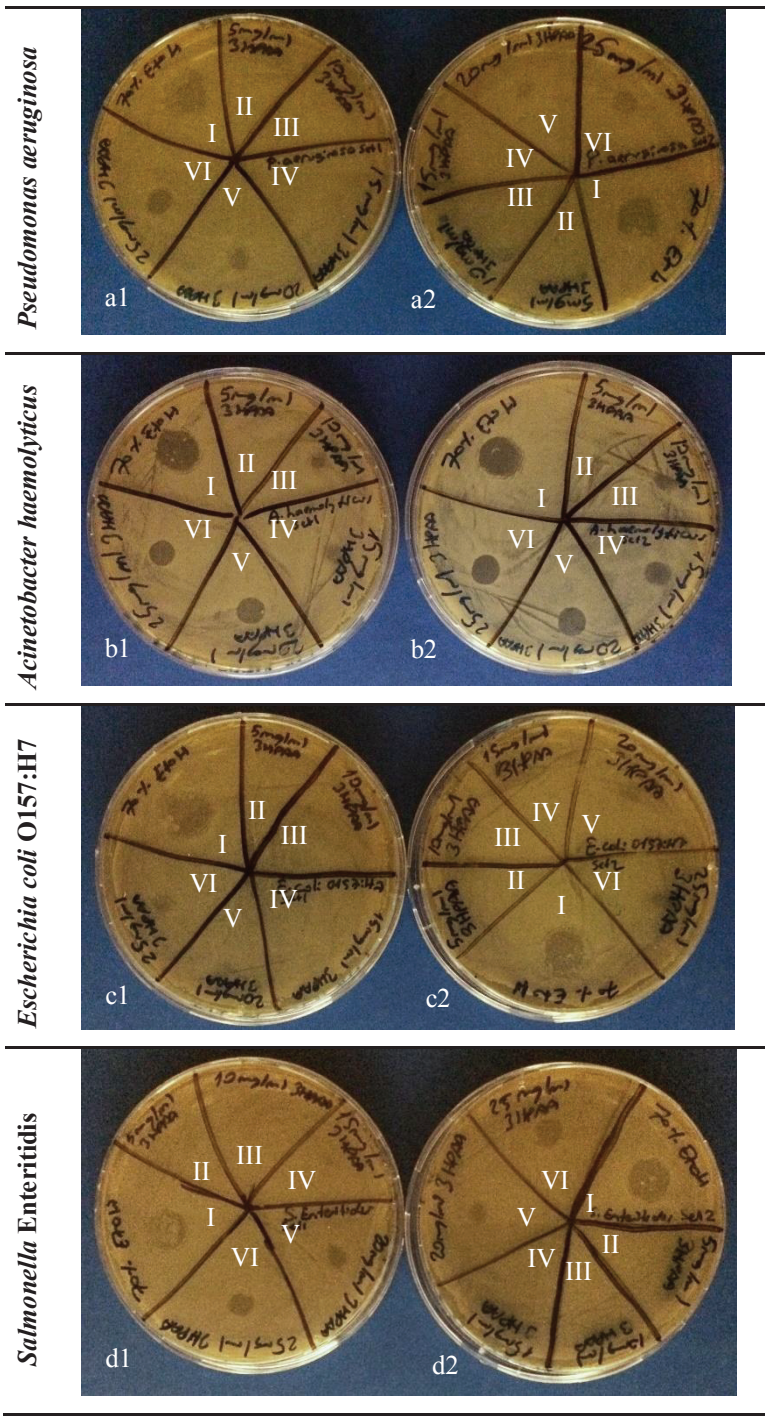

Figure 4.12. The effects of 3-HPAA solutions in a concentration range of 5-25 mg/ml (in ddH_2O) on Gram negative bacteria. Each bacteria was presented as 2 sets: *P. seruginosa* (a1, a2); *A. haemolyticus* (b1, b2); *E. coli* O157H:7 (c1, c2); *S.* Enteritidis (d1, d2). Each solution was indicated in a roman number as folllowing: 70% Ethanol (I); 5 mg/ml 3-HPAA (II); 10 mg/ml 3-HPAA (III); 15 mg/ml 3-HPAA (3mg/ml) (IV); 20 mg/ml 3-HPAA (V); 25 mg/ml 3-HPAA (VI).

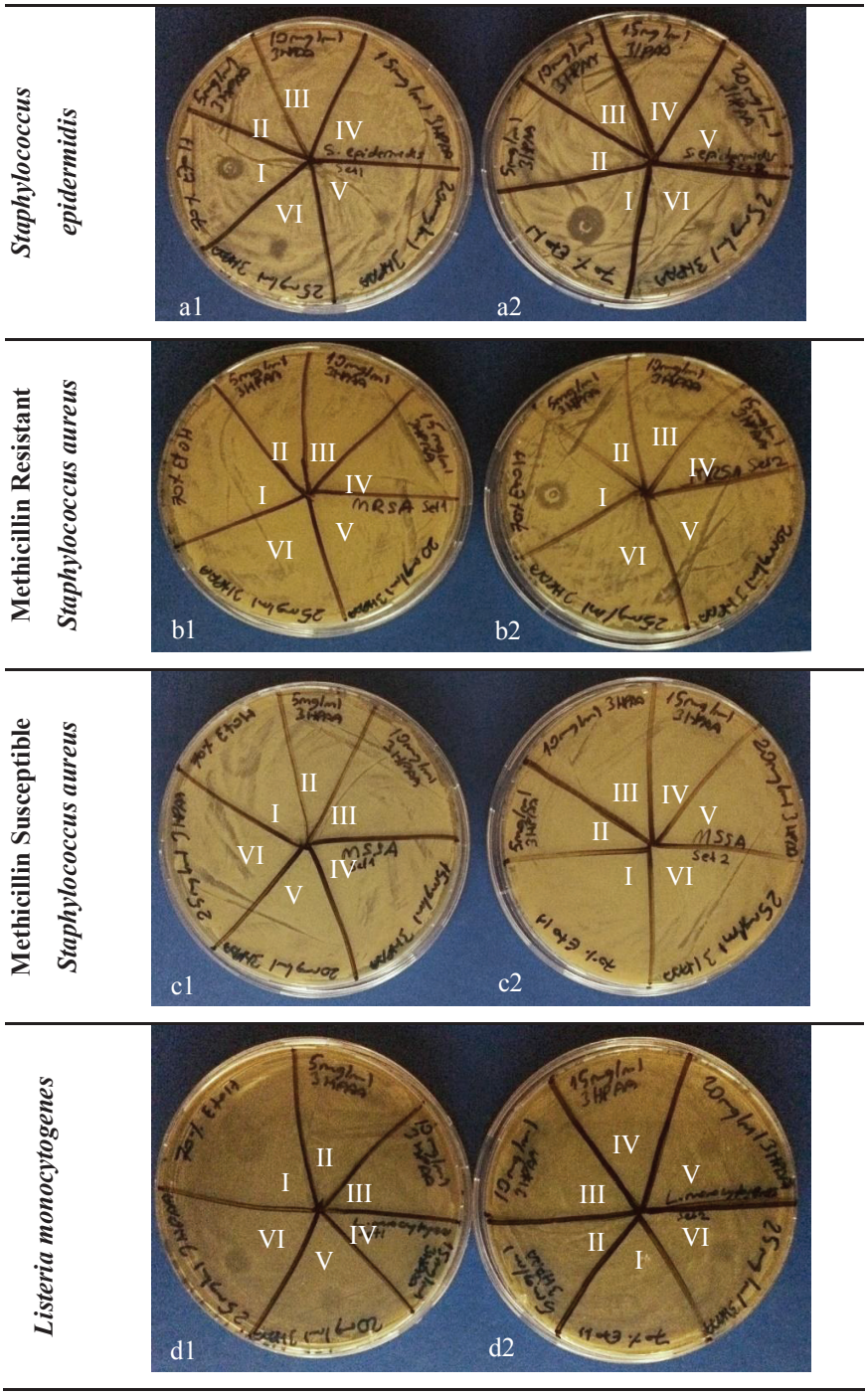

Figure 4.13. The effects of 3-HPAA solutions in a concentration range of 5-25 mg/ml (in ddH_2O) on Gram positive bacteria. Each bacteria was presented as 2 sets: *S. epidermidis* (a1, a2); MRSA (b1, b2); MSSA O157H:7 (c1, c2); *L. monocytogenes* (d1, d2). Each solution was indicated in a roman number as folllowing: 70% Ethanol (I); 5 mg/ml 3-HPAA (II); 10 mg/ml 3-HPAA (III); 15 mg/ml 3-HPAA (3mg/ml) (IV); 20 mg/ml 3-HPAA (V); 25 mg/ml 3-HPAA (VI).

Although 10% (v/v) concentration application caused only bacteriostatic effect (Figure 4.16 c, d), the 20% application displayed bacteriocidal effect on MRSA and MSSA (Figure 4.16 e, f). Although the result of 1% acetic acid application with 20% (v/v) final concentration showed significant antimicrobial effects different than that in our agar diffusion studies, it demonstrated the importance of the bacterial load on which the application done and the dose- dependent nature of antimicrobial agents. In the study of Jamil et al., it was also found that the antimicrobial effects of kefzole loaded chitosan nanoparticles presented different antimicrobial effects in agar diffusion and broth assays (Jamil et al., 2016 (a)). Similar to our results of acetic acid application, the lowest tested concentration in the agar diffusion tests, displayed much higher antimicrobial activity in the broth assays (Jamil et al., 2016 (a)).

All of these results indicated the antimicrobial effect of 3-HPAA was enhanced after encapsulation into alginate chitosan nanoparticles. In addition, 3-HPAA-Alg-Chi showed its antimicrobial effect on different bacteria with different levels: For the bacteriocidal effect on *P. aeruginosa* and *S. epidermidis* 10% (v/v) concentration was sufficient while 20% (v/v) concentration was required for MRSA and MSSA (Table 4.3). Consistent with our results, Madureira et al. demonstrated the growth inhibitions of various bacteria were changed between 60-90% in the presence of chitosan encapsulated rosmarinic acid (RA), protocatechuic acid (PA) and the 2,5-dihydroxybenzoic acid (DHBA) (Madureira et al., 2015).

These might display the strain-specific and dose-dependent properties of nanoparticles loaded with phenolic compounds in the case of their antimicrobial effects. The synergistic effect of 3-HPAA, alginate-chitosan and acetic acid might contribute the bacteriocidal effect of 3-HPAA-Alg-Chi solution. In addition, it showed bacteriostatic effect on the pathogenic bacteria with different concentrations regardless of their Gram properties. These results lead the conclusion that 3-HPAA-Alg-Chi solution might be studied in more detail as a promising natimicrobial agent for future usage.

4.5. Overall Conclusions and Future Aspects

This study presented that the water soluble phenolic acids 3-HPAA and 4-HBA showed high antimicrobial effects on *P. aeruginosa*, which is a serious pathogen.

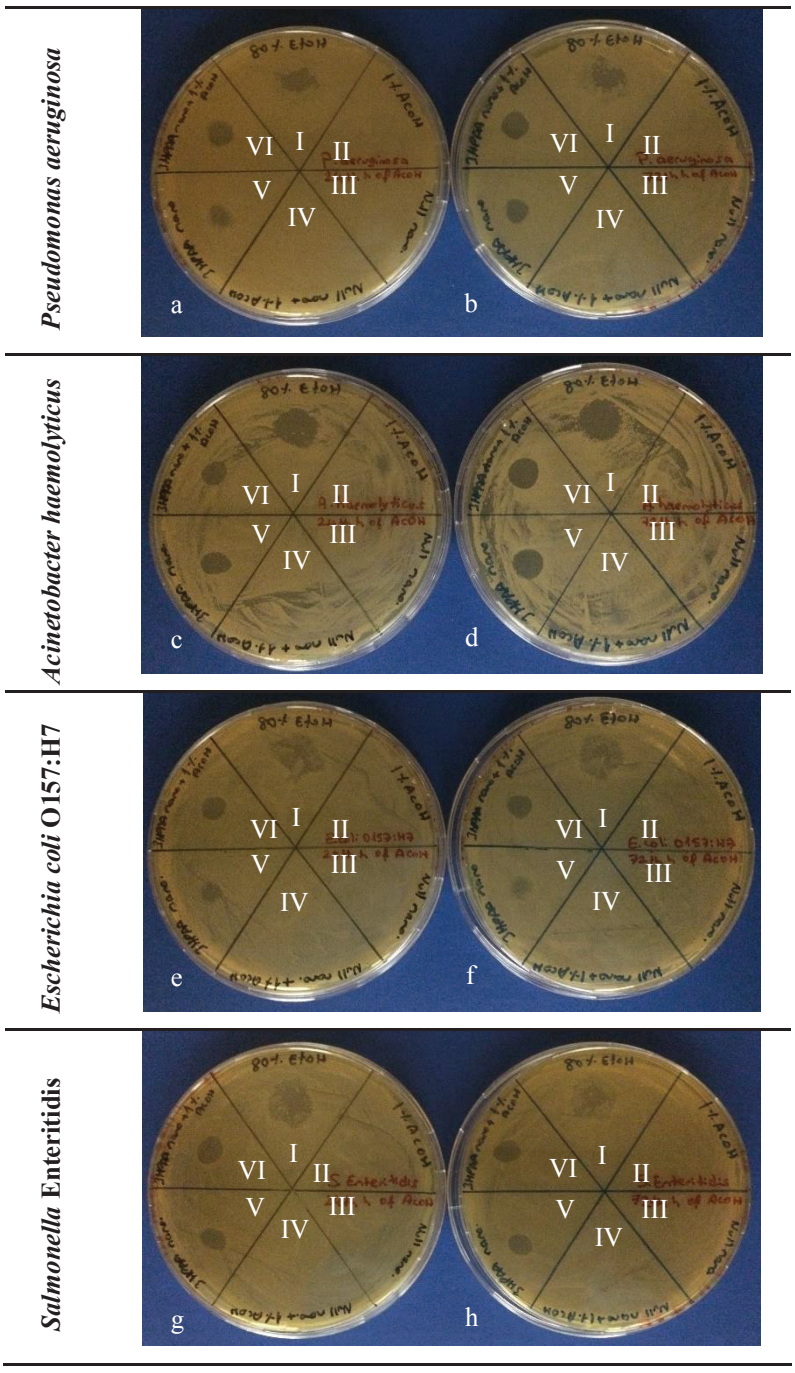

Figure 4.14. The effect of 25 mg/ml 3-HPAA loaded nanoparticles with or without acetic acid treatment for 24 (a, c, e, g) or 72 hours (b, d, f, h) on Gram negative bacteria. *P. seruginosa* (a, b); *A. haemolyticus* (c, d); *E. coli* O157H:7 (e, f); *S.* Enteritidis (g, h). Each solution was indicated in a roman number as folllowing: 80% Ethanol (I); 1% Acetic acid (II); Null nanoparticle solution (III); Null nanoparticle solution in acetic acid (IV); 3-HPAA-Alg-Chi solution (V); 3-HPAA-Alg-Chi solution in acetic acid (VI).

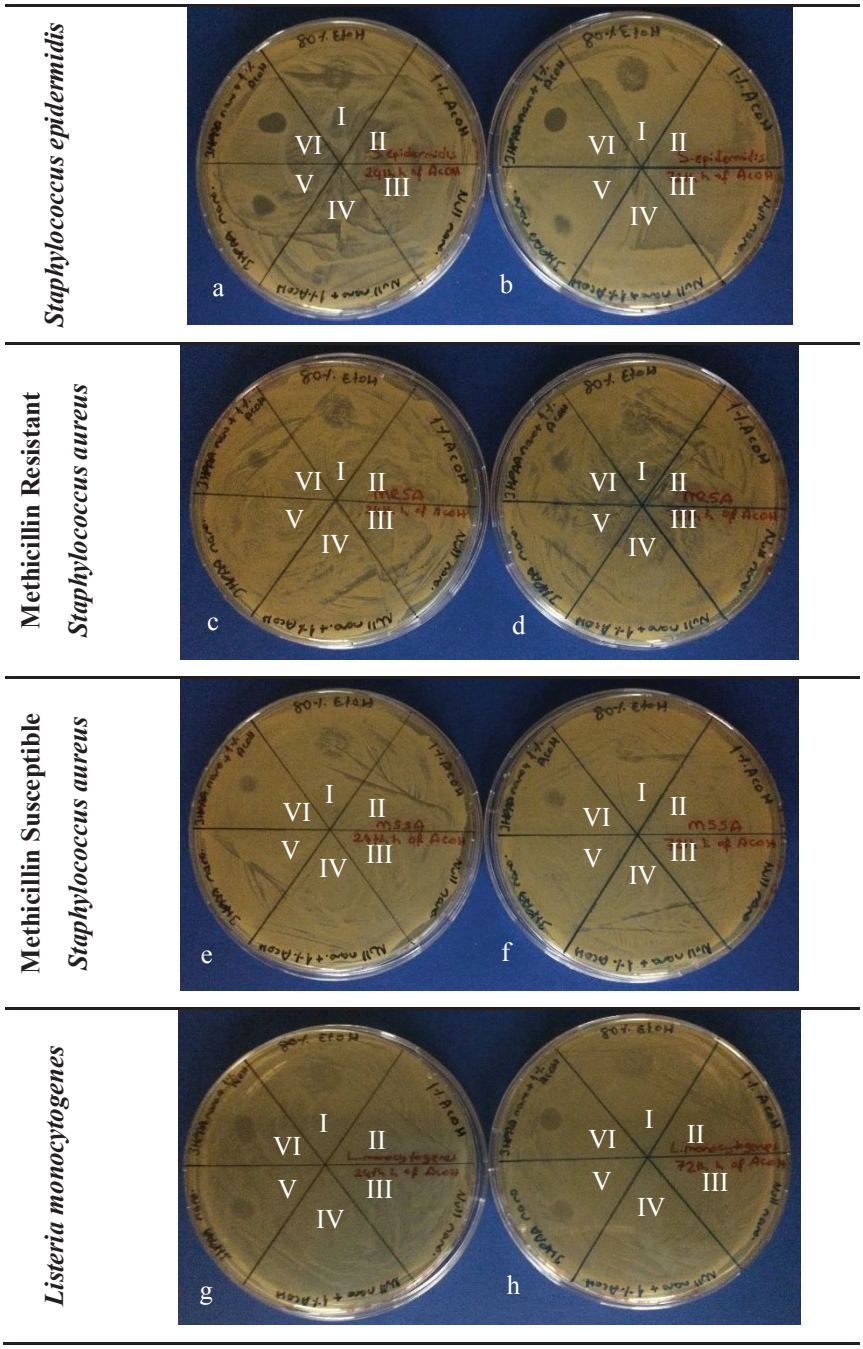

Figure 4.15. The effect of 25 mg/ml 3-HPAA loaded nanoparticles with or without acetic acid treatment for 24 (a, c, e, g) or 72 hours (b, d, f, h) on Gram positive bacteria. *S. epidermidis* (a, b); MRSA (c, d); MSSA (e, f); *L. monocytogenes* (g, h). Each solution was indicated in a roman number as folllowing: 80% Ethanol (I); 1% Acetic acid (II); Null nanoparticle solution (III); Null nanoparticle solution in acetic acid (IV); 3-HPAA-Alg-Chi solution (V); 3-HPAA-Alg-Chi solution in acetic acid (VI).

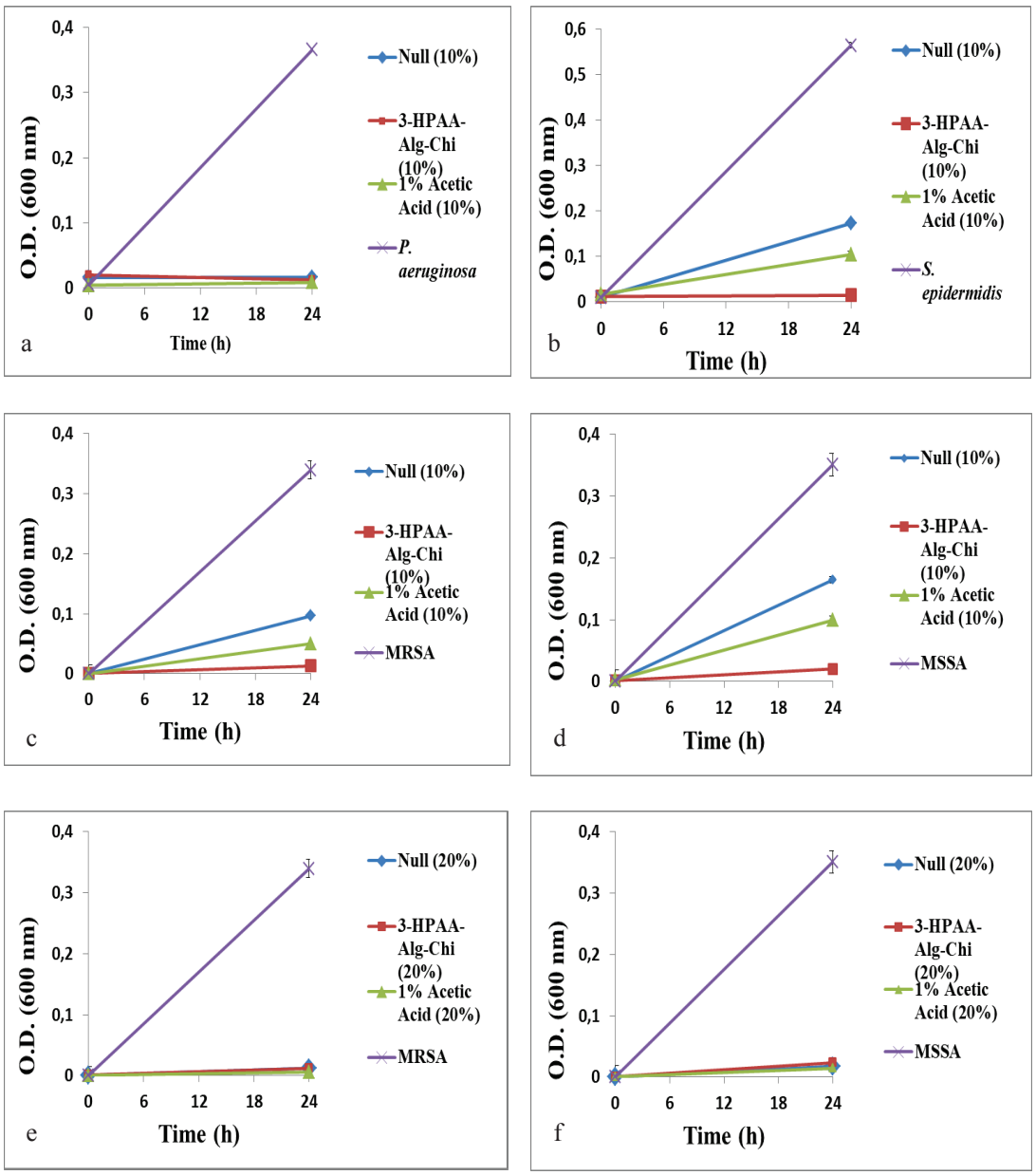

Figure 4.16. The antimicrobial effects of the nanoparticles and 1% acetic acid with 10% final concentration (a, b, c, d) and 20% final concentration (e,f) on bacterial growth of *P. aeruginosa* (a), *S. epidermidis* (b), MRSA (c, e) and MSSA (d, f). In each graph, the colors of lines correspond to the bacterial growth in the presence of the following: Null nanoparticles (blue); 3-HPAA-Alg-Chi (red); 1% acetic acid (green) and control bacteria (purple).

Table 4.3. Percent inhibitions and cfu/ml values of bacteria in the presence of nanoparticles in 10% or 20% volume application.

		Solutions	Percent Inhibition (%)	Cell viability (cfu/ml)
10% (v/v) APPLICATION	***P. aeruginosa***	Null nanoparticles	95	TMTC*
		3-HPAA loaded nanoparticles	97	No survivors
		Acetic acid (1%)	98	TMTC
	S. epidermidis	Null nanoparticles	69	TMTC
		3-HPAA loaded nanoparticles	97	No survivors
		Acetic acid (1%)	82	TMTC
	MRSA	Null nanoparticles	72	TMTC
		3-HPAA loaded nanoparticles	96	TMTC
		Acetic acid (1%)	85	TMTC
	MSSA	Null nanoparticles	55	TMTC
		3-HPAA loaded nanoparticles	94	TMTC
		Acetic acid (1%)	73	TMTC
20% (v/v) APPLICATION	**MRSA**	Null nanoparticles	96	TMTC
		3-HPAA loaded nanoparticles	96	No survivors
		Acetic acid (1%)	98	TMTC
	MSSA	Null nanoparticles	95	TMTC
		3-HPAA loaded nanoparticles	94	No survivors
		Acetic acid (1%)	96	TMTC

*TMTC: Too many to count

The free forms of the phenolics showed bacteriostatic and bacteriocidal effects in a dose-dependent manner. In addition, the treatment of *P. aeruginosa* with the subinhibitory concentrations of each phenolic resulted in morphological changes in bacteria. The distinct greenish-blue color of *P. aeruginosa* culture was disappeared which could be recognized by naked eye and invaginations were formed on the surface of the bacterial cells which were determined in the SEM images. The bacteria which were grown in the presence of phenolic acids were elucidated at the proteomic level to determine the molecular reasons of the antimicrobial effects of the phenolics, including the reasons of the mentioned morphological changes. It was presented that the proteins functioned in the biosynthesis of phenazine pigment which gives the blue color of *P. aeruginosa* were not detected after phenolic acids exposure. Since this pigment is also an important virulence factor, it could be pointed out that not only the color but also the virulence of *P. aeruginosa* were reduced with phenolic acids. Besides that, the proteomic data revealed various changes in metabolic pathways which were mostly due to the adaptation process of the bacteria to the phenolic acid-containing environment. However, some notable changes in the protein profile of the bacteria could give clues about the affected processes of the bacteria after phenolic exposure. The proteomic study showed the changes in the bacterial cell membrane proteins which could be the reasons of invaginations of bacterial surfaces seen in SEM images. For instance, the various changes in the carboxypeptidases and endopeptidases as well as lipid metabolism related proteins might demonstrate that the bacteria managed to fix the defects in their membranes. Another important point was the changes in the RNA metabolism which includes the changes in tRNA biosynthesis related proteins and structural ribosomal RNA proteins. These might show that phenolic acids might result in the problems of biosyntheses and structures of tRNAs, rRNAs and ribosomes, thereby the protein translation. The undetection of iron homeostasis related proteins such as Fe(3+)-pyochelin receptor and the newly detection of phosphate starvation response protein PhoB might point out that the bacteria suffered from the nutrient starvation (iron and phosphate, respectively) which might lead to the inhibition of bacterial growth. The phenolic acids also seemed to result in serious oxidative stress with newly detection of various redox homeostasis related proteins including OxyR. Besides, it was demonstrated that the phenolic acid exposure caused changes in the DNA replication and repair mechanisms. Although each phenolic acid resulted in the

changes in DNA replication and repair mechanisms, especially 3-HPAA resulted in the undetection of proteins functioned in NER and MMR which might lead to the serious DNA damage. The bacteria might manage to carry out horizontal gene transfer via recombination for survival since recombination related proteins were newly detected. All of these results were speculated as the phenolic acids may show their antimicrobial effects by causing defects in more than one bacterial processes which makes them multi-target antimicrobial agents.

The phenolic acids also demonstrated the antimicrobial effects after encapsulation into alginate-chitosan nanoparticles on various pathogens. The usage of high molarity of cross-linker $CaCl_2$ in nanoparticle production, resulted in the homogeneous nanoparticles with high encapsulation percentages. The phenolic acid loaded nanoparticles showed a dose- and strain-dependent bacteriostatic and/or bacteriocidal effects and the acetic acid treatment of the nanoparticle solutions 24 hours before their application aid their antimicrobial effect. The antimicrobial effects of the nanoparticle solutions continued as the same even after 72 hours of acetic acid treatment. Thus, they were presented as the effective antimicrobial solutions against nosocomial or food-borne pathogenic bacteria.

Although all the results of this study pointed out the important consequences of the phenolic acid applications, various related studies can be performed as the next steps. Undoubtfully the most important step would be the cytotoxicity studies for both free and nanoparticle forms of the phenolic acids. The two important concepts in antimicrobial agent development are the high antimicrobial effect on the pathogens as well as the low damage to eukaryotic cells. Hence, the cytotoxicity test such as MTT may be performed to determine the nontoxic concentrations of the phenolic acids and phenolic acid loaded nanoparticle solutions *in vitro* as well as the animal experimentation to determine their effects *in vivo*. Since our study presented the high antimicrobial effects of the phenolic acids with dose-dependency, the upcoming studies showing the useful doses without a toxic effect *in vitro* and *in vivo* would be highly supportive for phenolic acids/nanoparticles to be presented as promising antimicrobial agents. Besides that, additional studies can be performed to optimize the treatment time and concentration of acetic acid before the nanoparticle application as well as testing their effects more than after 72 hours. The shelf-life of the nanoparticles can be performed by periodically repeating the characterization and antimicrobial studies.

The proteomic study indicated various proteins functioned in the important metabolic pathways. However, these results can be supported via with other -omics studies. Especially the transcriptomic studies such as next generation sequencing may aid proteomics studies in the enlightening the mode of action of antimicrobial agents. The transcript profile of the same bacteria grown under the same conditions can be useful to determine the overlapped genes as targets of the antimicrobial agents. Additionally, the specific mutant strains of the targetted genes can be generated and tested under phenolic acid stresses to determine the exact function of these genes for enlightening the action mechanism of the tested compound. Although the usage of overlapped genes in –omics studies will give more precise results, the proteomics or transcriptomics results can also be used indivudually with the validation of gene expression changes with RT-qPCR. Since the phenolic acid loaded nanoparticles resulted in the notable antimicrobial effects, the similar mode of action studies including proteomic, transcriptomics and testing mutant strains can also be performed to investigate the action mechanism of nanoparticles. The phenolic acids and naoparticles loaded with phenolic acids were shown to display a strain-dependent antimicrobial effect in our study. Hence, these agents can be tested on other bacteria at the proteomic and transcriptomic level to be able to compare and point out the strain-dependent nature of these agents.

Our study can be accepted as the first step in the enlightening of phenolic acids action mechanism as well as their usage either in free or nanoparticle forms. To the best of our knowledge, the studies of the antimicrobial effects of phenolic acids at the molecular level is very limited. Hence, our results can be elucidated as the starting points of further studies for investigating the phenolic acids as new antimicrobial agents.

REFERENCES

Albano, M.; Crulhas, B. P.; Alves, F. C. B.; Pereira, A. F. M.; Andrade, B. F. M. T.; Barbosa, L. N.; Furlanetto, A.; da Silveira Lyra, L. P.; Rall, V. L. M.; Júnior, A. F. Antibacterial and anti-biofilm activities of cinnamaldehyde against *S. epidermidis*. *Microbial Pathogenesis* **2019**, *126*, 231-238.

Alegbeleye, O. O.; Singleton, I.; Sant'Ana, A. S. Sources and contamination routes of microbial pathogens to fresh produce during field cultivation: A review. *Food Microbiology* **2018**, *73*, 177-208.

Aloush, V.; Navon-Venezia, S.; Seigman-Igra, Y.; Cabili, S.; Carmeli, Y. Multidrug-Resistant *Pseudomonas aeruginosa*: Risk factors and clinical impact. *Antimicrobial Agents and Chemotherapy* **2006**, *50* (1), 43-48.

Aminov, R.; History of antimicrobial drug discovery: Major classes and health impact. *Biochemical Pharmacology* **2017**, *133*, 4-19.

Ananda, A. P.; Manukumar, H.M.; Krishnamurthy, N.B.; Nagendra, B.S.; Savitha, K.R. Assessment of antibacterial efficacy of a biocompatible nanoparticle PC@AgNPs against *Staphylococcus aureus*. *Microbial Pathogenesis* **2019**, *126*, 27-39.

Andjelkovic, M.; Camp, J. V.; De Meulenaer, B.; Depaemelaere, G.; Socaciu, C.; Verloo, M; Verhe, R. Iron-chelation properties of phenolic acids bearing catechol and galloyl groups. *Food Chemistry* **2006**, *98*, 23-31.

Andonova, M.; Urumova, V. Immune surveillance mechanisms of the skin against the stealth infection strategy of *Pseudomonas aeruginosa*-Review. *Comparative Immunology, Microbiology and Infectious Diseases*. **2013**, *36*, 433-448.

Argudin, M. A.; Vanderhaeghen, W.; Vandendriessche, S.; Vandecandelaere, I.; Andre, F.-X.; Denis, O.; Coenye, T.; Butaye, P. Antimicrobial resistance and population structure of *Staphylococcus epidermidis* recovered from animals and Humans. *Veterinary Microbiology* **2015**, *178*, 105-113.

Armengod, M. E.; Meseguer, S.; Villarroya, M.; Prado, S.; Moukadiri, I.; Ruiz-Partida, R.; Garzon, M. J.; Navarro-Gonzalez, C.; Martínez-Zamora, A. Modification of the wobble uridine in bacterial and mitochondrial tRNAs reading NNA/NNG triplets of 2-codon boxes. *RNA Biology* **2014**, *11* (12), 1495-1507.

Aseev, L. V.; Boni, I. V. Extraribosomal functions of bacterial ribosomal proteins. *Molecular Biology* **2011**, *45* (5), 739-750.

Atichartpongkul, S.; Vattanaviboon, P.; Wisitkamol, R.; Jaroensuk, J.; Mongkolsuk, S.; Fuangthong, M. Regulation of organic hydroperoxide stress response by two OhrR homologs in *Pseudomonas aeruginosa*. *PLoS ONE* **2016**, *11* (8), e0161982.

Azevedo, M. A.; Bourbon, A. I.; Vicente, A. A.; Cerqueira, M. A.; Alginate/chitosan nanoparticles for encapsulation and controlled release of vitamin B2. *International Journal of Biological Macromolecules* **2014**, *71*, 141-146.

Bakht azad, S.; Nikokar, I.; Faezi, S.; Rasooly, S.; Mahdavi, M. Evaluation of the immune responses following co-administration of PilQ and type b-flagellin from *Pseudomonas aeruginosa* in the burn mouse model. *Microbial Pathogenesis* **2018**, *123*, 426-432.

Bandounas, L.; Ballerstedt, H.; de Winde, J. H.; Ruijssenaars, H. J. Redundancy in putrescine catabolism in solvent tolerant *Pseudomonas putida* S12. *Journal of Biotechnology* **2011**, *154*, 1–10.

Barrera-Necha, L. L.; Correa-Pacheco, Z. N.; Bautista-Banos, S.; Hernandez-Lopez, M.; Jiménez, J. E. M.; Mejía, A. F. M. Synthesis and characterization of chitosan nanoparticles loaded botanical extracts with antifungal activity on colletotrichum gloeosporioides and Alternaria species. *Advances in Microbiology* **2018**, *8*, 286-296.

Basler, M.; Ho, B. T.; Mekalanos, J. J. Tit-for-Tat: Type VI Secretion system counterattack during bacterial cell-cell interactions. *Cell* **2013**, *152*, 884-894.

Batth, T. S.; Francavilla, C.; Olsen, J. V. Off-Line High-pH reversed-phase fractionation for in-depth phosphoproteomics. *Journal of Proteome Research* **2014**, *13*, 6176-6186.

Bergogne-Berezin, E.; Outbreaks caused by bacteria with novel multiple resistance: towards zero therapeutic options? The increasing significance of outbreaks of Acinetobacter spp.: the need for control and new agents. *Journal of Hospital Infection* **1995**, *30*, 441-452.

Bhattacharjee, S.; DLS and zeta potential-What they are and what they are not? *Journal of Controlled Release* **2016**, *235*, 337-351.

Bisht, S. C.; Joshi, G. K.; Mishra, P. K. CspA encodes a major cold shock protein in Himalayan psychrotolerant Pseudomonas Strains. *Interdiscip Sci Comput Life Sci* **2014**, *6*, 140-148.

Bitrus, A. A.; Zunita, Z.; Khairani-Bejo, S.; Othman, S.; Nadzir, N. A. A. Staphylococcal cassette chromosome mec (SCCmec) and characterization of the attachment site (attB) of methicillin resistant *Staphylococcus aureus* (MRSA) and methicillin susceptible *Staphylococcus aureus* (MSSA) isolates. *Microbial Pathogenesis* **2018**, *123*, 323-329.

Black, K. A.; Dos Santos, P. C. Abbreviated pathway for biosynthesis of 2-thiouridine in *Bacillus subtilis*. *Journal of Bacteriology* **2015**, *197*, 1952-1962.

Bleves, S.; Viarre, V.; Salacha, R.; Michel, G. P. F.; Filloux, A.; Voulhoux, R. Protein secretion systems in *Pseudomonas aeruginosa*: A wealth of pathogenic weapons. *International Journal of Medical Microbiology* **2010**, *300*, 534-543.

Borrero, N. V.; Bai, F.; Perez, C.; Duong, B. Q.; Rocca, J. R.; Jin S.; Huigens III, R. W. Phenazine antibiotic inspired discovery of potent bromophenazine antibacterial agents against *Staphylococcus aureus* and *Staphylococcus epidermidis*. *Organic & Biomolecular Chemistry* **2014**, *12*, 881.

Breidenstein, E. B. M.; de la Fuente-Nunez, C.; Hancock, R. E. W. *Pseudomonas aeruginosa*: all roads lead to resistance. *Trends in Microbiology* **2011**, *19* (8), 419.

Brown, S. P.; Cornforth, D. M.; Mideo, N. Evolution of virulence in opportunistic pathogens: generalism, plasticity, and control. *Trends in Microbiology* **2012**, *20* (7), 336.

Bubunenko, M.; Korepanov, A.; Court, D. L.; Jagannathan, I.; Dickinson, D.; Chaudhuri, B. R.; Garber, M. B.; Culver, G. M. 30S ribosomal subunits can be assembled in vivo without primary binding ribosomal protein S15. *RNA* **2006**, *12*, 1229-1239.

Buck, M.; Gallegos, M.-T.; Studholme, D. J.; Guo, Y.; Gralla, J. D. The bacterial enhancer-dependent σ54 (σN) transcription factor. *Journal of Bacteriology* **2000**, *182* (15), 4129-4136.

Budnyak, T. M.; Yanovska, E. S.; Kichkiruk, O. Yu.; Sternik, D.; Tertykh, V. A. Natural minerals coated by biopolymer chitosan: Synthesis, physicochemical, and adsorption properties. *Nanoscale Research Letters* **2016**, *11*, 492.

Cafarelli, T. M.; Desbuleux, A.; Wang, Y.; Choi, S. G.; De Ridder, D.; Vidal, M. Mapping, modeling, and characterization of protein–protein interactions on a proteomic scale. *Current Opinion in Structural Biology* **2017**, *44*, 201-210.

Caffrey, N.; Invik, J.; Waldner, C. L.; Ramsay, D.; Checkley, S. L. Risk assessments evaluating foodborne antimicrobial resistance in humans: A scoping review. *Microbial Risk Analysis* **2019**, *11*, 31-46.

Capaldi Arruda, S. C.; Silva, A. L. D.; Galazzi, R. M.; Azevedo, R. A.; Arruda, M. A. Z. Nanoparticles applied to plant science: A review. *Talanta* **2015**, *131*, 693-705.

Cardona, F.; Andres-Lacueva, C.; Tulipani, S.; Tinahones, F. J.; Queipo-Ortuno, M. I. Benefits of polyphenols on gut microbiota and implications in human health. *Journal of Nutritional Biochemistry* **2013**, *24*, 1415-1422.

Carmona, M.; de Lorenzo, V. Involvement of the FtsH (HflB) protease in the activity of σ54 promoters. *Molecular Microbiology* **1999**, *31* (1), 261-270.

Carrera, M.; Böhme, K.; Gallardo, J. M.; Barros-Velazquez, J.; Canas, B.; Calo-Mata, P. Characterization of foodborne strains of *Staphylococcus aureus* by shotgun proteomics: Functional networks, virulence factors and species-specific peptide biomarkers. *Frontiers in Microbiology* **2017**, *8*, 2458.

Carter, T.; Buensuceso, R. N. C.; Tammam, S.; Lamers, R. P.; Harvey, H.; Howell, P. L.; Burrows, L. L. The type IVa pilus machinery is recruited to sites of future cell division. *mBio* **2017**, *8* (1), e02103-16.

Chaban, B.; Hughes, H. V.; Beeby, M. The flagellum in bacterial pathogens: For motility and a whole lot more. *Seminars in Cell & Developmental Biology* **2015**, *46*, 91-103.

Chatterjee, M.; Anju, C.P.; Biswas, L.; Kumar, V. A.; Mohan, C. G.; Biswas, R. Antibiotic resistance in *Pseudomonas aeruginosa* and alternative therapeutic options. *International Journal of Medical Microbiology* **2016**, *306*, 48-58.

Chavali, A. K.; D'Auria, K. M.; Hewlett, E. L.; Pearson, R. D.; Papin, J. A. A metabolic network approach for the identification and prioritization of antimicrobial drug targets. *Trends in Microbiology* **March 2012**, *20* (3), 113.

Choksawangkarn, W.; Edwards, N.; Wang, Y.; Gutierrez, P.; Fenselau, C. Comparative study of workflows optimized for in-gel, in-solution, and on-filter proteolysis in the analysis of plasma membrane proteins. *Journal of Proteome Research* **2012**, *11*, 3030-3034.

Cisse, G. Food-borne and water-borne diseases under climate change in low- and middle-income countries: further efforts needed for reducing environmental health exposure risks. *Acta Tropica* **2019**, doi: 10.1016/j.actatropica.2019.03.012.

Cueva, C.; Moreno-Arribas M. V.; Martin-Alvarez, P. J.; Bills, G.; Vicente, M. F.; Basilio, A.; Rivas, C. L.; Requene, T.; Rodrigez J. M.; Bartolome, B. Antimicrobial activity of phenolic acids against commensal, probiotic and pathogenic bacteria. *Research in Microbiology* **2010**, *161*, 372-382.

Culver, G. M. Assembly of the 30S ribosomal subunit. *Biopolymers* **2003**, *68*, 234-249.

Daglia, M. Polyphenols as antimicrobial agents. *Current Opinion in Biotechnology* **2012**, *23*, 174-181.

Dalbey, R. E.; Wang, P.; Kuhn, A. Assembly of bacterial inner membrane proteins. *Annu. Rev. Biochem.* **2011**, *80*, 161-87.

Darzins, A.; Wang, S.-K.; Vanags, R. I.; Chakrabarty A. M. Clustering of mutations affecting alginic acid biosynthesis in mucoid *Pseudomonas aeruginosa*. *Journal of Bacteriology* **1985**, *164* (2), 516-524.

Darzins, A. The pilG gene product, required for *Pseudomonas aeruginosa* pilus production and twitching motility, is homologous to the enteric, single-domain response regulator CheY. *Journal of Bacteriology* **1993**, *175* (18), 5934-5944.

De Crecy-Lagard, V.; Haas, D.; Hanson, A. D. Newly-discovered enzymes that function in metabolite damage-control. *Current Opinion in Chemical Biology* **2018**, *47*, 101-108.

De Mol, M. L.; Snoeck, N.; De Maeseneire, S. L.; Soetaert, W. K. Hidden antibiotics: Where to uncover? *Biotechnology Advances* **2018**, *36*, 2201-2218.

Deka, C.; Deka, D.; Bora, M. M.; Jha, D. K.; Kakati, D. K. Synthesis of peppermint oil-loaded chitosan/alginate polyelectrolyte complexes and study of their antibacterial activity. *Journal of Drug Delivery Science and Technology* **2016**, *35*, 314-322.

Diaz-Gomez, R.; Lopez-Solis, R.; Obreque-Slier, E.; Toledo-Araya, H. Comparative antibacterial effect of gallic acid and catechin against *Helicobacter pylori*. *LWT - Food Science and Technology* **2013**, *54*, 331-335.

Dietrich, L. E. P.; Price-Whelan, A.; Petersen, A.; Whiteley, M.; Newman, D. K. The phenazine pyocyanin is a terminal signalling factor in the quorum sensing network of *Pseudomonas aeruginosa*. *Molecular Microbiology* **2006**, *61* (5), 1308-1321.

Drehe, I.; Simonetti, E.; Ruiz, J. A. Contribution of the siderophores pyoverdine and enantio-pyochelin to fitness in soil of *Pseudomonas* protegens Pf-5. *Current Microbiology* **2018**, *75*, 1560-1565.

Driessen, A. J. M. SecB, a molecular chaperone with two faces. *Trends in Microbiology* **2001**, *9* (5), 193.

Driscoll, J. A.; Brody, S. L.; Kollef, M. H. The epidemiology, pathogenesis and treatment of *Pseudomonas aeruginosa* infections. *Drugs* **2007**, *67* (3), 351-368.

Dubuisson, J.-F.; Vianney, A.; Hugouvieux-Cotte-Pattat, N.; Lazzaroni, J. C. Tol-Pal proteins are critical cell envelope components of *Erwinia chrysanthemi* affecting cell morphology and virulence. *Microbiology* **2005**, *151*, 3337-3347.

Dulcey, C. E.; Dekimpe, V.; Fauvelle, D. A.; Milot, S.; Groleau, M. C.; Doucet, N.; Rahme, L. G.; Lepine, F.; Deziel, E. The End of an old hypothesis: The *Pseudomonas* signaling molecules 4-hydroxy-2-alkylquinolines derive from fatty acids, not 3-ketofatty acids. *Chemistry & Biology* **2013**, *20*, 1481-1491.

Dumas, J.-L.; van Delden, C.; Perron, K.; Köhler, T. Analysis of antibiotic resistance gene expression in *Pseudomonas aeruginosa* by quantitative real-time-PCR. *FEMS Microbiol. Letters* **2006**, *254*, 217-225.

Dumelin, C. E.; Chen, Y.; Leconte, A. M.; Chen, Y. G.; Liu, D. R. Discovery and biological characterization of geranylated RNA in bacteria. *Nat Chem Biol.* **2012**, *8* (11), 913-919.

Durand, G. A.; Raoult, D.; Dubourg, G. Antibiotic discovery: history, methods and perspectives. *International Journal of Antimicrobial Agents* **2019**, *53*, 371-382.

Duthie, G. G.; Gardner, P. T.; Kyle, J. A. M. Plant polyphenols: are they the new magic bullet? *Proceedings of the Nutrition Society* **2003**, *62*, 599-603.

El-Fouly, M. Z.; Sharaf, A. M.; Shahin, A. A. M.; El-Bialy, H. A.; Omara, A. M. A. Biosynthesis of pyocyanin pigment by *Pseudomonas aeruginosa*. *Journal of Radiation Research and Applied Sciences* **2015**, *8*, 36-48.

Faure, L. M.; Llamas, M. A.; Bastiaansen, K. C.; de Bentzmann, S.; Bigot, S. Phosphate starvation relayed by PhoB activates the expression of the *Pseudomonas aeruginosa* svreI ECF factor and its target genes. *Microbiology* **2013**, *159*, 1315-1327.

Fernandez, L.; Breidenstein, E. B. M.; Taylor, P. K.; Bains, M.; de la Fuente-Nuñez, C.; Fang, Y.; Foster, L. J.; Hancock; R. E. W. Interconnection of posttranscriptional regulation: The RNA-binding protein Hfq is a novel target of the Lon protease in *Pseudomonas aeruginosa*. *Nature Scientific Reports* **2016**, *6*, 26811. 10.1038/srep26811.

Ferro, I.; Chelysheva, I.; Ignatova, Z. Competition for amino acid flux among translation, growth and detoxification in bacteria. *RNA Biology* **2018**, *15* (8), 991-994.

Fletcher, E.; Gao, K.; Mercurio, K.; Ali, M.; Baetz K. Yeast chemogenomic screen identifies distinct metabolic pathways required to tolerate exposure to phenolic fermentation inhibitors ferulic acid, 4-hydroxybenzoic acid and coniferyl aldehyde. *Metabolic Engineering* **2019**, *52*, 98-109.

Flynn, K.; Villarreal, B. P.; Barranco, A.; Belc, N.; Björnsdottir, B.; Fusco, V.; Rainieri, S.; Smaradottir, S. E.; Smeu, I.; Teixeira, P.; Jörundsdottir, H. O. An introduction to current food safety needs. *Trends in Food Science & Technology* **2019**, *84*, 1-3.

François, P.; Scherl, A.; Hochstrasser, D.; Schrenzel, J. Proteomic approaches to study *Staphylococcus aureus* pathogenesis. *Journal of Proteomics* **2010**, *73*, 701-708.

Franz, C. M. A. P.; den Besten, H. M. W.; Böhnlein, C.; Gareis, M.; Zwietering, M. H.; Fusco, V. Reprint of: Microbial food safety in the 21st century: Emerging challenges and foodborne pathogenic bacteria. *Trends in Food Science & Technology* **2019**, *84*, 34-37.

Galloway-Peña, J.; Brumlow, C.; Shelburne, S. Impact of the microbiota on bacterial infections during cancer treatment. *Trends in Microbiology* **2017**, *25* (12), 992.

Garg, A.; Kumari, B.; Singhal, N.; Kumar, M: Using molecular-mimicry-inducing pathways of pathogens as novel drug targets. *Drug Discovery Today* **2018**, doi: 10.1016/j. drudis.2018.10.010

Geissmann, T.; Marzi, S.; Romby, P. The role of mRNA structure in translational control in bacteria. *RNA Biology* **2009**, *6* (2), 153-160.

Gellatly, S. L.; Hancock, R. E. W. *Pseudomonas aeruginosa*: new insights into pathogenesis and host defenses. *Pathogens and Disease* **2013**, *67*, 159-173.

Ghaima, K. K.; Rahal, B. S.; Mohamed, M. M. Biodegradation of phenol by *Pseudomonas aeruginosa* isolated from soil contaminated with diesel fuel. *Bioscience Research* **2017**, *14* (4), 713-720.

Ghosh, C.; Sarkar, P.; Issa, R.; Haldar, J. Physiological functions of D-alanine carboxypeptidases in *Escherichia coli*. *Trends in Microbiology* **2008**, *16* (7), 309.

Gill, E. E.; Chan, L. S.; Winsor, G. L.; Dobson, N.; Lo, R.; Sui, S. J. H.; Dhillon, B. K.; Taylor, P. K.; Shrestha, R.; Spencer, C.; Hancock, R. E. W.; Unrau, P. J.; Brinkman, F. S. L. High-throughput detection of RNA processing in bacteria. *BMC Genomics* **2018**, *19*, 223.

Giltner, C. L.; Nguyen, Y.; Burrows, L. L. Type IV pilin proteins: Versatile molecular modules. *Microbiology and Molecular Biology Reviews* **2012**, *76* (4), 740-772.

Glonti, T.; Chanishvili, N.; Taylor, P.W. Bacteriophage-derived enzyme that depolymerizes the alginic acid capsule associated with cystic fibrosis isolates of *Pseudomonas aeruginosa*. *Journal of Applied Microbiology* **2010**, *108*, 695-702.

Gray, A. N.; Egan, A. J. F.; van't Veer, I. L.; Verheul, J.; Colavin, A.; Koumoutsi, A.; Biboy, J.; Altelaar, A. F. M.; Damen, M. J.; Huang, K. C.; Simorre, J.-P.; Breukink, E.; den Blaauwen, T.; Typas, A.; Gross, C. A.; Vollmer, W. Coordination of peptidoglycan synthesis and outer membrane constriction during *Escherichia coli* cell division. *Microbiology and infectious disease* **2015**, *4*, doi: 10.7554/eLife.07118.

Gurrola, R. C. Z.; Fu, Y.; Luna, I. C. R.; Cardoza, C. G. B.; López, M. de J. L.; Vidal, Y. L.; Gutíerrez, G. R. A.; Pérez, M.A. R.; Guo, X. Novel protein interactions with an actin homolog (MreB) of *Helicobacter pylori* determined by bacterial two-hybrid system. *Microbiological Research* **2017**, *201*, 39-45.

Gutiérrez-Larraínzar, M.; Rúa, J.; Caro, I.; de Castro, C.; de Arriaga, D.; García-Armesto, M. R.; del Valle, P. Evaluation of antimicrobial and antioxidant activities of natural phenolic compounds against foodborne pathogens and spoilage bacteria. *Food Control* **2012**, *26*, 555-563.

Ha D.-G.; O'Toole, G. A. c-di-GMP and its effects on biofilm formation and dispersion: a *Pseudomonas aeruginosa* review. *Microbiol Spectr.* **2015**, *3* (2), doi: 10.1128/microbiolspec.MB-0003-2014.

Hajnsdorf, E.; Kaberdin, V. R. RNA polyadenylation and its consequences in prokaryotes. *Phil. Trans. R. Soc. B* **2018**, *373*, 20180166.

Hannemann, L.; Suppanz, I.; Ba, Q.; MacInnes, K.; Drepper, F.; Warscheid, B.; Koch, H.-G. Redox activation of the universally conserved ATPase YchF by thioredoxin 1. *Antioxidants & Redox Signaling* **2016**, *24* (3), 141.

Hassett, D. J.; Sokol, P. A. ; Howell, M. L.; MA, J.-F.; Schweizer, H. T.; Ochsner, U.; Vasil, M. L. Ferric uptake regulator (Fur) mutants of *Pseudomonas aeruginosa* demonstrate defective siderophore-mediated iron uptake, altered aerobic growth, and decreased superoxide dismutase and catalase activities. *Journal of Bacteriology* **1996**, *178* (14), 3996-4003.

Heleno, S. A.; Martins, A.; Queiroz, M. J. R. P.; Ferreira, I. C. F. R. Bioactivity of phenolic acids: Metabolites versus parent compounds: A review. *Food Chemistry* **2015**, *173*, 501-513.

Heredia, N.; Garcia, S. Animals as sources of food-borne pathogens: A review. *Animal Nutrition* **2018**, *4*, 250-255.

Ho, J. M.; Bakkalbasi, E.; Söll, D.; Miller, C. A. Drugging tRNA aminoacylation. *RNA Biology* **2018**, *15* (4-5), 667-677.

Hogde-Hanson, K. M.; Downs, D. M. Members of the Rid protein family have broad imine deaminase activity and can accelerate the *Pseudomonas aeruginosa* D-arginine dehydrogenase (DauA) reaction in vitro. *PLoS ONE* **2017**, *12* (9), e0185544.

Huang, B.; Whitchurch, C. B.; Mattick, J. S. FimX, a multidomain protein connecting environmental signals to twitching motility in *Pseudomonas aeruginosa*. *Journal of Bacteriology* **2003**, *185* (24), 7068-7076.

Huang, N.; De Ingeniis, J.; Galeazzi, L.; Mancini, C.; Korostelev, Y. D.; Rakhmaninova, A. B.; Gelfand, M. S.; Rodionov, D. A.; Raffaelli, N.; Zhang, H. Structure and function of an ADP-ribose-dependent transcriptional regulator of NAD metabolism. *Structure* **2009**, *17*, 939-951.

Huber, P.; Basso, P.; Reboud, E.; Attree, I. *Pseudomonas aeruginosa* renews its virulence factors. *Environmental Microbiology Reports* **2016**, *8* (5), 564-571.

Hurtado-Fernandez, E.; Gomez-Romero, M.; Carrasco-Pancorbo, A.; Fernandez-Gutierrez, A. Application and potential of capillary electroseparation methods to determine antioxidant phenolic compounds from plant food material. *Journal of Pharmaceutical and Biomedical Analysis* **2010**, *53*, 1130-1160.

Hynes, A.; Scott, D. A.; Man, A.; Singer, D. L.; Sowa, M. G.; Liu, K.-Z. Molecular mapping of periodontal tissues using infrared Microspectroscopy. *BMC Medical Imaging* **2005**, *5* (2), doi:10.1186/1471-2342-5-2.

Jain, R.; Sliusarenko, O.; Kazmierczak, B. I. Interaction of the cyclic-di-GMP binding protein FimX and the Type 4 pilus assembly ATPase promotes pilus assembly. *PLOS pathogens* **2017**, *13* (8), e1006594.

Jamil, B.; Habib, H.; Abbasi, S.; Nasir, H.; Rahman, A.; Rehman, A.; Bokhari, H.; Imran, M. Cefazolin loaded chitosan nanoparticles to cure multi drug resistant Gram-negative pathogens. *Carbohydrate Polymers* **2016** (a), *136*, 682-691.

Jamil, B.; Abbasi, R.; Abbasi, S.; Imran, M.; Khan, S. U.; Ihsan, A.; Javed, S.; Bokhari, H.; Imran, M. Encapsulation of cardamom essential oil in chitosan nano-composites: In-vitro efficacy on antibiotic-resistant bacterial pathogens and cytotoxicity studies. *Frontiers in Microbiology* **2016** (b), *7*, 1580.

Jayakumar, R.; Menon, D.; Manzoor, K.; Nair, S.V.; Tamura, H. Biomedical applications of chitin and chitosan based nanomaterials-A short review. *Carbohydrate Polymers* **2010**, *82*, 227-232.

John, G. St.; Brot, N.; Ruan, J.; Erdjument-Bromage, H.; Tempst, P.; Weissbach, H.; Nathan, C. Peptide methionine sulfoxide reductase from *Escherichia coli* and *Mycobacterium tuberculosis* protects bacteria against oxidative damage from reactive nitrogen intermediates. *PNAS* **2001**, *98* (17), 9901-9906.

Johnson, L.; Mulcahy, H.; Kanevets, U.; Shi, Y.; Lewenza, S. Surface-localized spermidine protects the *Pseudomonas aeruginosa* outer membrane from antibiotic treatment and oxidative stress. *Journal of Bacteriology* **2011**, *194* (4), 813-826.

Kamariah, N.; Manimekalai, M. S. S.; Nartey, W.; Eisenhaber, F.; Eisenhaber, B.; Gruber, G. Crystallographic and solution studies of NAD(+)- and NADH-bound alkylhydroperoxide reductase subunit F (AhpF) from *Escherichia coli* provide

insight into sequential enzymatic steps. *Biochimica et Biophysica Scta-Bioenergetics* **2015**, *1847* (10), 1139-1152.

Karaosmanoglu, H.; Soyer, F.; Ozen, B.; Tokatlı, F. Antimicrobial and antioxidant activities of Turkish extra virgin olive oils. *Journal of Agricultural and Food Chemistry* **2010**, 58, 8238-8245.

Kazmierczak, B. I.; Lebron, M. B.; Murray, T. S. Analysis of FimX, a phosphodiesterase that governs twitching motility in *Pseudomonas aeruginosa*. *Mol Microbiol.* **2006**, *60* (4), 1026-1043.

Kazmierczak, B. I.; Schniederberend, M.; Jain, R. Cross-regulation of Pseudomonas motility systems: the intimate relationship between flagella, pili and virulence. *Current Opinion in Microbiology* **2015**, *28*, 78-82.

Khan, F.; Manivasagan, P.; Pham, D. T. N.; Oh, J.; Kim, S.-K.; Kim, Y.-M. Antibiofilm and antivirulence properties of chitosan-polypyrrole nanocomposites to *Pseudomonas aeruginosa*. *Microbial Pathogenesis* **2019**, *128*, 363-373.

Khatua, B.; Vleet, J. V.; Choudhury, B. P.; Chaudhry, R.; Mandal, C. Sialylation of outer membrane porin protein D: A mechanistic basis of antibiotic uptake in *Pseudomonas aeruginosa*. *Molecular & Cellular Proteomics* **2014**, *13* (6), 1412.

Kılıç, N. K.; Stensballe, A.; Otzen, D. E.; Donmez, G. Proteomic changes in response to chromium(VI) toxicity in *Pseudomonas aeruginosa*. *Bioresource Technology* **2010**, *101*, 2134-2140.

Kiefer, D.; Kuhn, A. YidC-mediated membrane insertion. *FEMS Microbiology Letters* **2018**, *365* (12), doi: 10.1093/femsle/fny106.

Kim, S. Y.; Park, C.; Jang, H.-J.; Kim, B.-o; Bae, H.-W.; Chung, I.-Y.; Kim, E. S.; Cho, Y.-H. Antibacterial strategies inspired by the oxidative stress and response Networks. *Journal of Microbiology* **2019**, *57* (3), 203-212.

Kirillov, S.; Vitali, L. A.; Goldstein, B. P.; Monti, F.; Semenkov, Y.; Makhno, V.; Ripa, S.; Pon, C. L.; Gualerzi, C. O. Purpuromycin: An antibiotic inhibitinf tRNA aminoacylation. *RNA* **1997**, *3*, 905-913.

Klockgether, J.; Tümmler, B. Recent advances in understanding *Pseudomonas aeruginosa* as a pathogen [version 1; referees: 3 approved]. *F1000Research* **2017**, *6*, 1261.

Krausz, A. E.; Adler, B. L.; Cabral, V.; Navati, M.; Doerner, J.; Charafeddine, R. A.; Chandra, D.; Liang, H.; Gunther, L.; Clendaniel, A.; Harper, S.; Friedman, J. M.; Nosanchuk, J. D.; Friedman, A. J. Curcumin-encapsulated nanoparticles as innovative antimicrobial and wound healing agent. *Nanomedicine: Nanotechnology, Biology, and Medicine* **2015**, *11*, 195-206.

Krishnan, B.; Kulothungan, S. R.; Patra, A. K.; Udgaonkar, J. B.; Varadarajan, R. SecB-mediated protein export need not occur via kinetic partitioning. *J. Mol. Biol.* **2009**, *385*, 1243-1256.

Langklotz, S.; Baumann, U.; Narberhaus, F. Structure and function of the bacterial AAA protease FtsH. *Biochimica et Biophysica Acta* **2012**, *1823*, 40-48.

Lee, S. A.; Gallagher, L. A.; Thongdee, M.; Staudinger, B. J.; Lippman, S.; Singh, P. K.; Manoil, C. General and condition-specific essential functions of *Pseudomonas aeruginosa*. *PNAS* **2015**, *112* (16), 5189-94.

Lee, E.-Y.; Kim, S.; Kim, M. H. Aminoacyl-tRNA synthetases, therapeutic targets for infectious diseases. *Biochemical Pharmacology* **2018**, *154*, 424-434.

Lewis, K. New approaches to antimicrobial discovery. *Biochemical Pharmacology* **2017**, *134*, 87-98.

Li, Z.; Jiang, H.; Xu, C.; Gu, L. A review: Using nanoparticles to enhance absorption and bioavailability of phenolic phytochemicals. *Food Hydrocolloids* **2015**, *43*, 153-164.

Li, W.; Zhang, S.; Wang, X.; Yu, J.; Li, Z.; Lin, W.; Lin, X. Systematically integrated metabonomic-proteomic studies of *Escherichia coli* under ciprofloxacin stress. *Journal of Proteomics* **2018**, *179*, 61-70.

Lima, M. C.; de Sousa, C. P.; Fernandez-Prada, C.; Harel, J.; Dubreuil, J. D.; de Souza, E. L. A review of the current evidence of fruit phenolic compounds as potential antimicrobials against pathogenic bacteria. *Microbial Pathogenesis* **2019**, *130*, 259-270.

Lister, P. D.; Wolter, D. J.; Hanson, N. D. Antibacterial-resistant *Pseudomonas aeruginosa*: Clinical impact and complex regulation of chromosomally encoded resistance mechanisms. *Clinical Microbiology Reviews* **2009**, *22*, 582-610.

Liu, Q.; Fredrick, K. Intersubunit bridges of the bacterial ribosome. *J Mol Biol.* **2016**, *428* (10 Pt B), 2146-2164.

Liu, J.; Xiao, J.; Li, F.; Shi, Y.; Li, D.; Huang, Q. Chitosan-sodium alginate nanoparticle as a delivery system forε-polylysine: Preparation, characterization and antimicrobial activity. *Food Control* **2018**, *91*, 302-310.

Iiyama, K.; Chieda, Y.; Lee, J. M.; Kusakabe, T.; Yasunaga-Aoki, C.; Shimizu, S. Effect of superoxide dismutase gene inactivation on virulence of *Pseudomonas aeruginosa* PAO1 toward the silkworm, *Bombyx mori*. *Applied and Environmental Microbiology* **2007**, *73* (5), 1569-1575.

Llamas, M. A.; Ramos, J. L.; Rodriguez-Herva, J. J. Transcriptional organization of the *Pseudomonas putida* tol-oprL genes. *Journal of Bacteriology* **2003**, *185* (1), 184-195.

Llanes, C.; Hocquet, D.; Vogne, C.; Benali-Baitich, D.; Neuwirth, C.; Plesiat, P. Clinical strains of *Pseudomonas aeruginosa* overproducing MexAB-OprM and MexXY efflux pumps simultaneously. *Antimicrobial Agents and Chemotherapy* **2004**, *48* (5), 1797-1802.

Lu, H. D.; Pearson, E.; Ristroph, K. D.; Duncan, G. A.; Ensign, L. M.;mSuk, J. S.; Hanes, J.; Prudhomme, R. K. *Pseudomonas aeruginosa* pyocyanin production reduced by quorum-sensing inhibiting nanocarriers. *International Journal of Pharmaceutics* **2018**, *544*, 75-82.

Ma, W.; Zhang, D.; Li, G.; Liu, J.; He, G.; Zhang, P.; Yang, L.; Zhu, H.; Xu, N.; Liang, S. Antibacterial mechanism of daptomycin antibiotic against *Staphylococcus aureus* based on a quantitative bacterial proteome analysis. *Journal of Proteomics* **2017**, *150*, 242-251.

Maldonado-Carmona, N.; Vazquez-Hernandez, M.; Chavez, O. J. P.; Rodriguez-Luna, S. D.; Rodriguez, O. J.; Sanchez, S.; Ceapa, C. D. Impact of ~omics in the detection and validation of potential anti-infective drugs. *Current Opinion in Pharmacology* **2019**, *48*, 1-7.

Madureira,A. R.; Pereira, A.; Castro,P. M.; Pintado, M. Production of antimicrobial chitosan nanoparticles against food pathogens. *Journal of Food Engineering* **2015**, *167*, 210-216.

Mathieu, S.; Cisse, C.; Vitale, S.; Ahmadova, A.; Degardin, M.; Perard, J.; Colas, P.; Miras, R.; Boturyn, D.; Coves, J.; Crouzy, S.; Michaud-Soret, I. From peptide aptamers to inhibitors of FUR, bacterial transcriptional regulator of iron homeostasis and virulence. *ACS Chem. Biol.* **2016**, *11*, 2519-2528.

Mejias, S. H.; Bahrami-Dizicheh, Z.; Liutkus, M.; Sommer, D. J.; Astashkin, A.; Kodis, G.; Ghirlanda, G.; Cortajarena, A. L. Repeat proteins as versatile scaffolds for arrays of redox-active FeS clusters. *Chem. Commun.* **2019**, *55*, 3305-3420.

Meyer, K.; Addy, C.; Akashi, S.; Roper, D. I:; Tame, J. R. H. The crystal structure and oligomeric form of *Escherichia coli* L,D-carboxypeptidase A. *Biochemical and Biophysical Research Communications* **2018**, *499*, 594-599.

Mintz, K. P.; Moskovitz, J.; Wu, H.; Fives-Taylor, P. M. Peptide methionine sulfoxide reductase (MsrA) is not a major virulence determinant for the oral pathogen *Actinobacillus actinomycetemcomitans*. *Microbiology* **2002**, *148*, 3695-3703.

Miryala, S. K.; Anbarasu, A.; Ramaiah, S. Discerning molecular interactions: A comprehensive review on biomolecular interaction databases and network analysis tools. *Gene* **2018**, *642*, 84-94.

Mladenovska, K.; Cruaud, O.; Richomme, P.; Belamie, E.; Raicki, R. S.; Venier-Julienne, M.-C.; Popovski, E.; Benoit, J. P.; Goracinova, K. 5-ASA loaded chitosan–Ca–alginate microparticles: Preparation and physicochemical characterization. *International Journal of Pharmaceutics* **2007**, *345*, 59–69.

Mohammadi, A.; Hashemi, M.; Hosseini, S. M. Effect of chitosan molecular weight as micro and nanoparticles on antibacterial activity against some soft rot pathogenic bacteria. *LWT - Food Science and Technology* **2016**, *71*, 347-355.

Monti, M. R.; Miguel, V.; Borgogno, M. V.; Argarana, C. E. Functional analysis of the interaction between the mismatch repair protein MutS and the replication processivity factor β-clamp in *Pseudomonas aeruginosa*. *DNA Repair* **2012**, *11*, 463-469.

Mori, N.; Ishii, Y.; Tateda, K.; Kimura, S.; Kouyama, Y.; Inoko, H.; Mitsunaga, S.; Yamaguchi, K.; Yoshihara, E. A peptide based on homologous sequences of the b-

barrel assembly machinery component BamD potentiates antibiotic susceptibility of *Pseudomonas aeruginosa*. *J Antimicrob Chemother* **2012**, *67*, 2173-2181.

Morita, Y.; Tomida, J.; Kawamura, Y. Responses of *Pseudomonas aeruginosa* to antimicrobials. *Frontiers in Microbiology* **2014**, *4*, 422.

Moschona, A.; Liakopoulou-Kyriakides, M. Encapsulation of biological active phenolic compounds extracted from wine wastes in alginate-chitosan microbeads. *Journal of Microencapsulation* **2018**, *35* (3), 229-240.

MubarakAli, D.; LewisOscar, F. ; Gopinath, V.; Alharbi, N. S.; Alharbi, S. A.; Thajuddin, N. An inhibitory action of chitosan nanoparticles against pathogenic bacteria and fungi and their potential applications as biocompatible antioxidants. *Microbial Pathogenesis* **2018**, *114*, 323-327.

Mujumdar, S. S.; Bashetti, S. P.; Chopade, B. A. Plasmid pUPI126-encoded pyrrolnitrin production by *Acinetobacter haemolyticus* A19 isolated from the rhizosphere of wheat. *World J Microbiol Biotechnol* **2014**, *30*, 495-505.

Murima, P.; McKinney, J. D.; Pethe, K. Targeting bacterial central metabolism for drug development. *Chemistry & Biology* **2014**, *21*, 1423.

Murray, J. L.; Kwon, T.; Marcotte, E. M.; Whiteley, M. Intrinsic antimicrobial resistance determinants in the superbug *Pseudomonas aeruginosa*. *mBio* **2015**, *6* (6), e01603-15.

Nakanishi, K.; Bonnefond, L.; Kimura, S.; Suzuki, T.; Ishitani, R.; Nureki, O. Structural basis for translational fidelity ensured by transfer RNA lysidine synthetase. *Nature* **2009**, *461*, 1144.

Nandan, A.; Nampoothri, K. Molecular advances in microbial aminopeptidases. *Bioresource Technology* **2017**, *245*, 1757-1765.

Narberhaus, F.; Obrist, M.; Führer, F.; Langklotz, S. Degradation of cytoplasmic substrates by FtsH, a membrane anchored protease with many talents. *Research in Microbiology* **2009**, *160*, 652-659.

Navare, A. T.; Chavez, J. D.; Zheng, C.; Weisbrod, C. R.; Eng, J. K.; Siehnel, R.; Singh, P. K.; Manoil, C.; Bruce, J. E. Probing the protein interaction network of

Pseudomonas aeruginosa cells by chemical cross-linking mass spectrometry. *Structure* **2015**, *23*, 762-773.

Neely, A. N.; Maley, M. P. Survival of *Enterococci* and *Staphylococci* on hospital fabrics and plastic. *Journal of Clinical Microbiology* **2000**, *38* (2), 724-726.

Nordmann, P.; Naas, T.; Fortineau, N.; Poirel, L. Superbugs in the coming new decade; multidrug resistance and prospects for treatment of *Staphylococcus aureus*, *Enterococcus* spp. and *Pseudomonas aeruginosa* in 2010. *Current Opinion in Microbiology* **2007**, *10*, 436-440.

Numata, T. Mechanisms of the tRNA wobble cytidine modification essential for AUA codon decoding in prokaryotes. *Bioscience, Biotechnology, and Biochemistry* **2015**, *79* (3), 347-353.

Ocakoglu, D.; Tokatli, F.; Ozen, B.; Korel, F. Distribution of simple phenols, phenolic acids and flavonoids in Turkish monovarietal extra virgin olive oils for two harvest years. *Food Chemistry* **2009**, *113*, 401-410.

Okon, E.; Dethlefsen, S.; Pelnikevich, A.; van Barneveld, A.; Munder, A.; Tümmler, B. Key role of an ADP - ribose - dependent transcriptional regulator of NAD metabolism for fitness and virulence of *Pseudomonas aeruginosa*. *International Journal of Medical Microbiology* **2017**, *307*, 83-94.

Oliver, A.; Baquero, F.; Blazquez, J. The mismatch repair system (mutS, mutL and uvrD genes) in *Pseudomonas aeruginosa*: molecular characterization of naturally occurring mutants. *Molecular Microbiology* **2002**, *43* (6), 1641-1650.

Pang, Z.; Raudonis, R.; Glick, B. R.; Lin, T.-J.; Cheng, Z. Antibiotic resistance in *Pseudomonas aeruginosa*: mechanisms and alternative therapeutic strategies. *Biotechnology Advances* **2019**, *37*, 177-192.

Paques, J. P.; van der Linden, E.; van Rijn, C. J. M.; Sagis, L. M. C. Preparation methods of alginate nanoparticles. *Advances in Colloid and Interface Science* **2014**, *209*, 163-171.

Parenti, M. A.; Hatfield, S. M.; Leyden, J. J. Mupirocin: a topical antibiotic with a unique structure and mechanism of action, *Clin Pharm.* **1987**, *6* (10), 761-70.

Parlet, C. P.; Brown, M. M.; Horswill, A. R. Commensal *Staphylococci* influence *Staphylococcus aureus* skin colonization and disease. *Trends in Microbiology* **2019**, 27 (6), 497-507.

Piette, A.; Verschraegen, G. Role of coagulase-negative *Staphylococci* in human disease. *Veterinary Microbiology* **2009**, *134*, 45-54.

Pinochet-Barros, A.; Helmann, J. D. Redox sensing by Fe2+ in bacterial Fur family metalloregulators. *Antioxidants & Redox Signaling* **2018**, *29* (18), 1858-1871.

Poole K. *Pseudomonas aeruginosa*: Resistance to the max. *Frontiers in Microbiology* **2011**, *2* (65), 10.3389/fmicb.2011.00065.

Potron, A.; Poirel, L.; Nordmann, P. Emerging broad-spectrum resistance in *Pseudomonas aeruginosa* and *Acinetobacter baumannii*: Mechanisms and epidemiology. *International Journal of Antimicrobial Agents* **2015**, *45* (6), 568-85.

Potvin, E.; Sanschagrin, F.; Levesque, R. C. Sigma factors in *Pseudomonas aeruginosa*. *FEMS Microbiol Rev* **2008**, *32*, 38-55.

Qi, L.; Xu, Z.; Jiang, X.; Hu, C.; Zou, X. Preparation and antibacterial activity of chitosan nanoparticles. *Carbohydrate Research* **2004**, *339*, 2693-2700.

Quesada, J. M.; Otero-Asman, J. R.; Bastiaansen, K. C.; Civantos, C.; Llamas, M. A. Activity of the *Pseudomonas aeruginosa* virulence regulator σVreI is modulated by the anti-σ factor VreR and the transcription factor PhoB. *Frontiers in Microbiology* **2016**, *7*, 1159.

Rada B.; Leto, T. L. Pyocyanin effects on respiratory epithelium: relevance in *Pseudomonas aeruginosa* airway infections. *Trends in Microbiology* **2013**, *21* (2), 73.

Rammelt, C.; Rossmanith, W. Repairing tRNA termini: News from the 3' end. *RNA Biology* **2016**, *13* (12), 1182-1188.

Rego, A. T.; Holding, A. N.; Kent, H.; Lamers, M. H.. Architecture of the Pol III–clamp–exonuclease complex reveals key roles of the exonuclease subunit in processive DNA synthesis and repair. *The EMBO Journal* **2013**, *32*, 1334-1343.

Ringel, P. D.; Hu, D.; Basler, M. The role of type VI secretion system effectors in target cell lysis and subsequent horizontal gene transfer. *Cell Reports* **2017**, *21*, 3927-3940.

Roig, A.; Cayuela, M. L.; Sanchez-Monedero M. A. An overview on olive mill wastes and their valorisation methods. *Waste Management* **2006**, *26*, 960-969.

Russell, A. B.; Singh, P.; Brittnacher, M.; Bui, N. K.; Hood, R. D.; Carl, M. A.; Agnello, D. M.; Schwarz, S.; Goodlett, D. R.; Vollmer, W.; Mougous, J. D. A Widespread bacterial type VI secretion effector superfamily identified using a heuristic approach. *Cell Host & Microbe* **2012**, *11*, 538-549.

Salih, O.; He, S.; Planamente, S.; Stach, L.; MacDonald, J. T.; Manoli, E.; Scheres, S. H. W.; Filloux, A.; Freemont, P. S. Atomic structure of type VI contractile sheath from *Pseudomonas aeruginosa*. *Structure* **2018**, *26*, 329-336.

Salomon, D.; Orth, K. Type VI secretion system. *Current Biology* **2015**, *25*, R255–R268.

Sanhueza, L.; Melo, R.; Montero, R.; Maisey, K.; Mendoza, L.; Wilkens, M. Synergistic interactions between phenolic compounds identified in grape pomace extract with antibiotics of different classes against *Staphylococcus aureus* and *Escherichia coli*. *PLoS ONE* **2017**, *12* (2), e0172273.

Schoenfelder, S. M. K.; Lange, C.; Eckart, M.; Hennig, S.; Kozytska, S.; Ziebuhr W., Success through diversity – How *Staphylococcus epidermidis* establishes as a nosocomial pathogen. *International Journal of Medical Microbiology* **2010**, *300*, 380-386.

Serganov A.; Polonskaia, A.; Ehresmann, B.; Ehresmann, C.; Patel, D. J. Ribosomal protein S15 represses its own translation via adaptation of an rRNA-like fold within its mRNA. *The EMBO Journal* **2003**, *22* (8), 1898-1908.

Serra, C.; Bouharkat, B.; Touil-Meddah, A. T.; Guenin, S.; Mullie, C. MexXY multidrug efflux system is more frequently overexpressed in ciprofloxacin resistant french clinical isolates compared to hospital environment ones. *Frontiers in Microbiology* **2019**, *10*, 366.

Shajani, Z.; Sykes, M. T.; Williamson, J. R. Assembly of bacterial ribosomes. *Annu. Rev. Biochem.* **2011**, *80*, 501-26.

Sharma, D.; Garg, A.; Kumar, M.; Khan, A. U. Proteome profiling of carbapenem-resistant *K. pneumoniae* clinical isolate (NDM-4): Exploring the mechanism of resistance and potential drug targets. *Journal of Proteomics* **2019**, *200*, 102-110.

Shen, X.; Sun, X.; Xie, Q.; Liu, H.; Zhao, Y.; Pan, Y.; Hwang, C.-A.; Wu, V. C. H. Antimicrobial effect of blueberry (*Vaccinium corymbosum* L.) extracts against the growth of *Listeria monocytogenes* and *Salmonella* Enteritidis. *Food Control* **2014**, *35*, 159-165.

Shi, C.; Zhang, X.; Zhao, X.; Meng, R.; Liu, Z.; Chen, X.; Guo, N. Synergistic interactions of nisin in combination with cinnamaldehyde against *Staphylococcus aureus* in pasteurized milk. *Food Control* **2017**, *71*, 10-16.

Shigi, N. Recent advances in our understanding of the biosynthesis of sulfur modifications in tRNAs. *Frontiers in Microbiology* **2018**, *9*, 2679.

Sidorenko, J.; Ukkivi, K.; Kivisaar, M. NER enzymes maintain genome integrity and suppress homologous recombination in the absence of exogenously induced DNA damage in *Pseudomonas putida*. *DNA Repair* **2015**, *25*, 15-26.

Sierant, M.; Leszczynska, G.; Sadowska, K.; Dziergowska, A.; Rozanski, M.; Sochacka, E.; Nawrot, B. S-Geranyl-2-thiouridine wobble nucleosides of bacterial tRNAs; chemical and enzymatic synthesis of S-geranylated-RNAs and their physicochemical characterization. *Nucleic Acids Research* **2016**, *44* (22), 10986-10998.

Silby, M. W.; Winstanley, C.; Godfrey, S. A. C.; Levy, S. B.; Jackson, R. W. *Pseudomonas* genomes:diverse and adaptable. *FEMS Microbiol Rev.* **2011**, *35*, 652-680.

Singh, K.; Kumar, A. Kinetics of complex formation of Fe(III) with caffeic acid: Experimental and theoretical study. *Spectrochimica Acta Part A: Molecular and Biomolecular Spectroscopy* **2019**, *211*, 148-153.

Srinivasan, R.; Rajeswari, H.; Ajitkumar, P. Analysis of degradation of bacterial cell division protein FtsZ by the ATP-dependent zinc-metalloprotease FtsH in vitro. *Microbiological Research* **2008**, *163*, 21-30.

Smirnova, G. V.; Oktyabrsky, O. N. Glutathione in bacteria. *Biochemistry (Moscow)* **2005**, *70* (11), 1199-1211.

Stapels, M. D.; Cho, J.-C.; Giovannoni, S. J.; Barofsky, D. F. Proteomic analysis of novel marine bacteria using MALDI and ESI mass spectrometry. *Journal of Biomolecular Techniques* **2004**, *15*, 191-198.

Stinnett, J. D.; Gilleland JR., H. E.; Eagon, R. G. Proteins released from cell envelopes of *Pseudomonas aeruginosa* on exposure to ethylenediaminetetraacetate: Comparison with dimethylformamide extractable proteins. *Journal of Bacteriology* **1973**, *114* (1), 399-407.

Strateva, T.; Yordanov, D. *Pseudomonas aeruginosa* – a phenomenon of bacterial resistance. *Journal of Medical Microbiology* **2009**, *58*, 1133–1148.

Sturgis, J. N. Organisation and evolution of the tol-pal gene cluster. *J. Mol. Microbiol. Biotechnol.* **2001**, *3* (1), 113-122.

Sutcliffe, J. A. Improving on nature: antibiotics that target the ribosome. *Current Opinion in Microbiology* **2005**, *8*, 534-542.

Swiecilo, A.; Zych-Wezyk, I. Bacterial stress response as an adaptation to life in a soil environment, *Pol. J. Environ. Stud.* **2013**, *22* (6), 11.

Sze, C. C.; Bernardo, L. M. D.; Shingler, V. Integration of global regulation of two aromatic-responsive σ54-dependent systems: A common phenotype by different mechanisms. *Journal of Bacteriology* **2002**, *184* (3), 760-770.

Takahashi, H.; Saito, R.; Miya, S.; Tanaka, Y.; Miyamura, N.; Kuda, T.; Kimura, B. Development of quantitative real-time PCR for detection and enumeration of Enterobacteriaceae. *International Journal of Food Microbiology* **2017**, *246*, 92-97.

Tamburro, A.; Allocati, N.; Masulli, M.; Rotilio, D.; Di Ilio, C.; Favaloro, B. Bacterial peptide methionine sulphoxide reductase: co-induction with glutathione S-transferase during chemical stress conditions. *Biochemical Journal* **2001**, *360* (3), 675-681.

Tang, D.-W.; Yu, S.-H.; Ho, Y.-C.; Huang, B.-Q.; Tsai, G.-J.; Hsieh, H.-Y.; Sung, H.-W.; Mi, F.-L. Characterization of tea catechins-loaded nanoparticles prepared from chitosan and an edible polypeptide. *Food Hydrocolloids* **2013**, *30*, 33-41.

Tang, Y.; Nakashima, S.; Saiki, S.; Myoi, Y.; Abe, N.; Kuwazuru, S.; Zhu, B.; Ashida, H.; Murata, Y.; Nakamura, Y. 3,4-Dihydroxyphenylacetic acid is a predominant

biologically-active catabolite of quercetin glycosides. *Food Research International* **2016**, *89*, 716-723.

Tark, M.; Tover, A.; Koorits, L.; Tegova, R.; Kivisaar, M. Dual role of NER in mutagenesis in *Pseudomonas putida*. *DNA Repair* **2008**, *7*, 20-30.

Tavita, K.; Mikkel, K.; Tark-Dame, M.; Jerabek, H.; Teras, R.; Sidorenko, J.; Tegova, R.; Tover, A.; Dame, R. T.; Kivisaar, M. Homologous recombination is facilitated in starving populations of *Pseudomonas putida* by phenol stress and affected by chromosomal location of the recombination target. *Mutation Research* **2012**, *737*, 12-24.

Templin, M. F.; Ursinus, A.; Höltje, J.-V. A defect in cell wall recycling triggers autolysis during the stationary growth phase of *Escherichia coli*. *The EMBO Journal* **1999**, *18* (15), 4108-4117.

Tripathi, P. C.; Gajbhiye,S. R.; Agrawal, G. N. Clinical and antimicrobial profile of Acinetobacter spp.: An emerging nosocomial superbug. *Adv Biomed Res.* **2014**, *3*, 13.

Tripoli, E.; Giammanco, M.; Tabacchi, G.; Di Majo, D.; Giammanco, S.; La Guardia, M. The phenolic compounds of olive oil: structure, biological activity and beneficial effects on human health. *Nutrition Research Reviews* **2005**, *18*, 98-112.

Ugurlu, A.; Karahasan Yagci, A.; Ulusoy, S.; Aksu, B.; Bosgelmez-Tinaz, G. Phenolic compounds affect production of pyocyanin, swarming motility and biofilm formation of *Pseudomonas aeruginosa*. *Asian Pac J Trop Biomed* **2016**, *6* (8), 698-701.

Valentini, M.; Gonzalez, D.; AI Mavridou, D.; Filloux, A. Lifestyle transitions and adaptive pathogenesis of *Pseudomonas aeruginosa*. *Current Opinion in Microbiology* **2018**, *41*, 15-20.

Walther, T. C.; Mann, M. Mass spectrometry–based proteomics in cell biology. *The Journal of Cell Biology*, **2010**, *190* (4): 491-500.

Wang, Y.; Yang, F.; Gritsenko, M. A.; Wang, Y.; Clauss, T.; Liu, T.; Shen, Y.; Monroe, M. E.; Lopez-Ferrer, D.; Reno, T.; Moore, R. J.; Klemke, R. L.; Camp II, D. G.; Smith, R. D. Reversed-phase chromatography with multiple fraction concatenation strategy for proteome profiling of human MCF10A cells. *Proteomics* **2011**, *11*, 2019-2026.

Wang X.; Liu, Q.; Zhang, B. Leveraging the complementary nature of RNA-Seq and shotgun proteomics data. *Proteomics* **2014**, *14*, 2676-2687.

Wang, R.; Vangaveti, S.; Ranganathan, S. V.; Basanta-Sanchez, M.; Haruehanroengra, P.; Chen, A.; Sheng, J. Synthesis, base pairing and structure studies of geranylated RNA. *Nucleic Acids Research* **2016**, *44* (13), 6036-6045.

Whitney, J. C.; Howell, P. L. Synthase-dependent exopolysaccharide secretion in Gram negative bacteria. *Trends in Microbiology* **2013**, *21* (2), 63.

Wei, Q.; Le Minh, P. N.; Dotsch, A.; Hildebrand, F.; Panmanee, W.; Elfarash, A.; Schulz, S.; Plaisance, S.; Charlier, D.; Hassett, D.; Haussler, S.; Cornelis, P. Global regulation of gene expression by OxyR in an important human opportunistic pathogen. *Nucleic Acids Research* **2012**, *40* (10), 4320-4333.

Wintachai, P.; Paosen, S.; Yupanqui, C. T.; Voravuthikunchai, S. P. Silver nanoparticles synthesized with *Eucalyptus critriodora* ethanol leaf extract stimulate antibacterial activity against clinically multidrug-resistant *Acinetobacter baumannii* isolated from pneumonia patients. *Microbial Pathogenesis* **2019**, *126*, 245-257.

Wu, T.; Li, Y.; Shen, N.; Yuan, C.; Hu, Y. Preparation and characterization of calcium alginate-chitosan complexes loaded with lysozyme. *Journal of Food Engineering* **2018**, *233*, 109-116.

Yang, J.-S.; Xie, Y.-J.; He, W. Research progress on chemical modification of alginate: A review. *Carbohydrate Polymers* **2011**, *84*, 33-39.

Yang, F.; Shen, Y.; Camp II, D. G.; Smith, R. D. High pH reversed-phase chromatography with fraction concatenation as an alternative to strong-cation exchange chromatography for two-dimensional proteomic analysis. *Expert Rev Proteomics* **2012**, *9* (2), 129-134.

Zafra, A.; Juarez, M. J. B.; Blanc, R.; Navalon, A.; Gonzalez, J.; Vilchez, J. L. Determination of polyphenolic compounds in wastewater olive oil by gas chromatography–mass spectrometry. *Talanta* **2006**, *70*, 213-218.

Zhou, X.; Yishake, M.; Li, J.; Jiang, L.; Wu, L.; Liu, R.; Xu, N. Genetic susceptibility to prosthetic joint infection following total joint arthroplasty: A systematic review. *Gene* **2015**, *563*, 76-82.

Zimet, P.; Mombru, A. W.; Faccio, R.; Brugnini, G.; Miraballes, I.; Rufo, C.; Pardo, H. Optimization and characterization of nisin-loaded alginate-chitosan nanoparticles with antimicrobial activity in lean beef. *LWT - Food Science and Technology* **2018**, *91*, 107-116.

APPENDIX A

THE GROWTH CURVE OF *P. aeruginosa*

The growth curve of *P. aeruginosa* was plotted as optical density versus time by measurement of optical density (O.D.) of bacteria spectrophotometrically at 600 nm. The intervals of measurement points were 3 hours during 24 hours of growth in MHB at 37^{o}C. In addition, for viable cell count, colony forming unit per mililiters (cfu/ml) were calculated by counting the colonies on agar plates which were inoculated by spread plating at least 3 hours of intervals for 24 hours. According to results of spectrophotometric measurements the bacteria displayed the growth curve which fit the general curve of bacterial growth with specific exponential and stationary phases. Figure A.1 demonstrates that the exponential phase of *P. aeruginosa* starts at about 18th hour of growth.*P. aeruginosa* culture starts to have a blue color and the cells start to make clumps by sticking to each other in test tubes from the 15th hour of growth. During the experiments, these clumps were achieved to be destroyed via vortex. However, at the 24th of its growth, the clumps were more adherent and difficult to be destroyed. These cell clumps might cause the O.D. of the *P. aeruginosa* at 24th hour of growth seemed a little more than that of 18th hour in the graph.

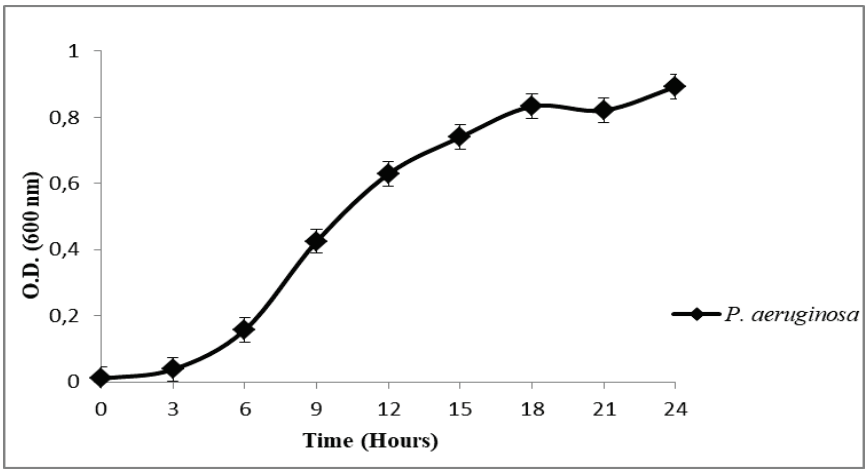

Figure A.1. The growth curve of *P. aeruginosa.*

APPENDIX B

THE ANTIMICOBIAL EFFECTS OF A NARROW RANGE OF CONCENTRATIONS

The antimicrobial effects of 3-HPAA and 4-HBA were tested on *P. aeruginosa* in a narrow range of concentrations. These additional experiments were performed by the same technique used in Chapter 2 with a different brand of media. In the main antimicrobial and protein experiments in Chapter 2 and 3, Mueller Hinton Media with Fluka Brand were used. Since Fluka MHB media was consumed in all previous experiments, the same media with Sigma brand was thought to be proper (Sigma-Aldrich was incorporated Fluka brand). Surprisingly, different MIC and MBC values were obtained than these values of previous experiments when the different brand media were used.

In the experiments which were carried out with with Fluka brand MHB, 1.9 mg/ml 3-HPAA showed 58% inhibition on *P. aeruginosa* (Table 2.1.) was chosen for using in shot-gun proteomics as a subinhibitory concentration. When the experiments were performed with Sigma brand MHB, the percent inhibition of 1.9 mg/ml 3-HPAA was found as 25%. Although it is still a subinhibitory concentration, the percent inhibition was found as decreased about half of the previous experiments. The MIC was determined as 2.1 mg/ml and 2.3 mg/ml for 3-HPAA in the experiments carried out with Fluka and Sigma, respectively.

In the case of 4-HBA, 1.5 mg/ml had 39% inhibition and 1.7 mg/ml had 71% inhibition in the previous experiments (Table 2.1.). Thus, 1.6 mg/ml was used for shot-gun proteomics experiments since it would show a percent inhibition between 39-71%. In addition, MIC was found as 1.9 mg/ml (Table 2.1.). However in the experiments performed by Sigma brand MHB, 1.6 mg/ml showed a 12% inhibition and the MIC was found as 2.0 mg/ml.

Therefore; it could be concluded that the bacteria might behave differently against different brands of broth media. The brand of the media should be considered as an important parameter for obtaining consistent results and brand of media with the same brand should be used during the experiments.

Table B.1. Inhibition of percentages of 3-HPAA and cfu/ml of *P. aeruginosa* of narrow range concentrations.

	3-HPAA		4-HBA	
Phenolic acid Concentrations (mg/ml)	**Percent Inhibition**	**Cell Survival**	**Percentage of Inhibition**	**Cell Survival**
1.5	-1	ND*	4	ND
1.6	2	ND	12	$4x10^8$ cfu/ml
1.7	3	ND	40	ND
1.8	21	ND	46	ND
1.9	25	$5x\ 10^8$ cfu/ml	55	ND
2.0	42	ND	98	TMTC
2.1	51	ND	98	TMTC
2.2	65	ND	99	TMTC
2.3	98	TMTC**	99	TMTC
2.4	98	TMTC	98	TMTC
2.5	98	TMTC	98	$5x10^2$ cfu/ml
2.6	98	TMTC	98	$1x10^1$ cfu/ml
2.7	98	TMTC	98	No survivors
2.8	98	No survivors	98	No survivors
2.9	98	No survivors	99	No survivors
3.0	98	No survivors	98	No survivors

*ND: Not determined.

**TMTC: Too many to count

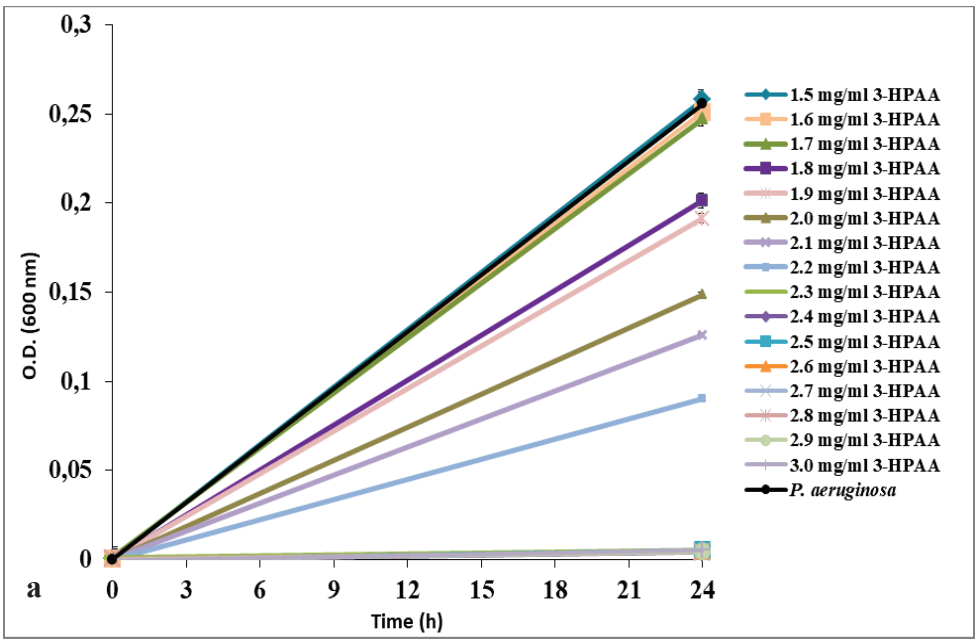

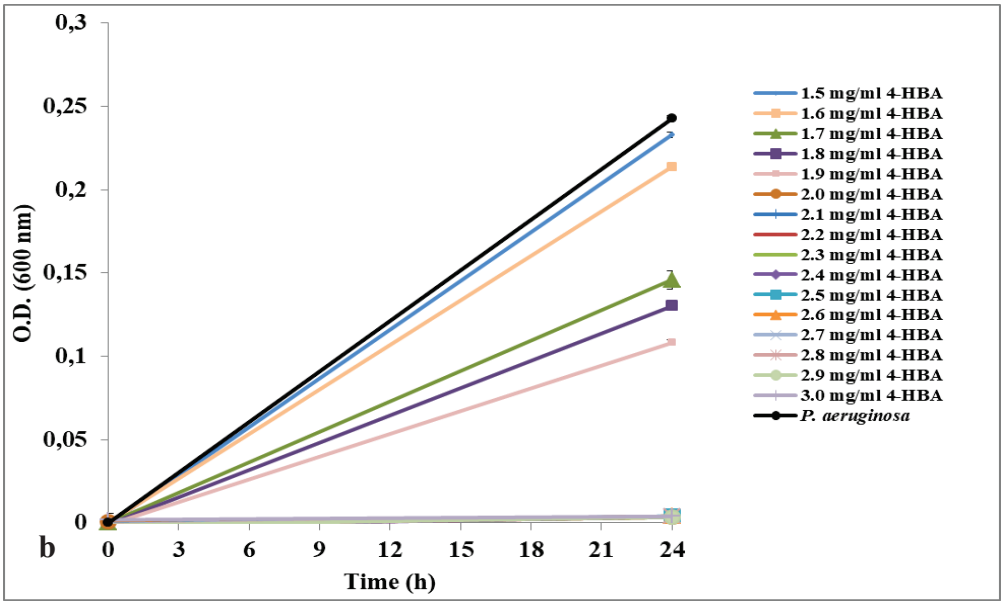

Figure B.1. The antimicrobial effect of phenolic acids in a narrow range of concentrations on *P. aeruginosa* grown with Sigma MHB media. a) 3-HPAA b) 4-HBA

APPENDIX C

BOVINE SERUM ALBUMIN STANDART CURVE

Since the proteins were dissolved in resuspension buffer for the LC-ESI-MS/MS studies, , Bovine serum albumin (BSA) was also dissolved in resuspension buffer 50-250 µg/ml concentrations. The absorbance values of BSA solutions were measured at 595 nm.

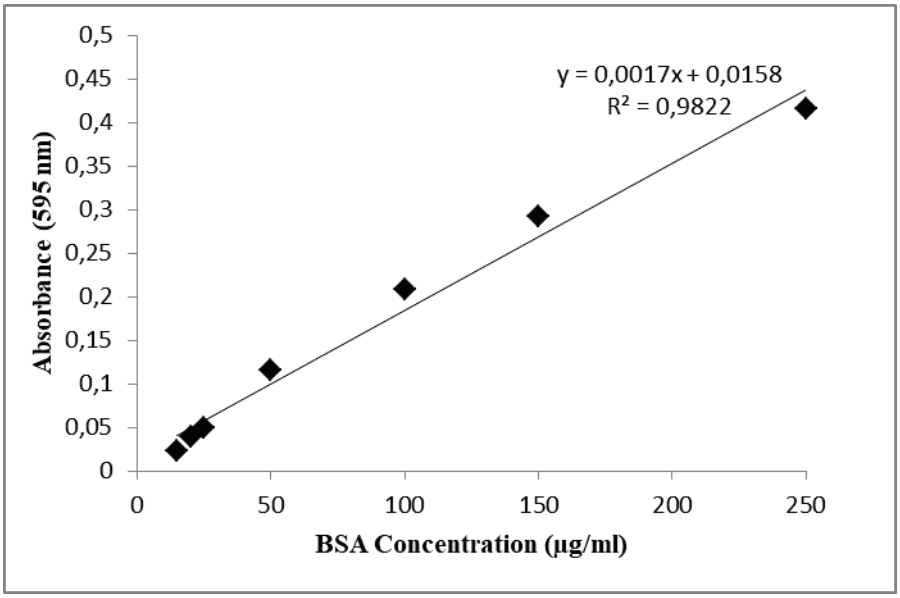

Figure C.1. The standart curve of bovine serum albumin.

APPENDIX D

MUTUAL PROTEINS

The mutual proteins which did not change either in control group or phenolic acid treated groups were shown in Table D.1.

Table D.1. Mutual proteins that did not change in *P. aeruginosa* protein profile.

ID	Protein Name	Gene Name
P48372	DNA gyrase subunit A	gyrA PA3168
P28811	3-hydroxyisobutyrate dehydrogenase	mmsB PA3569
O52760	DNA-directed RNA polymerase subunit alpha	rpoA PA4238
Q9HUC3	Polyhydroxyalkanoate synthesis protein PhaF	phaF PA5060
P13982	Carbamate kinase	arcC PA5173
Q9HVC5	Ribose-phosphate pyrophosphokinase	prs PA4670
Q9HZP5	Electron transfer flavoprotein-ubiquinone oxidoreductase	PA2953
Q59637	Pyruvate dehydrogenase E1 component	aceE aceA, PA5015
Q9I2W7	Putative 4-hydroxy-4-methyl-2-oxoglutarate aldolase	PA1772
Q9HY22	Response regulator ErdR	erdR PA3604
Q9HTD1	Probable transcarboxylase subunit	PA5435
Q9HW32	Insulin-cleaving metalloproteinase outer membrane protein	icmP PA4370
Q9I576	4-hydroxyphenylpyruvate dioxygenase	hpd PA0865
Q9HYX8	Peptidyl-prolyl cis-trans isomerase	PA3262
Q9HZH7	Molybdenum cofactor biosynthesis protein B	moaB2 PA3029
Q9I659	Probable ClpA/B protease ATP bindin...	PA0459
Q9I5E2	2-methylisocitrate lyase	prpB PA0796
Q9HYZ6	Site-determining protein	minD PA3244
P50987	Argininosuccinate lyase	argH PA5263
Q9I0A0	Translation initiation factor IF-3	infC PA2743
Q9I2V5	Aconitate hydratase B	acnB PA1787
O50175	N-succinylarginine dihydrolase	astB aruB, PA0899
P72173	Aspartate aminotransferase	aspC PA3139

(cont. on next page)

Table D.1. (continued)

Q9HXN2	Phosphoribosylformylglycinamidine synthase	purL PA3763
Q9I1M0	Lipoamide acyltransferase component of branched-chain alpha-keto acid dehydrogenase complex	bkdB PA2249
Q9I0K4	Isocitrate lyase	PA2634
Q9I6M4	5-aminovalerate aminotransferase DavT	davT PA0266
P47205	UDP-3-O-acyl-N-acetylglucosamine deacetylase	lpxC envA, PA4406
Q9HTM1	DNA-directed RNA polymerase subunit omega	rpoZ PA5337
Q9I6J1	Putrescine-binding periplasmic protein SpuD	spuD PA0300
Q9HZJ5	DNA topoisomerase 1	topA PA3011
Q9I3D3	2-oxoglutarate dehydrogenase (E1 subunit)	sucA PA1585
Q9HX05	Probable aldehyde dehydrogenase	PA4022
Q59636	Nucleoside diphosphate kinase	ndk PA3807
Q9I4X2	2-heptyl-4(1H)-quinolone synthase subunit PqsB	pqsB PA0997
Q9I747	Protein hcp1	hcp1 PA0085
Q9HTR6	Nitrogen regulatory protein P-II 2	glnK PA5288
Q9I5Y4	Phosphoglycerate kinase	pgk PA0552
Q9I636	Malate synthase G	glcB PA0482
Q9HW68	Fumarate hydratase class I	PA4333
Q9HZK4	Glyceraldehyde-3-phosphate dehydrogenase	PA3001
P13794	Outer membrane porin F	oprF PA1777
Q9I6Z3	Alkyl hydroperoxide reductase subunit C	ahpC PA0139
Q51404	Fumarate hydratase class II 2	fumC2 PA4470
Q9HVA8	Ferric iron-binding periplasmic protein HitA	hitA PA4687
Q9HVN5	Chaperone protein ClpB	clpB PA4542
Q9HUY5	Mg(2+) transport ATPase, P-type 2	mgtA PA4825
Q9I047	Transaldolase	tal PA2796
Q9I2W9	Phosphoenolpyruvate synthase	ppsA PA1770
Q9HTP2	Probable aldehyde dehydrogenase	PA5312
Q9HVT7	Aspartyl/glutamyl-tRNA(Asn/Gln) amidotransferase subunit B	gatB PA4484
Q9I344	Chorismate synthase	aroC PA1681
Q9HXJ4	4-hydroxy-3-methylbut-2-en-1-yl diphosphate synthase (flavodoxin)	ispG PA3803
Q9HW04	Arginine biosynthesis bifunctional protein ArgJ	argJ PA4402
P57112	Soluble pyridine nucleotide transhydrogenase	sthA sth, PA2991
Q9HV55	Translation initiation factor IF-2	infB PA4744
Q9I4W0	Phosphoribosylaminoimidazole-succinocarboxamide synthase	purC PA1013

(cont. on next page)

Table D.1. (continued)

Q9I5I4	Probable enoyl-CoA hydratase/isomerase	PA0745
Q9HZ98	Heat-shock protein IbpA	ibpA PA3126
Q9HT17	ATP synthase subunit delta	atpH PA5557
Q9I5Z0	S-adenosylmethionine synthase	metK PA0546
Q9HZE0	NAD-specific glutamate dehydrogenase	gdhB PA3068
Q9I5E4	Probable aconitate hydratase	PA0794
P08308	Ornithine carbamoyltransferase, catabolic	arcB PA5172
Q9HWD2	Elongation factor G 1	fusA fusA1, PA4266
Q9HUD3	Malic enzyme	PA5046
Q9HT21	ATP synthase epsilon chain	atpC PA5553
Q9HZP7	Electron transfer flavoprotein subunit alpha	etfA PA2951
Q9HZJ2	Fatty acid oxidation complex subunit alpha	fadB PA3014
Q9I4I2	Ribonucleoside-diphosphate reductase subunit beta	nrdB PA1155
P05384	DNA-binding protein HU-beta	hupB PA1804
Q9HV43	Chaperone protein DnaK	dnaK PA4761
Q9HZF5	Probable hydrolytic enzyme	PA3053
Q9I3D2	Dihydrolipoyllysine-residue succinyltransferase component of 2-oxoglutarate dehydrogenase complex	sucB PA1586
P53641	Superoxide dismutase [Fe]	sodB PA4366
Q9HWW7	Probable thioredoxin	PA4061
Q9HT16	ATP synthase subunit b	atpF PA5558
Q9I2U0	ATP-dependent Clp protease ATP-binding subunit ClpX	clpX PA1802
Q9I4Z4	Peptidoglycan-associated lipoprotein	pal oprL, PA0973
Q51344	Aspartate-semialdehyde dehydrogenase	asd PA3117
P57668	Thiol peroxidase	tpx PA2532
Q59638	Dihydrolipoyllysine-residue acetyltransferase component of pyruvate dehydrogenase complex	aceF aceB, PA5016
Q9HX76	Probable DNA binding protein	PA3940
Q9HV54	Transcription termination/antitermination protein NusA	nusA PA4745
Q9HXV4	Adenylate kinase	adk PA3686
Q9HW45	Xenobiotic reductase	xenB PA4356
Q9I0J6	NADH-quinone oxidoreductase subunit G	nuoG PA2642
Q9X2T1	Thioredoxin	trxA trx, PA5240
O30508	Succinylornithine transaminase/acetylornithine aminotransferase	aruC argD, astC, PA0895
P28810	Methylmalonate-semialdehyde dehydrogenase [acylating]	mmsA PA3570
Q9HU24	dTDP-glucose 4,6-dehydratase	rmlB PA5161

(cont. on next page)

Table D.1. (continued)

P52002	Multidrug resistance protein MexB	mexB PA0426
Q9I6H5	D-3-phosphoglycerate dehydrogenase	serA PA0316
Q9HVY4	Ubiquinol-cytochrome c reductase iron-sulfur subunit	PA4431
Q9HTD9	Alcohol dehydrogenase	adhA PA5427
Q9I4I1	Ribonucleoside-diphosphate reductase	nrdA PA1156
Q9HV46	Transcription elongation factor GreA	greA PA4755
Q9HUC5	ATP-dependent protease ATPase subunit HslU	hslU PA5054
Q9HVD1	Lipid A deacylase PagL	pagL PA4661
P37798	Biotin carboxylase	accC fabG, PA4848
P20580	Anthranilate synthase component 1	trpE PA0609
P43335	Pterin-4-alpha-carbinolamine dehydratase	phhB PA0871
Q9I3B2	Beta-ketoacyl-ACP synthase I	fabB PA1609
Q9I3G2	Cbb3-type cytochrome c oxidase subunit	ccoP2 PA1555
Q9I5U3	Chaperone SurA	surA PA0594
Q9I2Y7	Phospho-2-dehydro-3-deoxyheptonate aldolase	PA1750
O69077	Aspartokinase	lysC PA0904
Q9HW86	Transcriptional regulator MvaT, P16 subunit	mvaT PA4315
P30718	60 kDa chaperonin	groL groEL, mopA, PA4385
Q9HX01	Probable acetyltransferase	PA4026
P08280	Protein RecA	recA PA3617
Q9I0T1	Probable acyl-CoA thiolase	PA2553
P43501	Protein PilH	pilH PA0409
Q9I3D4	Succinate dehydrogenase (B subunit)	sdhB PA1584
Q9I407	Glutaminase-asparaginase	ansB PA1337
P00282	Azurin	azu PA4922
P13981	Arginine deiminase	arcA PA5171
Q9I3F5	Aconitate hydratase A	acnA PA1562
Q9I6M5	Glutarate-semialdehyde dehydrogenase	davD PA0265
O82852	Uridylate kinase	pyrH PA3654
Q9HVA2	Ketol-acid reductoisomerase (NADP(+))	ilvC PA4694
P15276	Transcriptional regulatory protein AlgP	algP algR3, PA5253
Q9I1L9	Dihydrolipoyl dehydrogenase	lpdV PA2250
Q9I137	Glycine dehydrogenase (decarboxylating) 1	gcvP1 PA2445
Q9I6G0	L-threonine dehydratase	ilvA1 ilvA, PA0331
Q9HVT8	Glutamyl-tRNA(Gln) amidotransferase subunit A	gatA PA4483
Q9I140	Glycine cleavage system protein T2	gcvT2 PA2442

(cont. on next page)

Table D.1. (continued)

P30720	10 kDa chaperonin	groS groES, mopB, PA4386
Q9I0D3	Cysteine synthase	cysK PA2709
P38100	Carbamoyl-phosphate synthase large chain	carB PA4756
Q9I2U2	Trigger factor	tig PA1800
Q9HXZ5	Enolase	eno PA3635
Q9I7C2	DNA gyrase subunit B	gyrB PA0004
Q51561	DNA-directed RNA polymerase subunit beta	rpoB PA4270
Q9HY77	Glutaredoxin	PA3533
Q9HWC9	DNA-directed RNA polymerase subunit beta'	rpoC PA4269
Q9I5Q9	N-acetyl-gamma-glutamyl-phosphate reductase	argC PA0662
Q9HZJ3	3-ketoacyl-CoA thiolase	fadA PA3013
Q9HT20	ATP synthase subunit beta	atpD PA5554
Q9I3C5	Chaperone protein HtpG	htpG PA1596
P14165	Citrate synthase	gltA PA1580
Q9HTU9	Glyoxalase	PA5245
P77915	Oxygen-independent coproporphyrinogen III oxidase	hemN PA1546
Q9HV59	Polyribonucleotide nucleotidyltransferase	pnp PA4740
P11221	Major outer membrane lipoprotein	oprI PA2853
Q9I083	Probable outer membrane protein	PA2760
Q9HYL8	Binding protein component of ABC phosphonate transporter	PA3383
Q9HU65	Glutamine synthetase	glnA PA5119
Q9I690	UPF0312 protein PA0423	PA0423
Q9I687	Methylenetetrahydrofolate reductase	metF PA0430
P09591	Elongation factor Tu	tufA PA4265 tufB PA4277
Q9I296	Putative isovaleryl-CoA dehydrogenase	liuA PA2015
Q9HX20	Gamma-glutamyl phosphate reductase	proA PA4007
Q9I0K9	Adenylosuccinate lyase	purB PA2629
Q9I138	Serine hydroxymethyltransferase 2	glyA2 PA2444
P72157	N5-carboxyaminoimidazole ribonucleotide mutase	purE PA5426
Q9I402	Probable binding protein component of ABC transporter	PA1342
Q9HTV1	Transcription termination factor Rho	rho PA5239
Q59643	Delta-aminolevulinic acid dehydratase	hemB PA5243
Q9HXZ4	CTP synthase	pyrG PA3637
Q9HWX4	3,4-dihydroxy-2-butanone 4-phosphate synthase	ribB PA4054
Q9HZZ2	Elongation factor P	efp PA2851
G3XD47	Arginine/ornithine binding protein AotJ	aotJ PA0888
Q9HZM8	Ribonuclease E	rne PA2976

(cont. on next page)

Table D.1. (continued)

O82853	Ribosome-recycling factor	frr PA3653
O52762	Catalase	katA PA4236
Q9HV42	Protein GrpE	grpE PA4762
P21175	Leucine-, isoleucine-, valine-, threonine-, and alanine-binding protein	braC PA1074
Q9I2U9	Peptidyl-prolyl cis-trans isomerase	ppiB PA1793
Q9HXM5	Inosine-5'-monophosphate dehydrogenase	guaB PA3770
Q9HT25	Glutamine--fructose-6-phosphate aminotransferase [isomerizing]	glmS PA5549
Q9I1N7	PslB	pslB PA2232
Q9HVJ1	Probable ATP-binding component of ABC transporter	PA4595
Q9I0L5	Isocitrate dehydrogenase [NADP]	icd PA2623
Q9HY81	Probable peroxidase	PA3529
Q9HVI7	Serine hydroxymethyltransferase 3	glyA2 PA4602
P0DP44	Polyphosphate kinase	ppk PA5242
O87125	Protein-glutamate methylesterase/protein-glutamine glutaminase 1	cheB1 PA1459
Q9I3D1	Dihydrolipoyl dehydrogenase	lpdG PA1587
Q9HY84	Argininosuccinate synthase	argG PA3525
Q9I0L4	Isocitrate dehydrogenase	idh PA2624
Q9HV50	Phosphoglucosamine mutase	glmM PA4749
O82851	Elongation factor Ts	tsf PA3655
Q9HVQ3	Ornithine decarboxylase	speC PA4519
Q9HWC4	Transcription termination/antitermination protein NusG	nusG PA4275
Q9I5G8	Elongation factor 4	lepA le, PA0767
Q9HXJ9	Probable aminotransferase	PA3798
Q9I685	Adenosylhomocysteinase	ahcY sahH, PA0432
O54438	3-oxoacyl-[acyl-carrier-protein] reductase FabG	fabG PA2967
Q9I6J2	Putrescine--pyruvate aminotransferase	spuC PA0299
Q9I6E0	Dihydroxy-acid dehydratase	ilvD PA0353
P38098	Carbamoyl-phosphate synthase small chain	carA PA4758
P24559	Twitching mobility protein	pilT PA0395
Q9HW72	Pyruvate kinase	pykA PA4329
Q9I0Y8	Efflux pump membrane transporter	mexF PA2494
Q9I185	PvdO	pvdO PA2395
P26275	Positive alginate biosynthesis regulatory protein	algR PA5261
Q9HT18	ATP synthase subunit alpha	atpA PA5556
Q9HVS8	RoxR	roxR PA4493
Q9HUM6	Adenylosuccinate synthetase	purA PA4938

(cont. on next page)

Table D.1. (continued)

Q9I4Z7	Probable dna-binding stress protein	PA0962
Q9I662	Probable cold-shock protein	PA0456
Q9HYK7	Ferredoxin--NADP+ reductase	fpr PA3397
P20577	Indole-3-glycerol phosphate synthase	trpC PA0651
G3XDA8	Phosphate-binding protein PstS	pstS PA5369
Q9HXZ2	Acetyl-coenzyme A carboxylase carboxyl transferase subunit alpha	accA PA3639
Q9HTQ0	D-amino acid dehydrogenase 1	dadA1 dadA, PA5304
Q9HZP6	Electron transfer flavoprotein subunit beta	etfB PA2952
Q9HWC6	50S ribosomal protein L1	rplA PA4273
Q9HWD8	50S ribosomal protein L2	rplB PA4260
Q9HWD5	50S ribosomal protein L3	rplC PA4263
Q9HWD6	50S ribosomal protein L4	rplD PA4262
Q9HWE7	50S ribosomal protein L5	rplE PA4251
Q9HWF0	50S ribosomal protein L6	rplF PA4248
Q9HWC8	50S ribosomal protein L7/L12	rplL PA4271
Q9HUN2	50S ribosomal protein L9	rplI PA4932
Q9HWC7	50S ribosomal protein L10	rplJ PA4272
Q9HWC5	50S ribosomal protein L11	rplK PA4274
Q9HVY2	50S ribosomal protein L13	rplM PA4433
Q9HWF4	50S ribosomal protein L15	rplO PA4244
Q9HWE2	50S ribosomal protein L16	rplP PA4256
O52761	50S ribosomal protein L17	rplQ PA4237
Q9HWF1	50S ribosomal protein L18	rplR PA4247
Q9HXQ2	50S ribosomal protein L19	rplS PA3742
Q9I0A2	50S ribosomal protein L20	rplT PA2741
Q9HVL6	50S ribosomal protein L21	rplU PA4568
Q9HWE6	50S ribosomal protein L24	rplX PA4252
Q9HVC4	50S ribosomal protein L25	rplY ctc, PA4671
Q9HTN8	50S ribosomal protein L28	rpmB PA5316
Q9HWE3	50S ribosomal protein L29	rpmC PA4255
Q9HWF3	50S ribosomal protein L30	rpmD PA4245
Q9HZN4	50S ribosomal protein L32	rpmF PA2970
Q9HZ71	30S ribosomal protein S1	rpsA PA3162
Q9HWE1	30S ribosomal protein S3	rpsC PA4257
O52759	30S ribosomal protein S4	rpsD PA4239
Q9HWF2	30S ribosomal protein S5	rpsE PA4246

(cont. on next page)

Table D.1. (continued)

Q9HUM9	30S ribosomal protein S6	rpsF PA4935
Q9HWD1	30S ribosomal protein S7	rpsG PA4267
Q9HWE9	30S ribosomal protein S8	rpsH PA4249
Q9HVY3	30S ribosomal protein S9	rpsI PA4432
Q9HWD4	30S ribosomal protein S10	rpsJ PA4264
Q9HWD0	30S ribosomal protein S12	rpsL PA4268
Q9HWF7	30S ribosomal protein S13	rpsM PA4241
Q9HWE8	30S ribosomal protein S14	rpsN PA4250
Q9HXP9	30S ribosomal protein S16	rpsP PA3745
Q9HWE4	30S ribosomal protein S17	rpsQ PA4254
Q9HWD9	30S ribosomal protein S19	rpsS PA4259
Q9I5V8	30S ribosomal protein S21	rpsU PA0579
Q9HXU0	Lysine--tRNA ligase	lysS PA3700
Q9I0M6	Serine--tRNA ligase	serS PA2612
Q51422	Aspartate--tRNA(Asp/Asn) ligase	aspS PA0963
Q9HX33	Leucine--tRNA ligase	leuS PA3987
Q9HUC8	Arginine--tRNA ligase	argS PA5051
Q9HVX6	Tryptophan--tRNA ligase	trpS PA4439
Q9I502	Proline--tRNA ligase	proS PA0956
Q9I7B8	Glycine--tRNA ligase beta subunit	glyS PA0008
Q9I553	Alanine--tRNA ligase	alaS PA0903
Q51567	Succinate--CoA ligase [ADP-forming] subunit alpha	sucD PA1589
Q9HYU4	Long-chain-fatty-acid--CoA ligase	fadD1 PA3299
P53593	Succinate--CoA ligase [ADP-forming] subunit beta	sucC PA1588
Q9I171	Uncharacterized protein	PA2410
Q9I500	Uncharacterized protein	PA0959
Q9I2R5	Uncharacterized protein	PA1830
Q9I0R1	Uncharacterized protein	PA2575
Q9HXL0	Uncharacterized protein	PA3785
Q9HYZ0	Uncharacterized protein	PA3250
Q9I5U9	Uncharacterized protein	PA0588
Q9I338	Uncharacterized protein	PA1689
Q9HU11	Uncharacterized protein	PA5178
Q9I0D5	Uncharacterized protein	PA2707
Q9I078	Uncharacterized protein	PA2765
Q51384	Uncharacterized protein PA3808	PA3808
Q9HVW4	Uncharacterized protein	PA4453

(cont. on next page)

Table D.1. (continued)

Q9HW49	Uncharacterized protein	PA4352
Q9HVV5	Uncharacterized protein	PA4463
Q9HYT5	Uncharacterized protein	PA3309
Q9I1F7	Uncharacterized protein	PA2318
Q9I658	Uncharacterized protein	PA0460
Q9HX12	Uncharacterized protein	PA4015
Q9HYG6	Uncharacterized protein	PA3440
Q9I0H1	Uncharacterized protein	PA2667
Q9HVF2	Uncharacterized protein	PA4639
Q9I4W2	Uncharacterized protein	PA1011

APPENDIX E

THE ANTIMICROBIAL EFFECTS OF THE CONCENTRATIONS OF PHENOLIC ACIDS USED IN NANOPARTICLE PRODUCTION

The concentrations of phenolic acids which were used in nanoparticle production demonstrated bacteriocidal effect on *P. aeruginosa* (Figure E.1; Table E.1)

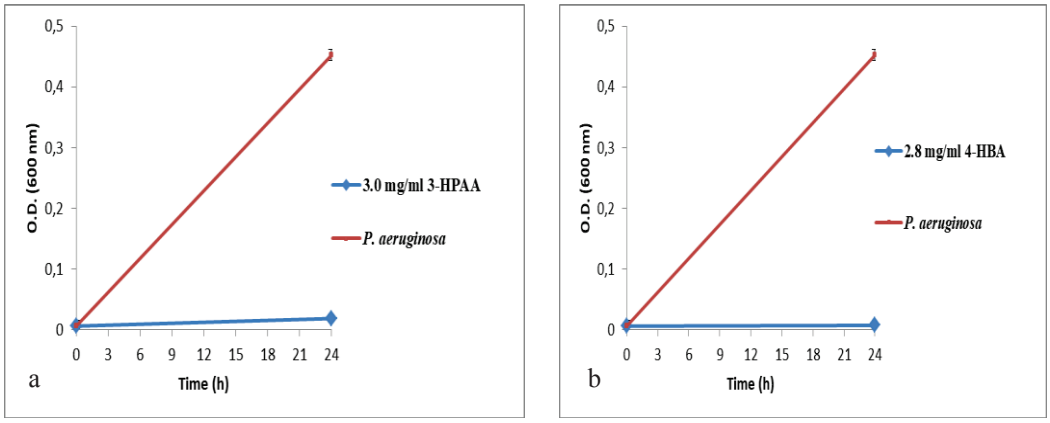

Figure E.1. The antimicrobial effect of concentrations which were used in nanoparticle production on *P. aeruginosa.* a) 3-HPAA b) 4-HBA

Table E.1. The effect of the phenolic acid concentrations used in nanoparticle production in terms of percent inhibition and cell survival.

Phenolic Acid Concentration	Percentage of Inhibition	Cell Survival
3-HPAA (3.0 mg/ml)	96	No survivors
4-HBA (2.8 mg/ml)	98	No survivors

APPENDIX F

THE EFFECT OF ETHANOL CONCENTRATIONS ON *Staphylococci*

Since 70% ethanol did not present inhibition zones for *S. epidermidis*, MRSA and MSSA in agar diffusion studies with nanoparticle solutions, the concentration range of ethanol was tested *on Staphylococci* and compared with inhibition of household bleach (Figure F.1.-a,b,c).

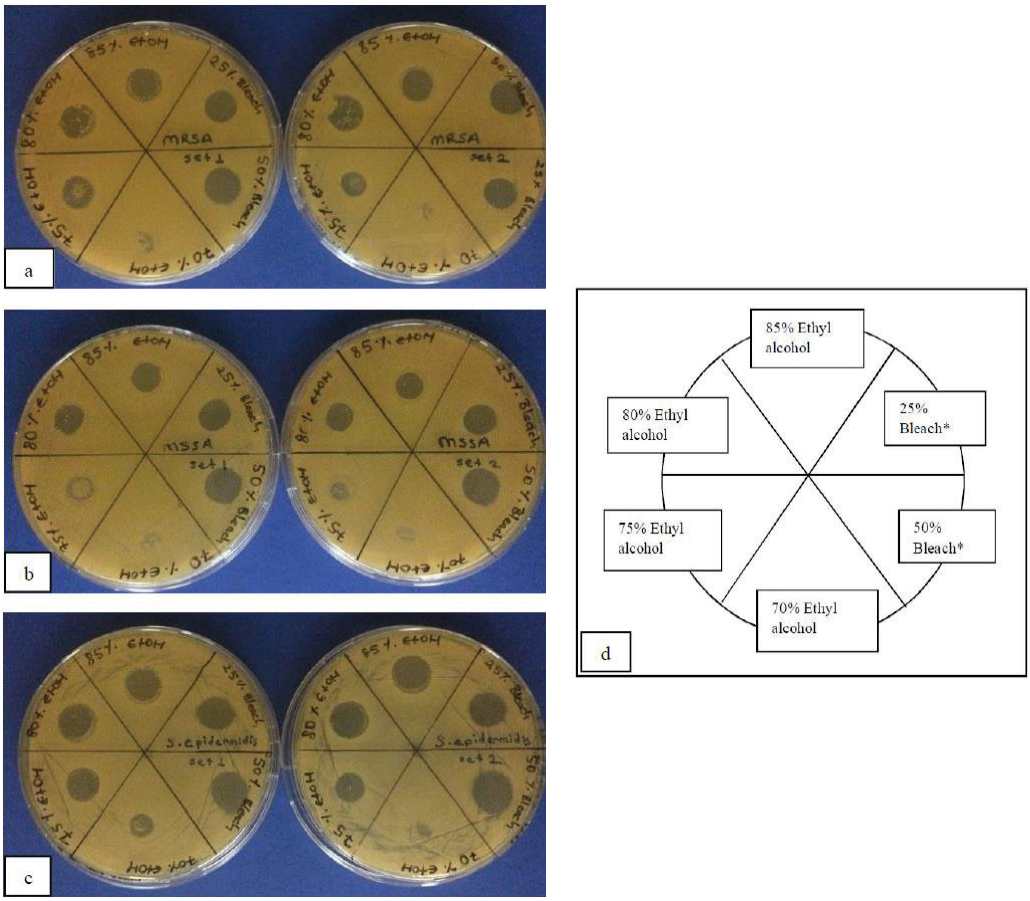

Figure F.1. The effect of ethanol on S*taphylococci*. Different sets (Set 1: left; Set 2: right) of the same bacteria; a) MRSA b) MSSA c) *S. epidermidis* d) The template which shows the regions of the solutions on agar plates

The solutions in agar plates has an exception in the template: The locations of 25% and 50% bleach are vice versa in MRSA Set 2 plate (Figure F.1.-d)

The results demonstrated that 70% ethanol caused a new growth on its own inhibition zone for each tested bacteria. The zone was full covered with bacteria in the cases of MRSA and MSSA while a ring-like growth pattern was determined for *S. epidermidis* on the inhibition zone of 70% ethanol. The concentrations of 80% and 85% showed clear inhibition zones similar to 25% household bleach had displayed for each tested bacterium. Therefore, it could be suggested that using ethanol in 80-85% rather than 70% would be much effective on pathogenic *Staphylococci* which are accepted as one of the main agents of many nosocomial infections.

VITA

Date/Place of Birth

12.01.1986/Ankara, Turkey

Educational Background

Undergraduate: Hacettepe University, Faculty of Science, Department of Biology (2004-2008)

Master of Science: İzmir Institute of Technology, Institute of Engineering and Science, Department of Molecular Biology and Genetics (2009 – 2012)

Publications

1. Telli, Nihat; Güner, Ahmet; Soyer Dönmez, Ferda; Özdemir, Özgün Öykü, Detection of the contamination sources of *Listeria monocytogenes* in pickled white cheese production process line and genotyping with the pulsed-field gel electrophoresis method, 2016, Turk J Vet Anim Sci, doi:10.3906/vet-1511-59.

Presentations in Symposiums

1. Ozdemir O. O., Soyer F.**,** Synthesis, characterization and antimicrobial effect of phenolic acid loaded alginate-chitosan nanoparticles, PPM, 2017. (Oral Presentation)
2. Keman, D., Özdemir, Ö., Fratebianchi de la Parra, D., Cavalitto, S.**,** Study of the Pectolytic Activities Produced by *Aspergillus sojae* in Solid State Cultures Utilizing Agroindustrial Residues, SaProBio, 2014. (Poster presentation)
3. Ozdemir O. O., Soyer F.**,** Inhibition of *Staphylococcus epidermidis* growth by 4-Hydroxybenzoic acid added bone cement, PPM, 2015. (Oral presentation)
4. Ozdemir O. O., Keman D., Soyer F., Profiling of Outer Membrane Proteins of *Salmonella* Enteritidis in Response to 3-hydroxyphenylacetic Acid, ISSMET, 2011. (Poster presentation)
5. Keman D., Ozdemir O. O., Soyer F.**,** Outer Membrane Protein Profiling of *Escherichia col*i O157:H7 in caffeic acid stress, ISSMET, 2011. (Poster presentation).

Certificates

Experimental Animal Use Certificate, Ege University, EÜHADYEK, 2017.